The Holocene cryptotephra record of Lake Kushu, northern Japan: Towards an integrated tephrostratigraphic framework for East Asia

Xuan-Yu Chen

Thesis submitted for the degree of Doctor of Philosophy at the University of London

September 2018

Institution of study:

Department of Geography & Department of Earth Sciences

Royal Holloway, University of London

Declaration

This thesis presents the results of original research undertaken by the author and none of the results, illustrations and text are based on published or unpublished work of others, except where specified and acknowledged.

Signature: …… Date: ……..……..

Abstract

Tephrochronology is the study of the stratigraphy, age, glass chemistry and distribution of volcanic ash (i.e. tephra) layers and the use of widely dispersed tephra isochrons for precise dating and correlation of geological, paleoclimate and archaeological records. Palaeoclimate records in East Asia, a region where environmental changes are primarily controlled by the Asian monsoon, are essential for our understanding of monsoon dynamics. Importantly, East Asia is a volcanically active region, which possesses great potential for offering widespread tephra layers. As such the region is an ideal area for optimising the use of tephra layers to synchronise palaeoclimate records. However, before this can be achieved, a comprehensive regional tephra framework is required, in order to guide future correlations and minimise miscorrelation.

In this PhD project, the proximal volcanic stratigraphy of Changbaishan volcano China/N Korea and a cryptotephra deposit from Lake Kushu northern Japan were investigated. These records were then compared to a range of data sources to attempt to correlate and, where possible provide independent ages for the tephra. Proximal-distal correlations of the Millennium eruption tephra (~1ka) allowed the clarification of controversial proximal stratigraphy of the Changbaishan volcano. In addition, precisely determined tephra ages were used to constrain the radiocarbon chronology of the distal lacustrine record. A detailed investigation of cryptotephra on the entire 16-m-long Holocene Kushu sequence was undertaken. The presented glass chemistry and age results based on Bayesian modelling of available radiocarbon dates for the core allowed the identification of several regional marker tephra layers and previously undocumented tephra horizons. The presented RK12 Holocene tephrostratigraphy integrated local and far-travelled tephras originating from regions in Japan, China, Russia and as far south as Indonesia, which facilitated the construction of an integrated tephra framework for East Asia through providing an important northern element of a regional tephra lattice. A prominent cryptotephra in the sequence exhibited chemical fingerprint that did not match with known Asian northern Hemisphere eruptions. With further investigation of southern Hemisphere tephra sources, this study proposed the identification of a cryptotephra from Krakatau volcano Indonesia, in northern Japan over 6700 km from the vent. An updated and integrated Holocene tephra framework

for East Asia was also summarised in this study, based on a thorough review of previous visible tephra work and recent developments of cryptotephra research in the region. A total of twenty-two widespread tephras originating from Russia, China/N Korea, S Korea, Japan and Indonesia were selected and incorporated in the proposed framework, which was an essential first step towards a regional master tephra framework. In addition, the chronostratigraphic relationships between these tephras and climate change events were fully evaluated, in particular the extent to which these isochrons could be used to constrain regional variations of short-lived climate oscillations. Given the fruitful results from recent pioneering cryptotephra studies in East Asia, it is now essential that a more systematic approach to the application of cryptotephra studies is applied to terrestrial and marine records from the region.

Acknowledgements

I owe a number of people significant gratitude, without them completion of this thesis would not have been possible.

To my supervisors at both RHUL and GIGCAS, Professors **Simon Blockley**, **Martin Menzies** and **Yigang Xu**, for their guidance and support over the last four years. Simon has advised me with the directions of the research and has had many stimulating discussions with me throughout the PhD project. Martin has patiently and meticulously revised my writing all the time and has encouraged and motivated me whenever I encountered difficulties or became frustrated. Yigang has initiated the collaborative programme between RHUL and GIGCAS and has provided me the opportunity for studying in the UK. They are all great scientists and advisors, and are role models to me.

To Prof. **Pavel Tarasov** and Dr. **Stefanie Müller** at the Free University Berlin for providing sub-samples of lake core sediment, and the discussions on sediment core correlation and radiocarbon chronology.

To Drs. **Emma Tomlinson** at the Trinity College Dublin, **Victoria Smith** and **Paul Albert** at the University of Oxford, **Chris Hayward** at the University of Edinburgh for their assistance during geochemical analyses, and the help with data processing.

To co-worker **Danielle McLean** at the University of Oxford, former CQR student for providing information on preliminary investigation of the core, and enlightening discussions on the manuscripts.

To Prof. **Ian Candy** for being my advisor and all the helpful suggestions on annual review meetings, Dr. **Simon Armitage** for the helpful discussion on the Changbaishan manuscript.

To **Katy Flowers** and Dr. **Marta Perez** for their great support during my three and half years' lab work period.

To all other staff in CQR and Earth Sciences for their support.

To friends in Geography and Earth Sciences for their support and discussion during the last four years: **Jacob Bendle, Rhys Timms, Ashley Abrook, Rachel Devine, Angharad Jones, Elizabeth Peneycad, Dorothy Weston, Yajun Li, Alice Carter-**

Champion, Richard Clark-Wilson, Amy Walsh, Yunting Qi, Shuang Zhang, Liang Liu, Yizhuo Sun, Jie Xiao, Hongdan Deng, Qiong Li.

To **Jiaqi Qin** in SYSU for remote teaching of the use of plotting software when I published my first manuscript, **Junting Qiu** in the University of Tokyo for the help with accessing Japanese literature, and **Cong Chen** in SYSU for the discussions of Quaternary scientific questions. To other friends in China who cared about me and encouraged me during the tough time of writing-up.

To **Tianshu** for being a great friend and housemate, our friendship will continue no matter where we are.

To **Aike** for the last four years of friendship and all the support and encouragement throughout my PhD.

To **Martin** again and his wife **Lesley Hunter**, for inviting me to their home for the tea and cakes, and for celebrating with me every Chinese Lunar New Year.

Finally to my family for their unconditional love and support. I am forever grateful to them.

Table of Content

List of Figures

Chapter 1

Chapter 2

Chapter 3

Chapter 4

Chapter 5

Chapter 6

List of Tables

Chapter 2

Chapter 3

Chapter 4

Chapter 5

Chapter 1: Introduction

1.1 General context

1.1.1 Tephrochronology as a dating and correlation tool

Tephrochronology is the study of the stratigraphy, age, glass chemistry and distribution of volcanic ash (i.e. tephra) layers and the use of widely dispersed tephra isochrons for precise dating and correlation of geological, paleoclimate and archaeological records (Lowe, 2011). Volcanic ash horizons, preserved in various sedimentary archives, exist as visible layers or as non-visible cryptotephra layers (Blockley et al., 2005). In Europe and the North Atlantic, considerable progress has been made in few decades in the development of tephrochronology as a dating and correlation method, among which the most significant breakthroughs are mainly from cryptotephra studies (c.f. Davies, 2015). Cryptotephra studies reveal the presence of tephras in sedimentary records which are not apparent from visible tephra studies (e.g. Davies et al., 2010; Lane et al., 2011, 2012, 2015; Abbott et al., 2016; Bourne et al., 2010, 2015a, 2015b, 2016; MacLeod et al., 2015; Matthews et al., 2015; Wulf et al., 2016, 2018; Watson et al., 2016, 2017a, 2017b; Jones et al., 2017; Timms et al., 2017, 2018). In addition, cryptotephra studies greatly enlarge the ash footprint of individual volcanic eruptions (e.g. Blockley et al., 2007; Lane et al., 2012; Jensen et al., 2014; Sun et al., 2014; Bourne et al., 2016; wan der Bilt et al., 2017; Cook et al., 2018; Kearney et al., 2018). These achievements allow a more comprehensive regional tephra framework to be established (e.g. Blockley et al., 2012, 2014; Davies et al., 2012, 2014), which facilitates the use of tephra isochrons in the synchronisation of widespread palaeoclimate records. More importantly, the identification of tephra layers that are closely associated with climatic/cultural changes in different records permits the investigation of long-standing questions such as the leads and lags in the climate system (Lane et al., 2013) or the causal links between climate change and human migration/evolution (Lowe et al., 2012).

1.1.2 Palaeoclimate studies in East Asia

Palaeoclimate records in East Asia, a region where environmental changes are primarily controlled by the Asian monsoon (An, 2000), are essential for our understanding of monsoon dynamics. The East Asian monsoon (EAM) regime is a sub-system of the Asian monsoon circulation, which affects an area to the east of the Bay of Bengal and the Tibetan Plateau, influencing the climate of Japan, the Koreas and much of China. The EAM is formed because of the thermal differences between the Asian continent and the Pacific Ocean, and is further enhanced by the thermal and dynamic effects of the Tibetan Plateau (An, 2000). The EAM is divided into the East Asian summer monsoon (EASM) and the winter monsoon (EAWM). In the northern summer season, warm and humid air originating from the low latitude oceans migrates north along with the seasonal changes of planetary scale circulations, and is further driven by the east-west pressure gradient in East Asia. While in the northern winter season, cold air from high latitudes is controlled by the continental high-pressure system, and propagates southward along the eastern margin of the Tibetan Plateau (An, 2000).

The history of the EAM is reconstructed using loess deposits that are widely distributed in central China (An, 2000). Previous research (e.g., Kukla and An, 1989) indicates that loess is the deposition of dust transported by the northerly winter monsoon. Particle size, aeolian flux and detrital quartz composition can be used as proxy indices of the EAWM (e.g., An et al., 1991a; Ding et al., 1994; Xiao et al., 1995). In contrast, the interbedded palaeosol is formed by pedogenesis under conditions where the summer monsoon dominates. Magnetic susceptibility, organic carbon content, stable carbon isotope ratio, ^{10}Be content, chemical weathering index and carbonate content of palaeosols can be used as proxy indices of the EASM (e.g., An et al., 1991b; Shen et al., 1992). The evidence from loess deposits indicates that the EAM evolution is driven by the nonlinear rhythm of the ocean and ice sheets, together with orbitally induced changes in insolation and global ice volume (An, 2000).

Although loess-palaeosol sequences are capable of providing information on long-term changes of the EAM, they are limited by resolution and dating problems (Wang et al., 2001). Recent progresses from Chinese speleothem have provided absolutely-dated high-resolution proxy records of past changes of the EAM. Studies have shown

that shifts in the oxygen isotope ratio ($\delta^{18}O$) of well-selected stalagmites largely reflect changes in $\delta^{18}O$ values of meteoric precipitation at the related sites, which in turn relate to changes in the amount of precipitation and thus characterize the EAM strength (Wang et al., 2001, 2005, 2008; Dykoski et al., 2005). The long-term speleothem records of the last glacial and deglacial periods appear to broadly follow summer insolation, suggesting that the latter is one of the key factors that affects the monsoon evolution. However, the records are also punctuated by numerous millennial-scale events, which suggest a link between the EAM and the North Atlantic climate (Wang et al., 2001). This indicates that the massive and rapid changes in oceanic and atmospheric circulation patterns which affects the North Atlantic region might have a wider impact (Wang et al., 2001). Studies on Holocene speleothem records (Wang et al., 2005; Dykoski et al., 2005) further demonstrate the similarities and correlations between the EAM and the North Atlantic climate during the Holocene. It is also possible that oceanic circulation changes in the North Atlantic triggered changes of the EAM (Wang et al., 2005). Nevertheless, it is clear that the decline trend of EAM intensity during the latter part of the Holocene results directly from the orbitally induced lowering of summer insolation that affects the Intertropical Convergence Zone (ITCZ) and low-latitude precipitation patterns (Wang et al., 2005). The conclusion that tropical monsoons vary dominantly and directly in response to changes in Northern Hemisphere summer insolation, on orbital scales, is further confirmed by speleothem records that date back to the last two interglacial-glacial cycles (Wang et al., 2008).

Some other studies, however, indicate that the interpretation of the $\delta^{18}O$ signal from speleothems as a proxy for the EAM strength is complex and sometimes controversial. For example, through mass balance calculations, Maher and Thompson (2012) propose that the cave $\delta^{18}O$ variations cannot not be simply explained by summer rainfall changes. Instead they might reflect changes in moisture source (Maher and Thompson, 2012). In addition, modelling studies suggest that the timing of light cave $\delta^{18}O$ peaks should not be interpreted as reflecting the timing of strong summer monsoons alone, and that there are additional forcing mechanisms (e.g., Clemens et al., 2010). If these were true, the interpretation of cave $\delta^{18}O$ signal needs to be re-evaluated. Furthermore, though most of the published stalagmite records show the same general trend of increasingly heavy $\delta^{18}O$ composition, thus weakened EASM, through the last 9 ka, the

timing of the Holocene monsoon maximum remains contentious. For instance, lacustrine records from SE China show that EASM was strong in the early part of the Holocene and weakened during the latter part of the Holocene (Wang et al., 2016), supporting the scenario indicated by the speleothem records (Wang et al., 2005; Dykoski et al., 2005). However, a well-dated quantitative precipitation reconstruction from an alpine lake in North China reveals a monsoon maximum in mid-Holocene, rather than in the early Holocene (Chen et al., 2015). The recorded ~4 ka delay in the response of the maximum monsoon intensity to the Northern Hemisphere summer insolation maximum challenges the prevailing view of Holocene monsoon evolution and suggests internal feedback processes in both high- and low-latitudes which have strong impacts on the monsoon system (Chen et al., 2015). In terms of the EAWM, its strength has been reconstructed using diatom assemblages (Wang et al., 2012) and Ti content of sediment (Yancheva et al., 2007) from maar lake in SE China. However, the two studies came to contradictory conclusions. The record based on diatom assemblages shows that EAWM shifted from strong to weak from the early to late Holocene, which is broadly in-phase with the EASM on orbital time scales (Wang et al., 2012). In contrast, the results from the other study indicate an anti-correlation between the EAWM and EASM during the last deglaciation and the Holocene (Yancheva et al., 2007).

In summary, though palaeoclimate records in East Asia provide important information of changes in the past, our understanding of the behaviour and dynamics of EAM is far away from comprehensive. It is thus very important to continue to search for reliable palaeoclimate records in the region, and to improve their chronologies as well as the ability of synchronising records. The latter is of particular importance for investigating rapid climate changes and testing leads and lags in climate archives.

1.1.3 East Asian tephrochronology

Active volcanic regions like East Asia, have significant potential for the development of an important tephra lattice due to the number and widespread dispersal of ash layers (Machida, 1999). Combined with the important role the region plays in understanding monsoon dynamics, East Asia is an ideal area for optimising the use of tephra isochrons to synchronise palaeoclimate records. Initial work such as Machida and Arai (1983) provided a sound basis for the investigation of tephra in this region.

Since then, tephrochronologists have been working on the construction of regional frameworks (e.g., Arai et al., 1986; Furuta et al., 1986; Machida, 1999; Machida and Arai, 2003; Moriwaki et al., 2016; Nakamura, 2016; Razzhigaeva et al., 2016). Meanwhile, long sedimentary cores have been increasingly utilized for distal tephra investigations, where multiple volcanic eruptions can be integrated into a single record (e.g., Aoki and Arai, 2000; Park et al., 2003; Nagahashi et al., 2004; Aoki et al., 2008; Okuno et al., 2011; Smith et al., 2013; Tsuji et al., 2018). For example, Machida (1999) summarised widespread late Quaternary tephra layers in and round Japan, which presented a tephrostratigraphic framework for East Asia during the past 1 Ma. The proposed framework includes twenty-six tephras, most of which originate from Japanese volcanoes (Machida, 1999). Arai et al (1986) systematically categorised marker tephras in northern Japan, which provides detailed information for tephra studies in the region. Recently, Nakamura (2016) and Razzhigaeva et al (2016) updated the glass chemistry of Holocene tephra layers in Hokkaido and Kuril Islands, respectively. A selection of widespread Holocene tephra markers in East Asia based on previous studies is shown in Fig. 1.1.

The outcome of the above-mentioned studies is important but has limitations, as they are based on the investigations of visible tephra layers. In contrast, recent cryptotephra work related to this region has made some significant breakthroughs. For example, tephras of East Asian provenance have been shown to have a very wide distribution (Sun et al., 2014; Bourn et al., 2016), connecting the region with the Greenland ice-core records. In addition, cryptotephra studies in continuous sequences from the region have been proven to provide more comprehensive eruptive records (e.g. Matsu'ura et al., 2017; McLean et al., 2018). These new findings provide substantial encouragement for further cryptotephra investigations in East Asia. In order to (a) expand the ash footprint of individual eruptions thus synchronise palaeoclimate records over greater geographical areas, and (b) identify previously unreported tephra isochrons, it is now essential that a more systematic approach to the application of cryptotephra studies is applied to lacustrine and marine records from the region.

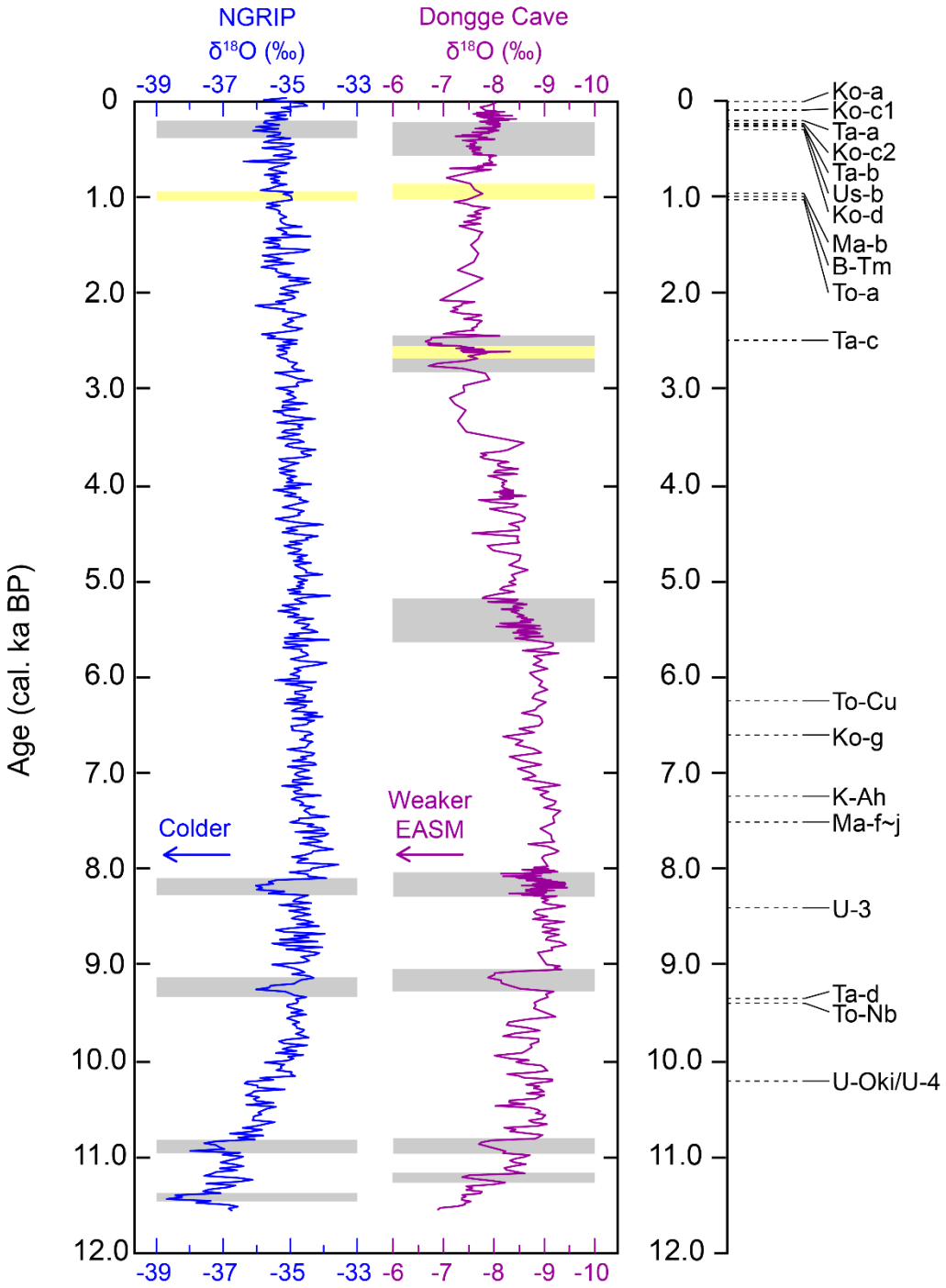

Fig. 1.1 A selection of widespread Holocene tephra markers in East Asia based on previous studies (e.g. Machida and Arai, 2003; Nakamura, 2016). The tephra layers were plotted using their ages (median values of age ranges), against the proxy records from Greenland (NGRIP members, 2004) and Chinese speleothem (Dykoski et al., 2005).

1.2 Regional settings

1.2.1 Distal site (Lake Kushu)

Rebun Island is situated in the northeastern part of the Sea of Japan, ca. 45 km west off the northern coast of Hokkaido (Fig. 1.2). The elongated-shaped island occupies an area of ca. 82 km^2, with its long axis (north-south) spanning about 20 km. Lake Kushu (45°25′55″N, 141°02′13″E, 4 m.a.s.l.) is a coastal freshwater lake located in the northern part of the island (Fig. 1.2). With a catchment area of ca. 10 km^2, the lake is fed by two inflows, the Oshonnai River from the south and a tiny stream from the east, and has one outlet connecting with the sea (Sato et al., 1998). About 300 m away from the coast, the lake is surrounded by dense vegetation, which effectively limits sediment in-washing to the lake, where sediment is made up primarily from autochthonous biological productivity, aeolian input and minor fluvial input (Schmidt et al., 2016).

Following a preliminary survey, sediment coring was undertaken in the central part of the lake when it was covered by a thick ice layer (February 2012; Müller et al., 2016). Two parallel sediment cores RK12-01 and RK12-02 were recovered using a hydro-pressure thin-walled piston corer. After the drilling campaign, the cores were transported to Hokkaido University and stored under cool temperature. In April 2012, the cores were opened by splitting each into two identical halves and the sediments were photographed, described, archived and sub-sampled for multi-proxy analyses. One set of subsampled core sections were sent to the Centre for Quaternary Research at Royal Holloway University of London for the tephra study presented here. A composite sequence was also shipped to the Institute of Geological Sciences at the Free University of Berlin where a range of proxy studies (e.g., pollen, diatom, geochemical analyses) were performed (Müller et al., 2016; Schmidt et al., 2016, 2019; Leipe et al., 2017, 2018).

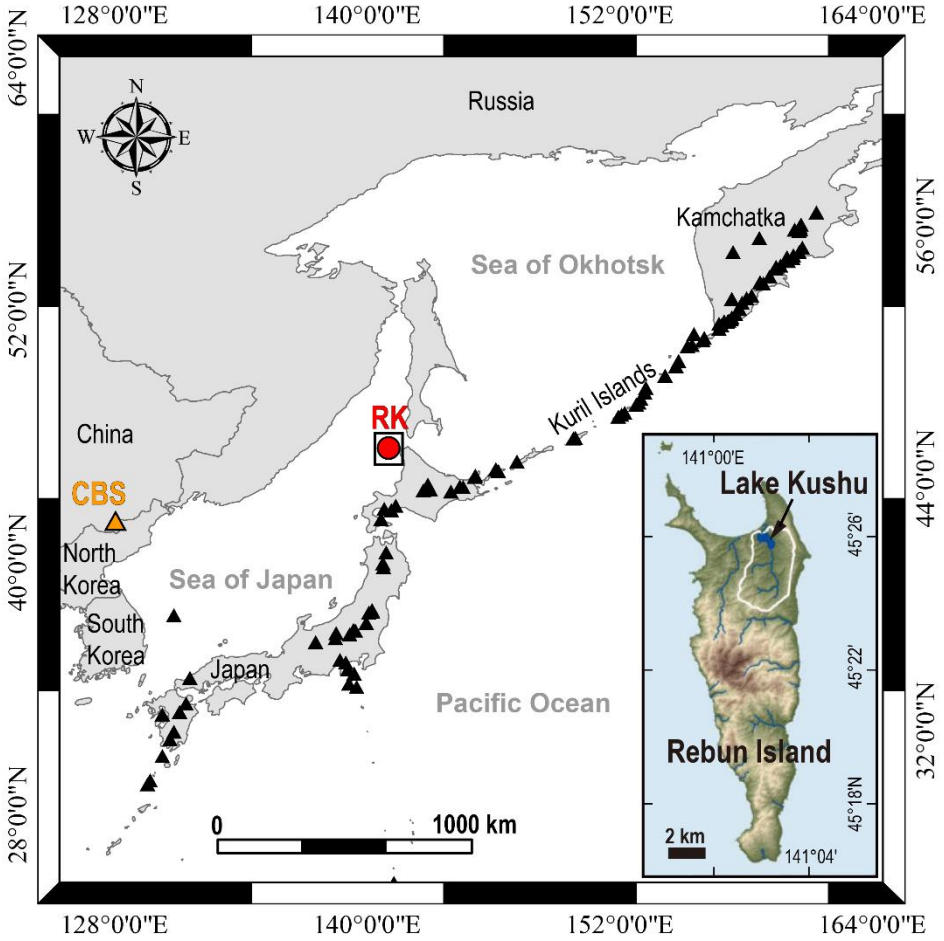

Fig. 1.2 Map of the East Asia region showing active volcanoes (triangle) and the location of Lake Kushu, Rebun Island (RK). The Changbaishan (CBS) volcano is highlighted in orange.

The composite RK12 sequence spans ca. 19.5 m long and is composed of continuous, partly laminated, organic-rich sediments (Fig. 1.3). A total of fifty-seven bulk 1 cm samples throughout the composite sequence were processed for AMS radiocarbon dating (Müller et al., 2016). The obtained results allow the construction of the RK12 age model (Fig. 1.3), which indicate the Holocene period spans the upper ca. 16.5 m sediment in composite sequence. The uppermost 50 cm sediment could not be recovered due to its unconsolidated state. As such this study focuses on core sediment between composite depth (CD) 50-1650 cm.

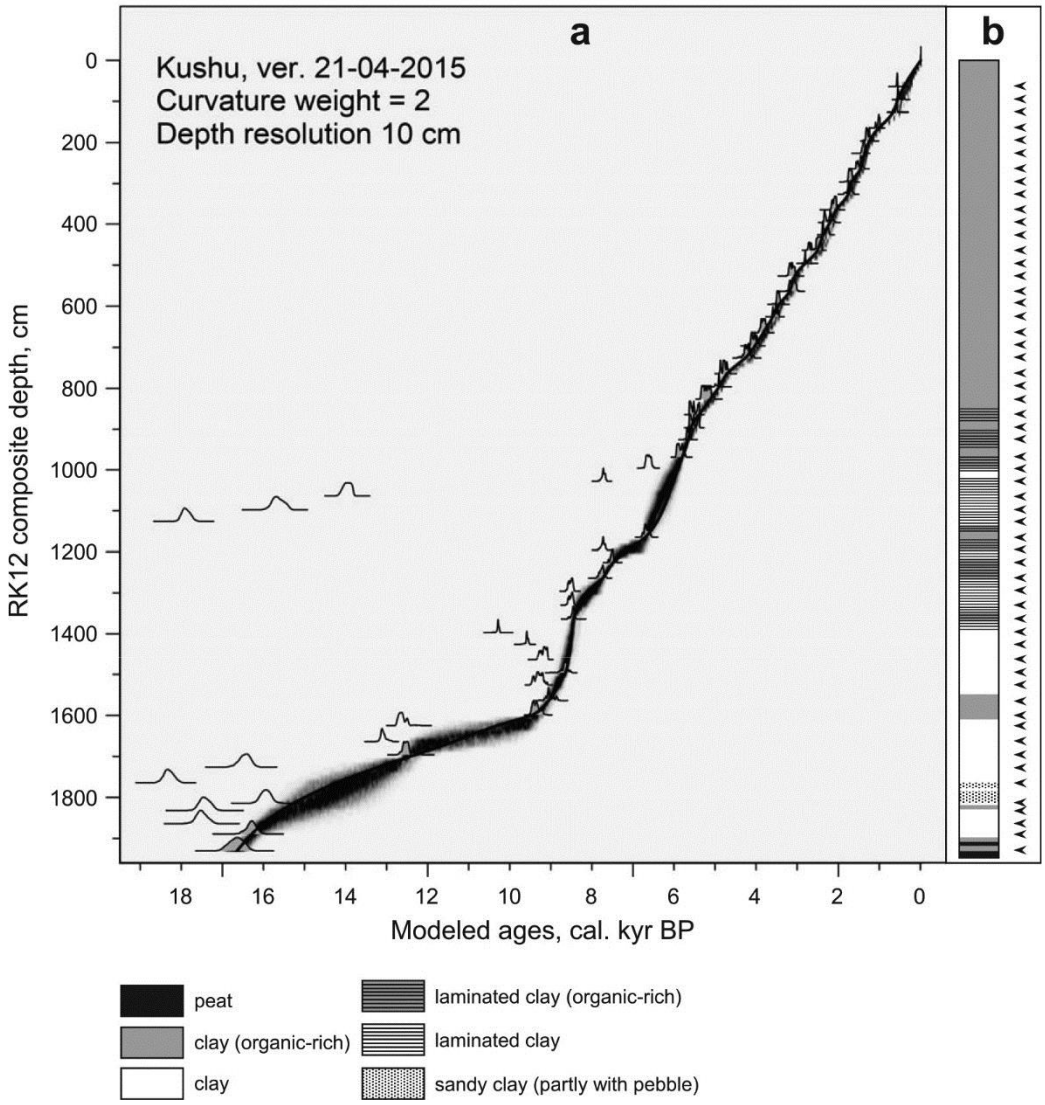

Fig. 1.3 (a) The age-depth model for the RK12 sediment core constructed using the free-shape algorithm based on 57 AMS radiocarbon dates (Müller et al., 2016), and (b) lithostratigraphy of the RK12 sediment core with radiocarbon samples marked in the corresponding depths (Müller et al., 2016).

The RK12 core from Lake Kushu is ideal for high-resolution cryptotephra investigations given that (a) the Holocene sediments span ca. 16.5 m and are well constrained by numerous radiocarbon ages (Müller et al., 2016), (b) the lake is not close to large active volcanic centres (Fig. 1.2) that would dominate the tephrostratigraphic record of the site and mask the cryptotephra record, (c) due to its positioning the Kushu sedimentary record provides a unique opportunity to understand more about ash dispersal reaching the northernmost regions of Japan and thus facilitate the construction

of an East Asia tephra lattice through providing an important northern element of the tephra lattice.

1.2.2 Proximal site (Changbaishan)

Changbaishan volcano is an intraplate stratovolcano on the border between China and North Korea, and ~1100 km SW of Lake Kushu (Fig. 1.2). The volcano is known for its Millennium Eruption (ME) that occurred at 946 CE (Xu et al., 2013; Sigl et al., 2015; Oppenheimer et al., 2017; Hakozaki et al., 2017) with tephra dispersed as far as Greenland (Sun et al., 2014a). Despite numerous studies having been carried out at the proximal sites (e.g., Wang et al., 2001; Yang et al., 2014; Ramos et al., 2016, Sun et al., 2017), the Holocene eruptive record is far from conclusive. This is largely due to

(a) the complexity of the proximal eruptive record due to resurgent activity & caldera collapse;
(b) inherent difficulties in dating proximal "young" (<50ka) volcanic rocks (e.g. Ramos et al., 2016),
(c) a focus on the ME deposits (see Sun et al., 2014b) to the detriment of younger & older eruptive deposits (see Wei et al., 2013).

The Holocene eruptive record of Changbaishan volcano is normally divided into three phases based on the prominent Millennium eruption: the younger post-Millennium activities, the ME and the older pre-Millennium activities (e.g. Wei et al., 2013; Sun et al., 2017).

Due to the ultra-young ages of the post-Millennium activities, these eruptions were largely inferred from historical records, and through geological mapping, assigned to some proximal deposits without the support of "in situ" dating. As such, they are not very reliable (Wei et al., 2013). Recent studies have revised the proximal ME stratigraphy to include deposits that were previously regarded as post-Millennium products via distal-proximal tephra correlations (Chen et al., 2016; Pan et al., 2017). More recently, Sun et al. (2017) has provided new dating results attempting to reliably constrain the post-Millennium deposits.

The profound Millennium eruption is continuously attracting attention, as on one hand, its precise eruptive age (i.e. 946 CE) is now cross-validated by ice-core chronology (Sigl et al., 2015) and ^{14}C spike-matching dendrochronology (Oppenheimer

et al., 2017; Hakozaki et al., 2017). On the other hand, its ash footprint (i.e. B-Tm) has been extended to cover a much larger geographic area than previously proposed (e.g. Machida, 1999). New localities include northeast China (Sun et al., 2015), Russian Far East (Razjigaeva et al., 2017), northern Japan (Chen et al., 2016), central Japan (McLean et al., 2016), and Greenland (Sun et al., 2014a). These recent developments permit the climatic event that is closely associated in time with the B-Tm tephra (i.e. Medieval Warm period, ca. 900-1300 CE) to be examined in detail for its climatic forcing and environmental responses across a vast distance.

As for the pre-Millennium activities, U-series, Ar-Ar and optically stimulated luminescence (OSL) methods have been applied to date the proximal eruptive products (e.g. Wang et al., 2001; Yang et al., 2014; Sun et al., 2017), however stratigraphic and chronological results vary from study to study. Recently, a distal study has reported that a previously unknown pre-Millennium tephra (i.e. SG14-1058) from Changbaishan was identified in Lake Suigetsu, central Japan, which highlights the importance of distal archives in resolving incomplete proximal eruptive histories (McLean et al., 2018).

1.3 Methodology

1.3.1 Cryptotephra extraction and identification

Preliminary tephra investigation on the RK12 core revealed that no visible tephra layer was recorded throughout the Holocene sequence, thus the core was analysed in detail for cryptotephra. Cryptotephra deposits were detected and extracted following the physical separation methods outlined by Blockley et al. (2005) (Fig. 1.4) with slight modifications. The RK12 Holocene sequence was first contiguously sub-sampled at a 10 or 20 cm resolution for range-finder scanning to determine tephra presence. If an elevated shard concentration was observed in the range-finder samples, the sediments were resampled at 1 or 2 cm resolutions for point sampling to locate the precise stratigraphic position of the cryptotephra. Sediments were first wet-sieved using 15 μm and 125 μm mesh. The 15-125 μm fraction was then separated using sodium polytungstate (SPT) prepared to specific densities. A cleaning float of 2.0 g/cm^3 was used, same as the one proposed by Blockley et al. (2005). An extraction float of 2.55 g/cm^3 that is slightly heavier than the density reported in Blockley et al. (2005), was adopted throughout the research following an updated protocol utilised at the

cryptotephra laboratory at Royal Holloway University of London. Blank samples were prepared alongside all the samples to monitor possible laboratory contamination. Each extracted sample was mounted on one or more slides and examined for tephra shards using a plane polarizing microscope. Tephra concentrations were measured by counts normalized to shards per gram dry sediment (shards/g). Individual shards of each cryptotephra were hand-picked from point-samples with the highest tephra counts and embedded in epoxy resin, which were then sectioned and polished for geochemical analysis.

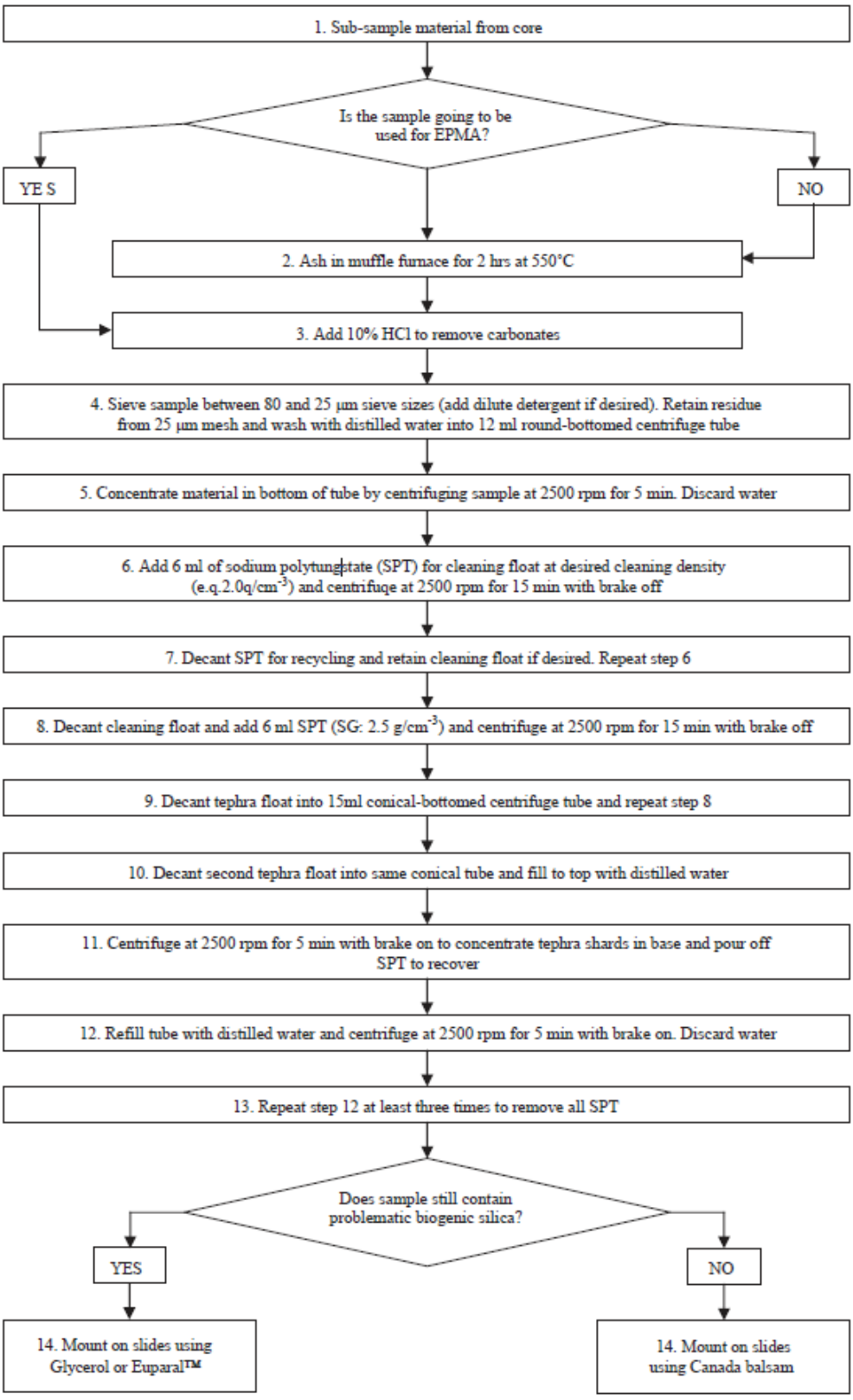

Fig. 1.4 Cryptotephra extraction procedures proposed by Blockley et al. (2005). Note that the method has been adopted in this study with two modifications: (1) a sieving size between 15-125 µm, and (2) a slightly heavier extraction float of 2.55 g/cm^3.

1.3.2 Analytical methods

Electron micro-probe analysis (EMPA)

Single-grain major and minor element concentrations were measured using wavelength-dispersive electron probe microanalysis (WDS-EPMA) at 1) the Research Laboratory for Archaeology and the History of Art, at the University of Oxford with a JEOL JXA-8600, and 2) the Grant Institute, School of Geosciences at the University of Edinburgh with a Cameca SX100. Spot sizes of 10, 5 and 3 µm were used depending on the size of the area available for analysis in different shards. Secondary glass standards were analysed in the same session in order to monitor instrumental accuracy and analytical precision. Detailed machine set-up for the electron probe JEOL JXA-8600 at Oxford see Kuehn et al. (2011) (lab#25), and for the Cameca SX100 at Edinburgh see Hayward (2011). Data were filtered to remove non-glass analyses, and those with analytical totals <93%. For comparative purposes, all data presented in text, table and plots were normalized to 100 wt % on a volatile-free basis.

Laser ablation inductively coupled plasma mass spectrometry (LA-ICP-MS)

Trace element analyses of glasses of proximal and distal tephras were performed using a Thermo Scientific iCAP Q ICP-MS coupled to an Analyte Excite excimer laser-ablation system at the Department of Geology, Trinity College Dublin. Spot sizes of 18, 24, 30 and 36 µm were used, depending on the size of the area available for analysis in different samples. The repetition rate was 5Hz and the count time was 40 s (200 pulses) on the sample and 40 s on the gas blank (background). The ablated sample was transported in He gas flow (0.65L/min) with additional N2 (5ml/min) via a signal smoothing device. Concentrations were calibrated using NIST612 with ^{29}Si as the internal standard. Data reduction was performed manually using Microsoft Excel that allowed removal of portions of the signal compromised by the microcryst, void or resin component. Full details of the analytical and data reduction methods are described in Tomlinson et al. (2010).

1.4 Aims and Objectives

The following chapters represent the bulk of the work undertaken as part of this PhD project at the Centre for Quaternary Research at Royal Holloway University of

London. The research focus is tephrochronology in East Asia, with the overall aims being to develop a Holocene tephrostratigraphy for the region and to explore its utility in palaeoclimate research. The achievement of the overall aims is through:

(1) A detailed investigation of proximal and distal tephras of the Changbaishan volcano China/N Korea which is one of the major volcanic centres that produced widespread tephra isochrons in the region, but has had limited study and has been the subject of only minimal cryptotephra investigation.

(2) A systematic search for cryptotephra horizons in a high resolution lacustrine record in northern Japan, which is a key study site for palaeoclimate research.

(3) A thorough review of widespread tephra isochrons in the region and an evaluation of how these tephras can be used for testing leads and lags in palaeoclimate archives.

These three objectives correspond to the three major components of this thesis:

First, a focus on tephrochronology using the Holocene tephrostratigraphy of Changbaishan volcano straddling the border between China and North Korea, and the uppermost sequence of a distal lake (Lake Kushu) in northern Japan. The main aim in Changbaishan was to use distal-proximal tephra correlations to resolve the proximal stratigraphy of the volcano. To date it has been problematic due to the inherent difficulty in dating ultra-young (< 1ka) volcanic rocks. The aim at Lake Kushu was to explore the potential of using high precision tephra ages to constrain the radiocarbon-based age model of the distal lacustrine record. The findings of this work are mainly reflected in Chapter 2.

Secondly, a detailed cryptotephra investigation was undertaken on an entire 16-m-long Holocene sequence of the Lake Kushu sedimentary record. In this study, the intention was to establish an integrated Holocene tephrostratigraphy for northern Japan. This would facilitate the construction of a master Holocene tephra framework for the East Asia. In the mean time the data can help test the capability of the cryptotephra technique in the identification of far-travelled tephras in a volcanically active region, as the method has been commonly employed in North Atlantic/Europe but not yet in East Asia. The findings of this work are mainly reflected in Chapter 3 and 4.

Thirdly, a thorough review was undertaken of tephra layers originating from or occurring in East Asia in order to establish criteria for selection of tephra isochrons. In this study, the intention was to propose an integrated Holocene tephra framework for future palaeoclimate research in the region. Furthermore, this was coupled with an evaluation of the chronostratigraphic relationships between these tephras and their associated climatic events and to discuss how these isochrons can be used to constrain regional variations of short-lived climate oscillations. The results of this work are mainly reflected in Chapter 5, taking the form of a review paper and serving as the discussion and critical evaluation of the thesis.

1.5 Thesis Outlines

The thesis consists of six chapters, including this introductory chapter and the studies mentioned above, as well as a concluding/summary chapter. They are entitled:

1. Introduction
2. Clarifying the distal to proximal tephrochronology of the Millennium (B-Tm) eruption, Changbaishan Volcano, northeast China
3. Developing a Holocene tephrostratigraphy for northern Japan using the sedimentary record from Lake Kushu, Rebun Island
4. Transhemispheric tephra dispersal: Krakatau tephra in northern Japan
5. An Integrated Holocene tephrostratigraphic framework for East Asia: implications for palaeoclimate research and future opportunities
6. Conclusions

The chapters are connected as part of a broader theme of understanding the full picture of East Asian tephrochronology, particularly those far-travelled tephra isochrons that could be used to facilitate the correlation of widespread palaeoclimate records, and are organised in such a manner that they build on one another, culminating in the conclusions presented in Chapter 5. Each chapter from chapter 2 to chapter 5 represents an independent study designed to be published as a peer-reviewed journal article. As a result, the chapters are similarly structured with their own introduction, methods, results, discussion and conclusion sections. References for all the chapters are combined into a single bibliography located at the end of the thesis.

Chapter 2, in full, is a reprint of the material as it appears in Quaternary Geochronology, vol. 33, 2016, doi.org/10.1016/j.quageo.2016.02.003. Authors include X.-Y. Chen, S. Blockley, P. Tarasov, Y.-G. Xu, D. McLean, E. Tomlinson, P. Albert, J.-Q. Liu, S. Müller, M. Wagner and M. Menzies. The thesis author was the lead author and corresponding author of this article.

Chapter 3, in part, is submitted for publication of the material. Authors include X.-Y. Chen, D. McLean, S. Blockley, P. Tarasov, Y.-G. Xu and M. Menzies. The thesis author was the primary investigator of the project and lead author of this manuscript.

Chapter 4, in part, is currently being prepared for submission for publication of the material. Authors include X.-Y. Chen, D. McLean, S. Blockley, P. Tarasov, Y.-G. Xu and M. Menzies. The thesis author was the primary investigator of the project and lead author of this manuscript.

Chapter 5, in part, is currently being prepared for submission for publication of the material. Authors include X.-Y. Chen, S. Blockley, Y.-G. Xu and M. Menzies. The thesis author was the primary investigator of the work and lead author of this manuscript.

Chapter 2: Clarifying the distal to proximal tephrochronology of the Millennium (B-Tm) eruption, Changbaishan Volcano, northeast China

2.1 Author List

Xuan-Yu Chen [a,b,c,d,*], Simon P.E. Blockley [b], Pavel E. Tarasov [e], Yi-Gang Xu [c], Danielle McLean [b,f], Emma L. Tomlinson [g], Paul G. Albert [f,h], Jia-Qi Liu [i], Stefanie Müller [e,j], Mayke Wagner [k] and Martin A. Menzies [a,c]

[a] Department of Earth Sciences, Royal Holloway University of London, Egham, Surrey TW20 0EX, UK

[b] Department of Geography, Royal Holloway University of London, Egham, Surrey TW20 0EX, UK

[c] State Key Laboratory of Isotope Geochemistry, Guangzhou Institute of Geochemistry, Chinese Academy of Sciences, Guangzhou 510640, China

[d] University of Chinese Academy of Sciences, Beijing 100049, China

[e] Institute of Geological Sciences, Palaeontology, Free University Berlin, Malteserstr. 74–100, Building D, 12249 Berlin, Germany

[f] Research Laboratory for Archaeology and the History of Art, University of Oxford, Oxford OX1 3QY, UK

[g] Department of Geology, Trinity College Dublin, Dublin 2, Ireland

[h] Department of Geography, Swansea University, Swansea SA2 8PP, UK

[i] Key Laboratory of Cenozoic Geology and Environment, Institute of Geology and Geophysics, Chinese Academy of Sciences, Beijing 100029, China

[j] Center for Ainu and Indigenous Studies, Hokkaido University, Kita 8, Nishi 6, Kita-ku, Sapporo 060-0808, Japan

[k] Eurasia Department and Beijing Branch Office, German Archaeological Institute, Im Dol 2–6, 14195 Berlin, Germany

2.2 Abstract

Tephra dispersed during the Millennium eruption (ME), Changbaishan Volcano, NE China provides one of the key stratigraphic links between Asia and Greenland for the synchronization of palaeoenvironmental records. However, controversy surrounds proximal-distal tephra correlations because (a) the proposed proximal correlatives of the distal ME tephra (i.e. B-Tm) lack an unequivocal chronostratigraphic context, and (b) the ME tephra deposits have not been chemically characterized for a full spectrum of element using grain-specific techniques. Here we present grain-specific glass chemistry, including for the first time, single grain trace element data, for a composite proximal sequence and a distal tephra from Lake Kushu, northern Japan (ca. 1100 km away from Changbaishan). We demonstrate a robust proximal-distal correlation and that the Kushu tephra is chemically associated with the ME/B-Tm. We propose that three of the proximal pyroclastic fall units were erupted as part of the ME. The radiocarbon chronology of the Kushu sedimentary record has been utilised to generate a Bayesian age-depth model, providing an age for the Kushu tephra which is consistent with high resolution ages determined for the eruption and therefore supports our geochemical correlation. Two further Bayesian age-depth models were independently constructed each incorporating one of two ice-core derived ages for the B-Tm tephra, providing Bayesian modelled ages of 933-949 and 944-947 cal AD (95.4%) for the Kushu tephra. The high-resolution ice-core tephra ages imported into the deposition models help test and ultimately constrain the radiocarbon chronology in this interval of the Lake Kushu sedimentary record. The observed geochemical diversity between proximal and distal ME tephra deposits clearly evidences the interaction of two compositionally distinct magma batches during this caldera forming eruption.

Keywords: Changbaishan; Millennium eruption; B-Tm tephra; Lake Kushu; Cryptotephra; Tephrochronology; Radiocarbon; Bayesian age modelling

2.3 Introduction

The Millennium eruption (ME) from the Changbaishan Volcano was a very large (VEI≈7) eruption with the potential for ash dispersal across the Northern Hemisphere. Whilst the eruption was estimated to have had substantial volatile and sulfate aerosol emissions (Horn and Schmincke, 2000; Guo et al., 2002), it lacked a global impact on climate (Xu et al., 2013; Sun et al., 2014a). Distal products of the ME (i.e. B-Tm) have been reported in many localities including the Sea of Japan, the Japanese Archipelago (Machida and Arai, 1983; Furuta et al., 1986; Machida et al., 1990; Fukusawa et al., 1998; Nanayama et al., 2003; Kamite et al., 2010; Okuno et al., 2011; Hughes et al., 2013), northeast China (Sun et al., 2015) and the Greenland ice cores (Sun et al., 2014a) (Fig. 2.1a). As such it provides one of the potential key stratigraphic links between Asia and Greenland for the synchronization of palaeoenvironmental records. The proposed correlations between the distal ME tephra deposits and the Changbaishan Volcano (Machida et al., 1990; Sun et al., 2014a; 2015) require detailed chronostratigraphic studies and geochemical analyses of the proximal deposits and distal records. However, the proximal correlatives reported therein lack chronostratigraphic context and the ME tephra units have not been chemically characterized for a full spectrum of element using grain-specific techniques. Here we present the results of geochemical investigations of tephra units from proximal deposits with chronostratigraphic context, and a distal archive from Japan. This is then used to re-evaluate the proximal deposits, distal correlatives and the overall chronology for this eruption.

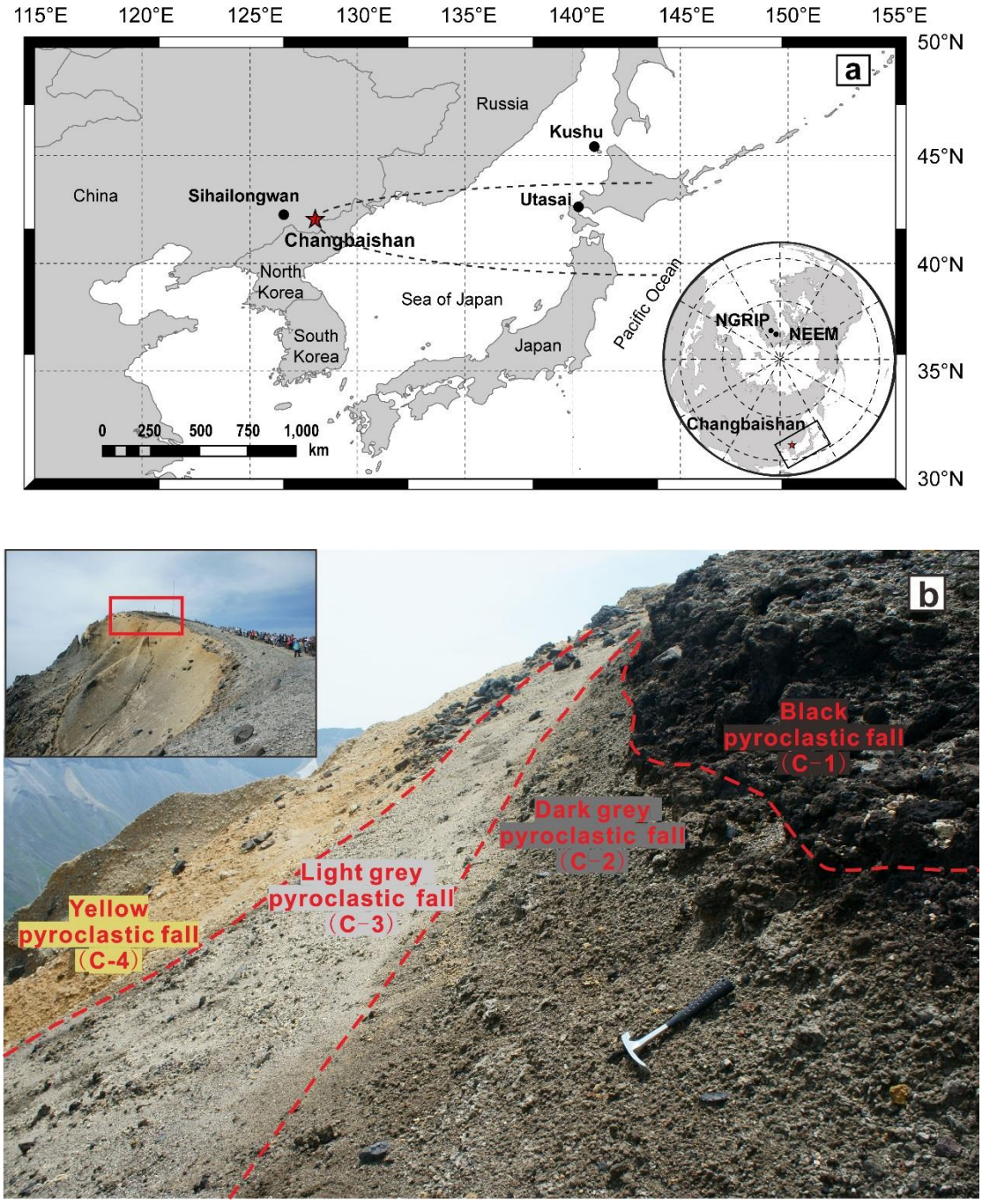

Fig. 2.1 (a) Location of the Changbaishan Volcano and the Lake Kushu distal archive on Rebun Island, northern Japan. The dashed line shows the previously reported distribution of B-Tm according to Machida and Arai (1983). Other occurrences of this tephra where the geochemical data used for comparison come from are marked on the map as well. (b) Sampled stratigraphy at the Tianwen summit on the Chinese flank of the Tianchi crater, Changbaishan Volcano, modified from Chen et al. (2014).

2.4 Background

2.4.1 Proximal volcanic deposits

The Changbaishan Volcano, situated on the border between China and North Korea (42°00' N, 128°03' E, Fig. 2.1a), is a polygenetic central stratovolcano with three main eruptive stages: early shield building, middle cone construction and a late explosive stage (Wei et al., 2007; 2013). During the latest explosive stage (<20ka: Wei et al., 2013), a major caldera-forming eruption occurring at ~AD 1000 (i.e. the "Millennium" eruption) produced a ca. 4.5 km wide caldera containing the crater lake called Tianchi (Machida et al., 1990).

The latest explosive stage recorded at Tianwen summit, on the Chinese flank of the crater contains four sequentially deposited pyroclastic fall units, C-4 [base], C-3, C-2 and C-1 [top], which are colored yellow, light grey, dark grey and black, respectively (Fig. 2.1b). Stratigraphic and chronological studies of the Tianwen summit profile are summarized in Figure 2.2. The lowermost C-4 yellow unit was dated by different methods and yielded ages around 4~5 ka (Liu et al., 1998; Wang et al., 2001; Yang et al., 2014). Hence, it was believed to be the product of an older pre-caldera forming eruption (Fig. 2.2). The overlying C-3 light grey unit is a very widespread pyroclastic fall which covers the crater rim and extends eastwards for more than 15 km from the crater (Horn and Schmincke, 2000; Sun et al., 2014b). At the Tianwen summit profile, this light grey unit has been dated at ~1 ka by U-series TIMS (Wang et al., 2001) and $^{40}Ar/^{39}Ar$ (Yang et al., 2014) methods. The same light grey-colored tephra was visually identified in the environs of the volcano where extensive radiocarbon dating studies of charcoal samples confirmed that it has an age consistent with the onset of the last millennium (e.g. Horn and Schmincke, 2000; Nakamura et al., 2007; Yatsuzuka et al., 2010; Yin et al., 2012; Xu et al., 2013; Table 2.1). Therefore, the C-3 unit was regarded as the product of the ME. However, there is considerable controversy regarding the stratigraphic and chronological significance of the overlying C-2 and C-1 units (Fig.

2.2). None of the previous studies reported a dark grey pyroclastic fall (here labelled C-2) overlying the C-3 light grey unit. Fan et al. (1999) described a light purplish red welded tuff unit with a post-ME age overlying the light grey unit. This cannot be correlated to our C-2 unit on the basis of their color and compositional discrepancies. Wang et al. (2001) mentioned two stratigraphically upper units without color description, whose age and compositional information did not help to clarify the stratigraphic correlation. The two more recent stratigraphic and chronological studies, Yu et al. (2012) and Yang et al. (2014), both failed to identify the dark grey unit sitting in between the light grey and the uppermost black units. For the C-1 black pyroclastic fall, no age has yet been conclusively confirmed. By reviewing the historical records of "abnormal natural phenomenon", Cui et al. (1995) proposed three possible dates (i.e. AD 1668, 1702 and 1903) for the post-caldera eruptions of the Changbaishan Volcano. Ji et al. (1999) used thermo-luminescence (TL) to date the K-feldspar from the black pumice (C-1) and reported an age of 0.34±0.03 ka. Based on these two pieces of evidence, Liu et al. (1999) concluded that the black unit (C-1) can be correlated to the AD 1668-1702 eruptive record. However, the "abnormal natural phenomenon" recorded by ancient people including "thunder" or "white ash rain" cannot be confidently and accurately attributed to a particular volcanic eruption. Moreover, the TL age from the black pumice cannot completely rule out the possibility that this C-1 unit could be an older eruptive, reset by a younger eruption. As such, the eruption age of the C-1 unit remains ambiguous and it could be either contemporaneous with the ME or post date the ME.

Table 2.1 Age results for the Millennium eruption from the dating of proximal and distal (B-Tm) tephra deposits.

Location	Method	Age	Ref.
Proximal			
Changbaishan environs (pyroclastic fall and flow deposits)	^{14}C wiggle-match dating	AD 940-952 (2σ)	Xu et al. (2013)
		AD 923-939 (2σ)	Yin et al. (2012)
		AD 945-960 (2σ)	Yatsuzuka et al. (2010)
		AD 930-943 (2σ)	Nakamura et al. (2007)
		AD 945-984 (2σ)	Horn and Schmincke (2000)
Tianwen summit (light grey fall)	^{40}Ar/^{39}Ar	1.24±0.51 ka	Yang et al. (2014)
	U-series TIMS	1.0±0.6 ka	Wang et al. (2001)
Distal			
Lake Kushu (Rebun, northern Japan)	Bayesian Modelling	AD 933-949 (2σ)	This study
		AD 944-947 (2σ)	
Greenland ice cores	Ice-core chronology	AD 946-947 (NS1-2011)	Sigl et al. (2015)
		AD 941±1 (GICC05)	Sun et al. (2014a)
		AD 945±4 (GISP2)	
Sihailongwan Maar Lake (NE China)	Varve chronology	AD 953±37	Sun et al. (2015)
	Conventional ^{14}C	AD 940-1020 (2σ)	
Lake Ni-no-Megata/ San-no-Megata (NE Japan)	Varve chronology	AD 929	Kamite et al. (2010)
Lake Ogawara (NE Japan)	Varve chronology	AD 937-938	Fukusawa et al. (1998)

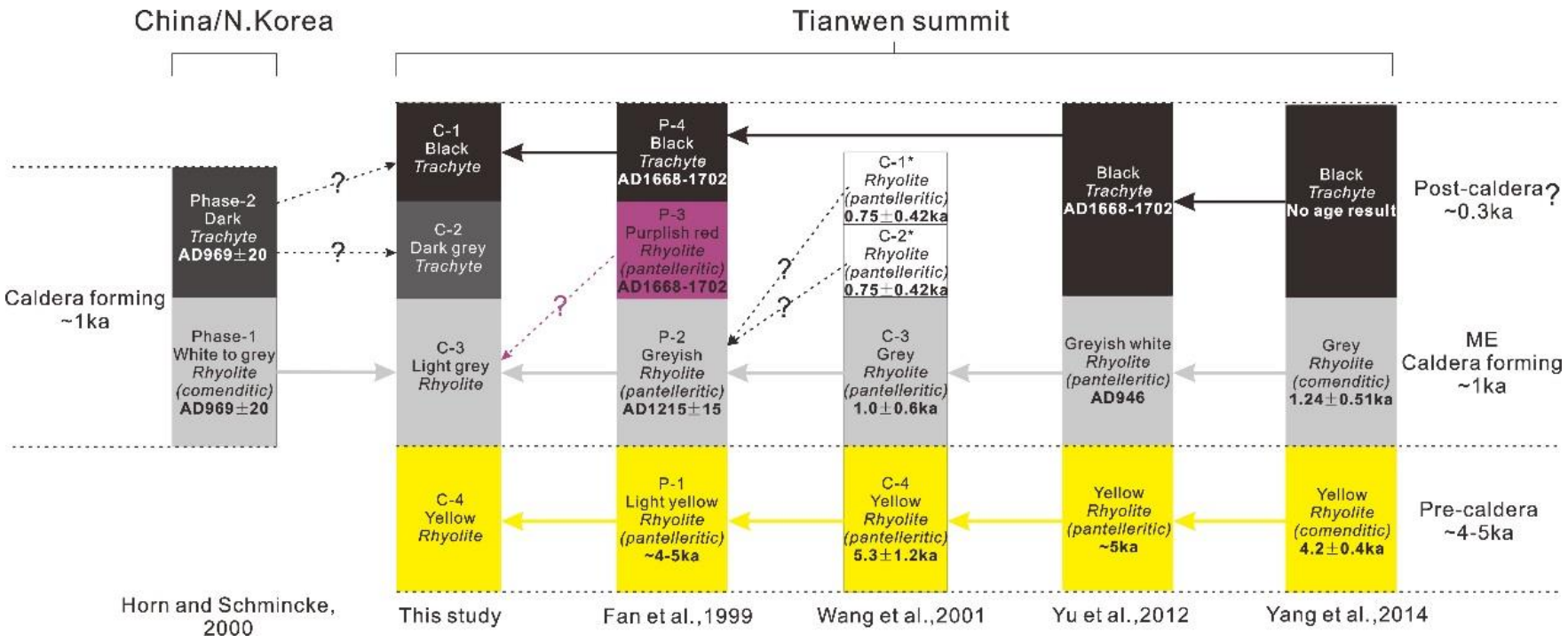

Fig. 2.2 Schematic illustration of previous stratigraphic and chronological studies of the Tianwen summit profile, Changbaishan Volcano. The solid arrows (black, grey, yellow) indicate correlations based on stratigraphy and the dashed arrows plus question mark indicate where correlations cannot be confirmed due to conflicting or inadequate stratigraphic information. Asterisks denote no color description of tephra units and a question mark denotes uncertainty about the nature of an eruptive deposit. This paper focuses on the three upper pyroclastic fall units above the yellow pumice (i.e. light grey, dark grey and black units).

Controversy also surrounds geochemical studies of the proximal ME stratigraphy on the crater rim. Fan et al. (1999) and Yu et al. (2012) suggested that, at Tianwen summit, only the light grey unit (i.e. C-3) is the ME product and that it can be classified as pantelleritic rhyolite based on bulk rock chemistry. However, Horn and Schmincke (2000) argued that the ME deposits should have included two phases: a major rhyolitic phase producing white to grey colored pumice, and a minor later phase forming trachytic agglutinates mantling the inner crater walls. Meanwhile, their electron microprobe glass data indicated that the widespread light grey pumice has a peralkalic composition akin to comendite rather than pantellerite. More recently, Sun et al. (2014a) reported major element glass chemistry for tephras sampled from the Korean side, indicating that the proximal ME deposits have bimodal compositions (i.e. trachyte and rhyolite). Although they described the outcrop containing white-yellow, grey and black pyroclastic fall, it is not easy to correlate this sequence to the Tianwen summit profile because no detailed stratigraphic context was provided.

2.4.2 Distal B-Tm records and the proximal correlatives

The B-Tm tephra, which was named after its source volcano Baegdusan (i.e. Changbaishan Volcano) and its type locality in Tomakomai, Hokkaido, was first reported to be found in the Sea of Japan and Hokkaido and the northern part of Honshu (Machida and Arai, 1983). It was suggested to be the distal equivalent of the ME on the basis of its composition and stratigraphic position (i.e. relative age), as well as petrographic features (Machida et al., 1990). Later on, the B-Tm tephra was reported in many localities across northeast Asia and in the Greenland ice cores (Furuta et al., 1986; Fukusawa et al., 1998; Nanayama et al., 2003; Kamite et al., 2010; Okuno et al., 2011; Hughes et al., 2013; Sun et al., 2014a; 2015). However, few of the above-mentioned studies have focused on the distal-proximal tephra correlation and the proposed proximal correlatives lack either independent dating to corroborate their “millennium” age (e.g. Machida et al., 1990) or unequivocal stratigraphic context (e.g. Sun et al., 2014a; 2015). As such hardly any clearly described outcrops have been reliably

confirmed as the proximal equivalent, which leaves the B-Tm tephra almost distally described only. Moreover, the identification, characterization and correlation of the B-Tm is typically based on major element glass chemistry. Whilst there are some effective major element discriminants that can be used to separate contemporaneous marker tephras (Sun et al., 2014a), one has to be careful because volcanoes can produce eruptions with similar compositions over a considerable time window (e.g. Smith et al., 2011a, 2011c; Lane et al., 2012b; MacLeod et al., 2015). Hence we highly recommend that a full spectrum of major, minor and trace elements should be applied when correlating tephras as this greatly increases the reliability of the resultant correlations. Since the abundances of trace elements are more sensitive to magmatic processes, they are widely used to secure tephra correlations (e.g. Allan et al., 2008; Smith et al., 2011a; Tomlinson et al., 2012; Lane et al., 2012b; Albert et al., 2012; 2013; Tomlinson et al., 2014; Albert et al., 2015; Tomlinson et al., 2015; Lane et al., 2015).

2.5 Sampling

2.5.1 Changbaishan tephra

Proximal fall lapilli samples from the C-1, C-2 and C-3 units were collected at the Tianwen summit (42°01’33” N, 128°04’00” E) under tight stratigraphic control. Sub-samples of the light grey pumice from Yang et al. (2014) are included in our C-3 sample set as they were collected from the same profile and the same unit, and were dated by $^{40}Ar/^{39}Ar$ to corroborate the millennium age. Lapilli sized samples were crushed, cleaned, dried and clean fragments were examined and picked under the microscope then mounted in epoxy resin for geochemical micro-beam analysis. The samples from these three fall units contain alkali feldspar as the dominant phenocryst phase, with some minor contributions of olivine, pyroxene and quartz. The C-1 unit contains the highest percentage of phenocryst among all the three units. SEM images were taken to reveal the vesicularity and the location of phenocrysts prior to micro-beam analysis (Fig. 2.3). SEM images show that the C-3 pumice samples are made up of both highly

vesiculated and less vesiculated glasses (Fig. 2.3a-b), with some highly vesiculated glasses being very stretched (Fig. 2.3a). The vesicularity of the C-3 sample was estimated to be ~60% (Yu et al., 2012). The C-2 pumice samples contain highly vesiculated glasses (Fig. 2.3c) and have a similar level of vesicularity with the C-3 samples. The C-1 pumice samples mainly contain poorly vesiculated glasses (Fig. 2.3d), with the mount of vesicles decreasing significantly relative to the C-2 and C-3 samples. The vesicularity of C-1 sample was estimated to be less than 50% (Yu et al., 2012), which is consistent with the observation that the C-1 samples are slightly welded whereas the C-2 and C-3 samples are not.

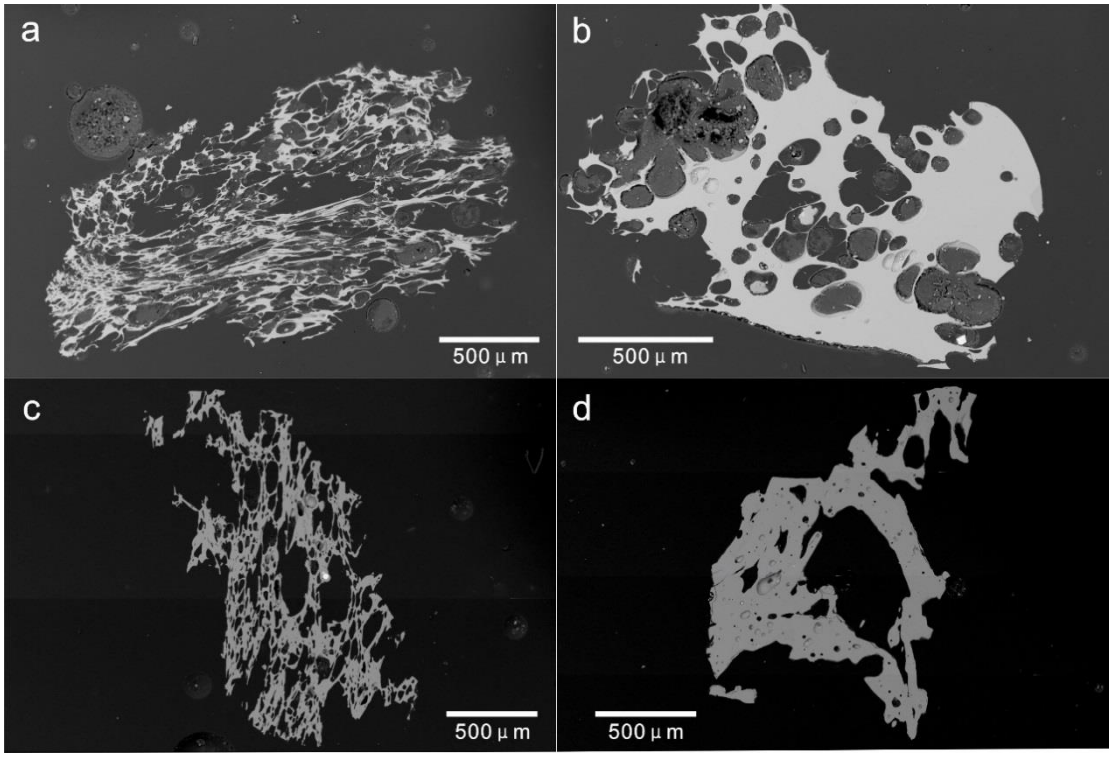

Fig. 2.3 SEM images of the proximal Changbaishan tephras. (a-b) the C-3 light grey pumice, both highly vesiculated and less vesiculated glasses with some highly vesiculated glasses being strongly stretched; (c) the C-2 dark grey pumice, vesicular and stretched glasses; (d) the C-1 black pumice samples that have the highest content of phenocryst and the least vesicularity among all the three proximal fall units.

2.5.2 Lake Kushu tephra

Lake Kushu (45°25’55” N, 141°02’13” E), ca. 1100 km away from the Changbaishan Volcano, is the only fresh-water lake of Rebun Island in the Sea of Japan, northwest off Hokkaido (Fig. 2.1a). Located in the northern part of the island, about 230-400 m from the coast, the lake has a kidney bean shape and a maximum length of ca. 1100 m. The maximum water depth reaches ca. 6 m in the eastern part of the lake with average depths of about 3 to 5 m. The bottom sediment of Lake Kushu has been considered as a valuable natural archive which stores detailed, high-resolution information about post-glacial environmental changes (Kumano et al., 1990). Therefore, Lake Kushu has been selected as one of the key study sites in the Baikal-Hokkaido Archaeology Project (BHAP), aiming to fill the existing gap in the current knowledge and to address the role of climate and environmental change in the life of northern hunter-gatherers (Weber et al., 2013). In February 2012, two parallel sediment cores (RK12-01 and RK12-02) were collected in the central part of the lake from the thick ice cover. The recovered composite core (RK12) revealed a continuous, partly laminated, organic-rich ca. 19.5 m long sediment column. The RK12 core age model built upon the 57 calibrated AMS radiocarbon dates suggests that the sedimentation continued over the past ca. 17,000 years (Müller et al., 2016).

This lake was also selected for visible tephra and crypto-tephra analyses due to the potential for tephras to be located from Japanese, Korean and Chinese volcanoes, and coupled with the high precision radiocarbon chronology and palaeoenvironmental record. The tephra study covered the entire core archive, although here we focus only on the tephra of approximate millennium age, based on the radiocarbon chronology. A detailed tephrochronological study of the whole core is currently in preparation (Chen et al., in progress). Distal tephras were separated using procedures outlined by Blockley et al. (2005). The extracted glass shards were mounted in Canada Balsam on glass slides and examined using an Olympus CX-41 microscope fitted with cross-polarising filters. In order to identify the location of each discrete tephra layer, two steps of sub-sampling

on the core materials were carried out. In the first scanning phase, 20 cm sampling interval was used to produce the range-finder counts that revealed the quantitative distribution of shards per gram of dry sediment for the complete composite core. A detailed analysis phase termed point-sample count, with 1 or 2 cm sampling interval, was undertaken later to locate the precise depth of the tephra where range-finders showed high concentration of glass shards. The point-sample counts relative to this research clearly show that the initial onset of the tephra input appears at the composite depth of 152-151 cm whilst the peak of it sits at 151-150 cm (Fig. 2.4). No visible ash layer was identified at these depths during core opening and sediment description though the tephra counts show quite large numbers. Individual shards (Fig. 2.5) were picked in the interval of 150-152 cm and embedded in resin, sectioned and polished ready for geochemical analysis.

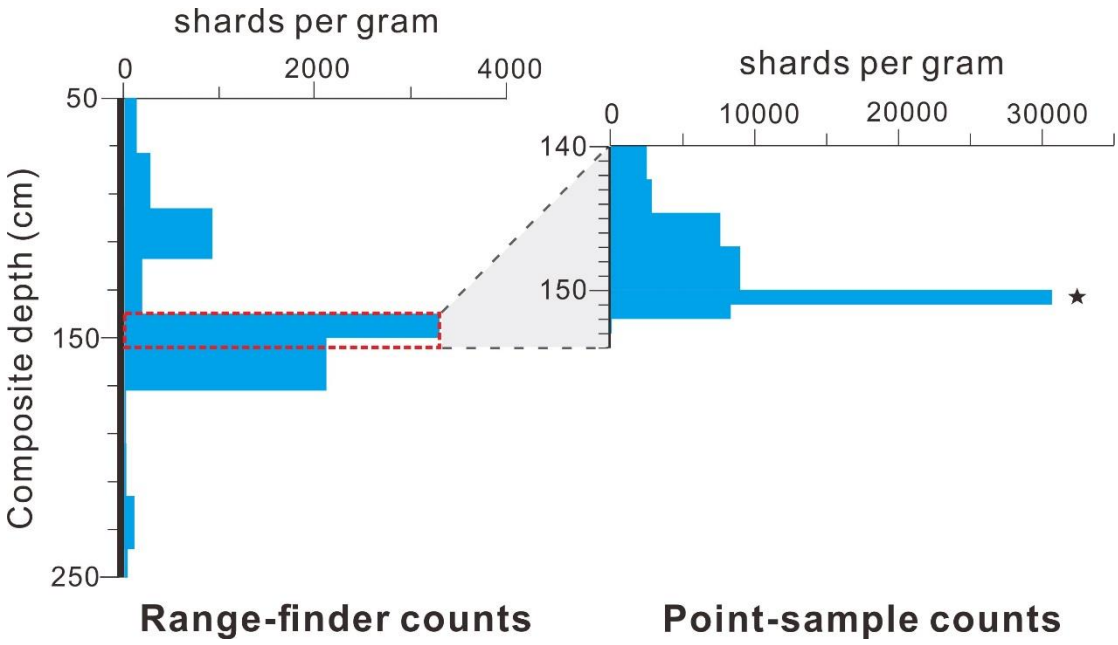

Fig. 2.4 Tephra shard concentrations measured in sediments in the top 2 meters of samples from Lake Kushu. Shard counts are given as numbers of shards per gram of dry sediment. The star marks the peak of the tephra input.

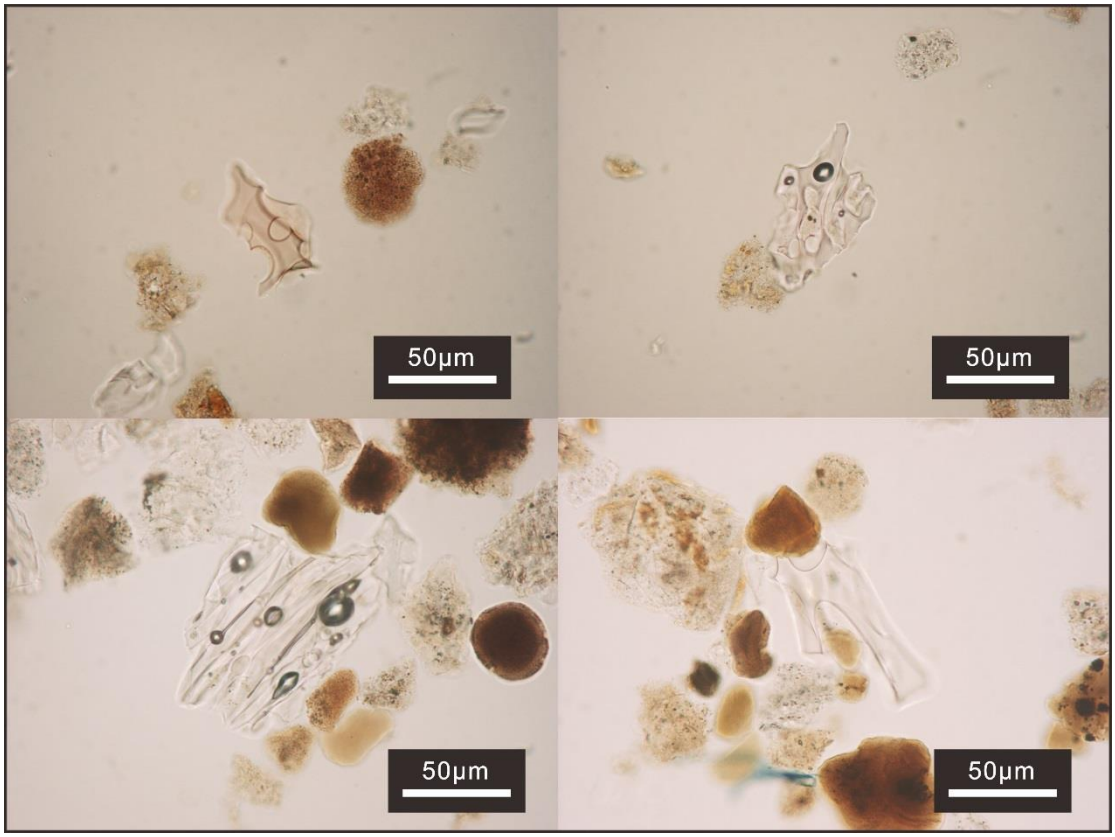

Fig. 2.5 Light microscope photographs of tephra shards extracted from Lake Kushu sediments at 150-152 cm composite depth.

2.6 Analytical methods

2.6.1 Electron micro-probe analysis (EMPA)

Major and minor element concentrations of glasses of proximal pumices and distal tephra shards were determined using Jeol JXA-8600 wavelength-dispersive electron microprobe (WDS-EMPA), equipped with 4 spectrometers and SamX software, at the Research Laboratory for Archaeology and the History of Art, University of Oxford. An accelerating voltage of 15 kV, low beam current (6 nA), and defocused (10 µm) beam were used to minimize Na migration. Count times were 30 s for Si, Al, Mg, Ti, Ca, K and Fe on each peak. Na was analysed for 12 s, Cl and Mn for 50 s and P for 60 s on each peak. The instrument was calibrated for each set of beam conditions using a suite

of appropriate mineral standards. The calibration was verified using a range of secondary glass standards (MPI-DING suite) including the ATHO-G (rhyolite), StHs6/80-G (andesite) and GOR132-G (komatiite) glasses from the Max Planck Institute (Jochum et al., 2006). Samples with analytical totals <94% were discarded. All the analyses presented in the text, plots and tables are normalised to 100 wt.% for comparative purposes. Analytical precision is typically <0.8% relative standard deviation (RSD) for Si; <5% RSD for analytes with concentrations >0.8 wt.% with the exception of Na (7-10%). All standard data is presented in the supplementary material.

2.6.2 Laser ablation inductively coupled plasma mass spectrometry (LA-ICP-MS)

Trace element analyses of glasses of proximal and distal tephras were performed using a Thermo Scientific iCAP Q ICP-MS coupled to an Analyte Excite excimer laser-ablation system at the Department of Geology, Trinity College Dublin. Spot sizes of 18, 24, 30 and 36 µm were used, depending on the size of the area available for analysis in different samples. The repetition rate was 5Hz and the count time was 40 s (200 pulses) on the sample and 40 s on the gas blank (background). The ablated sample was transported in He gas flow ($0.65 L min^{-1}$) with additional N_2 ($5 ml min^{-1}$) via a signal smoothing device. Concentrations were calibrated using NIST612 with ^{29}Si as the internal standard. Data reduction was performed manually using Microsoft Excel that allowed removal of portions of the signal compromised by the microcryst, void or resin component. Full details of the analytical and data reduction methods are described in Tomlinson et al. (2010). Accuracies of ATHO-G and StHs6/80-G MPI-DING glass analyses are typically <5% for most elements, <10% for Y, Zr, Nb, Gd and <15% for Ta. Reproducibility of ATHO-G analyses is <5% RSD for all trace elements with the exception of U (<7%).

2.7 Results

Glasses from juvenile clasts found in both proximal and distal deposits have compositions ranging from trachyte to rhyolite, with the rhyolitic population straddling the alkaline-subalkaline boundary (Fig. 2.6a). On a molecular basis, all the rhyolitic glasses and the majority of trachytic glasses reported herein have $(Na_2O+K_2O)>Al_2O_3$, whereas only few trachytic glasses show subtle $(Na_2O+K_2O)\leq Al_2O_3$. By definition, they are peralkaline trachyte and rhyolite. According to the classificatory scheme for peralkaline extrusive rocks (MacDonald, 1974), they can be further classified as comenditic trachyte and comendite, respectively (Fig. 2.6b). Representative major, minor and trace element glass compositions of proximal pumices and distal shards are given in Table 2.2. The full geochemical data sets are presented in the supplementary material.

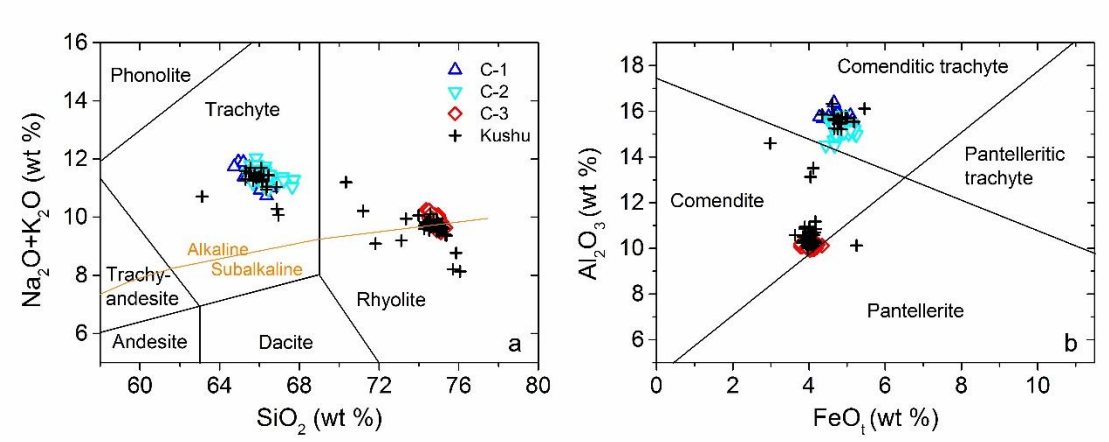

Fig. 2.6 (a) TAS classification (Le Bas et al., 1986) diagram showing the glass compositions of proximal fall deposits (i.e. C-1, C-2 and C-3) and distal Kushu tephra. The boundary separating the alkaline and subalkaline series is from Irvine and Baragar (1971). (b) Classificatory diagram for peralkaline extrusive rocks (MacDonald, 1974) showing the glasses compositions of the peralkaline proximal and distal tephras.

Table 2.2 Representative major, minor and trace element data for glasses from proximal volcanic deposits at Tianwen summit and distal Kushu tephra. Full geochemical data sets are available in the Supplementary material file.

Locality	Tianwen summit							Lake Kushu					
Unit/group	C-3			C-2		C-1		Rhyolite			Trachyte		
Sample	10CB-2-1	14-1-1	14-1-4	14-5-1	14-5-9	14-4-1	14-4-5	RH490-20	RH555-33	RH554-37	RH555-30	RH554-6	Rh554-8
Material	Pumice							Tephra shard					
Major elements wt.%													
SiO_2	74.98	74.73	74.93	66.06	66.42	66.08	66.24	74.90	74.97	70.34	66.15	66.12	66.20
TiO_2	0.21	0.23	0.19	0.41	0.52	0.45	0.44	0.24	0.20	0.30	0.48	0.48	0.42
Al_2O_3	10.06	10.15	10.23	15.37	15.26	15.69	15.09	10.58	10.36	14.60	15.49	15.66	15.86
FeO_t	4.15	4.23	4.08	4.96	4.91	4.37	4.92	3.92	4.13	2.98	4.81	4.64	4.35
MnO	0.13	0.10	0.02	0.13	0.12	0.08	0.20	0.10	0.08	0.09	0.17	0.16	0.12
MgO	0.00	0.04	0.00	0.19	0.17	0.22	0.17	0.00	0.00	0.00	0.23	0.18	0.17
CaO	0.20	0.16	0.21	1.25	1.30	1.25	1.23	0.23	0.23	0.19	1.25	1.26	1.26
Na_2O	5.12	5.45	5.26	5.68	5.54	6.06	5.90	5.27	5.25	6.05	5.45	5.67	5.81
K_2O	4.51	4.27	4.50	5.76	5.57	5.58	5.65	4.26	4.30	5.16	5.76	5.62	5.63
P_2O_5	0.01	0.02	0.00	0.04	0.06	0.09	0.04	0.00	0.00	0.03	0.06	0.07	0.05
Cl	0.63	0.62	0.57	0.15	0.13	0.14	0.12	0.51	0.48	0.25	0.15	0.14	0.13
Analytical total	98.02	99.61	98.08	99.29	98.47	98.13	99.89	97.02	97.97	98.60	98.98	98.26	99.19
K_2O+Na_2O	9.63	9.72	9.76	11.44	11.11	11.64	11.55	9.53	9.55	11.21	11.21	11.29	11.44
Trace elements ppm													
Rb	419	426	428	153	157	143	143	417	403	308	143	157	150
Sr	2.7	3.0	6.1	6.3	5.9	8.4	6.8	2.8	2.7	2.7	6.6	10.6	8.6
Y	125	143	156	43	43	37	42	144	130	66	37	48	38
Zr	2152	2377	2305	655	682	564	653	2395	2252	1260	589	792	585
Nb	280	302	299	93	95	79	88	303	286	195	84	107	87
Ba	7.7	9.1	9.9	19.2	17.6	28.6	19.9	8.5	9.7	10.8	19.9	31.0	30.1
La	135	152	173	89	92	77	87	163	148	127	82	101	79
Ce	288	316	336	175	175	154	170	328	307	246	159	197	155

Pr	31.8	35.4	39.6	19.0	19.1	16.5	18.3	34.7	33.2	23.6	17.2	20.6	17.7
Nd	118	130	149	71	71	62	69	136	123	78	63	77	61
Sm	26.0	29.3	32.2	13.4	14.3	11.7	13.0	31.6	26.6	16.5	12.1	14.3	13.1
Eu	<LOD	0.4	<LOD	<LOD	<LOD	0.4	0.4	0.4	<LOD	<LOD	<LOD	<LOD	<LOD
Gd	23.9	27.2	29.3	10.3	10.5	9.6	10.1	27.4	23.0	13.3	9.3	11.4	9.1
Dy	23.3	28.2	29.7	9.1	9.3	7.8	8.7	25.9	24.0	12.6	7.7	9.7	8.0
Er	12.9	14.4	15.0	4.6	4.5	3.8	4.2	13.7	11.9	7.3	4.1	5.0	4.0
Yb	10.7	12.7	12.9	4.0	4.1	3.5	4.0	11.9	10.7	5.9	3.5	4.9	3.6
Hf	52.2	60.9	56.7	16.2	16.2	13.2	15.1	58.1	51.3	30.3	13.9	18.2	13.9
Ta	15.9	17.1	17.0	4.7	4.8	4.0	4.5	15.4	14.3	9.7	4.0	5.4	4.1
Th	48.9	56.8	52.4	15.1	15.2	12.4	14.5	52.9	46.1	30.1	12.9	17.7	13.4
U	11.4	12.7	12.8	3.4	3.4	2.8	3.0	11.5	10.7	7.0	2.7	3.7	3.0

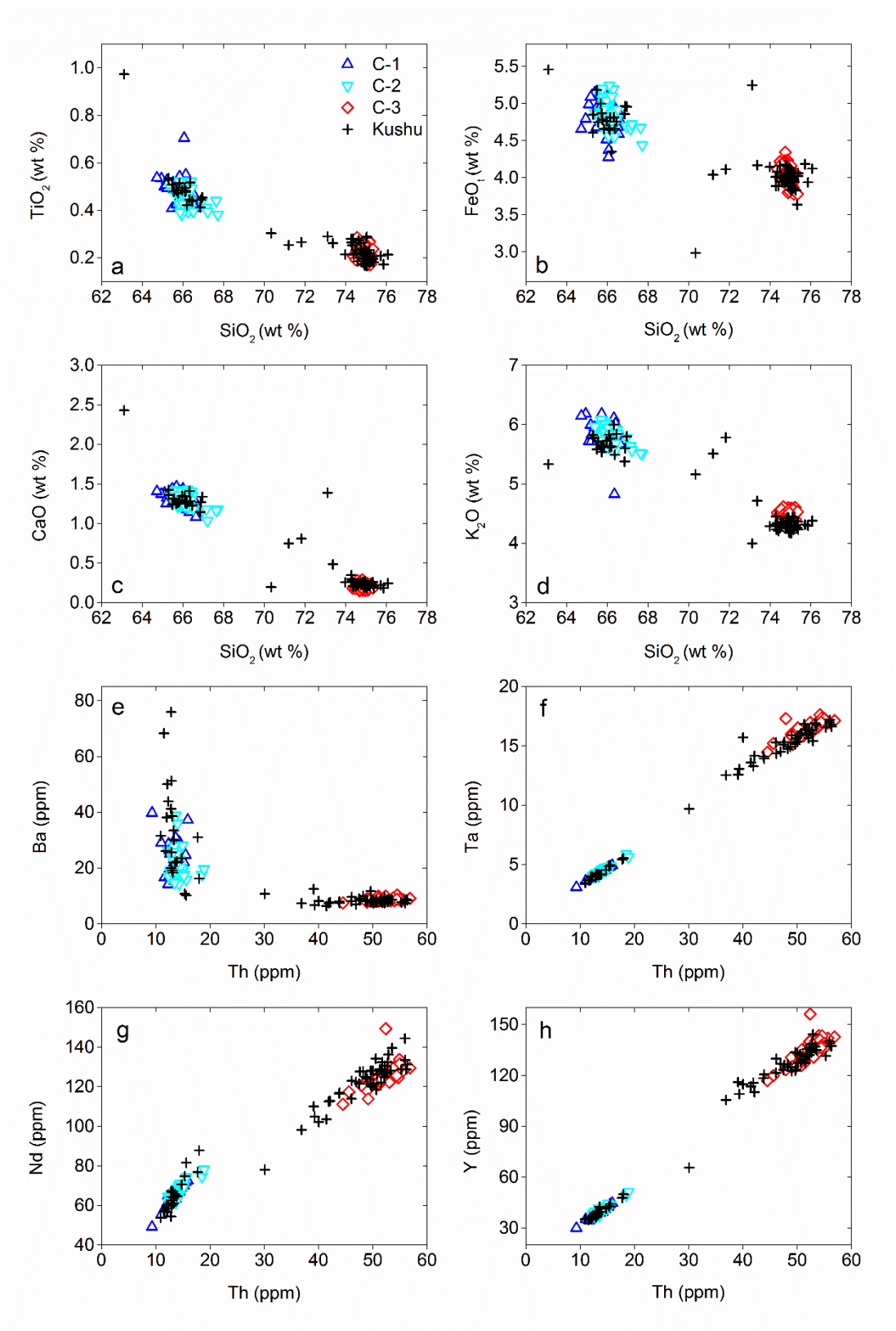

Fig. 2.7 Major and trace element variation diagrams showing the glass compositions of proximal fall deposits and distal Kushu tephra.

2.7.1 Glass chemistry of proximal deposits

The uppermost C-1 fall unit at Tianwen summit has a comenditic trachyte glass composition (Fig. 2.6b). The glasses are characterized by low CaO (1.1-1.5 wt.%) and MgO (0.1-0.3 wt.%), high K_2O (4.8-6.2 wt.%) and significantly high FeO_t (4.3-5.1 wt.%) with homogeneous SiO_2 (64.7-66.6 wt.%; Fig. 2.7a-d). They show an overall trend of decreasing total alkalis with increasing SiO_2 (Fig. 2.6a). Trace element data reveal that these glasses have limited compositional variations with 9-16 ppm Th, 14-40 ppm Ba, 3-5 ppm Ta, 49-73 ppm Nd and 30-45 ppm Y. They form compositional clusters in most of the trace element bi-plots (Fig. 2.7f-h). C-1 glasses have light rare earth element (LREE) enrichment relative to the heavy rare earth element (HREE) with La/Yb ratios ranging from 21 to 25. Mantle-normalised spider diagram reveals that C-1 glasses are up to more than 200 times more enriched than the primitive mantle (Fig. 2.8). They are characterized by pronounced negative anomalies in Ba, Sr and Eu in response to the fractionation of K-feldspar, which is a dominant phenocryst phase in the juvenile clasts.

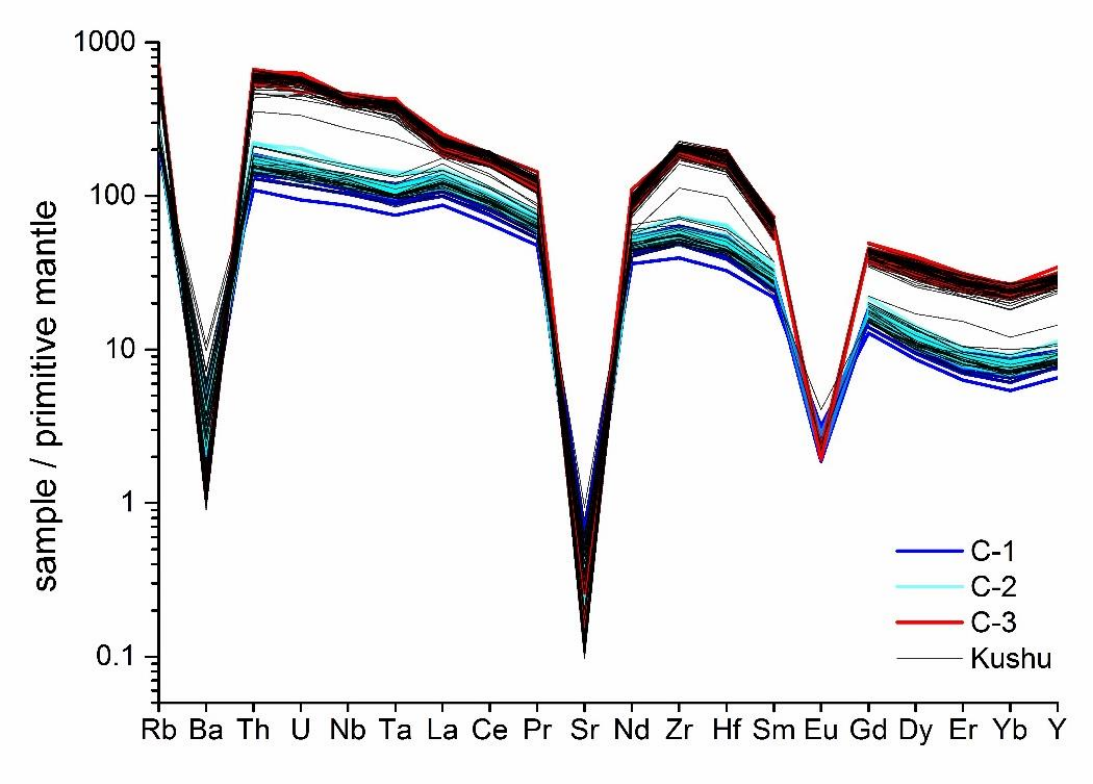

Fig. 2.8 Primitive mantle normalized trace element compositions of glasses from proximal fall deposits and distal Kushu tephra. Primitive mantle values are from Sun and McDonough (1989).

There is significant overlap in glass compositions of the C-2 fall unit and the overlaying C-1 unit. The C-2 glasses are also classified as comenditic trachyte (Fig. 2.6b). They extend to slightly more evolved SiO_2 (65.4-67.7 wt.%), have less variable K_2O (5.5-6.1 wt.%), comparable CaO (1.0-1.4 wt.%), FeO_t (4.4-5.2 wt.%) and MgO (0.1-0.3 wt.%) relative to those of the C-1 glasses (Fig. 2.7a-d). The compositional similarity between the two units can also be seen in the trace element data. C-2 glasses show trace element concentrations of 12-19 ppm Th, 14-39 ppm Ba, 4-6 ppm Ta, 61-78 ppm Nd, and 36-51 ppm Y, which form almost identical compositional clusters overlapping the C-1 glasses (Fig. 2.7e-h). Mantle-normalised spider diagram reveals that the multi-element profiles of C-2 glasses have similar distribution pattern and incompatible element enrichment level with those of the C-1 glasses (Fig. 2.8).

Nevertheless, some subtle differences in composition can be observed: (1) C-1 glasses have some least evolved components that are not seen in C-2 deposits (e.g. lower SiO_2 content and lower incompatible element enrichment level; Figs. 2.6a, 2.8); (2) C-2 glasses extend to more evolved compositions than C-1 glasses (e.g. higher SiO_2 content and higher incompatible element enrichment level; Figs. 2.6a, 2.8).

Glasses of the lower C-3 fall unit have a composition straddling the boundary between alkaline and subalkaline rhyolite (Fig. 2.6a) and can be specifically classified as comendite (Fig. 2.6b). C-3 glasses are highly homogeneous with restricted major element compositional ranges. They have concentrations of highly evolved SiO_2 (74.4-75.3 wt.%) with lower CaO (0.1-0.3 wt.%), MgO (<0.1 wt.%), K_2O (4.3-4.6 wt.%) and FeO_t (3.8-4.3 wt.%) than those of the overlying trachytic units (i.e. C-1 and C-2; Fig. 2.7a-d). Trace element concentration data for C-3 glasses form linear clusters in element bi-plots (Fig. 2.7e-h). They have higher contents of Th (44-57 ppm), Ta (14-18 ppm), Nd (111-149 ppm), Y (117-156 ppm) and lower Ba (7-10 ppm) relative to the upper trachyte units (Fig. 2.7e-h). C-3 glasses show LREE enrichment relative to the HREE with a lower LREE/HREE fractionation level (La/Yb=11-13) than those of the trachytic glasses. Mantle-normalised spider diagram shows that the C-3 glasses are up to more than 600 times more enriched than the primitive mantle, with more pronounced depletions in Ba, Sr and Eu relative to the trachytic units (Fig. 2.8). It is worth noting that, in their multi-element profiles, the trachytic glasses and the C-3 rhyolitic glasses show different trends in anomalies of Nb-Ta (Fig. 2.8).

2.7.2 Glass chemistry of distal tephra

The distal tephra found in Lake Kushu shows significant heterogeneity with compositions ranging from trachyte to rhyolite (Fig. 2.6a). This can be further classified as comenditic trachyte and comendite respectively (Fig. 2.6b). The less evolved trachytic components are characterized by relatively homogeneous SiO_2 (typically between 65.3-67.0 wt.%), low CaO (typically between 1.1-1.4 wt.%) and MgO (typically between 0.1-0.3 wt.%), high K_2O (5.3-6.0 wt.%) and FeO_t (4.4-5.5 wt.%),

while the more evolved rhyolitic shards have heterogeneous SiO_2 (70.3-76.1 wt.%), lower CaO (typically <0.8 wt.%), MgO (<0.1 wt.%), K_2O (typically <4.7 wt.%) and FeO_t (typically < 4.2wt.%; Fig. 2.7a-d). The two populations collectively show an overall trend of decreasing TiO_2, CaO, MgO, FeO_t and K_2O (Fig. 2.7a-d) with increasing SiO_2, while the Na_2O contents between the trachyte and rhyolite remain fairly constant (4.3-6.0 wt.% and 3.3-6.0 wt.% respectively).

Mantle-normalized spider diagrams shows that the distal trachytic and rhyolitic glasses are comparable in incompatible element distribution patterns and enrichment levels to the proximal trachytic and rhyolitic glasses respectively (Fig. 2.8). All the distal glasses show LREE enrichment relative to HREE and pronounced negative anomalies in Ba, Sr and Eu (Fig. 2.8). Nevertheless, the less evolved trachytic glasses show more pronounced fractionation of LREE/HREE (La/Yb=21-29) and less significant Ba, Sr and Eu anomalies relative to the highly evolved rhyolitic glasses (La/Yb typically <15). The two compositional groups clearly define two evolutionary trends in most of the trace element bi-plots (Fig. 2.7e-h). The trachytic glasses have trace element variations with 11-18 ppm Th, 10-76 ppm Ba, 4-6 ppm Ta, 54-88 ppm Nd and 37-50 ppm Y, while the rhyolitic glasses show significantly higher contents of Th (30-56 ppm), Ta (10-17 ppm), Nd (78-144 ppm), Y (66-144ppm) and lower Ba (6-12 ppm; Fig. 2.7e-h). The rhyolitic glasses contain an analysis that is characterized by noticeably lower concentrations in most of the measured trace elements (Th=30 ppm, see Table 2.2: RH554-37) and higher La/Yb ratio (La/Yb=22) than any other rhyolite. Nevertheless, this analysis lies on the evolutionary trend of the rhyolitic members (Fig. 2.7g).

2.8 Interpretation

2.8.1 Proximal-distal glass correlation

Proximal-distal relationships are assessed in this section based on the glass geochemistry presented above. Overall, glass shards found in Lake Kushu are highly

heterogeneous and broadly overlap all three proximal fall units at a major, minor and trace element level (Figs. 2.7, 2.8).

The two proximal trachytic units, C-1 and C-2, share broadly overlapping major, minor and trace element glass chemistries, which makes it problematic to distinguish between these two units based on glass chemistry alone. The trachytic glasses of the distal Kushu tephra overlap with the two proximal trachytic units (Figs. 2.7, 2.8). Subtle differences can be recognized between the proximal and distal trachytic glasses: a) Kushu trachytic glasses have a least evolved composition that is not seen in proximal trachytic glasses (Fig. 2.7a); b) Kushu trachytic glasses have greater compositional variations of highly depleted trace element (e.g. Ba and Sr) than proximal trachytic glasses (Fig. 2.7e), which might be affected by analysis of microlite of distal shards in LA-ICP-MS.

The proximal rhyolitic unit C-3 geochemically overlaps the most evolved compositions of the distal rhyolitic glasses. These most evolved distal compositions ($SiO_2 \geq 74.0$ wt.%, n=41) make up the majority of the Kushu rhyolitic glasses (n=46) and could not be separated from the C-3 glasses in the major or trace element bi-plots (Fig. 2.7). The mantle-normalised spider diagram corroborates the geochemical overlaps at a full spectrum of element level (Fig. 2.8). Nevertheless, Kushu rhyolitic glasses have some less fractionated compositions that are not seen in the C-3 glasses (Fig. 2.6a).

In summary, the distal Kushu tephra shows compositional heterogeneity and a continuum of compositions ranging from trachyte to rhyolite. The three proximal fall units collectively comprise compositionally identical trachyte and rhyolite but without the intervening compositional continuum. Given the similarity between the trachyte and rhyolite end-members we propose a correlation between the distal Kushu tephra and all three of the investigated proximal units.

2.8.2 Comparison with the published data

In order to determine the provenance of the tephras reported herein and to investigate the geochemical diversity between the well-correlated proximal and distal tephras, we compare our glass chemistries with those of the published proximal ME tephra and B-Tm, along with other widespread late Quaternary marker tephras in and around the Northeast Asia area. Since all the available data are major element glass chemistry, comparison can only be made at a major element level.

Major element glass chemistry provides some basic discriminants for the identification of the B-Tm tephra. The B-Tm tephra has distinctive compositional heterogeneity ranging from trachyte to alkaline/subalkaline rhyolite with a fairly high total alkali content (8-12 wt.%; Fig. 2.9a). However, the late Quaternary Kyushu tephra layers (e.g. K-Ah, AT, Aso-4 and Ata) and Holocene Kamchatka tephra deposits typically plot into the subalkaline area, and the early Holocene Ulleungdo tephra (i.e. U-Oki) straddles the boundary between phonolite and trachyte (Fig. 2.9a). The B-Tm tephra has lower CaO than that of the Kyushu and Kamchatka tephras in a given SiO_2, and higher SiO_2 than that of the Ulleungdo tephra (Fig. 2.9b). The FeO_t vs. CaO bi-plot is an excellent discriminant (Fig. 2.9c) since the B-Tm tephra has a fairly high FeO_t content (typically between 3.8-5.6 wt.%) coupled with a relatively low CaO content (typically <1.5 wt.%), given its highly evolved composition (SiO_2 >63 wt.%). All the proximal and distal tephras reported herein show major element compositions that correspond precisely to the published B-Tm chemistries, and can be separated from tephras from other volcanic settings in the same region (Fig. 2.9). On this basis we conclude that all our proximal and distal tephra deposits are the product of the ME.

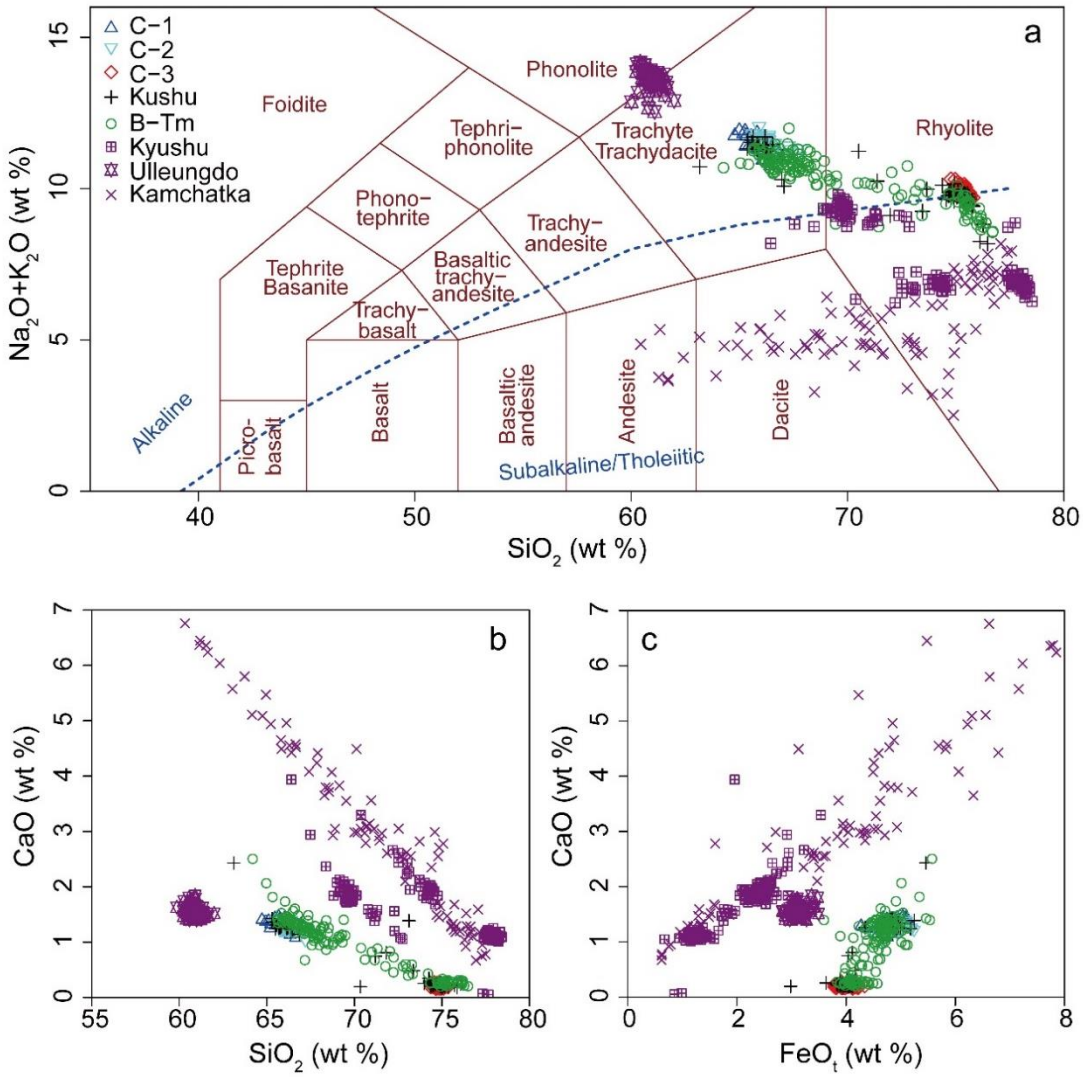

Fig. 2.9 (a) TAS classification (Le Bas et al., 1986) diagram and (b-c) major element variation diagrams showing the glass compositions of tephras reported herein along with the published data for comparison. The published data are glass compositions of the B-Tm and the widespread late Quaternary tephras from other volcanic settings in the Northeast Asia area. B-Tm includes the reported distal ME tephra deposits found in northeast China (Sun et al., 2015), Sea of Japan (Machida et al., 1990), Hokkaido (Hughes et al., 2013) and Greenland (Coulter et al., 2012; Sun et al., 2014a). Kyushu represents late Quaternary tephras (e.g. K-Ah, AT, Aso-4 and Ata) from volcanoes in Kyushu Island, Japan (Smith et al., 2013). Ulleungdo represents the early Holocene U-Oki tephra erupted from Ulleungdo, South Korea (Smith et al., 2011b). Kamchatka

represents the tephra layers from major Holocene eruptions in Kamchatka Peninsula, Russia (Kyle et al., 2011).

Sun et al. (2014a) reported the major element glass chemistry for a proximal ME sequence in North Korea which included the white-yellow, grey and black fall pumice. The major element chemistry for glasses from this ME sequence reveal an overlap with the proximal units described herein (Fig. 2.10a-b), suggesting both sequences relate to the ME. Most importantly, the proximal ME tephra units at Chinese and Korean sequences on the crater rim are both characterized by significant geochemical bimodality (i.e. trachyte and rhyolite) with no composition continuum plotting in the range of 69-74 wt.% of SiO_2 (Fig. 2.10a-b). This is in contrast to the B-Tm glass chemistries. The mid-range to distal ME tephra layers found in the Sihailongwan Lake (NE China; Sun et al., 2015), Sea of Japan (Machida et al., 1990), Utasai Bog (Hokkaido; Hughes et al., 2013) and Lake Kushu (Hokkaido, this study) reveal continuous compositions with data plotting in the compositional gap between the end-member compositions defined by proximal samples (Fig. 2.10c-d). Interestingly, although the ultra-distal B-Tm found in the Greenland ice cores contains very few shards (Coulter et al., 2012; Sun et al., 2014a), their compositions plot within the proximal compositional gap (Fig. 2.10c-d). Overall the proximal fall units deposited on the crater rim only preserve bimodal compositions for the caldera forming eruption, whereas the mid-range to distal tephras preserve a complete compositional range including the bimodal end-member compositions and intermediate compositions.

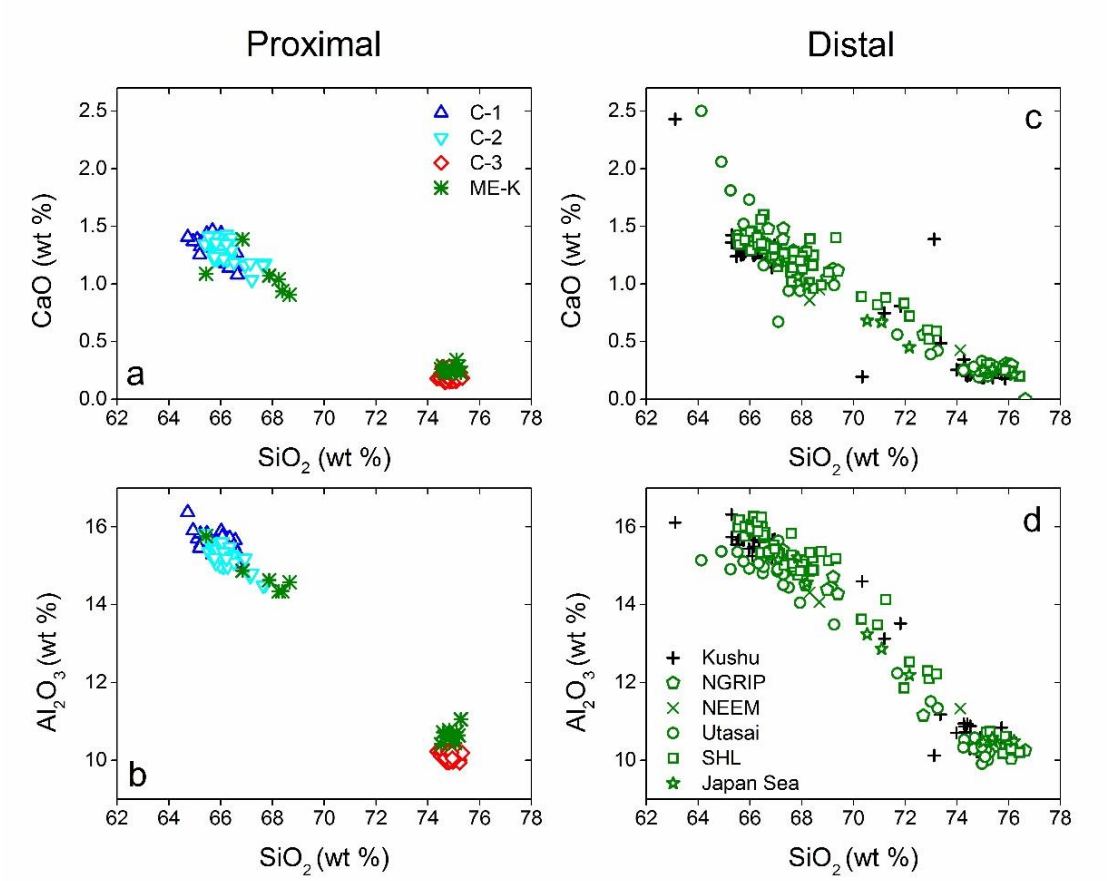

Fig. 2.10 Major element variation diagrams showing the glass compositions of (a-b) proximal tephra deposits in both Chinese (this study) and N. Korean ME sequences; (c-d) distal ME tephra deposits found in northeast China, Sea of Japan, Hokkaido and Greenland. ME-K represents the proximal ME sequence in N. Korean side of the crater (Sun et al., 2014a). Kushu represents the Lake Kushu in Rebun Island, Hokkaido, Japan (this study). Utasai represents the Utasai Bog in Hokkaido, Japan (Hughes et al., 2013). SHL represents the Sihailongwan Lake in northeast China (Sun et al., 2015). Japan Sea represents the distal ME tephra deposits found in Sea of Japan marine cores (Machida et al., 1990). NGRIP and NEEM represent the ultra-distal ME tephra deposits found in Greenland ice cores (Coulter et al., 2012; Sun et al., 2014a).

2.9 Discussion

2.9.1 Proximal-distal expression of the ME

As in the case of B-Tm tephra deposits reported from other localities, the single distal tephra layer found in Lake Kushu has compositional variation ranging from trachyte to rhyolite. This indicates the magmatic system that produced this distal ME tephra must have had the same compositional heterogeneity. In contrast the proximal C-3 unit is characterized by homogeneous rhyolite without any trachytic component. As such the C-3 unit alone cannot be the proximal equivalent of the B-Tm, though it is the most widespread unit in the Changbaishan volcanic region (Horn and Schmincke, 2000). Our glass chemistry shows that the geochemical bimodality observed between the proximal units C-3 to C-1 is comparable to the end-member compositions of the distal Kushu tephra. Importantly there is major, minor and trace element geochemical overlap between the proximal and distal end-member compositions which significantly increases the reliability of the tephra correlation. Hence, we propose that the proximal record of the ME at Tianwen summit is a composite sequence that includes the light grey, dark grey and black (i.e. C-3 to C-1) sub-units. This is also consistent with the field observation that there is no time break/erosional unconformity or paleosol between the three investigated fall units.

Proximal fall deposits preserved on the crater rim are dominated by bimodal compositions whereas distal tephras record a full range of geochemical heterogeneity. The presence of intermediate glass compositions in the distal tephras, not currently observed in the proximal records, clearly evidences the interaction of two compositionally distinct magma batches during the caldera forming eruption. Moreover, the interaction of the two magma batches was not substantial otherwise this would be reflected in the proximal record with evidence of mingling in the pumices. In fact, there is no such evidence in our pumice samples. Overall, the observed compositional diversity indicates that the trachytic and rhyolitic magmas were not thoroughly mixed

so only a minor portion of intermediate compositions were generated during magmatic interaction, which were then transferred into the stratosphere during the syn-eruptive process and were consequently recorded in the distal realms.

The preservation of bimodal proximal deposits (comprising the least and most fractionated components) has been reported from calderas elsewhere including in Afro-Arabia (Ukstins Peate et al., 2003; Ukstins Peate et al., 2008). As reported herein, the proximal units in Arabia are markedly bimodal and contrast with the contemporaneous distal tephra layers from 3000 km away in the Indian Ocean. These distal tephras display a continuum of compositions with end-members identical to the bimodal end-members found proximally. The bias between proximal and distal magma sequences is controversial and may relate to high level sub-volcanic processes that include fractionation processes involving silica rich magmas (Grove and Donnelly-Nolan, 1986), large scale liquid immiscibility (Charlier et al., 2011) and/or melt-crystal dynamics (Dufek and Bachmann, 2010).

2.9.2 Bayesian age modelling for Kushu tephra

The ME tephra deposits have been dated either directly or indirectly by multiple methods in many localities over the past two decades (Table 2.1). The proximal ages are mainly derived from the indirect dating method of ^{14}C dating of charcoals preserved in the pyroclastic fall and flow deposits (e.g. Horn and Schmincke, 2000; Nakamura et al., 2007; Yatsuzuka et al., 2010; Yin et al., 2012; Xu et al., 2013). Besides, direct dating of primary minerals using U-series TIMS (Wang et al., 2001) and $^{40}Ar/^{39}Ar$ (Yang et al., 2014) methods has also provided additional age constraints on the eruption. Distally, B-Tm tephra deposits were found in varve lakes in Japan and northeast China where the eruption was dated by varve chronology (Fukusawa et al., 1998; Kamite et al., 2010; Sun et al., 2015). Ultra-distal B-Tm tephra deposits were reported from the Greenland ice cores and as such the eruption has ages derived from the GICC05 and GISP2 ice-core chronologies (Sun et al., 2014a). Most recently, Sigl et al. (2015) has proposed a slight revision to the GICC05 chronology for the past 2,500 years. This new NS1-2011

chronology, based on ^{10}Be and ^{14}C synchronization of ice-core and tree-ring timescales, has shifted the age of the ME from AD 941±1 (GICC05) to AD 946-947 (Sigl et al., 2015).

In order to test our chemical correlation of the Kushu tephra to the proximal units and distal B-Tm, we have constructed a formal Bayesian age model for the late Holocene radiocarbon ages in the Kushu core (Fig. 2.11), for comparison with the highest resolution distal age reported for this tephra. In this age model, we have modelled the AMS ^{14}C dates reported in Müller et al. (2016), for Kushu along with the depth information (Table 2.3) in a Bayesian *P_Sequence* model with the addition of sediment deposition modelling to calculate the highest likelihood age ranges for every 1.6 cm, incorporating formal outlier detection (Bronk Ramsey, 2009a; 2009b; 2013). As there are no radiocarbon dates in the same centimeter of the core as the proposed B-Tm tephra, it was necessary to determine the age range for its depth at 151.5 cm, which is the average position in the core for the initial onset of Kushu tephra. The age range for the depth of 151.5 cm is 913-1395 cal AD (Fig. 2.11; supplementary material), and while at fairly low resolution this comfortably overlaps with the ice-core ages of the ME/B-Tm.

Table 2.3 Summary of radiocarbon dates from Kushu sediments and ice-core ages for B-Tm that were used to construct the Bayesian age-depth models, the modelled date results shown in 95% confidence, and the relative depth information. AMS ^{14}C uncal. dates are from Müller et al. (2016). Date shown in *italic* font may be an age inversion although after calibration this still contributes significant probability to the deposition model. GICC05 ice-core tephra age for the B-Tm is from Sun et al. (2014a), the revised B-Tm age based on NS1-2011 timescale is from Sigl et al. (2015). The Bayesian age-depth models are produced using OxCal v4.2.4 (Bronk Ramsey, 2013). The modelled date results for the set of 6 AMS-dated samples are from the model with GICC05 tephra age imported as shown in Fig. 2.12a.

Laboratory number	Composite depth	AMS ^{14}C date	Modelled date (OxCal v4.2.4), 95% range			
	cm	uncal. yr BP	From, cal. BP	To, cal. BP	From, cal. AD	To, cal. AD
Poz-51689	*64.5*	*470 ± 25*	528	325	1422	1626
Poz-51700	96.5	415 ± 30	569	449	1381	1502
Poz-51713	126.5	510 ± 35	653	500	1297	1450
Poz-51721	164.5	1065 ± 25	1055	1004	895	947
Poz-51731	196.5	1290 ± 30	1285	1180	666	771
Poz-51735	226.5	1445 ± 30	1386	1296	565	655
Imported tephra	Imported position	Imported ice-core ages				
B-Tm	151	AD 941±1 (GICC05)	1017	1001	933	949
		AD 946-947 (NS1-2011)	1006	1003	944	947

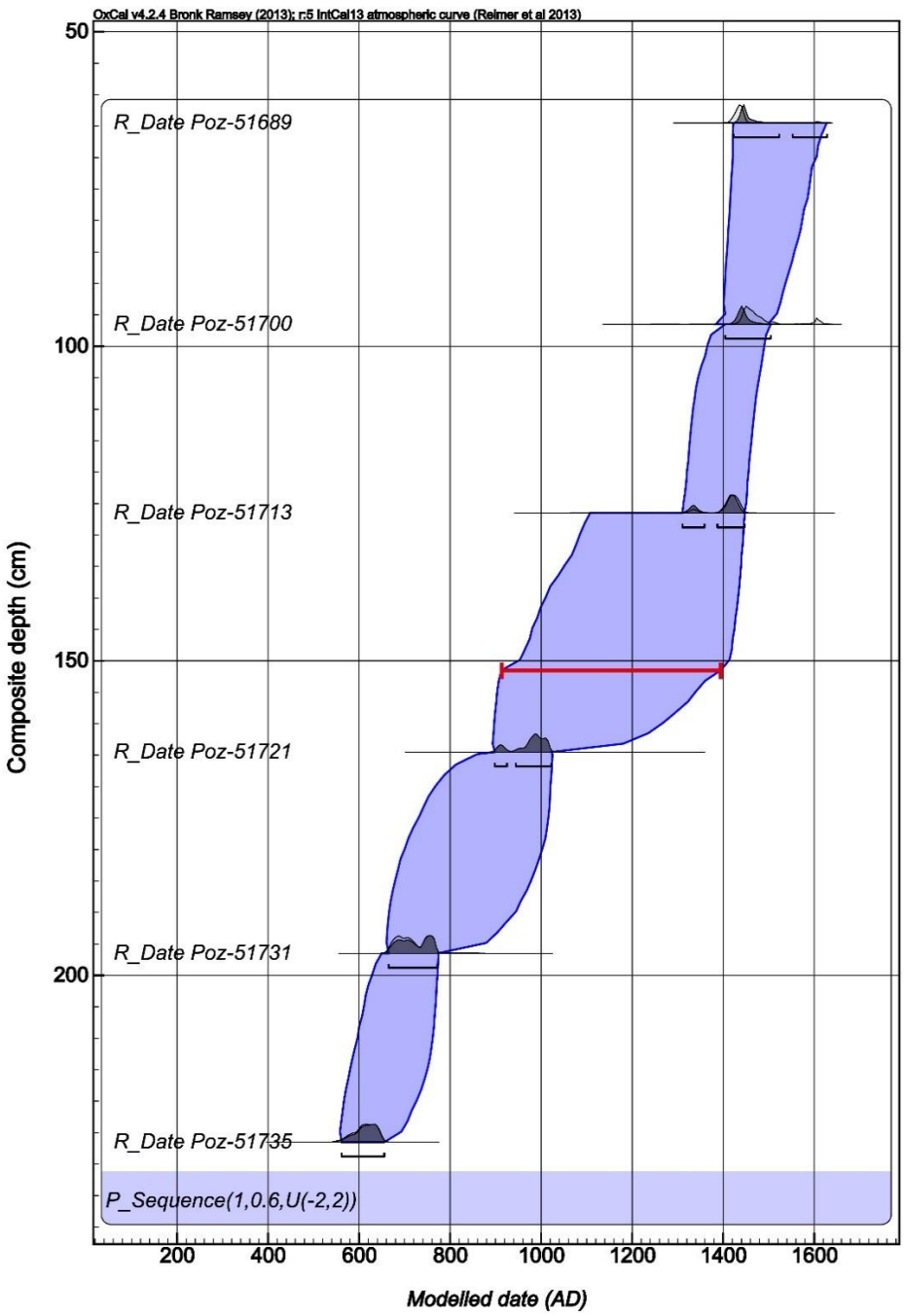

Fig. 2.11 95% confidence Highest Probability Density output for radiocarbon-based Bayesian age-depth model for the uppermost 2 meters sequence of Lake Kushu (run using a Poisson process model). The model was constructed purely using AMS ^{14}C dates of Kushu sediments from Müller et al. (2016), for providing independent age constraint on the Kushu tephra. The deposition model age range for the depth of 151.5 cm, which is the average position for the initial onset of the Kushu tephra, is 913-1395 cal AD.

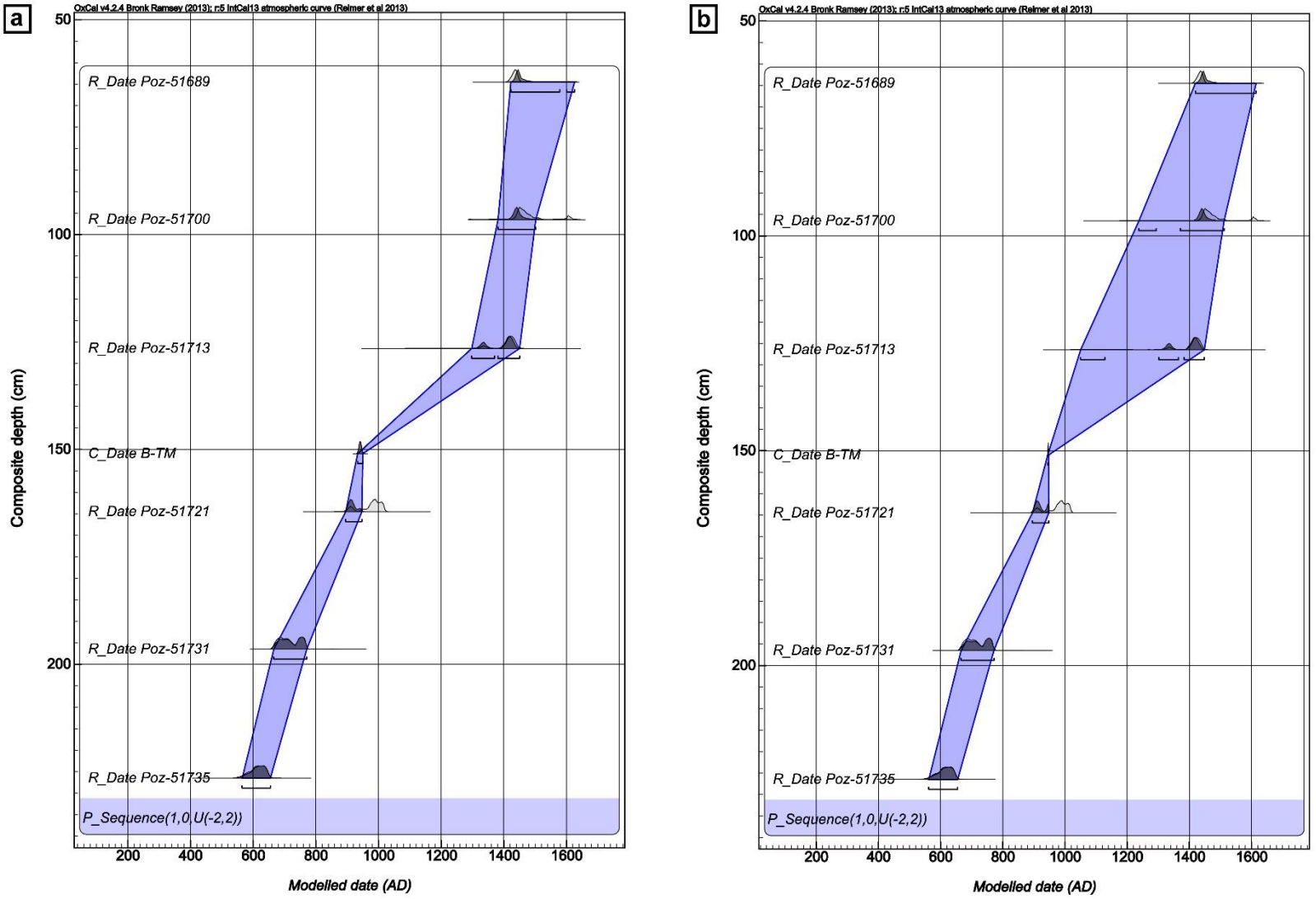
a
OxCal v4.2.4 Bronk Ramsey (2013); r:5 IntCal13 atmospheric curve (Reimer et al 2013)
R_Date Poz-51689
R_Date Poz-51700
R_Date Poz-51713
C_Date B-TM
R_Date Poz-51721
R_Date Poz-51731
R_Date Poz-51735
P_Sequence(1,0,U(-2,2))
Composite depth (cm)
Modelled date (AD)
b
OxCal v4.2.4 Bronk Ramsey (2013); r:5 IntCal13 atmospheric curve (Reimer et al 2013)
R_Date Poz-51689
R_Date Poz-51700
R_Date Poz-51713
C_Date B-TM
R_Date Poz-51721
R_Date Poz-51731
R_Date Poz-51735
P_Sequence(1,0,U(-2,2))
Composite depth (cm)
Modelled date (AD)

Fig. 2.12 (a) 95% confidence Highest Probability Density output for Bayesian age-depth model for the uppermost 2 meters sequence of Lake Kushu (run using a Poisson process model). The model was constructed using the AMS ^{14}C dates reported in Müller et al. (2016) and the GICC05 ice-core age for B-Tm tephra (Sun et al., 2014a) imported in the appropriate position where our proposed correlative tephra was identified; (b) As above but with the B-Tm age from the revised NS1-2011 timescale after Sigl et al. (2015).

Due to the low resolution generated by the requirement to model the ages and associated uncertainty of the depths between the radiocarbon ages in this approach we also attempted to test the chronological relationship between the Kushu tephra and the high resolution age for the B-Tm in more detail. The logic of the test is that, while the radiocarbon ages for the Kushu site (Fig. 2.11) show a broadly last millennium age for the tephra sitting at 151 cm, if our correlation is correct then the tephra and radiocarbon ages should all be compatible with a high precision age model. We have thus constructed two more constrained age models (Fig. 2.12). We again use the above radiocarbon ages and their depths (Table 2.3), without interpolation and have also imported the GICC05 (Sun et al., 2014a; Fig. 2.12a) and NS1-2011 (Sigl et al., 2015; Fig. 2.12b) ages for the ME/B-Tm at the depth of our proposed correlative tephra in Kushu. We have applied a *P_Sequence* depositional model in Oxcal (Bronk Ramsey, 2013), with a variable K factor and automatic outlier detection, following Bronk Ramsey (2008; 2009a; 2009b) with boundaries at the top and bottom of the selected 2 meters sequence. The outlier model selection used the general outlier model and outlier probabilities were set to 0.05%. The results of the modelling exercise are reported as 95% confidence highest probability density function and depositional model plots. In these higher resolution, more constrained models, we are testing if the B-Tm ages are fully consistent with the Kushu radiocarbon ages and the depths in the core in which they sit. If our data is incompatible with the B-Tm on chronological grounds we would expect that the B-Tm ages we have incorporated, or the radiocarbon ages above and

below the tephra would be reported as being anomalous by the outlier detection software. In these cases, however only the uppermost date Poz-51689 reported significant potential to be an outlier and thus the weighting of this date was reduced automatically in each age model. The dates close to the tephra layer, were, however, in reasonable agreement with the imported tephra ages. The two final modelled ages associated with GICC05 and NS1-2011 timescales, taking into account the depth and all chronological information are 933-949 and 944-947 cal AD (95.4%), respectively (Fig. 2.12; Table 2.3). We, thus, suggest on this rigorous basis, using formal deposition models the Kushu tephra is both chemically and chronologically well correlated to the ME/B-Tm.

2.9.3 Implication for future studies

High-resolution (annual to decadal-scale) reconstructions of past environments, and better understanding which role environmental and climatic changes played in the cultural dynamics remains extremely important, though an empirically challenging question for the Hokkaido region (Weber et al., 2013). Despite, the northern part of Japan, including Hokkaido and adjacent islands are rich in archaeological and environmental archives, the main challenge remains the scarcity of published records with high temporal resolution and adequate dating control (Nakagawa et al., 2012; Müller et al., 2016 and references therein). These two common problems hinder direct correlation between individual archives, thus preventing inter-regional comparison and identification of leads and lags in reconstructed climate variability. A multidisciplinary research on the RK12 core from Lake Kushu started in 2012 has a significant potential to fill the existing gap in the current knowledge and to build up the high-resolution environmental archive spanning the past ca. 17,000 years (Müller et al., 2016). However, in order to serve as a link between the high-resolution and accurately-dated records from central Japan (e.g. Lake Suigetsu: Nakagawa et al., 2012), China (e.g. Sihailongwan Maar Lake: Stebich et al., 2009; 2015), and North Atlantic region, the Kushu ^{14}C chronology must be checked, and when necessary, improved. The current

study demonstrates the potential of cryptotephra analysis for improving the age constraints on the Kushu sedimentary record. The ice-core ages imported into the deposition models significantly help constrain the age of the sediments around the tephra layer and improve the radiocarbon chronology in this interval (Fig. 2.12). This provides encouragement for the identification of additional cryptotephra layers in the Lake Kushu sediment. Though it still could be improved, we believe that the existing RK12 core chronology based on the 57 AMS dates (Müller et al., 2016) is robust enough to provide reliable age estimations for the tephra layers preserved in the sediment. This will facilitate search of the source volcano and identification of the eruption, which produced each given tephra.

2.10 Conclusions

a) Three proximal pyroclastic fall units (i.e. C-3 to C-1) from Tianwen summit on the crater rim of Changbaishan Volcano, NE China display bimodal glass compositions comprising trachyte and rhyolite end-member compositions.
b) A distal tephra layer in Lake Kushu of northern Japan contains glass shards that define a complete compositional continuum ranging from trachyte to rhyolite that in themselves are chemically identical to the investigated proximal glasses.
c) The chemical constraint and radiocarbon-based Bayesian age-depth model indicate that the analysed Kushu tephra is the distal expression of the Millennium eruption.
d) Proximal-distal geochemical correlation at a full spectrum of element level (i.e. major, minor and trace elements) requires that the three proximal pyroclastic fall units were erupted as part of the Millennium eruption as alluded to by previous studies (Horn and Schmincke, 2000; Sun et al., 2014a).
e) Bayesian age-depth modelling of Kushu sediments involving the AMS ^{14}C dates and two ice-core derived ages for the B-Tm provides 95% confidence interval ranges of 933-949 and 944-947 cal AD for the Kushu tephra. The high resolution ice-core tephra ages imported into the deposition models help test and ultimately constrain the radiocarbon chronology in this interval of the Lake Kushu

sedimentary record.

f) The presence of intermediate glass compositions in the distal tephra layers, not currently observed in the proximal records, clearly evidences the interaction of two compositionally distinct magma batches (with end-member compositions) during the caldera forming eruption.

2.11 Acknowledgements

This study was supported by the External Cooperation Program of BIC, Chinese Academy of Sciences, Grant No.132744KYSB20130005. XYC's stay at RHUL was supported by the collaboration scheme between GIGCAS and RHUL. Coring of Lake Kushu and core transportation costs were covered by the Japanese MEXT-Japan Kakenhi research grant No. 21101002 held by Dr. H. Yonenobu, whose generous help we greatly acknowledge. The Baikal–Hokkaido Archaeology Project and BHAP-related research activities on Rebun Island are supported by the Major Collaborative Research Initiative (MCRI) program of the Social Sciences and Humanities Research Council of Canada, and collaborating institutions, including University of Alberta, German Archaeological Institute (DAI), Free University Berlin and German Science Foundation (DFG TA 540/5), Hokkaido University, and Japan Society for the Promotion of Science. We would like to thank Prof. F. Wang for providing proximal tephra sub-samples; Dr. C. J. Manning for the assistance in sample preparation; Dr. S. Armitage for beneficial discussions; Dr. V. C. Smith and an anonymous reviewer for their detailed and constructive feedback. We thank N. Holloway for preparing samples in epoxy resin stubs; K. Flowers and S. Gibbons for their assistance in the lab.

Chapter 3: Developing a Holocene tephrostratigraphy for northern Japan using the sedimentary record from Lake Kushu, Rebun Island

3.1 Author List

Xuan-Yu Chen [a,b,c,d,*], Danielle McLean [e], Simon Blockley [b], Pavel Tarasov [f], Yi-Gang Xu [a], Martin Menzies [a,c]

[a] State Key Laboratory of Isotope Geochemistry, Guangzhou Institute of Geochemistry, Chinese Academy of Sciences, Guangzhou, 510640, China

[b] Department of Geography, Royal Holloway University of London, Egham, Surrey, TW20 0EX, UK

[c] Department of Earth Sciences, Royal Holloway University of London, Egham, Surrey, TW20 0EX, UK

[d] University of Chinese Academy of Sciences, Beijing, 100049, China

[e] Research Laboratory for Archaeology and the History of Art, University of Oxford, Oxford, OX1 3QY, UK

[f] Institute of Geological Sciences, Palaeontology, Free University Berlin, Malteserstr. 74-100, Building D, 12249, Berlin, Germany

3.2 Abstract

Palaeoclimate records in East Asia preserve valuable information on monsoon dynamics and serve as a link between North Atlantic and tropical climate systems. Precise alignment of proxy records within and beyond the region is aided by the use of isochronous marker horizons such as volcanic ash (tephra) layers. A comprehensive regional tephrostratigraphic framework is fundamental for correlating widespread archives. In this study, we present the first cryptotephra stratigraphy in northern Japan using the high resolution lacustrine archive from Lake Kushu, Rebun Island, which aids the construction of a master tephra framework for the East Asia region. Grain-specific major element glass chemistry and independent age estimates for each tephra layer are presented, which enable primary tephra horizons to be correlated to their source volcanoes or specific eruptions. The detailed RK12 tephrostratigraphy integrates local and far-travelled tephras originating from multiple regions such as Russia, China/N Korea, northern Japan, southern Japan and as far south as Indonesia. This cryptotephra study has significantly enlarged the known dispersal of several key tephra layers in the region and identified a number of previously undocumented tephra horizons. These tephras provide useful isochrons for dating and correlating sequences and call into question the currently known tephrostratigraphy in northern Japan which is based on visible tephra study. These results highlight the importance of the cryptotephra method even in a volcanically active region. Given that the tephra isochrons recorded in the Lake Kushu sequence have very wide distributions, ranging from high northern latitudes (e.g. Greenland, Kamchatka) to low southern latitudes (e.g. Indonesia), the RK12 record serves as a hub for linking widespread palaeoclimate archives spanning a vast geographic area, and therefore is one of the very few Holocene tephrostratigraphies that are suitable for correlating records in and beyond the East Asia region.

Keywords: Cryptotephra, Tephrostratigraphy, Glass chemistry, Lake Kushu, Northern Japan, Bayesian Modelling, Holocene, East Asia, Changbaishan, Shiveluch

3.3 Introduction

Palaeoclimate records in East Asia, a region largely affected by the East Asian monsoon system, preserve valuable information of climate changes, linking the North Atlantic climate system and the tropical western Pacific Ocean where the monsoon originates (e.g. Dykoski et al., 2005; Wang et al., 2005; Wang et al., 2012). Direct comparison of widespread paleoclimate records, however, can be difficult which is largely due to the inherent dating uncertainties of various dating techniques (e.g. 14C, U-series, Ar-Ar, varve chronology, ice-core chronology) that were applied to different types of sedimentary archive (e.g. ice, marine, lacustrine, speleothem), in particular when investigating short-lived (e.g. centennial or multi-decadal scale) climate changes (Lowe et al., 2015). Precise alignment of proxy records is thus aided by the use of isochronous marker horizons and in this respect volcanic ash (tephra) horizons preserved within sedimentary archives are becoming increasingly useful (Lowe et al., 2008b; Davies et al., 2012; Blockley et al., 2012). These volcanic ash horizons can be detected as visible layers or as non-visible cryptotephra layers (e.g. Blockley et al., 2005). In either case well dated tephra layers or ones that fall close to a palaeoclimatic/cultural transition are particularly useful (e.g. Lowe et al., 2012; Lane et al., 2013a), however, all widespread tephra horizons are important for the development of a regional tephra lattice (Blockley et al., 2014; Davies et al., 2014).

Active volcanic regions, for example the East Asia, have significant potential for the development of important tephrostratigraphic frameworks (McLean et al., 2018). Combined with its important role in understanding the monsoon dynamics, East Asia is an ideal area for optimising the use of tephra layers to synchronise widespread palaeoclimate records. Initial work such as Machida and Arai (1983) provided a sound basis for the investigation of tephra in this region. Later on, tephrochronologists started constructing regional tephrostratigraphic frameworks based on mapping widespread tephra layers (e.g. Arai et al., 1986; Furuta et al., 1986; Machida, 1999; Machida and Arai, 2003; Nagahashi et al., 2004; Moriwaki et al., 2016; Nakamura, 2016; Razzhigaeva et al., 2016). On the other hand, continuous sedimentary sequences were also increasingly utilised for distal tephra investigations, where stratigraphic relationships between tephra horizons help unravel the correct order of multiple volcanic eruptions (e.g. Aoki and Arai, 2000; Park et al., 2003; Aoki et al., 2008;

Takemura et al., 2010; Okuno et al., 2011; Smith et al., 2013; Tsuji et al., 2018). Continuous sequences are particularly useful when integrating multiple ash layers that are closely spaced in time into the regional tephra framework, given the dating uncertainties of the tephra layers.

The outcomes of these previous studies are important but also limited, as the results are based on identification of visible tephra layers only. In contrast, the cryptotephra technique has been demonstrated to effectively magnify the footprints of numerous volcanic eruptions (e.g. Pyne-O'Donnell et al., 2012, 2016; Lane et al., 2013b; Jensen et al., 2014; Sun et al., 2014a; Bourne et al., 2016; Mackay et al., 2016; wan der Bilt et al., 2017; Cook et al., 2018b; Kearney et al., 2018). These include the identification of several Asian tephra horizons in Greenland (Sun et al., 2014a; Bourne et al., 2016; Cook et al., 2018b) and probably in North America (Mackay et al., 2016). Moreover, the cryptotephra method also permits eruptions that are not revealed by visible tephra study to be identified, providing valuable information on volcanic resurgence and eruption forecasting (c.f. Davies, 2015). This method has now been widely employed in Europe and the North Atlantic regions (e.g. Abbott et al., 2016; Albert et al., 2015; Blockley et al., 2007, 2015; Bourne et al., 2010, 2015a, 2015b; Cook et al., 2018a; Jones et al., 2017; Lane et al., 2011, 2012a, 2015; MacLeod et al., 2015; Matthews et al., 2015; Timms et al., 2017, 2018; Watson et al., 2016, 2017; Wulf et al., 2016, 2018) and North America (e.g. Pyne-O'Donnell et al., 2012, 2016; Mackay et al., 2016; Spano et al., 2017; Davies et al., 2018), but has very limited applications in East Asia (Sun et al., 2015; Chen et al., 2016; McLean et al., 2018).

Given the need for developing a comprehensive tephrostratigraphy for the East Asia and building on the important but limited visible tephra work and the pioneering cryptotephra work in Lake Suigetsu, central Japan (McLean et al., 2018), this study presents the first detailed cryptotephra stratigraphy in northern Japan. The results below, show the potential of the cryptotephra method in facilitating the identification of far-travelled tephra horizons and the importance of the Lake Kushu as a hub for linking widespread sedimentary archives in and beyond the East Asia region.

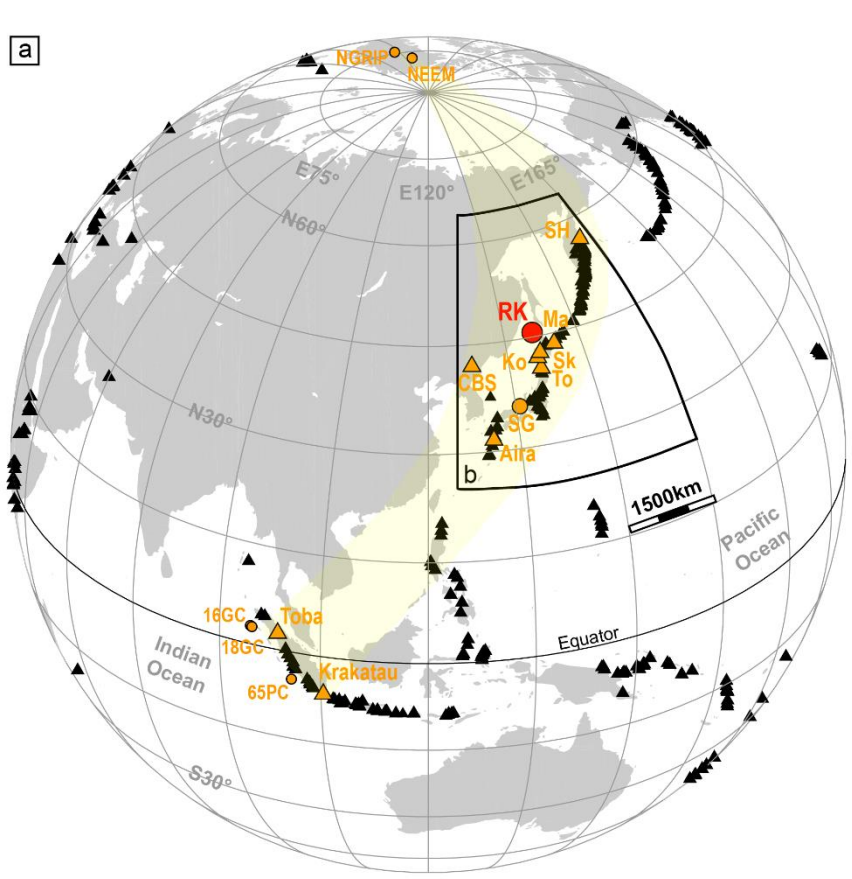
a
NGRIP
NEEM
E75°
E120°
E165°
N60°
N30°
SH
RK
Ma
Ko
Sk
To
CBS
SG
Aira
b
1500km
Pacific Ocean
16GC
Toba
18GC
Krakatau
65PC
Indian Ocean
Equator
S30°

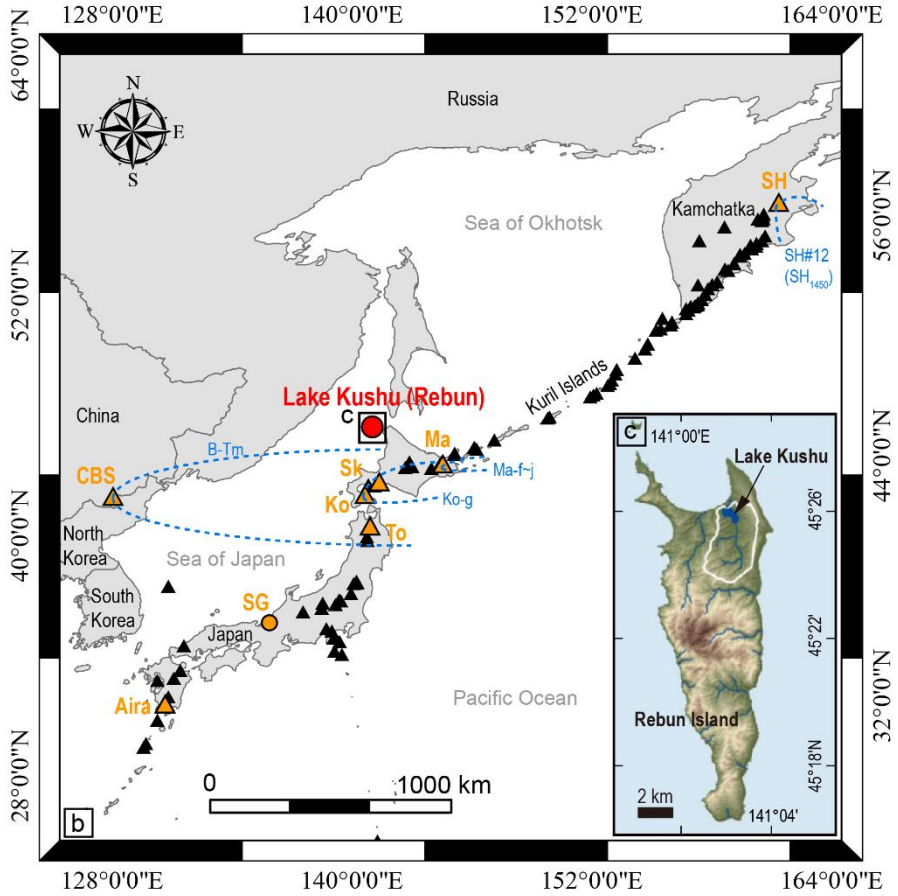
128°0'0"E
140°0'0"E
152°0'0"E
164°0'0"E
64°0'0"N
52°0'0"N
40°0'0"N
28°0'0"N
56°0'0"N
44°0'0"N
32°0'0"N
N
W
E
S
Russia
Sea of Okhotsk
Kamchatka
SH
SH#12
(SH1450)
Kuril Islands
China
Lake Kushu (Rebun)
C
B-Tm
Ma
Ma-f~j
CBS
Sk
Ko
Ko-g
To
North Korea
Sea of Japan
South Korea
SG
Japan
Aira
Pacific Ocean
0
1000 km
b
c
141°00'E
Lake Kushu
45°26'
45°22'
45°18'N
Rebun Island
2 km
141°04'

Fig. 3.1 (a) Map of the western Pacific rim region showing active volcanoes (triangle) and distal archives (circle) for tephra studies. The distal archive of this study – Lake Kushu (RK) is highlighted in red. Volcanoes and distal archives mentioned in the text are highlighted in orange. The yellow colour banded shape indicates an area within which widespread palaeoclimate records could probably be linked by tephra isochrons recorded in the Kushu sequence. (b) Enlarged map of the NE Asia showing volcanoes in Kamchatka Peninsula, Kuril Islands, Japanese Archipelago, China/North Korea and South Korea. The previous known dispersals of several marker tephras based on visible tephra studies are indicated using blue dashed lines. Dispersal data for B-Tm, Ko-g, Ma-f~j and SH#12 (SH_{1450}) tephras are from Machida (1999), Furakawa and Nanayama (2006), Katsui et al. (1975) and Kyle et al. (2011) respectively. The identification of these tephra horizons as cryptotephra layers in Lake Kushu has significantly enlarged their known distribution areas. (c) Detailed location of Lake Kushu in Rebun Island. Abbreviations: SH-Shiveluch volcano, RK-Lake Kushu Rebun Island, Ma-Mashu volcano, Sk-Shikotsu caldera, Ko-Komagatake volcano, To-Towada volcano, SG-Lake Suigetsu, CBS-Changbaishan volcano. 16GC, 18GC and 65PC are marine cores off Sumatra Island in Indian Ocean.

3.4 Study site

3.4.1 Rebun Island and Lake Kushu

Rebun Island, situated in the northeastern part of the Sea of Japan, is ca. 45 km W off the northern coast of Hokkaido (Fig. 3.1). The elongated-shaped island occupies an area of ca. 82 km^2, with its long axis (north-south) spanning about 20 km. Lake Kushu (45°25′55″N, 141°02′13″E, 4 m.a.s.l.) is a coastal freshwater lake located in the northern part of the Island (Fig. 3.1c). With a catchment area of ca. 10 km^2, the lake is fed by two inflows, the Oshonnai River from the south and a tiny stream from the east and has one outlet connecting with the sea (Sato et al., 1998). About 300 m away from the coast, the lake is surrounded by dense vegetation, which effectively limits sediment in-washing to the lake, where sediment is made up primarily from autochthonous biological productivity, aeolian input and minor fluvial input (Schmidt et al., 2016). As with Lake Suigetsu (Mclean et al., 2018), Lake Kushu is not close to large active

volcanic centres (Fig. 3.1b) that would dominate the tephrostratigraphic record of the site and mask a more regional tephra signal. In addition, the Kushu sequence is 16 m long through the Holocene which permits high resolution tephra investigation. Moreover, there is extensive radiocarbon dating on the core (Müller et al., 2016) and the potential to employ a range of age modelling approaches, including Bayesian deposition modelling (Bronk Ramsey, 2008). Given the northerly location of Rebun Island, in relation to most currently published tephra studies from the region (e.g. Nakamura, 2016; Razzhigaeva et al., 2016) and the good state of preservation of the sediments, the Kushu sedimentary record is ideal for aiding the development of a regional tephra framework for East Asia through providing an important northern element of a regional tephra lattice.

3.4.2 Lake Kushu RK12 composite core archive

Following a preliminary survey of the lake to determine the best coring point, coring was performed in the central part of the lake when it was covered by a thick ice layer in February 2012 (Müller et al., 2016). Two parallel sediment cores RK12-01 and RK12-02 were recovered using a hydro-pressure thin-walled piston corer. After the coring campaign, the cores were transported to the Hokkaido University and stored under cool temperature. In April 2012, the cores were opened by splitting each of them into two identical halves. The sediments were photographed, described, archived and sub-sampled for multi-proxy analyses. One complete set of the subsample was sent to the Centre for Quaternary Research at Royal Holloway University of London for tephra study. Other sets of the subsample from the same core were shipped to the Institute of Geological Sciences at the Free University of Berlin where a range of proxy studies (e.g. pollen, diatom, geochemical analyses) were performed (Müller et al., 2016; Schmidt et al., 2016; Leipe et al., 2018).

The composite core RK12 revealed a continuous, partly laminated, organic-rich ca. 19.5 m long sediment column. A total of fifty-seven bulk 1 cm samples throughout the composite core were processed for AMS radiocarbon dating (Müller et al., 2016). The obtained results allow the construction of the RK12 age model, suggesting a continuous sedimentary record covering the last ca. 17 ka. This study focuses on the Holocene part of the RK12 core, which includes the upper 16 m sediments of the sequence between

composite depth (CD) 50 cm and 1650 cm and age modelling of this section is discussed below.

3.5 Methods

3.5.1 Tephra separation and identification

Preliminary tephra investigation on the RK12 core revealed that no visible tephra layer was recorded throughout the Holocene sequence (McLean, 2013), thus the core was analysed in detail for cryptotephra. Cryptotephra deposits were detected and extracted using the physical separation methods outlined by Turney (1998) and Blockley et al. (2005). The RK12 Holocene sequence was first contiguously sub-sampled at a 10 or 20 cm resolution for range-finder scanning to determine tephra presence. If an elevated shard concentration was observed in the range-finder samples, the sediments were resampled at 1 or 2 cm resolutions for point sampling to locate the precise stratigraphic position of the cryptotephra. Blank samples were prepared alongside all the samples to monitor possible laboratory contamination. Each extracted sample was mounted on a slide and examined for tephra shards using a plane polarizing microscope. Tephra concentrations were measured by counts normalized to shards per gram dry sediment (shard g^{-1}). Individual shards of each cryptotephra were hand-picked from point-samples with the highest tephra counts and embedded in epoxy resin, which were then sectioned and polished for geochemical analysis.

3.5.2 Glass geochemical analysis

Single-grain major and minor element concentrations were measured using wavelength-dispersive electron probe microanalysis (WDS-EPMA) at 1) the Research Laboratory for Archaeology and the History of Art, at the University of Oxford with a JEOL JXA-8600, and 2) the Grant Institute, School of Geosciences at the University of Edinburgh with a Cameca SX100. Spot sizes of 10, 5 and 3 um were used depending on the size of the area available for analysis in different shards. Secondary glass standards were analysed in the same session in order to monitor instrumental accuracy and analytical precision. Detailed machine set-up for the electron probe JEOL JXA-8600 at Oxford see Kuehn et al. (2011) (lab#25), and for the Cameca SX100 at Edinburgh see Hayward (2011). Data were filtered to remove non-glass analyses, and

those with analytical totals <93%. For comparative purposes, all data presented in text, table and plots were normalized to 100 wt % on a volatile-free basis. All raw data and glass standards are presented in the supplementary material.

3.5.3 Chronology

Forty-nine AMS dates of the RK12 core reported by Müller et al. (2016) were re-modelled in a formal Bayesian age model for the Kushu Holocene sequence. The model utilises a *P_Sequence* in Oxcal ver. 4.3 (Bronk Ramsey, 2008, 2009a), with a variable K factor and automatic outlier detection (Bronk Ramsey and Lee, 2013; Bronk Ramsey, 2009b), applying the IntCal13 calibration curve (Reimer et al., 2013). In this model there is the addition of sediment deposition modelling to calculate the highest likelihood age ranges for every 1 cm CD, in order to provide age estimate for cryptotephra identified in the sequence. While estimating the ages, we used the depth range instead of sub-sampling mid-point for each cryptotephra to account for the full age uncertainty. Three conspicuous age reversals within the mid-Holocene (i.e. Poz-51838, 51840 and 51715) were removed from the age model as the program cannot run through with these dates incorporated, suggesting they are significantly at odds with the overall model assumptions and the remaining dates. Other ages with probability of being outliers were automatically down-weighted by the *Outlier_Model* (Bronk Ramsey, 2009b) as a proportion of their likelihood of being outlying. This is an objective way of dealing with outliers because no seeming age reversal was intentionally excluded, which could possibly represent a true age. As such no subjective bias was created while constructing the age model.

3.6 Results

3.6.1 Stratigraphy and ages

Detailed tephra stratigraphy and age model results for the Lake Kushu RK12 Holocene sequence are presented in Figs. 3.2 and 3.3 and summarised in Table 3.1. In total, twelve cryptotephra layers were identified, with four in each of the early, mid- and late Holocene. Subdivision of the Holocene Epoch follows the scheme proposed by Walker et al. (2012). Cryptotephra layers were labelled by the mid-point of the CD in 2 cm samples or the lower point in 1 cm samples (e.g. RK12-0225 for CD 224-226

cm and RK12-0151 for CD 150-151 cm). Counts of range-finders revealed that shard concentrations differ by one to two orders of magnitude between the first 1 m segment and the remaining 15 m sediment core. The largest range-finder sample within the first 1m segment reaches a peak of 3286 shards/g, due to the continuous reworking of the massive tephra RK12-0151 (Fig. 3.2a), whereas range-finder samples for the rest of the core barely exceed 50 shards/g (Fig. 3.2). Note that a sample at CD 1590-1600 cm was studied at higher resolution but the low tephra concentration meant that geochemical analysis was impossible (Fig. 3.2k).

3.6.1.1 Early Holocene (11.7-8.2 ka)

Age modelling of the RK12 composite core indicates that the early Holocene period covers the lowermost ca. 350 cm sediment (i.e. CD 1650-1300 cm, Fig. 3.3), within which four cryptotephra layers are identified: RK12-1507, RK12-1495, RK12-1391 and RK12-1361 (Fig. 3.2). Tephra layers RK12-1507 and RK12-1495 are closely located within the same range-finder. They have tephra concentrations of 60-80 shards/g that form peaks doubling the background value (ca. 20-30 shards/g) of the same time interval (Fig. 3.2j). The upper two tephra layers RK12-1391 and RK12-1361 also stand out from the background reaching 58 shards/g and 120 shards/g, respectively (Fig. 3.2h-i).

The radiocarbon dates within the early Holocene of the RK12 sequence comprise several age reversals (Fig. 3.3), which were dealt with by the *Outlier_Model* and were discussed above. The age estimates on the four identified tephra layers have reasonable resolution given their early Holocene timeframe and age ranges are 8914-9366 cal yrs BP, 8622-9309 cal yrs BP, 8440-8983 cal yrs BP and 8395-8586 cal yrs BP for RK12-1507, RK12-1495, RK12-1391 and RK12-1361 respectively. Note that significant age discrepancy occurred between radiocarbon samples Poz-51729 (CD 1599.5 cm) and Poz-51730 (CD 1625.5 cm) (Fig. 3.3), which indicates a major change in sedimentation rate or a depositional hiatus of the record at the beginning of the Holocene period.

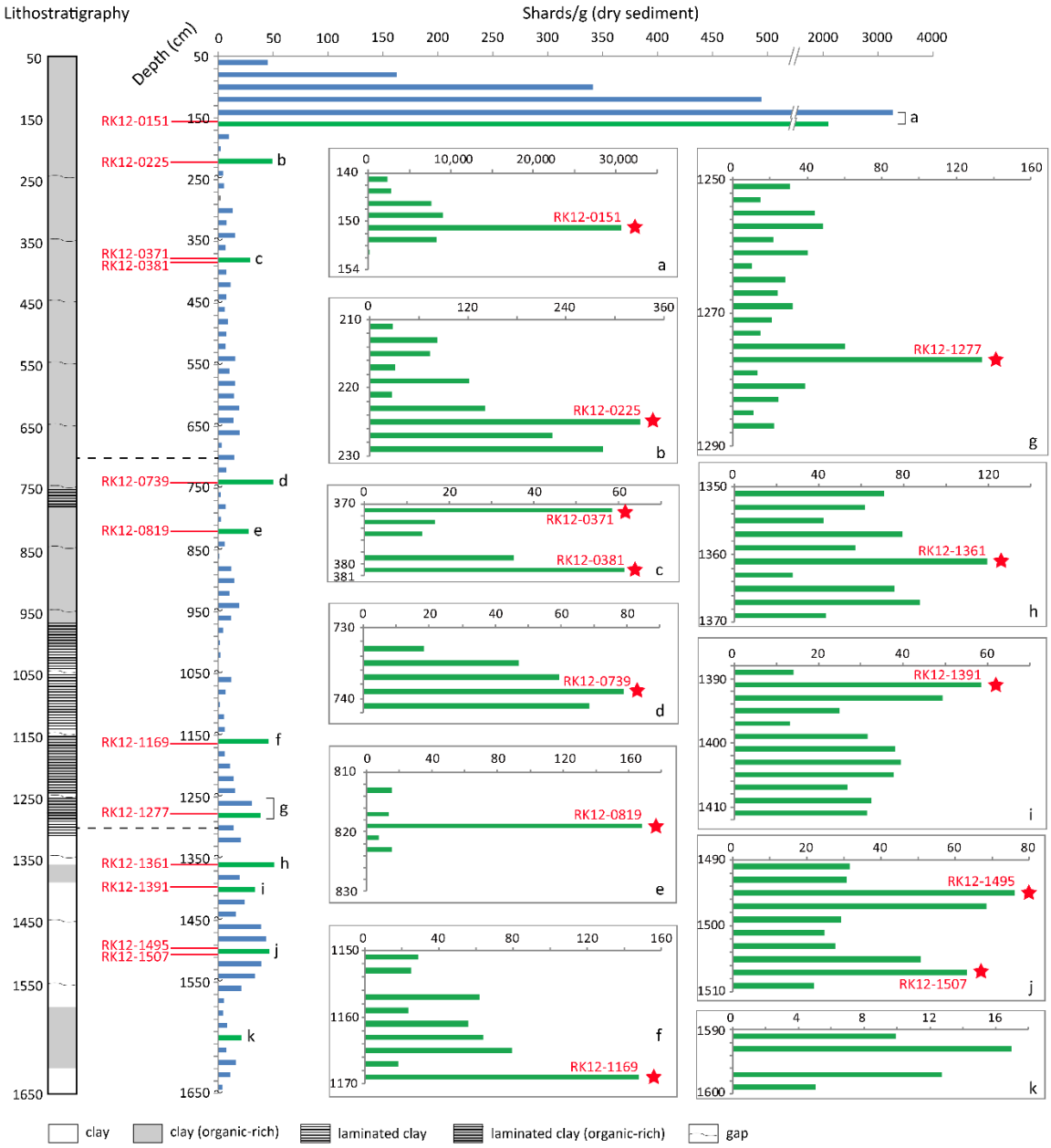

Fig. 3.2 Glass shards concentrations (shards per gram of dry sediment) measured in the Holocene sediments of the Lake Kushu RK12 core. The lithostratigraphy of the sediment core is also shown. Concentrations of range-finder samples (~10 or 20 cm resolution) are shown in blue colour, with samples revealing elevated shard concentrations highlighted in green colour. Highlighted range-finder samples were further studied at higher resolution (1 or 2 cm) which were termed point-samples. Inserted diagrams (a-k) showing tephra concentrations of the high-resolution point-samples. The pentagram denotes the stratigraphic position of each identified cryptotephra layer. Note that the tilde at the end of each 1 m core segment (except the first 1 m) indicates a 9 cm gap of sediment due to a technical issue while coring. The

dashed lines indicate the boundaries between early, mid- and late Holocene based on the age-depth model presented in Fig. 3.3. The Holocene subdivision follows the scheme proposed by Walker et al. (2012).

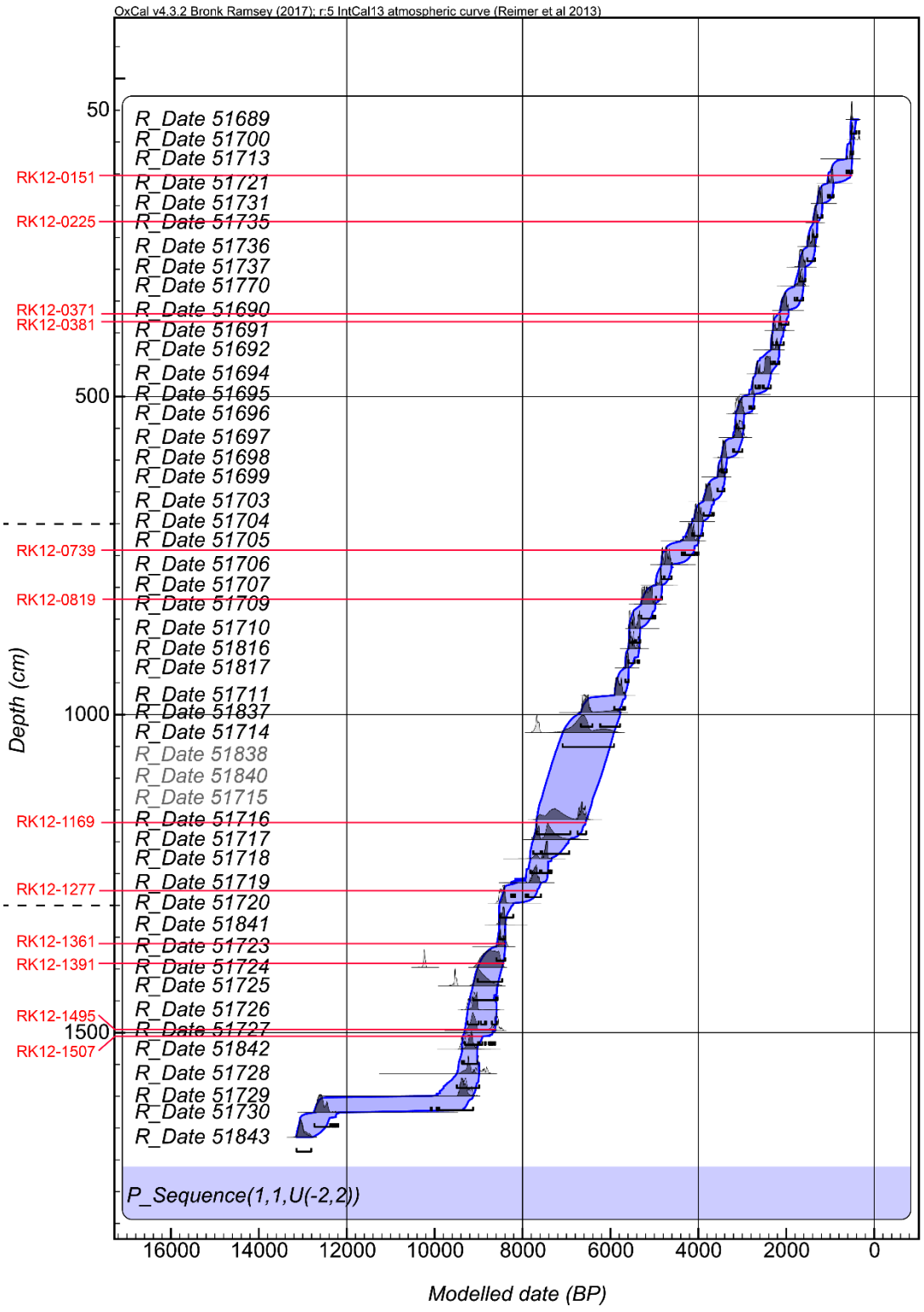

Fig. 3.3 95.4% confidence Highest Probability Density output for the Bayesian age model for Kushu RK12 Holocene sequence. The model was constructed using 49 AMS dates of the RK12 core reported by Müller et al. (2016), run using a *P_Sequence* model in Oxcal ver. 4.3 (Bronk Ramsey 2008, 2009a), with a variable K factor and outlier analysis (Bronk Ramsey and Lee, 2013; Bronk Ramsey, 2009b), applying the IntCal13 calibration curve (Reimer et al., 2013), for providing independent age constraint on tephra identified in the sequence. Identified cryptotephra layers are illustrated based on their stratigraphic positions. The age results are listed in Table 3.1. Note that the dates of three contaminated samples (Poz-51838, 51840, 51715) were removed from the age model as the program can not run through with these dates incorporated. The dashed lines indicate the boundaries between early, mid- and late Holocene. The Holocene subdivision follows the scheme proposed by Walker et al. (2012).

3.6.1.2 Mid-Holocene (8.2-4.2 ka)

The mid-Holocene period spans ca. 600 cm (i.e. CD 1300-700 cm) in the RK12 composite core. Compared with the early Holocene, this section has a lower tephra background revealed by range-finder counts (Fig. 3.2). Four cryptotephra layers are recognised at this interval: RK12-1277, RK12-1169, RK12-0819 and RK12-0739. The lower three (i.e. RK12-1277, 1169 and 0819) are prominent tephra layers with very well defined stratigraphic positions and relatively high concentrations of 130-170 shards/g, more than tripling the background concentrations at their respective intervals (Fig. 3.2e-g). The uppermost tephra RK12-0739 has lower shard counts with concentration of 79 shards/g (Fig. 3.2d).

The age model within the mid-Holocene period comprises higher and lower resolution sections with a split at ca. 6 ka BP (Fig. 3.3). In the lower part (ca. 8.2-6 ka) the age modelling is of lower resolution due to the removal of contaminated ^{14}C dates, and tephras RK12-1277 and RK12-1169 are dated to 7663-8431 cal yrs BP and 6559-7683 cal yrs BP, respectively. The age model displayed higher resolution in the period 6-4.2 ka, where the tephras RK12-0819 and RK12-0739 are dated at 4861-5287 cal yrs BP and 4089-4735 cal yrs BP, respectively.

3.6.1.3 Late Holocene (4.2-0 ka)

The late Holocene covers the uppermost ca. 650 cm sequence (i.e. CD 700-50 cm) in the RK12 composite core. This section includes four cryptotephra layer: RK12-0381, RK12-0371, RK12-0225 and RK12-0151. The RK12-0381 and RK12-0371 are closely located, with glass concentrations of 61 and 59 shards/g respectively (Fig. 3.2c). The upper RK12-0225 is a prominent tephra layer having 331 shards/g dry sediment (Fig. 3.2b). The previously reported layer RK12-0151 (>30,000 shard/g) was correlated to B-Tm tephra from Changbaishan by Chen et al. (2016). Based on the age model, the three newly identified tephra layers RK12-0381, RK12-0371 and RK12-0225 are dated to 1993-2281 cal yrs BP, 1947-2202 cal yrs BP and 1275-1389 cal yrs BP, respectively.

Table 3.1 Summary information of forty geochemical groups identified within twelve tephra layers extracted from the Lake Kushu RK12 Holocene sequence. Geochemical populations highlighted in bold are unique in time and chemistry thus can serve as isochrons for dating and correlating records.

Label	Composite depth (cm)	Age range (cal yr BP)	Tephra concentration (shards/g)	Total analyses (n)	Compositional populations	Correlation for dominant population	Correlation for subordinate population(s)
RK12-0151	150-151	528-1041	30671	66	1	**B-Tm, Changbaishan (n=66)**	NA
RK12-0225	224-226	1275-1389	331	15	2	**SH#12, Shiveluch (n=14)**	Sumatra (n=1)
RK12-0371	370-372	1947-2202	59	4	2	Sumatra (n=3)	Shikotsu (n=1)
RK12-0381	380-381	1993-2281	61	5	2	Shikotsu (n=4)	Sumatra (n=1)
RK12-0739	738-740	4089-4735	79	23	6	**Krakatau (n=8)**	Shikotsu (n=5); **Changbaishan (n=4)**; Komagatake (n=2); **Towada (n=2)**; Sumatra (n=2)
RK12-0819	818-820	4861-5287	168	28	2	**Krakatau (n=26)**	Sumatra (n=2)
RK12-1169	1168-1170	6559-7683	148	21	3	**Ko-g, Komagatake (n=16)**	Shikotsu (n=3); Sumatra (n=2)
RK12-1277	1276-1278	7663-8431	134	24	4	**Ma-f~j, Mashu (n=17)**	Sumatra (n=4); Shikotsu (n=2); Komagatake (n=1)
RK12-1361	1360-1362	8395-8586	120	36	4	Shikotsu (n=14)	Sumatra (n=8); Komagatake (n=7); Aira (n=7)
RK12-1391	1390-1392	8440-8983	58	35	5	N/A	Sumatra (n=12); Shikotsu (n=9); Komagatake (n=8); Aira (n=5); **Changbaishan (n=1)**
RK12-1495	1494-1496	8622-9309	76	17	4	N/A	Shikotsu (n=6); Komagatake (n=4); Aira (n=4); Sumatra (n=3)
RK12-1507	1506-1508	8914-9366	63	15	5	Shikotsu (n=8)	Aira (n=3); Sumatra (n=2); Komagatake (n=1); **Changbaishan (n=1)**

Table 3.2 Summary table of the compositions of geochemical populations identified in the Lake Kushu RK12 Holocene sequence grouped by the provenance.

Area	Rusian		China/N Korea				N Japan										S Japan		Indonesia					
Volcano or sub-region	Shiveluch		Changbaishan				Mashu		Komagatake				Towada		Shikotsu		Aira		Krakatau				Sumatra	
Correlated tephra	SH#12		B-Tm		Unknown		Ma-f~j		Ko-g		Unknown		unknown		Unknown		Unknown		Unknown		Unknown		Unknown	
Ralated horizons in RK12 core	RK12-0225 (D, n=14)		RK12-0151 (D, n=66)		RK12-0739 (S, n=4) RK12-1391 (S, n=1) RK12-1507 (S, n=1)		RK12-1277 (D, n=17)		RK12-1169 (D, n=16)		Group 2: RK12-0739 (S, n=2) RK12-1277 (S, n=1) RK12-1361 (S, n=7) RK12-1391 (S, n=8) RK12-1495 (S, n=4) RK12-1507 (S, n=1)		RK12-0739 (S, n=2)		Group 1: RK12-0371 (S, n=1) RK12-0381 (D, n=4) RK12-0739 (S, n=5) RK12-1169 (S, n=3) RK12-1277 (S, n=2) RK12-1361 (D, n=14) RK12-1391 (S, n=9) RK12-1495 (S, n=6) RK12-1507 (D, n=8)		Group A : RK12-1361 (S, n=7) RK12-1391 (S, n=5) RK12-1495 (S, n=4) RK12-1507 (S, n=3)		RK12-0739 (D, n=8)		RK12-0819 (D, n=26)		Group 3: RK12-0225 (S, n=1) RK12-0371 (D, n=3) RK12-0381 (S, n=1) RK12-0739 (S, n=2) RK12-0819 (S, n=2) RK12-1169 (S, n=2) RK12-1277 (S, n=4) RK12-1361 (S, n=8) RK12-1391 (S, n=12) RK12-1495 (S, n=3) RK12-1507 (S, n=2)	
K- series	Medium-K		High-K		High-K		Low-K		Medium-K		Medium-K		Low-K		Medium-K		Medium-K		Medium-K		Medium-K		High-K	
Composition	Rhyolitic		Trachytic-rhyolitic		Rhyolitic		Dacitic-rhyolitic		Rhyolitic		Rhyolitic		Rhyolitic		Rhyolitic		Rhyolitic		Dacitic-rhyolitic		Dacitic-rhyolitic		Rhyolitic	
wt. (%)	Avg.	±1σ	Avg.	±1σ	Avg.	±1σ	Avg.	±1σ	Avg.	±1σ	Avg.	±1σ	Avg.	±1σ	Avg.	±1σ	Avg.	±1σ	Avg.	±1σ	Avg.	±1σ	Avg.	±1σ
SiO2	76.75	0.57	71.97	4.15	75.04	1.25	73.26	1.39	73.56	0.66	76.43	0.97	74.51	0.56	77.95	0.73	77.82	1.02	72.55	1.29	70.61	1.83	77.56	0.92
TiO2	0.27	0.04	0.31	0.15	0.24	0.04	0.62	0.10	0.58	0.03	0.43	0.04	0.47	0.01	0.15	0.05	0.12	0.07	0.51	0.27	0.53	0.07	0.12	0.13
Al2O3	12.60	0.47	12.15	2.44	10.21	0.49	13.55	1.07	13.26	0.41	12.08	0.40	13.31	0.28	12.27	0.56	12.19	0.50	13.90	0.78	14.81	0.66	12.31	0.64
FeOt	1.18	0.18	4.25	0.45	4.20	0.44	3.09	0.44	2.92	0.18	2.11	0.30	2.39	0.05	1.26	0.41	1.26	0.40	2.83	0.58	2.90	0.52	0.96	0.37
MnO	0.04	0.01	0.10	0.04	0.08	0.04	0.14	0.02	0.11	0.02	0.08	0.01	0.11	0.01	0.06	0.01	0.06	0.02	0.09	0.02	0.11	0.03	0.04	0.02
MgO	0.24	0.03	0.08	0.12	0.01	0.01	0.78	0.16	0.71	0.06	0.41	0.09	0.62	0.03	0.15	0.04	0.10	0.06	0.61	0.23	0.81	0.20	0.09	0.06
CaO	1.13	0.12	0.60	0.54	0.24	0.09	3.48	0.58	3.02	0.17	2.17	0.43	2.88	0.18	1.46	0.14	1.06	0.41	2.59	0.53	3.16	0.55	0.74	0.23
Na2O	4.61	0.34	5.34	0.49	5.31	0.46	4.15	0.27	4.00	0.17	4.28	0.41	4.41	0.02	4.15	0.25	4.04	0.52	4.11	0.19	4.27	0.31	3.42	0.44
K2O	3.15	0.13	4.78	0.65	4.49	0.08	0.77	0.08	1.72	0.07	1.95	0.10	1.22	0.01	2.53	0.18	3.33	0.17	2.71	0.37	2.54	0.27	4.72	0.56
P2O5	0.04	0.01	0.03	0.04	0.01	0.01	0.16	0.03	0.10	0.01	0.06	0.01	0.08	0.01	0.02	0.01	0.02	0.01	0.11	0.06	0.15	0.13	0.02	0.02
n	14		66		6		17		16		23		2		52		19		8		26		40	
Representative compositions (wt.%)																								
SiO2	77.44	76.70	65.67	74.49	72.78	75.89	72.80	74.10	74.13	73.27	76.34	76.74	74.11	74.91	78.32	78.46	78.67	78.30	73.52	73.55	65.78	74.43	77.01	78.06
TiO2	0.27	0.28	0.48	0.23	0.33	0.24	0.69	0.68	0.59	0.58	0.44	0.43	0.47	0.46	0.13	0.14	0.13	0.09	0.30	0.30	0.58	0.34	0.07	0.02
Al2O3	12.45	12.48	15.72	10.29	10.96	9.78	13.54	13.16	12.91	13.77	12.02	11.91	13.51	13.11	11.79	11.21	11.67	11.72	13.96	13.77	16.98	13.92	12.42	12.20
FeOt	0.96	1.12	5.00	4.16	5.06	3.87	3.62	3.29	2.82	2.81	2.18	2.10	2.43	2.36	1.48	1.47	1.35	1.44	2.29	2.26	3.73	1.70	1.24	0.90
MnO	0.04	0.04	0.13	0.14	0.11	0.09	0.17	0.14	0.12	0.12	0.07	0.08	0.12	0.10	0.07	0.07	0.04	0.03	0.08	0.09	0.14	0.07	0.05	0.04
MgO	0.22	0.26	0.18	0.03	0.02	0.00	0.83	0.75	0.68	0.77	0.46	0.50	0.64	0.60	0.13	0.19	0.11	0.08	0.40	0.44	1.24	0.36	0.08	0.03
CaO	1.05	1.11	1.25	0.24	0.42	0.19	3.50	3.17	2.86	2.89	2.39	2.40	3.01	2.75	1.54	1.48	1.17	1.11	2.27	2.50	4.52	2.33	0.71	0.59
Na2O	4.46	4.88	5.64	5.62	5.87	5.38	3.93	3.74	4.02	4.06	4.02	3.73	4.40	4.42	4.25	4.40	3.60	3.82	3.92	4.02	4.72	3.94	3.76	3.50
K2O	3.07	3.09	5.62	4.26	4.44	4.54	0.74	0.80	1.78	1.61	2.03	2.04	1.23	1.21	2.28	2.57	3.26	3.40	3.19	3.01	2.08	2.86	4.64	4.64
P2O5	0.03	0.04	0.07	0.01	0.01	0.02	0.18	0.16	0.10	0.12	0.06	0.08	0.09	0.08	0.02	0.02	0.01	0.01	0.06	0.06	0.22	0.05	0.02	0.02

3.6.2 Glass geochemistry

Major element glass compositions of the RK12 Holocene tephra layers are presented in Table 3.2 grouped by the provenance outlined in section 3.7, and in selected bi-plots in Fig. 3.4. Geochemical analyses regarded as outliers from the main group of data within each sample, based on multiple bi-plots, are excluded from the presented datasets but included in the supplementary material. Glass compositions of Holocene tephra layers in Lake Kushu are mainly rhyolitic, with the exception of RK12-1277, RK12-0819 and one of the populations of RK12-0739 extending to less silicic dacitic compositions, and RK12-0151 to trachytic compositions (Fig. 3.4a). Glasses are classified into four series: the tholeiitic low-K series, the calc-alkaline medium-K and high-K series, and the shoshonitic high-K series (Fig. 3.4b).

The low-K series includes the dominant population of RK12-1277 (n=17) and a subordinate population from RK12-0739 (n=2). The medium-K series encompasses most of the prominent mid- to late Holocene tephra layers, including the dominant population of RK12-1169 (n=16), RK12-0819 (n=26), RK12-0739 (n=8) and RK12-0225 (n=14). A large amount of glasses from four early Holocene layers (i.e. RK12-1507, 1495, 1391 and 1361) were also plotted within the medium-K series and glasses from each layer cannot be distinguished from one anther (Fig. 3.4b). Interestingly, however, these early Holocene glasses seem to collectively form three populations separated by their K_2O values. Note that the glass compositions of two of these populations are not restricted only in the early Holocene period, as minor population glasses of mid- to late Holocene layers were also plotted in their compositional envelops. Therefore they were highlighted using ellipses to define them as compositional groups 1&2 (Fig. 3.4b-d). Group 1 encompasses glasses from nine tephra layers with the exception of RK12-0819, RK12-0225 and RK12-0151, whereas group 2 includes glasses from six layers with four in early Holocene and two in mid-Holocene (Table 3.2). Glasses in the calc-alkaline high-K series also show a special compositional group hereby named group 3 (Fig. 3.4b). This group contains glasses from eleven tephra layers except for RK12-0151, and they cannot be distinguished from each other (Fig. 3.4b-d). Given that the compositions of the three groups repeatedly occur within the Holocene period, for clarity these data will be dealt with separately, and excluded from diagrams while correlating specific chemical groups of a given layer. The calc-alkaline

high-K series also comprises the rhyolitic components of RK12-0151 and the subordinate populations of RK12-0739 (n=4), RK12-1391 (n=1) and RK12-1507 (n=1). The high-K shoshonite series mainly comprises the trachytic glasses of tephra layer RK12-0151 (Fig. 3.4b).

To summarise, two main characteristics of the RK12 Holocene tephra layers can be seen from the selected bi-plots:

1) most of the tephra layers comprise more than one compositional population, with some of them displaying a dominant composition (see Table 3.1);
2) certain compositions occur repeatedly in several samples while these samples are stratigraphically separated (e.g. compositional groups 1, 2 and 3, see Table 3.2).

These mixing and repeating of compositions, however, does not necessarily indicate reworking of tephra from the catchment or within the core. On the one hand, a 2 cm sub-sampling interval within the core equals ca. 12 years in time based on our age model, which allows multiple eruptions to be recorded in one single sample, given the observed frequency of volcanic eruptions in the region in historical time (Global Volcanism Program, 2018). Additionally, the absence of compositions of prominent tephra layers (e.g. RK12-1277, RK12-1169) in overlying samples, eliminates a prolonged reworking process in the RK12 sedimentary record. Taken together these two points suggest that all the glasses reported from the RK12 core are highly likely to be primary deposits. Therefore, samples with mixed populations can be explained as recording eruptions from different volcanic centres that occur within the sampling resolution, and the recurrence of the same compositions at different times can be explained by resurgence of the same volcanic centre or volcanoes within the tephra fall catchment of the lake that have very similar chemical signatures.

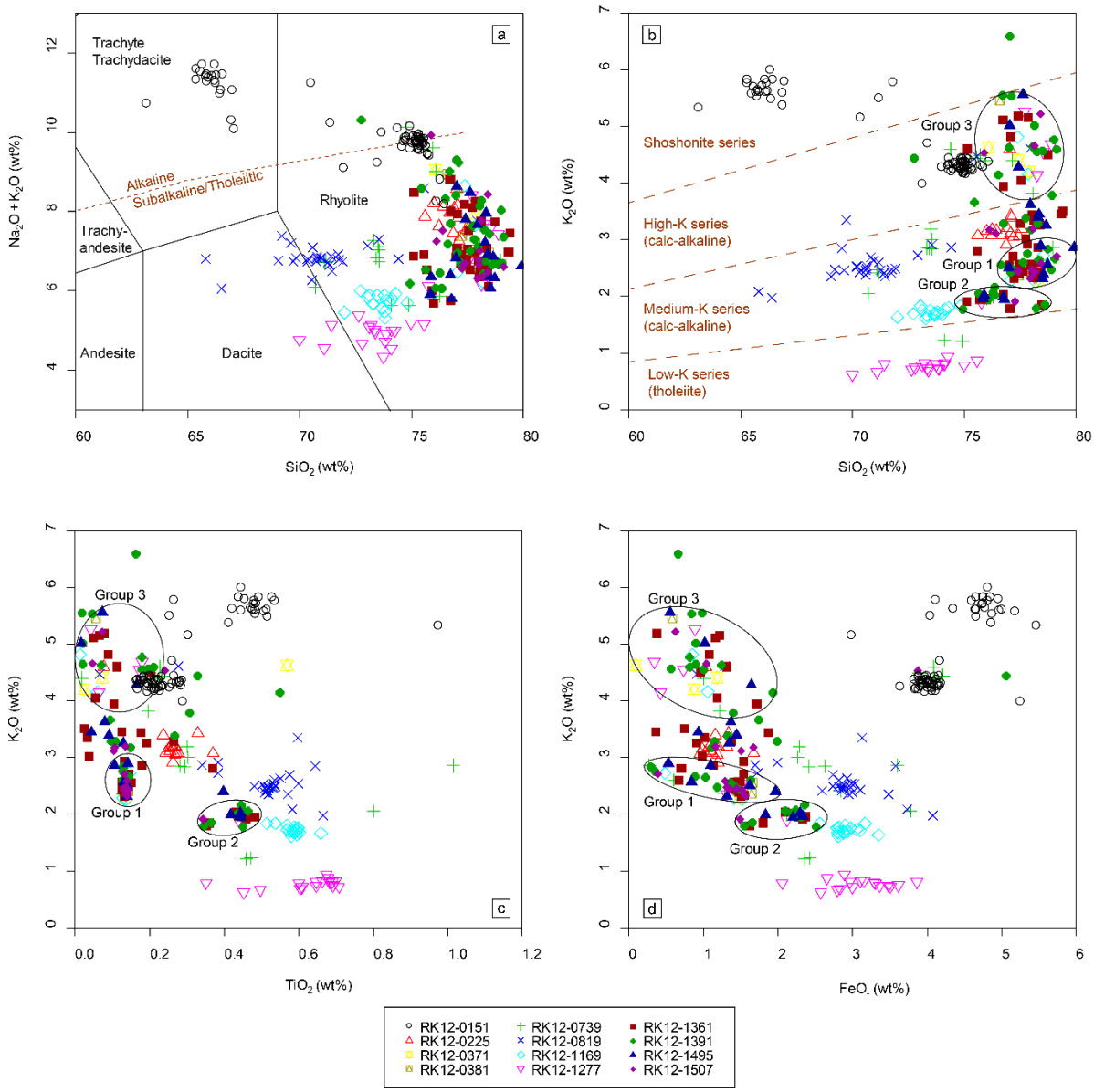

Fig. 3.4 Glass shard major element compositions of cryptotephra layers identified in the Lake Kushu RK12 Holocene sequence. The tephra layers are labelled using their composite depths. (a) Total alkaline versus silica (TAS) diagram (classification scheme based on Le Bas et al. (1986)), (b) K-classification diagram (classification scheme based on Peccerillo and Taylor (1976)), (c-d) Bivariate plots of TiO_2 and FeO_t versus K_2O. Glass shards from stratigraphically separated layers with indistinguishable compositions are highlighted as compositional groups 1, 2 and 3. Given that the compositions of the three groups repeatedly occur within the Holocene period, for clarity these data will be dealt with separately, and excluded from diagrams while correlating tephra layers.

3.7 Tephra correlation

A combination of relative stratigraphy, geochemical compositions and depositional modelled age were used to correlate the RK12 Holocene tephra layers to their source volcanoes and if possible, to specific eruptions. A summary of the correlations for RK12 glasses is presented in Table 3.1. Given the geographic proximity of Lake Kushu to Hokkaido, glass compositions of RK12 tephra layers were first compared to the Hokkaido Holocene tephras (Nakamura, 2016; Razzhigaeva et al., 2016). A list of eighteen Hokkaido Holocene marker tephras were compiled in Table 3.3. These tephras were erupted from six major volcanic centres in Hokkaido and with EPMA glass data available. Where no match to the local database was found, tephra from a broader region were then considered. Detailed geochemical comparisons and correlations are discussed below.

In summary, glass compositions of the RK12 tephra layers indicate that they are from the following volcanoes or regions:

1) Russia: Shiveluch volcano – RK12-0225
2) China/North Korea: Changbaishan volcano – RK12-0151, RK12-0739 (subordinate), RK12-1391 (subordinate), RK12-1507 (subordinate)
3) Northern Japan: Mashu volcano – RK12-1277; Komagatake volcano – RK12-1169, Group 2; Towada volcano – RK12-0739 (subordinate); Shikotsu caldera – Group 1
4) Southern Japan: Aira caldera – Group A
5) Indonesia: Krakatau volcano – RK12-0819, RK12-0739; Sumatra – Group 3

Table 3.3 Summary information of major marker tephras originating from Hokkaido volcanoes during the Holocene.

Volcano	Tephra	VEI	Tephra volume (km3)	Age	Age ref	EPMA glass chemistry ref
Usu	Us-b	5	2.78	1663 CE	Ōba et al 1983	Nakamura 2016
Komagatake	Ko-a	4	0.34	1929 CE	Katsui et al 1984	Nakamura 2016
	Ko-c1	4	0.21	1856 CE	Katsui et al 1984	Nakamura 2016
	Ko-c2	4	0.36	1694 CE	Katsui et al 1984	Nakamura 2016
	Ko-d	5	2.9	1640 CE	Katsui et al 1984	Nakamura 2016
	Ko-g	5	3	6.5-6.6 cal ka BP	Nakamura and Hirakawa 2004	Nakamura 2016
Tarumai	Ta-a	5	4	1739 CE	Nakamura 2016 and refs therein	Nakamura 2016
	Ta-b	5	2.8	1667 CE	Nakamura 2016 and refs therein	Nakamura 2016
	Ta-c	5	3.3	2.5-2.8 cal ka BP	Nakamura 2016 and refs therein	Nakamura 2016
	Ta-d	5	1.9	9.0-9.7 cal ka BP	Nakamura 2016 and refs therein	Nakamura 2016
Mashu	Ma-b	5	4.6	1.0 cal ka BP	McLean et al 2018	Nakamura 2016
	Ma-d1	4	0.32	4.0 cal ka BP	Yamamoto et al 2010	Nakamura 2016
	Ma-f~j	6	18.6	7.4-7.6/8.4-8.6 cal ka BP	Yamamoto et al 2010, Nakamura and Hirakawa 2004	Razzhigaeva et al 2016
Rausu	Ra-1	3	0.04	0.5-0.7 cal ka BP	Miyaji et al 2000	Nakamura 2016
	Ra-2	4	0.2	1.3-1.5 cal ka BP	Miyaji et al 2000	Nakamura 2016
	Ra-3	N/A	N/A	2.1-2.3 cal ka BP	Miyaji et al 2000	Nakamura 2016
	Ra-S	N/A	N/A	5.3-5.6 cal ka BP	Razzhigaeva et al 2016	Razzhigaeva et al 2016
Tenchozan	Ten-a	3	0.02	1.8-2.0 cal ka BP	Goto 2011	Razzhigaeva et al 2016

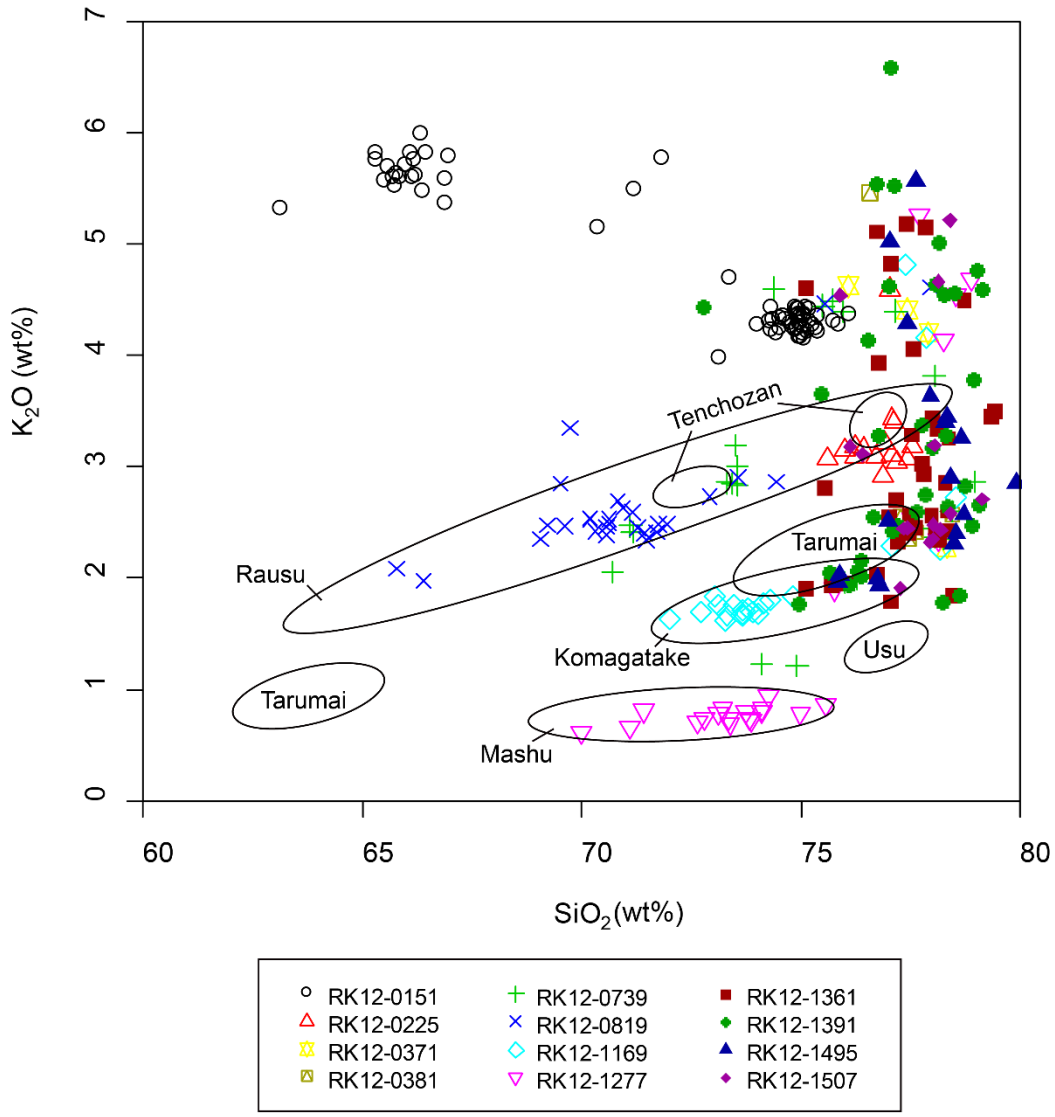

Fig. 3.5 Comparison of glass shard major element compositions between RK12 Holocene cryptotephra layers and Holocene marker tephras from major volcanic centres in Hokkaido Island. The referential compositional fields are defined by compositions of eighteen tephra layers from six Holocene volcanoes which are listed in Table 3.3. Reference EPMA data are from Nakamura (2016) and Razzhigaeva et al. (2016).

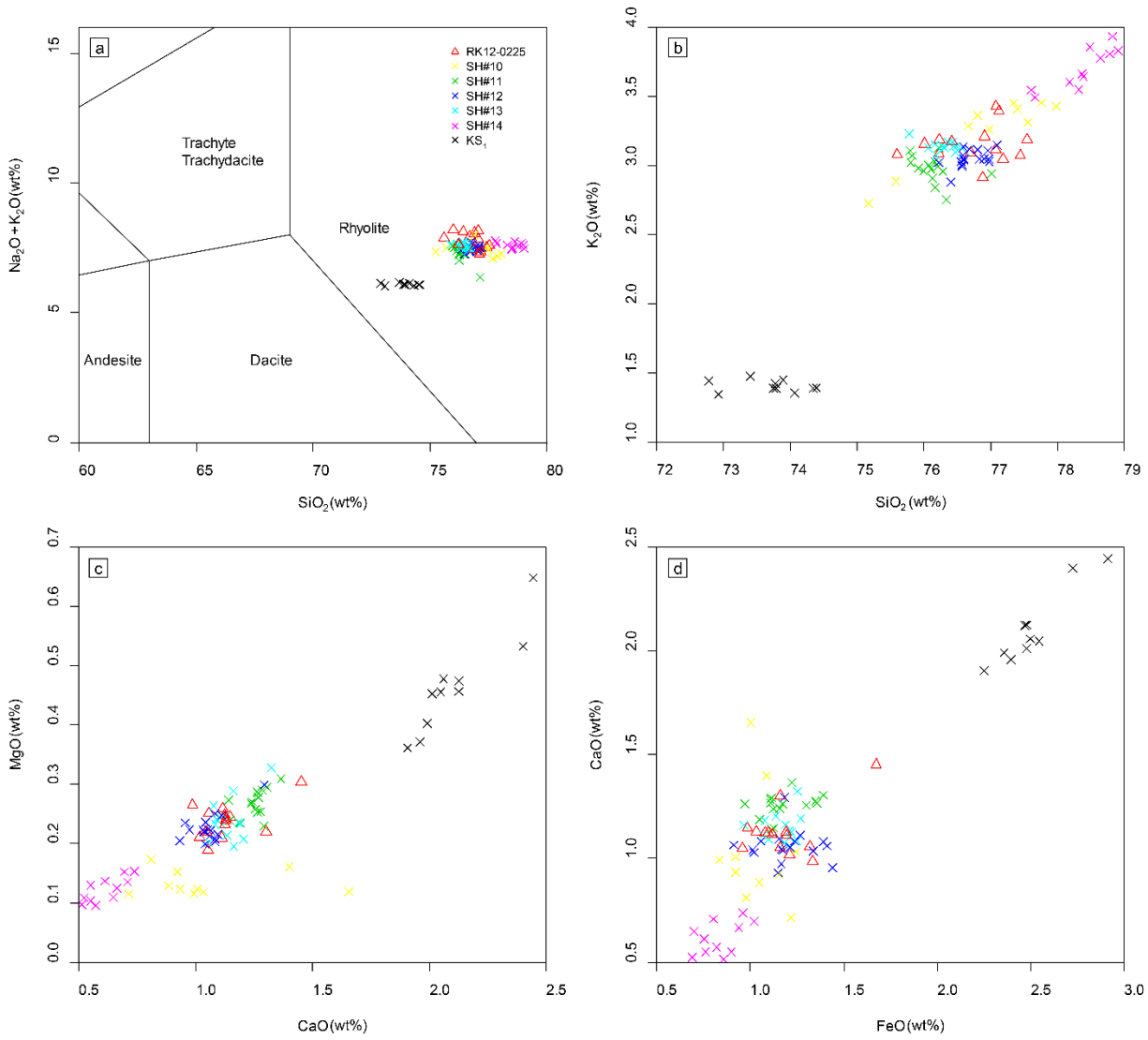

Fig. 3.6 (a) TAS classification diagram (classification scheme based on Le Bas et al. (1986)) and (b-d) major element bivariate plots showing glass compositions of distal RK12-0225 tephra in Lake Kushu and contemporaneous proximal units (SH#10-14) from Shiveluch volcano in Kamchatka Peninsular (Ponomareva et al., 2015), along with glass composition of a prominent regional marker tephra KS_1 from Ksudach volcano (Kyle et al., 2011).

3.7.1 Tephra layer from volcanoes in Russia (RK12-0225)

3.7.1.1 Shiveluch volcano

Shiveluch volcano is a highly explosive eruptive centre, located at the northern end of central Kamchatka Peninsula, Russia, and ~1900 km NE of Lake Kushu (Fig. 3.1). The most recent eruption occurred in January 2018 (https://www.volcanodiscovery.com/shiveluch/news.html), and Shiveluch is known to have had over sixty large eruptions during the Holocene (Global Volcanism Program, 2018). Detailed proximal tephrostratigraphic studies have identified and dated 77 individual pyroclastic units erupted since ~11 ka (Ponomareva et al., 2015). The proximal units were labelled SH followed with the ascending number from young to old (e.g. SH#12; Ponomareva et al., 2017). Geochemical fingerprinting of the Shiveluch Holocene tephras revealed that their glasses display significant compositional variation (Ponomareva et al., 2015), though the time intervals between each eruption during the Holocene were relatively short, with an average eruptive frequency of 100-200 years (Kyle et al., 2011). An updated Bayesian age model, with a total of 223 ^{14}C dates, was presented by Ponomareva et al. (2017). This detailed tephrostratigraphy, chronology and comprehensive geochemical dataset allows any distal Shiveluch tephra to be closely correlated to specific proximal eruptions.

3.7.1.2 Tephra correlation for RK12-0225

The glasses from RK12-0225 tephra are rhyolitic in composition and plot in the calc-alkaline medium-K series (Fig. 3.4a-b). Comparison with the Hokkaido dataset revealed that this tephra is less likely to come from Hokkaido (Fig. 3.5). The strong calc-alkaline medium-K and highly evolved characteristics of RK12-0225 glasses indicate that Shiveluch is a more likely source, whose Holocene glasses also display such characteristics and can be reliably distinguished from the majority of other Holocene tephras in Kamchatka (Ponomareva et al., 2015).

The RK12-0225 tephra has been dated to 1275-1389 cal yrs BP by our age model. Five Shiveluch proximal units chronologically match the RK12-0225 tephra. They are units SH#10, SH#11, SH#12, SH#13 and SH#14, dated to 1260-1365 cal yrs BP, 1295-1371 cal yrs BP, 1311-1408 cal yrs BP, 1326-1499 cal yrs BP and 1358-1553 cal yrs BP respectively (Ponomareva et al., 2017). Glass chemistry reveals that the RK12-0225

tephra can be reliably distinguished from the Shiveluch proximal units SH#10, SH#11, SH#14 and a prominent regional marker tephra KS_1 from Ksudach volcano dated slightly older at 1590-1705 cal yrs BP (Fig. 3.6). Units SH#12 and SH#13 glasses are indistinguishable from glasses of the RK12-0225 tephra on most major elements, except that the SH#13 glasses display slightly elevated CaO values compared to the SH#12 and RK12-0225 glasses (Fig. 3.6c-d).

Importantly a detailed tephrostratigraphic study of eastern Kamchatka has been reported at a distance of 50-100 km east of the Shiveluch volcano (Ponomareva et al., 2017). This study revealed that the SH#12 is the only unit among five (i.e., SH#10-SH#14) which can be traced across all the study sites, while the other four units are absent in any of the mid-range tephra sites. At these localities, SH#12 occurred as a reverse graded tephra layer with a salt-and-pepper colour, comprising fine to coarse sandy ash, with a thickness ranging from 1-4 cm. Based on the field observation and tephra correlation, the study concluded that the SH#12 unit is one of the major tephra markers in this region (Ponomareva et al., 2017).

We propose that the RK12-0225 tephra can be reliably correlated to the proximal SH#12 unit in Kamchatka on the basis of:

(a) independent chronologies that support a match between the proximal SH#12 unit and the distal RK12-0225 tephra;
(b) indistinguishable glass chemistries for proximal SH#12 and distal RK12-0225 that are different from other contemporaneous proximal tephra units (i.e. SH#10, SH#11, SH#13 and SH#14);
(c) a detailed mapping and correlation study suggesting that proximal SH#12 is the only unit among the five contemporaneous units which has the potential to be developed as a regional tephra marker.

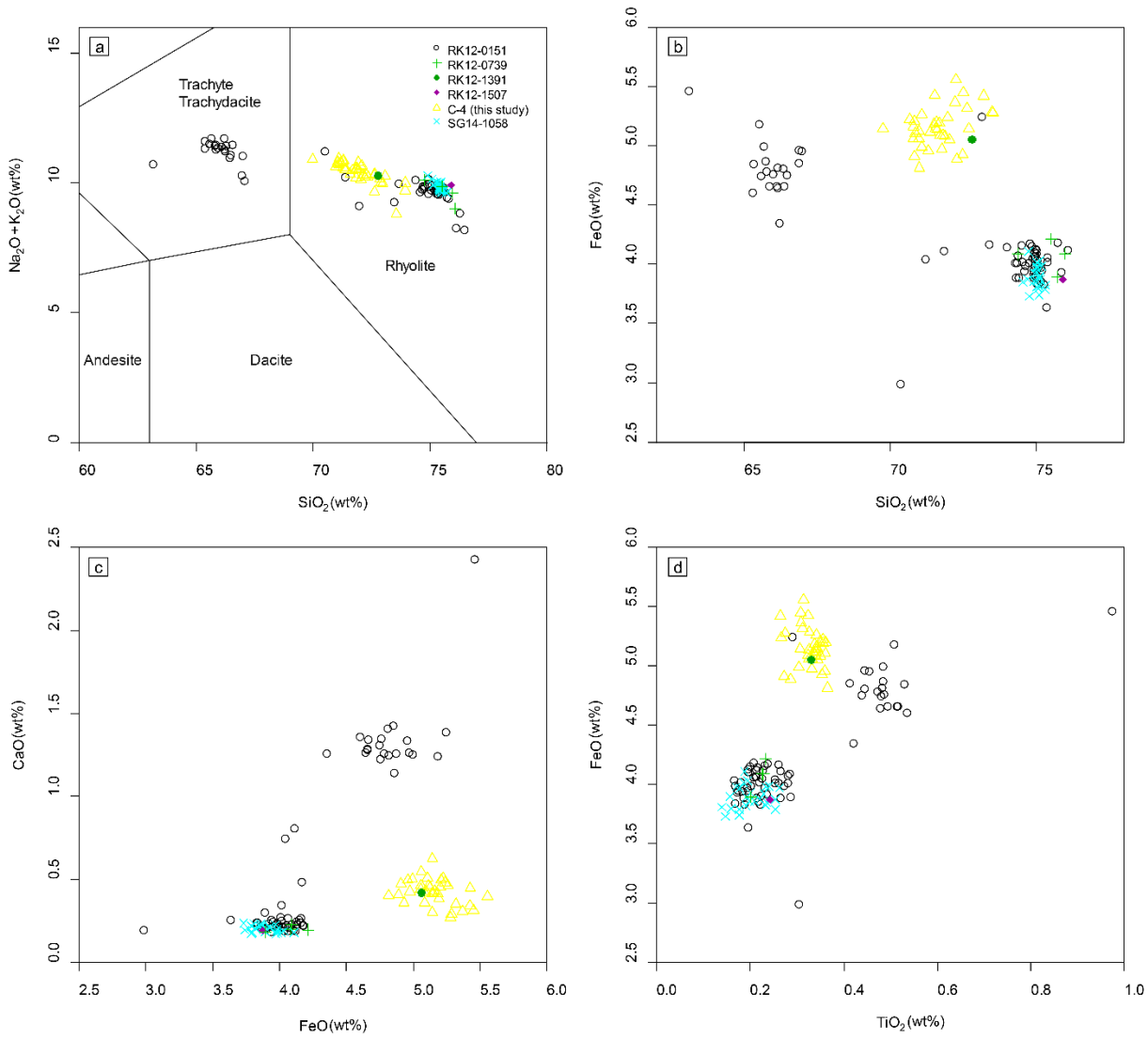

Fig. 3.7 (a) TAS classification diagram (classification scheme based on Le Bas et al. (1986)) and (b-d) major element bivariate plots showing glass compositions of subordinate populations of distal tephra layers (RK12-0739, 1391 and 1507) in Lake Kushu exhibiting typical Changbaishan characteristics, along with glass compositions of a proximal unit sampled from the crater rim of the Changbaishan volcano (C-4, this study) and a distal Changbaishan tephra identified in Lake Suigetsu (SG14-1058, McLean et al., 2018). The RK12-0151 layer was correlated to the B-Tm tephra by Chen et al. (2016) and plotted for comparison.

3.7.2 Tephra layers from volcanoes in China/North Korea (RK12-0151, RK12-0739, RK12-1391, RK12-1507)

3.7.2.1 Changbaishan volcano

Changbaishan volcano is an intraplate stratovolcano on the border between China and North Korea, and ~1100 km SW of Lake Kushu (Fig. 3.1). The volcano is known for its Millennium Eruption (ME) that occurred at 946 CE (Xu et al., 2013; Sigl et al., 2015; Oppenheimer et al., 2017; Hakozaki et al., 2017) with tephra dispersed to northern and central Japan (Chen et al., 2016; McLean et al., 2016) as well as Greenland (Sun et al., 2014a). Despite a number of studies with various dating methods (e.g. ^{14}C, U-series, Ar-Ar, TL and OSL) were undertaken at the proximal sites (e.g., Ji et al., 1999; Wang et al., 2001; Yang et al., 2014; Ramos et al., 2016; Sun et al., 2017), the volcano's Holocene eruptive record is far from conclusive. This is largely due to

(a) the complexity of the proximal eruptive record resulted from resurgent activity and caldera collapse,
(b) inherent difficulties in dating proximal young (<50ka) volcanic rocks (e.g. Ramos et al., 2016),
(c) a focus on the ME deposits (c.f. Sun et al., 2014b) to the detriment of younger and older eruptive deposits (c.f. Wei et al., 2013).

Recently, a previously unknown pre-Millennium Changbaishan tephra (SG14-1058) was reported from Lake Suigetsu, central Japan, which highlighted the importance of distal archives in resolving incomplete proximal eruptive histories (McLean et al., 2018). This layer has later been correlated to a controversial proximal unit (Sun et al., 2018). In the following section we will investigate a proximal pre-Millennium deposit, the C-4 yellow pumice, along with our distal tephras. This unit directly underlies the ME deposits at the proximal crater rim (c.f. Chen et al., 2016) and was dated to 5.3±1.2 ka and 4.2±0.4 ka by U-series and Ar-Ar respectively (Wang et al., 2001; Yang et al., 2014), but considerably younger at 1.9±0.6 ka by OSL method (Sun et al., 2017). We have obtained glass chemistry for this proximal unit to compare with our distal glass chemistry.

3.7.2.2 Tephra correlation for RK12-0151, RK12-0739 (subordinate), RK12-1391 (subordinate) and RK12-1507 (subordinate)

Proximal Changbaishan tephra deposits have distinctive high K_2O and FeO, trachytic to rhyolitic glass compositions (Chen et al., 2016). These glasses can easily be distinguished from the low-K to medium-K Holocene glasses produced from the Japanese arc volcanoes (c.f. McLean et al., 2018), the majority of the Kamchatka Holocene glasses that also display low-K to medium-K characteristics or high-K but less evolved compositions (c.f. Ponomareva et al., 2017), and the phonolitic Holocene glasses from Ulleungdo, South Korea (c.f. Shiihara et al., 2011).

Four stratigraphically separated layers in the Kushu RK12 core contain glasses that are comparable with Changbaishan glass compositions. The youngest one, RK12-0151, was correlated to the proximal ME units based on multi-elemental glass chemistry and independent chronology, thus reliably represents the B-Tm tephra in the RK12 sequence (Chen et al., 2016). The remaining three layers are RK12-0739, RK12-1391 and RK12-1507, dated to 4089-4735 cal yrs BP, 8440-8983 cal yrs BP and 8914-9366 cal yrs BP, respectively. They contain subordinate population of glasses exhibiting typical Changbaishan compositions (e.g. high FeO, Fig. 3.4d).

The subordinate population of RK12-0739 (n=4, 4089-4735 cal yrs BP) and RK12-1507 (n=1, 8914-9366 cal yrs BP) overlap the rhyolitic components of the RK12-0151 (i.e. B-Tm) at major element level (Fig. 3.7). Along with the geochemically indistinguishable SG14-1058 from Lake Suigetsu (8099-8166 cal yrs BP; McLean et al., 2018) (Fig. 3.7), the rhyolitic compositions of B-Tm tephra, which was regarded as a unique ME signature, in fact occurred another three times pre-dated the ME. The distal pre-ME ages of ~4.1-4.7 ka, ~8.1-8.2 ka and ~8.9-9.4 ka overlap with proximal U-series ages (e.g. C-6: 4.3±0.4 ka; C-8: 9.7±1.5 ka; Wang et al., 2001). However, if proximal-distal tephra correlations are to be reliably established, further stratigraphic and geochemical studies from both proximal and distal sites are required.

The subordinate population of RK12-1391 (n=1, 8440-8983 cal yrs BP) has a composition that is similar to the Changbaishan chemistry and matches closely with the proximal C-4 unit (Fig. 3.7). The pre-Millennium C-4 unit has higher FeO_t content coupled with lower CaO content compared to typical ME chemistry thus are distinctive among Changbaishan Holocene tephras (Fig. 3.7c). However, the distal and proximal

ages do not compare as the C-4 unit is considerably younger at ~2 ka to ~4-5 ka (Wang et al., 2001; Yang et al., 2014; Sun et al., 2017). This could be explained as either the C-4 type chemistry has been erupted twice during the Holocene, or that the proximal ages for C-4 are inaccurate. The results we presented here highlight the complexity of the volcano's Holocene eruptive history.

3.7.3 Tephra layers from volcanoes in Northern Japan (RK12-1277, RK12-1169 and RK12-0739)

3.7.3.1 Mashu, Komagatake and Towada volcano

Mashu volcano is situated on the eastern side of Kutcharo caldera in eastern Hokkaido and is 350 km SE of Lake Kushu (Fig. 3.1). The history of Mashu volcano during the past 14 ka can be divided into two stages: the caldera forming stage (ca. 14-7 ka) and the central cone building stage (ca. 6-1 ka) (Kishimoto et al., 2009). At least ten individual Holocene eruptions were identified at proximal sites, of which only two had bulk deposit volume > 1 km^3 (Kishimoto et al., 2009). The two associated tephra markers are Ma-b (4.6 km^3) and Ma-f~j (18.6 km^3) (Table 3.3). The younger Ma-b tephra (ca. 1 cal ka) was recently identified in Lake Suigetsu (McLean et al., 2018), whereas the identification of the volumetrically larger Ma-f~j tephra still remains in the proximal to mid-range sites (e.g. Furukawa and Nanayama, 2006). The Ma-f~j tephra is associated with the caldera-forming activity (VEI=6, LaMEVE database; Crosweller et al., 2012), which began with a phreatomagmatic eruption (Ma-j), followed by Plinian falls (Ma-i,h,g) and ended up with a catastrophic pyroclastic flow (Ma-f) (Katsui et al., 1975). Although the ^{14}C dates of the eruption vary considerably, ranging from ca. 7.4-7.6 cal ka (Yamamoto et al., 2010) to ca. 8.4-8.6 cal ka (Nakamura and Hirakawa, 2004) (Tables 3.3 and 3.4), the Ma-f~j tephra can be distinguished from the proceeding and succeeding eruptions of the same volcano, which produced the small volume phreatomagmatic Ma-k (ca. 11.7 cal ka) and Ma-e (ca. 5.5 cal ka) tephra deposits (Yamamoto et al., 2010).

Komagatake volcano is situated on the Oshima Peninsula in southwestern Hokkaido, 375 km S of Lake Kushu (Fig. 3.1). With numerous small eruptions continuing until recent times (e.g. 2000 CE; Nakagawa et al., 2001), the volcano was believed to have had six major Plinian eruptions during the Holocene, producing two marker tephras in

the mid-Holocene and four tephras in historic time (c.f. Nakamura, 2016). These are tephra layers Ko-g dated precisely at 6.5-6.6 cal ka (Nakamura and Hirakawa, 2004) (or with a larger uncertainty at 6.5-7.2 cal ka (Yoshimoto et al., 2008)), Ko-f dated at 6.2-6.4 cal ka (Okuno et al., 1999), and deposits Ko-d, Ko-c2, Ko-c1 and Ko-a dated precisely by historical records at 1640 CE, 1694CE, 1856 CE and 1929 CE, respectively (Katsui and Komuro, 1984). The eruption that produced the widespread Ko-g tephra was estimated to have a bulk deposit volume of 2.4-3.8 km^3, with a VEI of 5 (Nakamura and Hirakawa, 2004). The Ko-g tephra was dispersed towards the east-northeast (ENE) and has covered most of southern and eastern Hokkaido (Nakamura and Hirakawa, 2004; Furukawa and Nanayama, 2006).

Towada volcano is located in northern Honshu, 555 km S of Lake Kushu (Fig. 3.1). The volcano is believed to have erupted repeatedly throughout the Holocene. At least eight eruptive episodes were identified by previous studies and named using an alphabetical code (Hayakawa, 1985). They are episodes A, B, C, D, D', E, F and G dated at ca. 1.1, 2.8, 6.2, 7.6, 8.3, 9.4, 10.1 and 10.6 cal ka, respectively (Kudo and Sasaki, 2007). The 915 CE To-a tephra (Hayakawa and Koyama, 1998) and the ca. 6.2-6.3 cal ka To-Cu tephra (Inoue et al., 2011), derived from episodes A and C respectively, are the two volumetrically largest Plinian deposits from the volcano during the Holocene (Hayakawa, 1985). Recently, the distal To-Cu tephra was identified in Lake Suigetsu ~700 km away from the source volcano (McLean et al., 2018), illustrating the occurrence of Towada tephra deposits in distal sites.

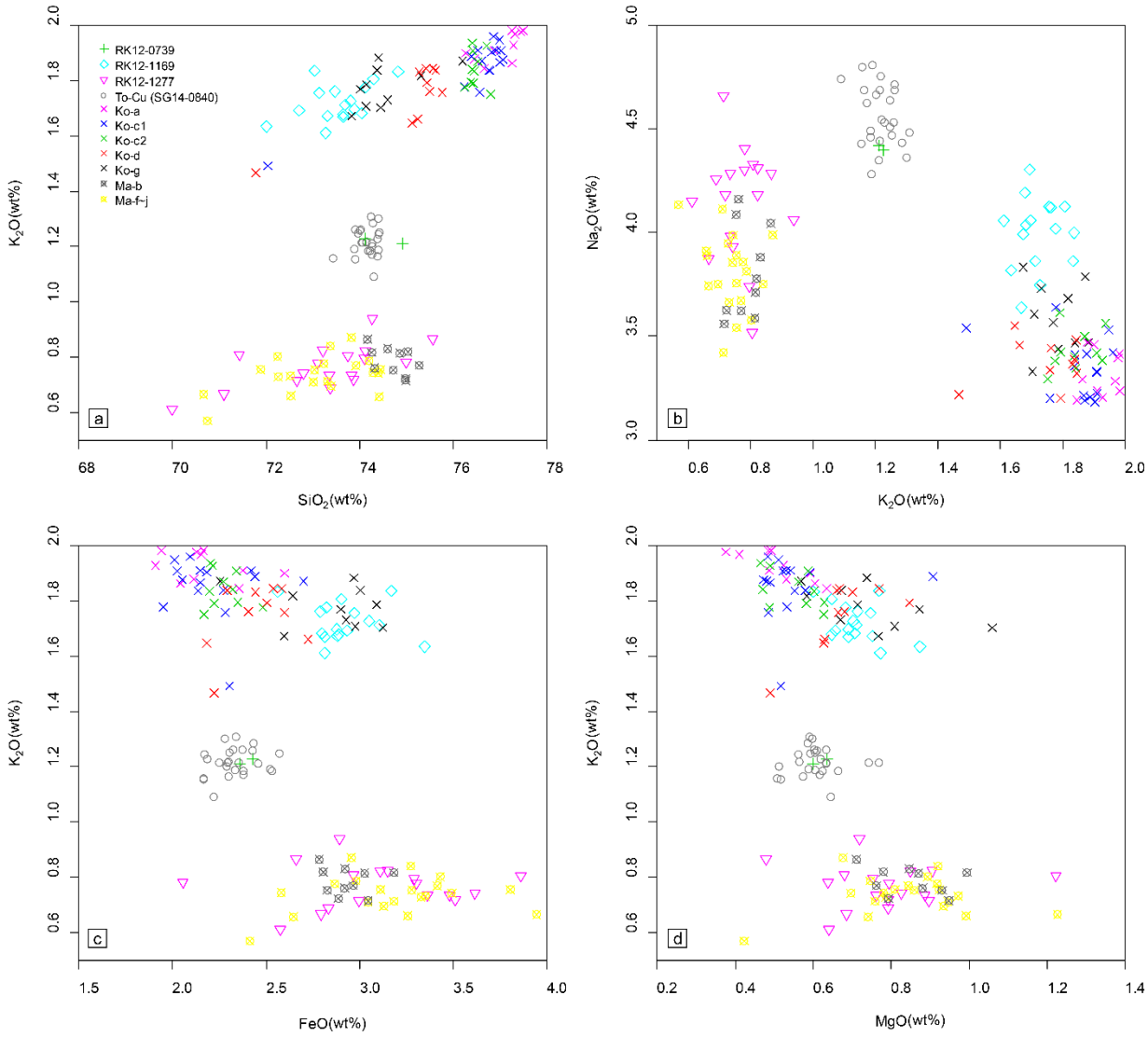

Fig. 3.8 Major element bivariate plots showing glass compositions of distal tephra layers RK12-1169, RK12-1277 and a subordinate population of RK12-0739 in Lake Kushu, along with glass compositions of tephras from Mashu (Nakamura, 2016; Razzhigaeva et al., 2016), Komagatake (Nakamura, 2016) and Towada (McLean et al., 2018) volcanoes in northern Japan.

3.7.3.2 Tephra correlation for RK12-1277, RK12-1169 and RK12-0739 (subordinate)

Glasses of tephra layer RK12-1277 (n=17, 7663-8431 cal yrs BP) ranges from dacitic to rhyolitic in composition (Fig. 3.4a). They have the lowest K_2O values among

all the RK12 glasses and belong to the low-K tholeiite series (Fig. 3.4b). Comparison of glass chemistry with published data revealed that they are from Mashu volcano (Fig. 3.5) and are comparable with the Ma-f~j tephra (Fig. 3.8). Both the RK12-1277 and Ma-f~j tephras can be distinguished from a younger marker tephra Ma-b from the same volcano (Fig. 3.8a). More importantly, the distal age of RK12-1277 matches the proximal ages of Ma-f~j (7.4-8.6 cal ka; Nakamura and Hirakawa, 2004; Yamamoto et al., 2010), and there is no other contemporaneous tephras from the same volcano (see section 3.7.3.1). We thus propose that the RK12-1277 tephra can be confidently correlated to the Ma-f~j tephra, on the basis of glass chemistry and independent chronology.

Glasses of tephra layer RK12-1169 (n=16, 6559-7683 cal yrs BP) are rhyolitic and belong to the medium-K series (Fig. 3.4a-b). Detailed compositional investigation revealed that they are from Komagatake volcano (Fig. 3.5) and closely resemble the Ko-g tephra (Fig. 3.8). On a SiO_2-K_2O diagram, RK12-1169 glasses display slightly lower SiO_2 values than the published Ko-g data (Fig. 3.8a). However, this is due to the apparent Na loss of the published Ko-g data (Fig. 3.8b), resulting in the increase of their SiO_2 values. Glasses of tephra layers from historical eruptions of Komagatake volcano (i.e. Ko-a, Ko-c1, Ko-c2 and Ko-d, Table 3.3) are shown for comparison, and the compositions are more evolved than those of the Ko-g glasses (Fig. 3.8). Chronologically, RK12-1169 matches with the Ko-g tephra (ca. 6.5-7.2 cal ka; Nakamura and Hirakawa, 2004; Yoshimoto et al., 2008), which again, is the only known Plinian tephra deposit in the same time window (see section 3.7.3.1). On these geochemical and chronological grounds, we propose that the RK12-1169 tephra represents the Ko-g tephra in the RK12 sequence.

Tephra layer RK12-0739 contains a subordinate population (n=2, 4089-4735 cal yr BP) which is the only group that plots in the low-K series among the six populations of the RK12-0739 glasses (Fig. 3.4b). The distinctive low-K feature indicates that these glasses are highly likely to come from a volcano in Hokkaido or Northern Honshu. However, comparison with Hokkaido glasses reveal that they were not from major volcanic centres in Hokkaido (Fig. 3.5). On major element bi-plots, these glasses are indistinguishable from glasses of the distal To-Cu tephra (SG14-0840, McLean et al., 2018) from the Towada volcano (Fig. 3.8). Chronologically, this subordinate population of RK12-0739 does not match any known Towada eruptions, as it falls

between the age of two contiguous eruptive episodes (i.e. episodes C and B) which produced the marker tephras To-Cu and To-b dated at ca. 6.2-6.3 cal ka (Inoue et al., 2011) and ca. 2.6-2.8 cal ka (Kudo and Sasaki, 2007) respectively. Given that the absence of (a) the To-Cu tephra in RK12 sequence, and (b) the To-Cu type chemistry in the underlying sample RK12-0819 dated at 4861-5287 cal yr BP, this subordinate population of RK12-0739 seems to indicate the presence of unknown activity from Towada volcano that dispersed the tephra to Lake Kushu, rather than represent the reworked tephra from the ca. 6.2-6.3 cal ka To-Cu eruption despite their geochemical affinity. However, to confirm these conclusions more research is needed in both proximal and distal localities.

3.7.4 Tephra layers from volcanoes in Southern Japan (RK12-1507, RK12-1495, RK12-1391 and RK12-1361)

3.7.4.1 Volcanoes in southern Kyushu

Situated on the subduction zone between the Philippine Sea Plate and the Eurasian Plate, southern Kyushu hosts some of the largest calderas of all Japanese volcanoes (Fig 1). These include Kikai, Aira, Aso and Ata calderas which produced large caldera-forming eruptions during the Holocene and late Pleistocene and dispersed tephra layers that mantled most of the Japanese archipelago (Machida, 1999). The K-Ah tephra (ca. 7.2 cal ka; Smith et al., 2013) from Kikai caldera, the AT tephra (ca. 30 cal ka; Smith et al., 2013) from Aira caldera, the Aso-4 tephra (ca. 87 ka; Aoki 2008) from Aso caldera and the Ata tephra (ca. 105-110 ka; Machida and Arai, 2003) from Ata caldera are the most representative and were estimated to have extremely large bulk deposit volume of >150 km^3, >450 km^3, >600 km^3 and >300 km^3, respectively (Machida, 1999).

Shortly after the large-scale AT formation of the Aira caldera, Sakurajima volcano, constructed on the southern rim of the Aira caldera, began its eruptions at ca. 26 cal ka (Okuno et al., 1997; Kobayashi and Sasaki, 2014). The eruptions of the Sakurajima volcano were believed to be fed from the magma chamber beneath the Aira caldera (Takahashi et al., 2013). In the last 26 cal ka, the volcano has erupted seventeen times producing tephra units Sz-P17 to Sz-P1 (c.f. Kobayashi and Sasaki, 2014). However, most of these are small volume eruptions with bulk volume <1.5 km^3, except for the 12.8 cal ka Sz-S(P14) eruption which was estimated to have a bulk volume of 14 km^3

(Kobayashi and Sasaki, 2014). Therefore, the Sz-S tephra was regarded as one of the prominent tephra markers within the last deglaciation in southern Japan (Moriwaki et al., 2011).

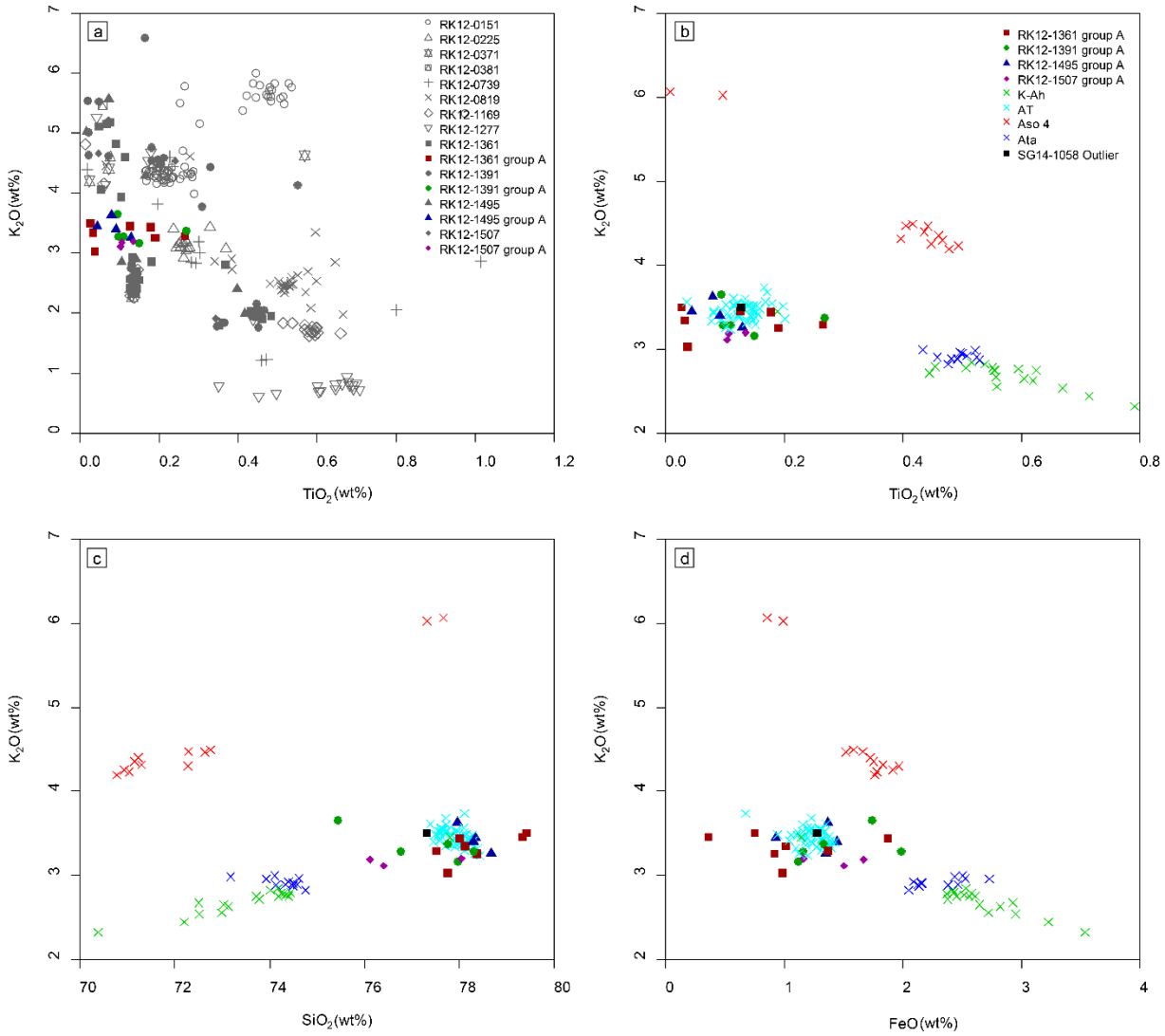

Fig. 3.9 Major element bivariate plots (a) showing glass compositions of group A tephra comprising subordinate populations from four early Holocene distal tephra layers (RK12-1361, 1391, 1495 and 1507) in Lake Kushu which collectively define unique compositional fields among all RK12 glasses, (b-d) showing compositional comparison of glasses between group A tephra and late Quaternary marker tephras derived from large caldera-forming eruptions in southern Kyushu, including K-Ah tephra from Kikai caldera, AT tephra from Aira caldera, Aso-4 tephra from Aso caldera and Ata tephra from Ata caldera (Smith et al., 2013). An outlier analysis of tephra layer SG14-1058

from Lake Suigetsu (McLean et al., 2018), whose composition matches those of the AT and group A glasses, is also shown for comparison.

3.7.4.2 Tephra correlation for RK12-1507, RK12-1495, RK12-1391 and RK12-1361 (Group A)

Early Holocene tephra layers RK12-1507 (8914-9366 cal yrs BP), RK12-1495 (8622-9309 cal yrs BP), RK12-1391 (8440-8983 cal yrs BP) and RK12-1361 (8395-8586 cal yrs BP) each contain subordinate populations of glasses (n=3, 4, 5 and 7 respectively) that collectively define unique compositional fields among all RK12 glasses (Fig. 3.9a, hereby named group A). Although they are from four different layers, the group A glasses are geochemically indistinguishable from one another and they can be separated from all other RK12 glasses on a TiO_2-K_2O diagram, on the basis of their low TiO_2 (<0.3 wt.%) and medium K_2O (~3.0-3.7 wt.%) contents (Fig. 3.9a). Unlike other populations of the four early Holocene layers which were accompanied by glasses from mid- or late Holocene layers (e.g. populations in groups 1, 2 and 3), the group A compositions were restricted to the early Holocene samples only (Fig. 3.4c). Comparison with the Holocene Hokkaido tephra failed to reveal the provenance of the group A glasses (Fig. 3.5). Neither did the contemporaneous Shiveluch glasses (i.e. proximal units SH#44 to SH#52, Ponomareva et al., 2015) provide a match, despite being evolved and medium-K similar to the group A glasses.

Comparison with the compositions of the late Quaternary marker tephras derived from large caldera-forming eruptions in southern Kyushu revealed that the group A glasses exhibit a strong geochemical affinity with the ~30 ka AT tephra from Aira caldera (Fig. 3.9b-d). Despite the matches on most major element bi-plots, group A glasses display a larger compositional variation (Fig. 3.9b-d). Chronologically, the huge age discrepancy between group A glasses (ca. 8.4-9.4 cal ka) and the AT tephra precludes a possible correlation. Meanwhile, the group A glasses are less likely to represent reworked AT tephra, as the tephra counts profile revealed relatively low shard concentrations in underlying samples (CD: 1640-1560 cm) whereas increases of shard concentrations occurred in CD 1560-1350 cm where these group A glasses located in (Fig. 3.2).

It is worth noting that a cryptotephra layer at ca. 8.1 cal ka in Lake Suigetsu (SG14-1058, McLean et al., 2018) contains one analysis which was regarded as an outlier but perfectly matches the compositions of both the AT tephra and our group A glasses (Fig. 3.9b-d). During the time frame of ca. 8.4-9.4 cal ka where the group A glasses were identified in Lake Kushu, the Suigetsu sequence recorded two tephras (i.e. SG14-1091 and SG14-1185) but neither of them contains any AT-type glass. Nevertheless, the single outlier analysis in Suigetsu SG14-1058 and the multiple layers in Kushu (i.e. group A) collectively indicate that tephra shards exhibiting AT-type chemistry were somehow erupted and transported to central and northern Japan during the time frame of ca. 8.1-9.4 ka. Importantly, the Aira caldera is clearly one of the possible provenances of these previously unknown tephra deposits, given their geochemical affinity, and that the caldera once dispersed AT tephra towards the ENE, covering most of Kyushu, Honshu and probably some part of Hokkaido (Machida, 1999).

Further comparison between group A glasses and glasses of late glacial to early Holocene tephra layers from the Sakurajima volcano (i.e. current Aira volcanic centre) however, revealed no close match. Tephra layers from Sakurajima volcano, including the Sz-S (P14), Sz-Tk3 (P13) and Sz-Ub (P12) dated at ca. 12.8 cal ka, 10.6 cal ka and 9.0 cal ka respectively, are clearly separated from the AT compositions on major element bi-plots (c.f. Fig. 3.4 in Moriwaki et al., 2016) hence are not matching the group A glasses either. Therefore, the group A glasses should not directly erupt from this known Aira volcanic centre, whose magma chamber system was believed to be closely related to that of the Aira caldera (Takahashi et al., 2013). As a result, the identification of early Holocene AT-type glasses in Lake Kushu and Suigetsu seems to call into question the post-caldera eruptive history of Aira caldera. No matter which volcanic centre these early Holocene AT-type glasses are from, the volcano must have tapped a different magma chamber from those which have continuously fed the Sakurajima volcano.

3.7.5 Tephra layers from volcanoes in Indonesia (RK12-0819 and RK12-0739)

3.7.5.1 Krakatau volcano

Krakatau volcano at 6° S, ~6700 km SW of Lake Kushu, is located in the Sunda Strait between the islands of Sumatra and Java, Indonesia (Fig. 3.1a). Causing more than 36000 fatalities, the colossal eruption (VEI=6) of the volcano on August 26-27, 1883 was ranked as one of the largest eruptions in historic time (Newhall and Self, 1982). The eruption destroyed most of the origin island and left the Krakatau as a 300 m deep and 6 km wide submarine caldera (Sigurdsson et al., 1991). A bulk tephra volume of 22.4 km^3 was estimated, the majority of which was deposited in the sea (Mandeville et al., 1996b). Although this eruption was well documented by eyewitness accounts and previous studies, the pre-historic eruptive record of the volcano remains largely unknown, owing to the difficulties in accessing the remnant islands and reconstructing Indonesian volcanism (e.g. high erosion rates, dense vegetation covers; Salisbury et al., 2012). Recently, Chen et al. (in preparation) proposed identification of Indonesian tephra with a probable Krakatau provenance in northern Japan, on the basis of distal-proximal tephra correlation.

3.7.5.2 Tephra correlation for RK12-0819 and RK12-0739 (subordinate)

Tephra layer RK12-0819 (n=26, 4861-5287 cal yr BP) has heterogeneous compositions ranging from dacitic to rhyolitic and belongs to the medium K series (Fig. 3.10a-b). Although its compositions fall within the Rausu chemical envelop in the K classification diagram (Fig. 3.5), other major element bi-plots (e.g. SiO_2-FeO_t) do not support a match with known Rausu tephras. Further investigation of major Holocene tephra layers within NE Asia also revealed no close match. The provenance of the tephra has eventually been traced into Indonesia and the Krakatau volcano was proposed as a most probable source (Chen et al., in preparation). The RK12 core contains an additional tephra layer RK12-0739 that has a dominant population of glasses whose compositions closely resemble the RK12-0819 tephra. These glasses from RK12-0739 (n=8, 4089-4735 cal yr BP) are also dacitic to rhyolitic and overlap with the RK12-0819 glasses on most major element bi-plots (Fig. 3.10). Differences include the RK12-0739 glasses exhibit less variation in SiO_2 contents but larger variation in TiO_2 contents compared to the RK12-0819 glasses (Fig. 3.4b-c).

Stratigraphically, the RK12-0739 and the underlying RK12-0819 are separated by over 60 cm sediment that exhibits very low tephra counts (Fig. 3.2). Moreover, point-sample counts suggest that tephra distribution of RK12-0819 within the sequence is largely restricted between CD 818-820 cm (Fig. 3.2e). These together indicate that the recurrence of the RK12-0819 type chemistry in the overlying RK12-0739 sample is less likely due to post-depositional processes. As for the mixing chemistry of all RK12-0739 glasses, we have explained earlier that this does not necessarily indicate tephra reworking (see section 3.6.2). In fact, a lack of corresponding major layers in the underlying sequence for the two subordinate populations of the RK12-0739 that are correlated to Changbaishan and Towada volcanoes, indicates that these glasses are probably syn-depositional product, though they are in a multiple populations layer. However, given that the related RK12-0739 glasses only display part of the geochemical variation of the RK12-0819 glasses (Fig. 3.10), we tentatively propose that the RK12 sequence recorded a younger event from the Krakatau volcano. Further geochemical analyses on RK12-0739 glass are needed to confirm these conclusions.

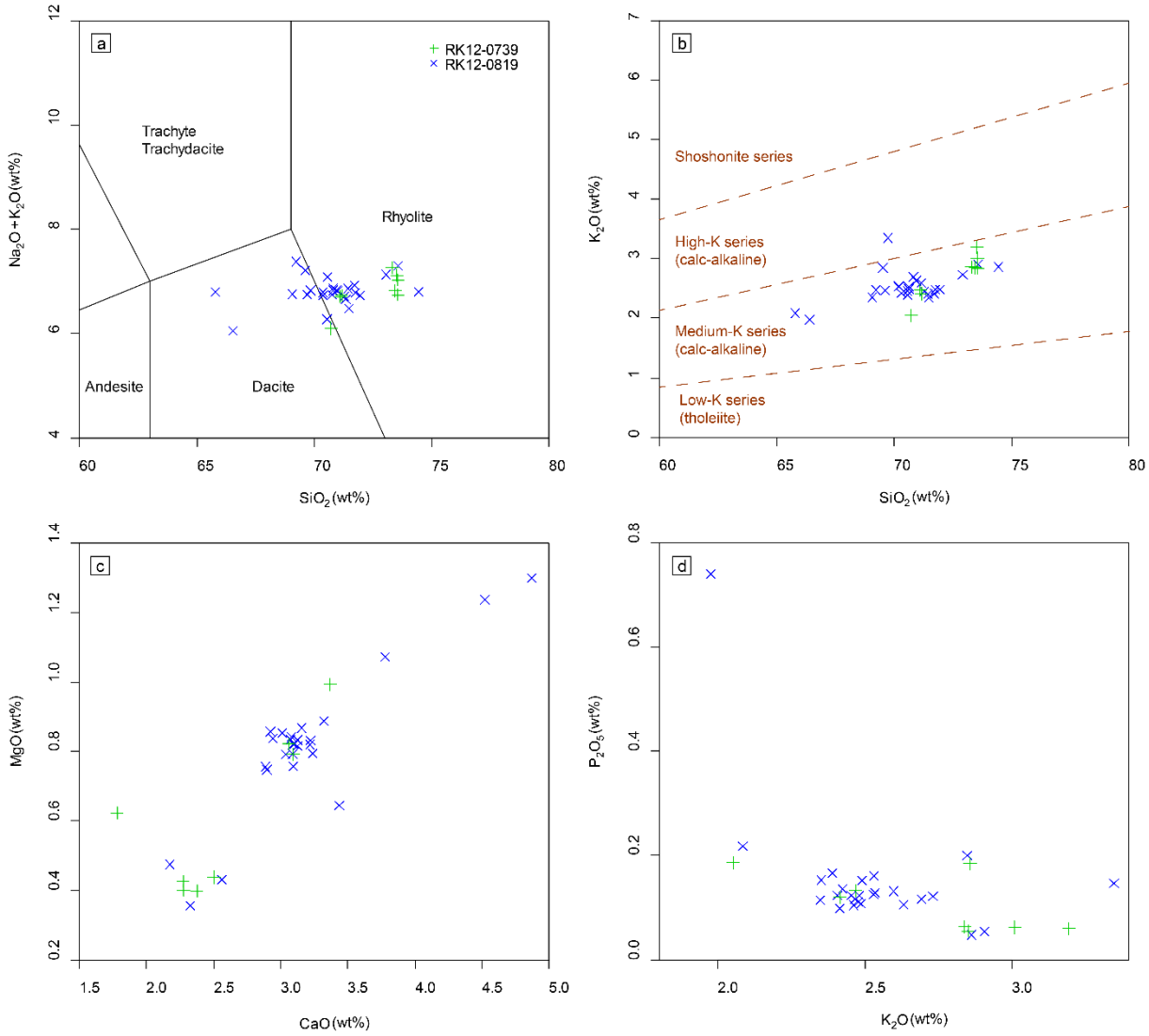

Fig. 3.10 (a) TAS classification diagram (classification scheme based on Le Bas et al. (1986)), (b) K-classification diagram (classification scheme based on Peccerillo and Taylor (1976)) and (c-d) major element bivariate plots showing glass compositions of tephra layer RK12-0819 and a subordinate population of RK12-0739 in Lake Kushu. The RK12-0819 layer has recently been correlated to the Krakatau volcano representing a previously undocumented eruption (Chen et al., in preparation).

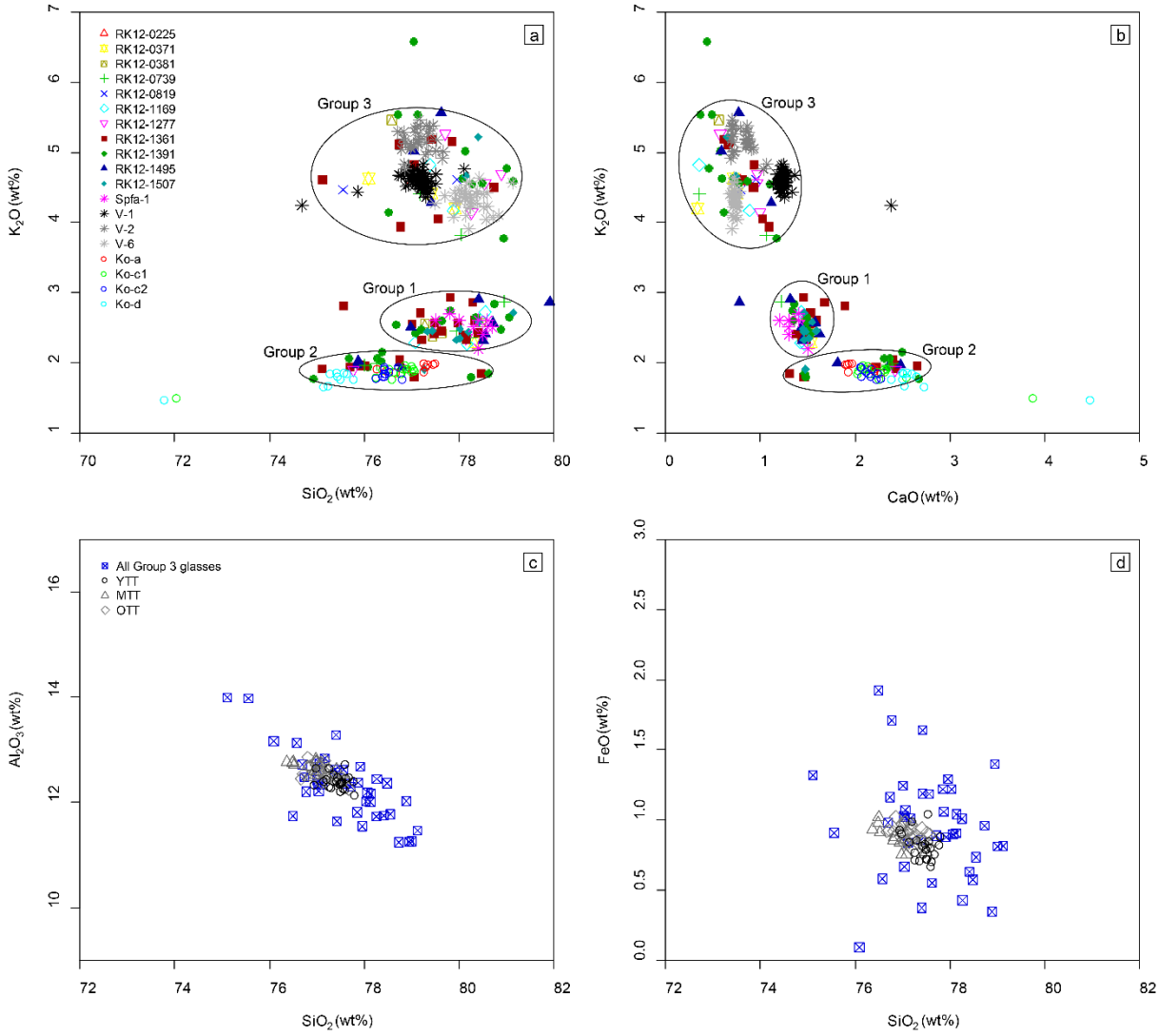

Fig. 3.11 Major element bivariate plots (a-b) showing glass compositions of compositional groups 1, 2 and 3 each containing tephras from multiple layers in Lake Kushu which share similar glass compositions, along with tephras from Shikotsu caldera (Spfa-1; Machida and Arai, 2003), Komagatake volcano (Ko-a, Ko-c1, Ko-c2 and Ko-d; Nakamura, 2016) and Indian Ocean marine cores (V-1, V-2 and V-6; Salisbury et al., 2012) for comparison, (c-d) showing compositional comparison of glasses between the group 3 tephra and Youngest Toba Tuff (YTT), Middle Toba Tuff (MTT) and Oldest Toba Tuff (OTT) from Toba caldera (Smith et al., 2011c).

3.7.6 Recurrent tephra layers (compositional groups 1, 2 and 3)

3.7.6.1 Proposed correlation for Group 1 tephra

The Shikotsu caldera is situated in southwestern Hokkaido and is 300 km S of Lake Kushu (Fig. 3.1). The caldera was formed ~40 ka ago (Katoh et al., 1995) during the climactic eruption that produced the pumice fall deposit Spfa-1 and the subsequent pumice flow deposits Spfl-2 and Spfl-1 (Katsui, 1963). The widespread fall unit Spfa-1 was mainly dispersed towards the southeast and had a thickness of 50 cm at a distance of ~180 km from the volcano (Katsui, 1963). Rishiri Island is the nearest location to Lake Kushu containing the Spfa-1 tephra. Although not situated in the main dispersal axis, Rishiri Island, ~40 km SE of Lake Kushu, recorded the Spfa-1 tephra as a 2 cm thick layer (Ishizuka, 1999). After the caldera was formed, a stratovolcano Tarumai was constructed on the caldera's southeastern rim and has been one of Hokkaido's most active Holocene volcanoes (Table 3.3).

The compositional group 1 contains subordinate populations of glasses from 9 layers with the exception of RK12-0819, RK12-0225 and RK12-0151 (Table 3.2). These glasses are medium-K rhyolitic in compositions and range from early to late Holocene in ages (Fig. 3.4a-b, Table 3.1). Geochemically, they match the late Pleistocene Spfa-1 tephra on most major element bi-plots (e.g. Fig. 3.11a-b) but can be distinguished from Holocene tephras (i.e. Ta-d, Ta-c, Ta-b and Ta-a) from the Tarumai volcano. The Holocene Tarumai tephras have bimodal and less evolved compositions compared to the group 1 tephras (Fig. 3.5). Chronologically, however, the Shikotsu caldera itself does not have any known Holocene activities (Arai et al., 1986).

We propose that the group 1 glasses are more likely to represent undocumented eruptions from the Shikotsu caldera rather than reworked Spfa-1 tephras. This is because the major marker tephras recorded in the RK12 sequence (e.g. RK12-1277, RK12-1169) did not show evidence of a prolonged reworking process. In addition, the continuous reworking of Spfa-1 tephra from ~40 cal ka into the late Holocene will require a fairly thick deposit in the catchment area. However, the Rishiri Island that is located closer to the caldera compared to the Rebun Island only recorded a 2 cm thick Spfa-1 layer, thus it is unlikely for the tephra with a < 2 cm thickness on the further Rebun Island to be reworked for a time period of over 38 ka into the RK12-0371 (ca. 1.9-2.2 cal ka) layer.

3.7.6.2 Proposed correlation for group 2 tephra

Compositional group 2 includes subordinate populations of glasses from four early Holocene layers and two mid-Holocene layers (Table 3.2). These rhyolitic glasses are classified into the medium-K series (Fig. 3.4a-b). Comparison with the Hokkaido Holocene tephras revealed that they are from the Komagatake volcano (Fig. 3.5). The Komagatake volcano is known to have produced six Plinian eruptions during the Holocene, two of which were in the mid-Holocene while the other four were in historic time (< 0.4 cal ka, Table 3.3). Glass compositions of its historic tephras (i.e. Ko-d, Ko-c2, Ko-c1 and Ko-a) are more evolved compared to the mid-Holocene ones (e.g. Ko-g), thus they can be easily distinguished (Fig. 3.8a). The RK12 sequence recorded the mid-Holocene Ko-g tephra of the volcano (see section 3.7.3.2). The additional early to mid-Holocene group 2 glasses in the sequence have very similar chemical affinities to the historic glasses (Fig. 3.11a-b), and do not show a clear match to any reported tephra in their timeframe for geographically closer volcanoes. While there are major differences in the age of the tephras, their chemical similarity indicates that the volcano probably produced geochemically indistinguishable tephras throughout the Holocene. As no eruptive record was known to predate the volcano's ca. 6.6-6.5 cal ka Ko-g tephra during the Holocene (Ganzawa et al., 2005), this work provides evidence of previously unknown early Holocene eruptions from the volcano, illustrating the importance of distal and cryptotephra studies for unravelling incomplete eruptive records. Nevertheless, considering that the group 2 glasses do not display dominant population in each respective layer, we are not assigning any tephra ages to the volcano in this study.

3.7.6.3 Proposed correlation for group 3 tephra

Compositional group 3 encompasses subordinate populations of glasses from eleven layers except for the youngest RK12-0151 (Table 3.2). These highly evolved rhyolitic glasses are characterised by high K_2O and low TiO_2 contents coupled with large K_2O variation (Fig. 3.4). The distinctive high K_2O characteristic of the group 3 glasses precludes a correlation with Hokkaido Holocene tephras (Fig. 3.5). Aoki and Machida (2006) systematically studied late Quaternary widespread tephras in Japan and the results indicated that the back-arc volcanoes are the most probable sources of tephra with low TiO_2 (<0.2 wt%) and high K_2O (4-6 wt%) contents. However, the Japanese back-arc volcanoes such as Daisetsu-Ohachidaira, Toga, Midagahara (Tateyama) and

Sambe do not have known large eruptions throughout the Holocene (Global Volcanism Program, 2018), whereas their mid- to late Pleistocene tephras do not fully match the group 3 compositions (c.f. Aoki and Machida, 2006; group 3 compositions see Table 3.2). Neither did Holocene tephras from Kamchatka (Kyle et al., 2011; Ponomareva et al., 2015, 2017), China/N Korea (Sun et al., 2017; McLean et al., 2018) and S Korea (Shiihara et al., 2011) provide a match.

Provenance studies for these tephras were thus expanded to include Philippine and Indonesia. Late Pleistocene tephras V-1, V-2 and V-6, found in Indian Ocean marine cores ~300 km away from Sumatra (16GC, 18GC and 65PC, Fig. 3.1a) and dated between ca. 27-110 ka by sedimentation rates (Salisbury et al., 2012), provide geochemical matches. Glasses from these three layers exhibit distinctive low TiO_2 and high K_2O characteristics and can be distinguished from other late Pleistocene to Holocene marine tephras found in the same region (Salisbury et al., 2012). These three tephra layers, though can be separated from one another, collectively define compositional fields that overlap the group 3 tephras in Lake Kushu on all major elements (e.g. Fig. 3.11a-b). Owing to the scarcity of available microprobe data on Indonesian tephras and a lack of direct dating constraints on the three marine tephras, Salisbury et al. (2012) failed to correlate them to their proximal counterparts. However, they suggested that these tephras are very likely to come from volcanoes in Sumatra given the geographic proximity between the marine cores and the island. Meanwhile they pointed out that the V-2 tephra (~110 ka) is geochemically similar to the Youngest Toba Tuff (~75 ka; Mark et al., 2014) from the Toba caldera in northern Sumatra (Fig. 3.1a). Comparison of glass chemistry with the known Toba tuffs (i.e. Oldest, Middle and Youngest Toba tuffs dated at ~790 ka, ~500 ka and ~75 ka respectively; Chesner et al., 1991; Lee et al., 2004) revealed that the group 3 glasses are similar to all three of the Toba tuffs but have greater compositional variation (Fig. 3.11c-d; Smith et al., 2011c). These multiple lines of evidence indicate that the group 3 tephras probably originated from Sumatra, Indonesia. We thus tentatively propose that Lake Kushu continuously received far-travelled tephras erupted from Sumatran volcanoes throughout the entire Holocene. Nevertheless, considering the long distance between Sumatra and northern Japan, and a lack of available glass chemistry dataset on Sumatran Holocene tephra at the moment, the proposed provenance for group 3 glasses is open to falsification, but awaits the discovery of definitive supporting evidence.

3.8 Age modelling

Correlation of distal tephra layers with their proximal counterparts allows the use of proximal ages to constrain the chronology in distal realm (Lowe, 2011). In the RK12 sequence, these include the B-Tm tephra (RK12-0151), the SH#12 tephra (RK12-0225), the Ko-g tephra (RK12-1169) and the Ma-f~j tephra (RK12-1277). Age modelling of the B-Tm tephra was demonstrated by Chen et al. (2016), whereas the distal age of RK12-0225 (i.e. 1275-1389 cal yr BP) shares a similar range and largely overlaps the proximal age of the SH#12 unit (i.e. 1311-1408 cal yr BP), therefore we are not dealing with them in this section. In contrast, we focus on the two mid-Holocene tephras Ko-g (RK12-1169) and Ma-f~j (RK12-1277), whose ages are better constrained in the proximal sites compared to in the distal RK12 sequence.

3.8.1 Ages for Ko-g and Ma-f~j tephras

Past attempts have been made to precisely date the two regional markers, Ko-g and Ma-f~j, using radiocarbon dating, however, individual samples results show considerable variation between studies (Table 3.4). In order to make full use of the available radiocarbon dates, along with their stratigraphic relationship, we followed the method outlined by Blockley et al. (2008) and have applied Bayesian modelling method to integrate all the available information, attempting to provide ages with the highest precision while retaining the accuracy. The dates used in the modelling exercises and their related information are listed in Table 3.4.

Taking the reported ages and the stratigraphic relationship between the dated material and the tephra layer itself, we constructed a Bayesian *Sequence* model for the Ko-g tephra. This model comprises two depositional phases: (1) a phase of dates derived from materials sampled immediately below the Ko-g tephra (i.e. pre-eruption phase), and (2) a phase of dates for eruptions or materials known stratigraphically to be slightly younger than the Ko-g (i.e. post eruption phase). The dates within each phase are stratigraphically unordered in relation to each other, but the two phases have relative stratigraphic order. The logic of the model is that although the Ko-g eruption is considered as a single event in geological terms, the sampling resolution of the available radiocarbon dates allows them to be grouped into different phases, and they provide complimentary chronological information in relation to the timing of the eruption itself.

The pre- and post eruption phases are separated by a boundary, whose age indicates the timing of the Ko-g eruption. The output for this model is presented in Fig. 3.12a with the agreement index [A], which is a measure of the proportion of the overlap between prior and posterior distributions. In the final output, most of the dates have agreement index above 100% and the agreement index for the overall model [Amodel] arises to 109%, suggesting an improvement in precision. As such the final modelled age for the Ko-g tephra, 6478-6657 cal yr BP (95.4%), taking into account all available chronological and stratigraphic information, is accepted to be imported into the RK12 age model later.

The Ma-f~j tephra, dated by charred materials within and below the deposit, has scattered calibrated ages derived from different dated samples, ranging from ca. 7.4-7.6 cal ka (Yamamoto et al., 2010) to ca. 8.4-8.6 cal ka (Nakamura and Hirakawa, 2004). Although the tephra lacks a minimum age constrained by date of stratigraphically overlaying material or eruption, it is still possible to use the Bayesian modelling process to derive reliable calibrated age estimate for the tephra. Here we again take the stratigraphically unordered but related group of dates as a *Phase*. We consider the phase comprising dates derived from materials buried by the tephra as a pre-eruption phase rather than a syn-eruption phase. This is because although the plants were killed by the pyroclastic deposits generated during the eruption, they are more likely to record the atmospheric $^{14}CO_2$ level right before the eruption happened. As such the phase (hereby named pre-eruption phase 2) includes ages that are slightly older than that of the eruption. The sequence model contains another pre-eruption phase (phase 1) that has ages known to be slightly order than the phase 2, which are derived from materials underlaying the tephra itself. There is a boundary separating the two pre-eruption phases, and in this case, the eruption age is indicated by the boundary placing at the top of the sequence. The final output for this model is presented in Fig. 3.12b, with the AI for the overall model being 97%, which is way higher than the reliable cut off value of 60% (Bronk Ramsey, 2008). As a consequence, the final modelled age for the Ma-f~j tephra, 6964-7566 cal yr BP (95.4%), is accepted for our next modelling exercise. This modelled age, taking into account the detailed stratigraphic information, indicates that the age for the Ma-f~j tephra reported by Nakamura and Hirakawa (2004) is apparently too old.

Table 3.4 Summary information of radiocarbon dates used for Bayesian age modelling for the Ko-g and Ma-f~j tephras.

Tephra	Material	Stratigraphic relationship with the tephra	Lab code	14C Age (BP)	Uncertainty 1 sigma	Source Ref	Detailed description	Phase
Ko-g	Plant	Above	Beta-132530	5770	40	Nakamura and Hirakawa 2004	13C corrected	Post eruption
	Humus	Above	JNC Tono-3773	5484	63	Nakamura and Hirakawa 2004	13C corrected	Post eruption
	Charcoal	Above	TKa-12988	5740	130	Yoshimoto et al 2008	Charcoal in tephra P1 overlaying P2 above Ko-g	Post eruption
	Charcoal	Above	TKa-12984	5640	70	Yoshimoto et al 2008	Charcoal in tephra P1 overlaying P2 above Ko-g	Post eruption
	Charcoal	Above	TKa-12989	5470	110	Yoshimoto et al 2008	Charcoal in tephra P2 immediately above Ko-g	Post eruption
	Charcoal	Above	TKa-12985	5440	70	Yoshimoto et al 2008	Charcoal in tephra P2 immediately above Ko-g	Post eruption
	Paleosol	Above	NUTA-5783	5480	90	Okuno et al 1999	Below Ko-f，above Ko-g	Post eruption
	Paleosol	Above	NUTA-5785	5530	80	Okuno et al 1999	Below Ko-f，above Ko-g	Post eruption
	Charcoal	Above	NUTA-5384	5730	80	Okuno et al 1999	10cm Below Ko-f，above Ko-g	Post eruption
	Charcoal	Within	TKa-12987	5970	110	Yoshimoto et al 2008	Charcoal within bottom part of Ko-g	Pre-eruption
	N/A	Below	GIN-8945	5900	40	Razzhigaeva et al 2016	Below unit L1-16 which is correlated with Ko-g	Pre-eruption
	Plant	Below	Beta-132531	5760	40	Nakamura and Hirakawa 2004	13C corrected	Pre-eruption
	Wood	Below	JNC Tono-4269	5825	62	Nakamura and Hirakawa 2004	13C corrected	Pre-eruption
Ma-f~j	Charcoal	Within	DHT201	6510	70	Yamamoto et al 2010	Charred material within Ma-f	Pre-eruption 2
	Charcoal	Within	DHT202	6730	60	Yamamoto et al 2010	Charred material within Ma-f	Pre-eruption 2
	Charcoal	Within	GaK-247	6460	130	Katsui 1963	Charcoal within Ma-f, old research	Pre-eruption 2
	Humus	Below	DHT103	6920	50	Yamamoto et al 2010	Charred sample from soil below Ma-j	Pre-eruption 1
	N/A	Below	GIN-13454	7270	50	Razzhigaeva et al 2016	Below unit L1-17 which is correlated with Ma-f~j	Pre-eruption 1
	N/A	Below	LU-6103	7610	60	Razzhigaeva et al 2016	Below unit L1-17 which is correlated with Ma-f~j	Pre-eruption 1
	N/A	Below	GIN-13470	6880	70	Razzhigaeva et al 2016	Below unit L1-17 which is correlated with Ma-f~j	Pre-eruption 1
	N/A	Below	GIN-8629	7180	100	Razzhigaeva et al 2016	Below unit L1-17 which is correlated with Ma-f~j	Pre-eruption 1
	Humus	Below	JNC Tono-3774	7700	69	Nakamura and Hirakawa 2004	Below Ma-f while Ma-g~j missing, 13C corrected	Pre-eruption 1
	Humic acid	Below	GaK-2594	7120	180	Katsui et al 1975	Old research	Pre-eruption 1

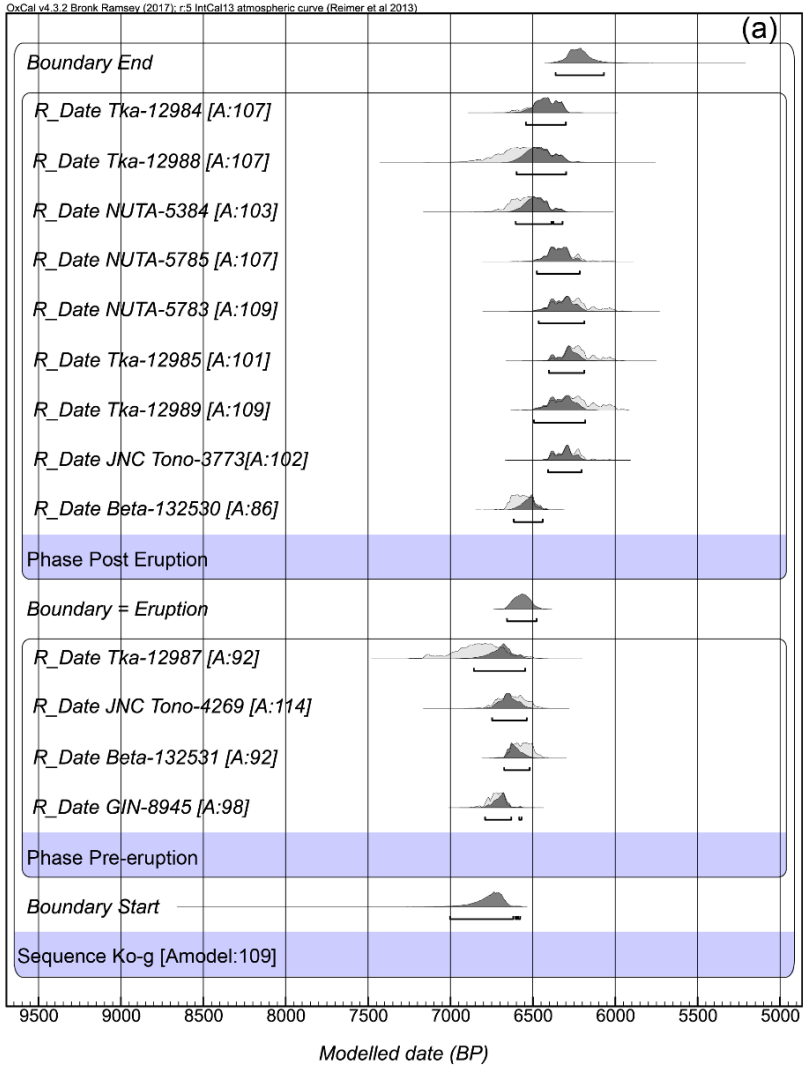
OxCal v4.3.2 Bronk Ramsey (2017); r:5 IntCal13 atmospheric curve (Reimer et al 2013)
(a)
Boundary End
R_Date Tka-12984 [A:107]
R_Date Tka-12988 [A:107]
R_Date NUTA-5384 [A:103]
R_Date NUTA-5785 [A:107]
R_Date NUTA-5783 [A:109]
R_Date Tka-12985 [A:101]
R_Date Tka-12989 [A:109]
R_Date JNC Tono-3773[A:102]
R_Date Beta-132530 [A:86]
Phase Post Eruption
Boundary = Eruption
R_Date Tka-12987 [A:92]
R_Date JNC Tono-4269 [A:114]
R_Date Beta-132531 [A:92]
R_Date GIN-8945 [A:98]
Phase Pre-eruption
Boundary Start
Sequence Ko-g [Amodel:109]
9500 9000 8500 8000 7500 7000 6500 6000 5500 5000
Modelled date (BP)

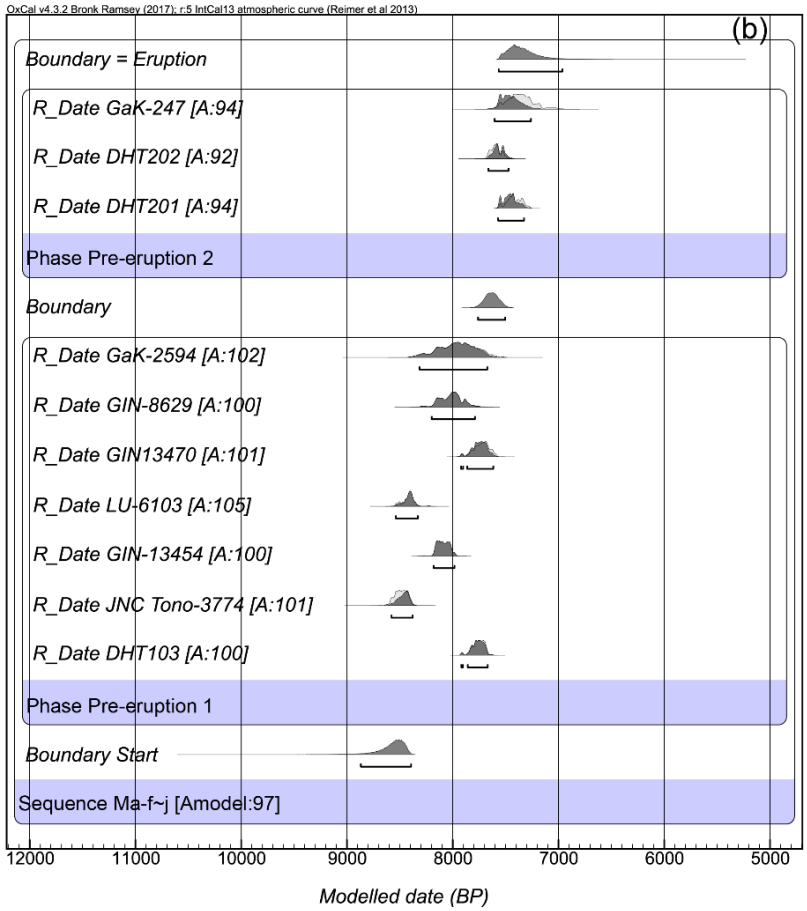
OxCal v4.3.2 Bronk Ramsey (2017); r:5 IntCal13 atmospheric curve (Reimer et al 2013)
(b)
Boundary = Eruption
R_Date GaK-247 [A:94]
R_Date DHT202 [A:92]
R_Date DHT201 [A:94]
Phase Pre-eruption 2
Boundary
R_Date GaK-2594 [A:102]
R_Date GIN-8629 [A:100]
R_Date GIN13470 [A:101]
R_Date LU-6103 [A:105]
R_Date GIN-13454 [A:100]
R_Date JNC Tono-3774 [A:101]
R_Date DHT103 [A:100]
Phase Pre-eruption 1
Boundary Start
Sequence Ma-f~j [Amodel:97]
12000 11000 10000 9000 8000 7000 6000 5000
Modelled date (BP)

Fig. 3.12 95.4% confidence Highest Probability Density Function for the Bayesian *Sequence* age models for the (a) Ko-g (6478-6657 cal yr BP, 95.4%) and (b) Ma-f~j (6964-7566 cal yr BP, 95.4%) tephras. The models are constructed following method outlined by Blockley et al. (2008), run in Oxcal ver. 4.3 (Bronk Ramsey, 2009a), applying the IntCal13 calibration curve (Reimer et al., 2013), for constraining the ages of the two Hokkaido tephras. Radiocarbon dates using in the models and their detailed descriptions are listed in Table 3.4. Based on their stratigraphic relationships with the tephra layers, the dates are separated into different depositional phases and the phases are modelled in stratigraphic order. Boundaries between the phases in (a) and at the top of the sequence in (b) indicate the timing of the eruptions. The percentage of the agreement indices [A] indicates how well the posterior distributions of each date, and the overall model [Amodel], fall within the initial probability distributions of the dates when they are just calibrated without any Bayesian constraints being imposed. See text for methodological details.

3.8.2 Improving the RK12 Holocene age model

In order to apply the tephra ages to constrain the RK12 ^{14}C-based chronology, we again constructed a formal Bayesian age model to integrate all available chronological, stratigraphic and depositional information. Same as the original deposition model shown in Fig. 3.3, we applied a *P_Sequence* model (Bronk Ramsey 2008, 2009a), with a variable K factor and outlier analysis (Bronk Ramsey and Lee, 2013; Bronk Ramsey, 2009b), applying the IntCal13 calibration curve (Reimer et al., 2013). On top of that, this time we have the three tephra ages of the B-Tm, Ko-g and Ma-f~j inserted in the model at the positions where we identified their correlative tephras. Detailed information on the inserted dates and model output are listed in Table 3.5. The deposition model is also illustrated in Fig. 3.13, for comparison with the original deposition model that is not constrained by any tephra ages (Fig. 3.3). The results show that dates for the three correlative tephras in the RK12 sequence have been significantly improved (Table 3.5), which in turn place remarkable constraints on the ages of the sediments that surround these tephra layers (Fig. 3.13).

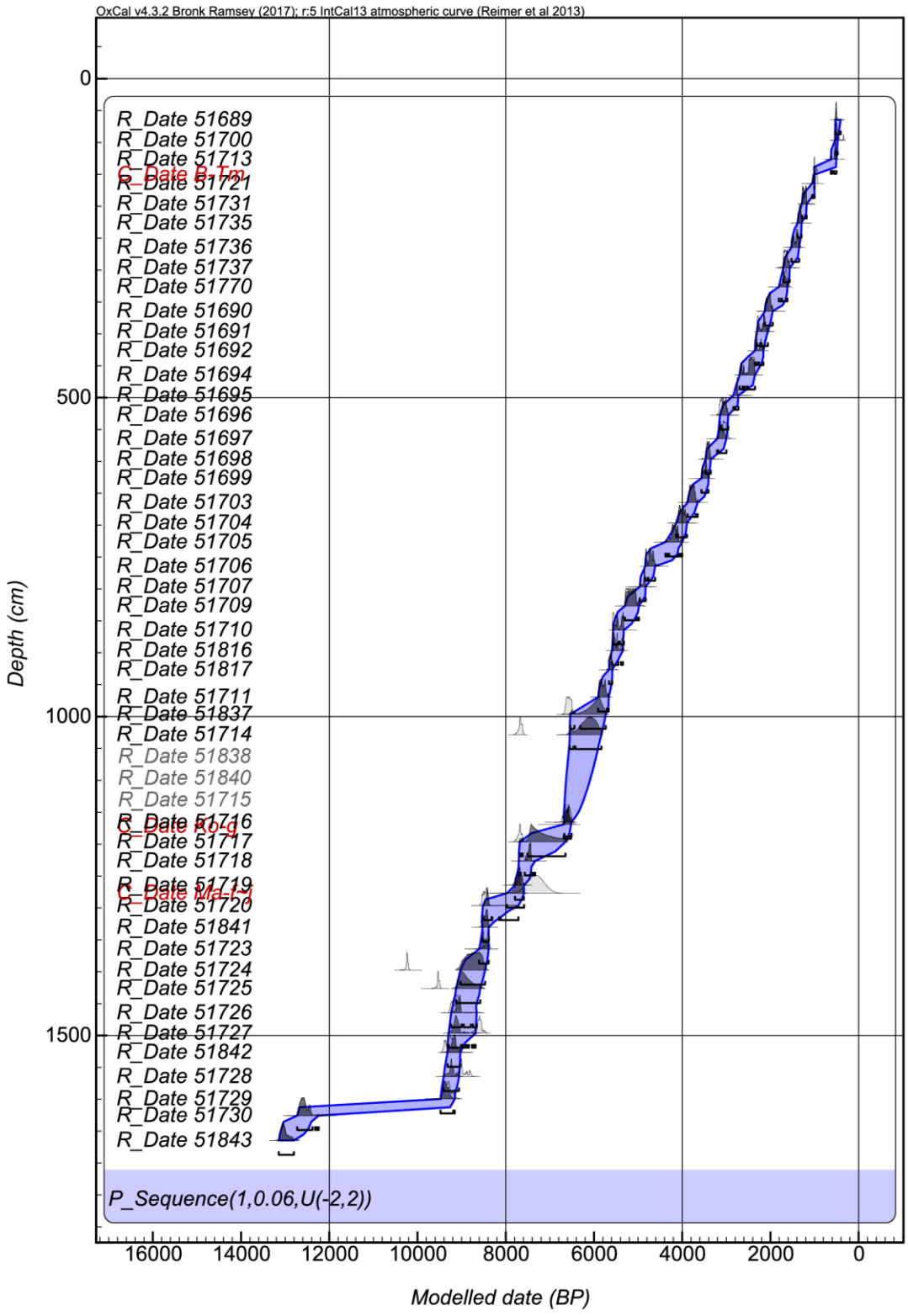

Fig. 3.13 95.4% confidence Highest Probability Density output for the improved Bayesian age model for Kushu RK12 Holocene sequence. Method for construction of this model is the same as that of the model shown in Fig. 3. Apart from the radiocarbon dates used in the original age model, three additional tephra ages of the B-Tm, Ko-g

and Ma-f~j have been inserted in the model at the positions where we identified their correlative tephras. Detailed information on the inserted dates and model output are listed in Table 3.5.

Table 3.5 Summary information of tephra ages that were used to constrain the RK12 age model and the improved ages for the tephra layers after deposition modelling.

Tephra	RK12 correlative layer	CD (cm)	Phase modelled date (95.4%, cal yr BP)	Inserted cal date (μ±σ, cal yr BP)	Age Ref	Final deposition modelled date (95.4%, cal yr BP)	Initial deposition modelled date (95.4%, cal yr BP)
B-Tm	RK12-0151	150.5	N/A	1004±1	Oppenheimer et al 2017	1002-1006	528-1041
Ko-g	RK12-1169	1169	6478-6657	6567±47	this study	6520-6686	6559-7683
Ma-f~j	RK12-1277	1277	6964-7566	7321±189	this study	7585-7976	7663-8431

3.9 Integrated RK12 tephrostratigraphy and its implications

The Lake Kushu RK12 record presents, to our best knowledge, the first comprehensive Holocene cryptotephra stratigraphy in northern Japan, which integrates tephras from multiple regions including Russia, China/N Korea, northern Japan, southern Japan and as far south as Indonesia. A total of twelve cryptotephra layers were extracted from the sequence, within which forty geochemical groups were identified, dated and correlated to their source volcanoes or region of provenance (Tables 1 and 2). Among them, ten unique geochemical groups (highlighted in Table 3.1) within specific layers can serve as isochrons for dating and correlating records while the rest recurrent populations in different layers provide evidence of magma resurgence of the related volcanic centres (Table 3.2). Given that each of the tephra isochrons has its own distribution area, the Lake Kushu record provides a valuable tie-point linking widespread palaeoclimate records. For example, the RK12-0151 was correlated to the B-Tm tephra that has been identified in the Greenland ice-cores (NGRIP and NEEM, Fig. 3.1a; Sun et al., 2014a), the RK12-0225 and RK12-0819 were correlated to tephras identified in Kamchatka and Indonesia respectively. As a result, palaeoclimate archives that span a vast geographic area from high northern latitudes to low southern latitudes, are now possible to be linked through the Lake Kushu record (Fig. 3.1a). We thus suggest that the detailed RK12 tephrostratigraphic record, coupled with an improved

chronology (Fig. 3.13), is one of the very few available Holocene tephrostratigraphy for correlating and linking records in and beyond the East Asia region.

A high-resolution pollen study is published for the upper part of the RK12 Holocene sequence (last ca. 6 ka; Leipe et al., 2018). This record documents the mid- to late Holocene vegetation and climate changes in northern Japan at a bi-decadal resolution. Three key maker tephra layers have been identified within this time period, they are the B-Tm erupted from Changbaishan (Chen et al., 2016), the SH#12 and RK12-0819 derived from Kamchatka and Indonesia, respectively. Interestingly, the oldest RK12-0819 (CD: 820-818 cm) falls very closely to the pollen boundary (CD: 822.5 cm) between local pollen zones 3 and 2b (Fig. 3.14; Leipe et al., 2018). At this time, the lake conditions significantly changed from an unstable lagoon phase characterising by short-term but intensive sea water influxes, to a stable freshwater lake system (Leipe et al., 2018; Schmidt et al., 2019), which might be related to past sea level changes. Identification of this tephra layer in other high-resolution records will permit an assessment of whether this change occurs simultaneously in other regions, which will provide a better understanding of regional variations of past climatic/environmental changes. In addition, the identification of the B-Tm tephra in the sequence (Chen et al., 2016), coupled with the pollen record (Leipe et al., 2018), indicates that the Millennium Eruption of Changbaishan volcano, though with the ability to disperse tephra to Greenland (Sun et al., 2014), had limited or no impact on environments of northern Japan, given that no significant changes were observed on the Kushu pollen record immediately after the eruption (Fig. 3.14). This provides additional evidence to support the limited regional environmental effects of the eruption, despite its great magnitude (6.8; Xu et al., 2013).

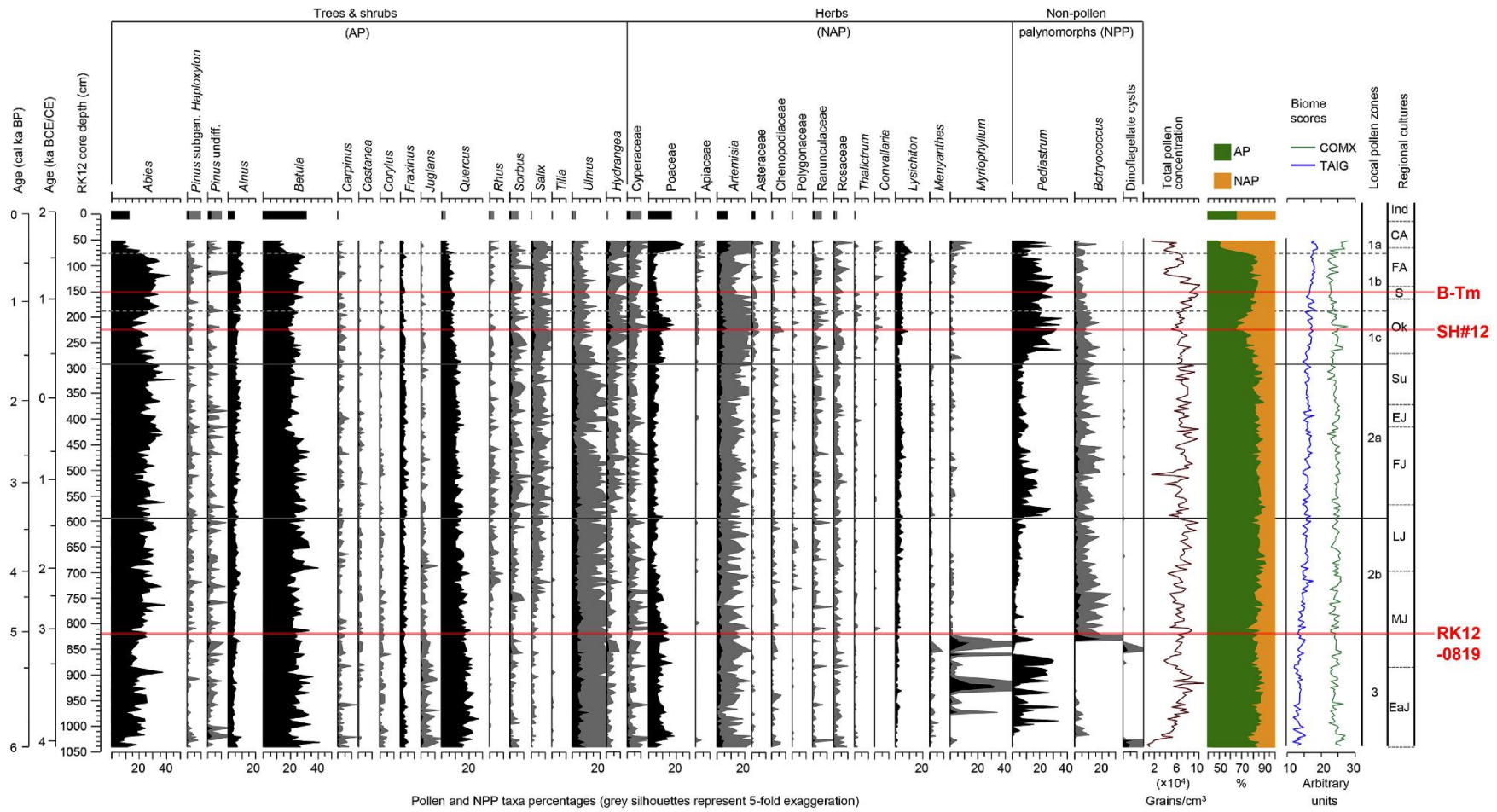

Fig. 3.14 Key marker tephra layers identified in this study plotted against the last 6 ka high-resolution pollen record from the RK12 composite sequence (Leipe et al., 2018).

The cryptotephra study from Lake Kushu has significantly extended the known ash dispersal of several key marker layers, including the SH#12, Ko-g and Ma-f~j tephras. The SH#12 (SH_{1450}) tephra from the Shiveluch volcano, was known to have a SE dispersal axis (Kyle et al., 2011) and was mainly identified in the eastern Kamchatka around 50-100 km east of the volcano (Ponomareva et al., 2017). The presence of the SH#12 tephra in Lake Kushu northern Japan (i.e. RK12-0225), is the first occurrence of the tephra outside the Kamchatka region, confirming a distance of ~1900 km from its source. More importantly, the lake is located SW of the Shiveluch volcano, not in the main axis of the eruption's primary plume dispersal (Fig. 3.1b). This indicates that the tephra is highly likely to be traced following its main dispersal axis over 1900 km into the Aleutian Arc, the Bering Sea and probably the SW of Alaska, which has the potential to be developed as a widespread marker linking archives across the northwestern Pacific Ring of Fire. Owing to the prevailing westerlies, the Hokkaido Ko-g and Ma-f~j tephras were dispersed towards ENE and ESE respectively (Furukawa and Nanayama, 2006; Katsui, 1963). Lake Kushu, neither in the main dispersal axes nor within the known distribution areas of the two tephras, recorded both of them as cryptotephras, confirming the distances of over 350 km from the sources in both cases. The correlative layers in Lake Kushu (i.e. RK12-1169, RK12-1277), currently represent the most northerly occurrence of the two isochrons, indicating that the Ko-g definitely covers the entire Hokkaido Island and the Ma-f~j probably as well (Fig. 3.1b). These findings clearly demonstrate the ability of cryptotephra study in extending the footprint of any given eruption.

Importantly this study has highlighted a number of previously unreported tephra layers that have now been reliably dated by the new Kushu age model (Table 3.1), which in turn placed significant constraints on the tempo and frequency of the related volcanic centres. For example, the typical Changbaishan composition has been found repeatedly occurring four times at ca. 1 ka, 4.1-4.7 ka, 8.4-8.9 ka and 8.9-9.3 ka throughout the RK12 Holocene sequence (see section 3.7.2.2). This represents currently the maximal record of multiple Changbaishan ash layers recorded in a single distal archive during the Holocene timeframe, allowing a much clearer insight into the explosive history of this volcano. The two layers that are correlated to the Krakatau volcano (i.e. dominant population of RK12-0819 and RK12-0739; Chen et al., in preparation and this study), probably indicate two previously undocumented large

eruptions that are capable of dispersing ultra-distal tephras from the southern hemisphere to the mid-latitude northern hemisphere. These currently represent the furthest known latitudinal tephra dispersal. The compositional group 1, 2, 3 and group A tephras, each containing shards from multiple layers within the RK12 sequence, are correlated to their possible source volcanoes or region based on glass chemistry (Table 3.2). However, the ages of these tephras do not match any known eruptions of their respective source volcanoes (e.g. Shikotsu, Komagatake and Aira). Therefore, our findings seem to call into question the currently known eruptive records of these volcanoes which mainly based on proximal and visible tephra studies. We thus advocate that the state-of-the-art cryptotephra method (e.g. Turney, 1998; Blockley et al., 2005) should be more frequently applied in the active volcanic regions, preferably in distal archives, in order to fully decipher the tempo of Asian volcanism.

3.10 Conclusions

This study presents the first detailed Holocene cryptotephra stratigraphy in northern Japan, a volcanically active region that is ideal for optimising the use of tephra isochrons to synchronise palaeoclimate records. The Kushu RK12 tephrostratigraphy integrates local and far-travelled tephras originating from multiple regions such as Russia, China/N Korea, northern Japan, southern Japan and as far south as Indonesia. A total of twelve cryptotephra layers are extracted from the sequence, within which forty geochemical groups are identified, dated and correlated to their source volcanoes or probable place of origin. These tephra layers provide useful isochrons for dating and correlating records and important information on volcano resurgence. Several prominent tephra horizons are now confirmed widespread thus can be incorporated into the East Asian master tephra framework. A large number of previously undocumented tephra horizons identified in this research call into question the current known tephrostratigraphy in northern Japan which is based on visible tephra studies, and highlight the importance of cryptotephra method even in volcanically active regions. A refined chronology for the Lake Kushu RK12 sequence is presented, which is based on our tephra correlation results. Given that the tephra isochrons recorded in the Lake Kushu sequence have very wide distributions, for example the correlatives of RK12-0151, RK12-0225 and RK12-0819 in Greenland, Kamchatka and Indonesia respectively, the RK12 record serves as a hub for linking palaeoclimate archives that

span a vast geographic area from high northern latitudes to low southern latitudes. Therefore, it is one of the very few Holocene tephrostratigraphies that are suitable for correlating records in and beyond the East Asia region.

3.11 Acknowledgements

This study was supported by the External Cooperation Program of Bureau of International Co-operation, Chinese Academy of Sciences (Grant No. 132744KYSB20130005) and CAS Strategic Priority Research Program (B) (XDB18000000). XYC's stay at RHUL was supported by the collaboration scheme between GIGCAS and RHUL. We thank Drs. Yugo Nakamura and Akiko Matsumoto for providing the full dataset of the published tephra chemistry, Victoria Smith, Paul Albert and Chris Hayward for their assistance during geochemical analyses, Stefanie Müller for providing additional lake core samples.

Chapter 4: Transhemispheric tephra dispersal: Krakatau tephra in northern Japan

4.1 Author List

Xuan-Yu Chen [a,b,c,d,*], Danielle McLean [e], Simon Blockley [a], Pavel Tarasov [f], Yi-Gang Xu [b], Martin Menzies [b,c]

[a] Department of Geography, Royal Holloway University of London, Egham, Surrey, TW20 0EX, UK

[b] State Key Laboratory of Isotope Geochemistry, Guangzhou Institute of Geochemistry, Chinese Academy of Sciences, Guangzhou, 510640, China

[c] Department of Earth Sciences, Royal Holloway University of London, Egham, Surrey, TW20 0EX, UK

[d] University of Chinese Academy of Sciences, Beijing, 100049, China

[e] Research Laboratory for Archaeology and the History of Art, University of Oxford, Oxford, OX1 3QY, UK

[f] Institute of Geological Sciences, Palaeontology, Free University Berlin, Malteserstr. 74-100, Building D, 12249, Berlin, German

4.2 Abstract

A comprehensive inventory of far-travelled volcanic ash (i.e. tephra) layers is essential for the development of tephrochronology as a global scale correlation and dating tool, to allow the investigation of synchroneity and/or diachroneity of climate change events across widely spaced climate systems. Recent development and employment of the cryptotephra technique has given rise to the identification of a number of intercontinentally dispersed tephra layers. However, most of these tephra layers are erupted from mid- to high latitudes and dispersed longitudinally thus are restricted to one hemisphere. The only known transhemispheric tephra distribution is the Toba ash in East Africa from the largest Quaternary eruption. In this study, we propose the identification of a cryptotephra from Krakatau volcano Indonesia, in northern Japan over 6700 km from the vent. This provides the first empirical evidence of transhemispheric latitudinal distribution of volcanic ash, which significantly improves our knowledge of the dispersal capacity of tephra erupted at low-latitude, especially with regard to the dispersal of tephra to the polar regions. The finding not only provides information on a previously undocumented large eruption, but also opens up an opportunity for developing an interhemispheric cryptotephra lattice in the region. Given that there are so few cryptotephra studies in the western Pacific rim region, we recommend the cryptotephra method to be more systematically employed, particularly in the tropics, where the atmospheric dispersal pattern is most likely to disperse volcanic ash globally.

4.3 Introduction

Geochemically unique and widely distributed volcanic ash (tephra) layers can be used to link a variety of volcanic, archaeological and palaeoclimatic archives, and serves as a dating tool when the age is well constrained (e.g. Lowe et al., 2015; Bronk Ramsey et al., 2015; Albert et al., 2015; Barton et al., 2015). These tephra horizons can be detected as visible layers or as non-visible cryptotephra layers (Blockley et al., 2005). The increased use of the cryptotephra technique has greatly extended the range of tephra-based correlation and, within some regions such as Europe has facilitated precise investigation of problems such as leads and lags in the climate system (Lane et al., 2013a), or the timing of climatic changes and regional species extinctions (Lowe et al., 2012). Developing a better inventory of far-travelled tephra, is essential for the development of tephrochronology as a global scale correlation tool and this is a significant goal for the technique as it would allow for the correlation of climate archives in regions where they are influenced by different drivers within the climate system and can, thus, help with testing ideas of how climatic changes propagate globally.

Recently, an increasing number of widespread tephras with intercontinental distributions have been identified, including for example, the north American Mazama Ash found in Greenland (Zdanowicz et al., 1999), the Alaskan White River Ash found in northern Europe (Jensen et al., 2014), the Kamchatkan tephras found in north America, Arctic circle and Greenland (Mackay et al., 2016; van der Bilt et al., 2017; Cook et al., 2018b), the Chinese and Japanese tephras found in Greenland (Sun et al., 2014a; Bourne et al., 2016), and the Sumatran Toba ash found in East Africa (Lane et al., 2013b). Most of these tephras were erupted at mid- to high latitudes and probably dispersed by the tropospheric westerlies and stratospheric jet stream (e.g. Davies et al., 2010; Bursik et al., 2009), thus their distributions are largely longitudinal (c.f. Lane et al., 2017). Until now, very little is known about long distance transportation of tephra erupted at low-latitudes and dispersed latitudinally. This lack of knowledge is largely due to the fact that cryptotephra studies at these latitudes are in their infancy. At these latitudes, the trade winds and Hadley cell convection might be involved which complicates the mechanism of tephra dispersal. Nevertheless, here we discuss the potential for new far-travelled cryptotephra correlations based on work in East Asia.

This study is based on the analyses of a mid-Holocene cryptotephra from Lake Kushu northern Japan (Fig. 4.1). Cryptotephra layers from this site have been predominantly correlated to volcanic eruptions in the northern Hemisphere, from Japan, China and Russia (Chen et al., 2016; Chen et al., submitted), however a remaining cryptotephra horizon, as discussed below exhibits chemical affinity that does not match with known Asian northern Hemisphere eruptions. We, thus, in this study, explore the possibility of a far-travelled southern Hemisphere tephra source.

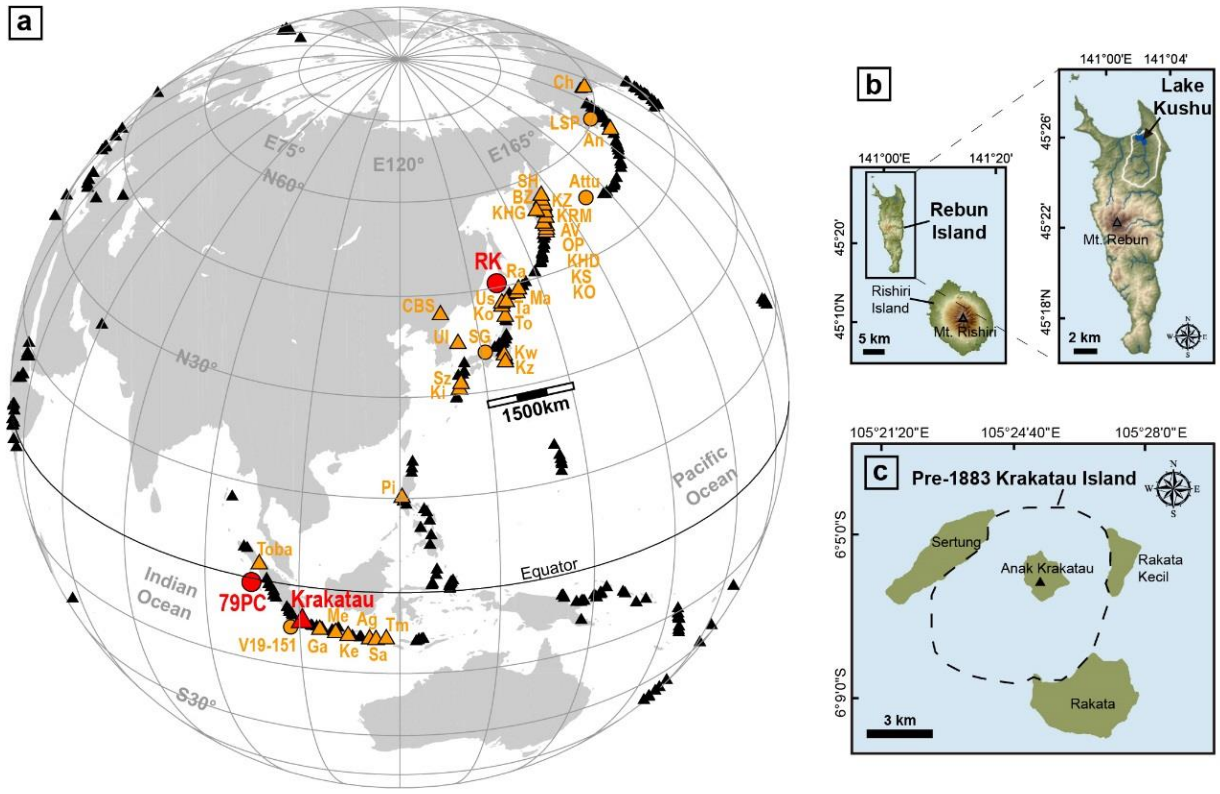

Fig. 4.1 (a) Map of the western Pacific rim showing active volcanoes (triangle) and distal archives for tephra studies (circle). The red colour highlights the volcano and distal archives where the tephra correlations established herein. The orange colour highlights the volcanoes and archives with major Holocene tephra markers whose glass chemistry were well characterised by electron probe techniques and were used for comparison in this study. An additional thirty late Quaternary major volcanic centres in Japan were not highlighted on the map though sixty widespread tephras from them, ranging from 15 ka to 1 Ma in age, were also used for compositional comparison (averaged compositions only). (b) Detailed location of Lake Kushu, Rebun Island in

Sea of Japan northwest of Hokkaido. (c) Schematic location of the pre-1883 Krakatau island volcano and current remnant islands, as well as the new volcanic centre Anak Krakatau.
Abbreviations: Japan: RK-Rebun Island Lake Kushu, Ra-Rausu, Ma-Mashu, Us-Usu, Ta-Tarumai, Ko-Komagatake, To-Towada, SG-Lake Suigetsu, Kw-Kawagodaira, Kz-Kozushima, Sz-Sakurajima, Ki-Kikai; China/N Korea: CBS-Changbaishan; S Korea: Ul-Ulleungdo; Kamchatka: SH-Shiveluch, BZ-Bezymianny, KHG-Khangar, KZ-Kizimen, KRM-Karymsky, AV-Avachinsky, OP-Opala, KHD-Khodutkinsky, KS-Ksudach, KO-Kurile Lake; Aleutians and Alaska: Ch-Churchill, LSP-Lone Spruce Pond, An-Aniakchak, Attu-Attu Island; Philippines: Pi-Pinatubo; Indonesia: Ga-Galunggung, Me-Merapi, Ke-Kelut, Ag-Agung, Sa-Samalas, Tm-Tambora; 79PC and V19-151 are marine cores near Sumatra Island. Detailed information on volcanoes, major eruptions and tephras, VEI, bulk tephra volumes, ages and glass chemistries references see Tables S4.1 and S4.2.

4.4 Regional setting, sample and methods

4.4.1 Distal archive

Kushu is the only fresh-water lake of Rebun Island in the Sea of Japan, northwest of Hokkaido (Fig. 4.1a, b). In February 2012, composite core RK12 was recovered in the central part of the lake, which revealed a continuous, partly laminated, organic-rich ca. 19.5 m long sedimentary record. The RK12 core age model built upon fifty-seven calibrated AMS radiocarbon dates indicates that the sedimentation continued over the past ca. 17,000 years (Muller et al., 2016). Forty-nine dates within the Holocene were remodelled in a Bayesian P_Sequence model with outlier detection analysis in Oxcal (Bronk Ramsey 2008, 2009a, 2009b), applying the IntCal13 calibration curve (Reimer et al., 2013), with the incorporation of a high-resolution age of the B-Tm tephra (Chen et al., 2016), to provide age estimate for any tephra found in the sequence.

Preliminary tephra investigation on RK12 core revealed no visible tephra layer throughout the entire sequence (McLean, 2013), thus the core was analysed in detail for cryptotephra following the methods outlined in Blockley et al. (2005). The core

segment related to this study is between composite depth (CD) 750-930 cm. This segment was first contiguously sub-sampled at a 20 cm resolution for range-finder scanning to determine tephra presence. If an elevated shard concentration was observed in the range-finder samples, the sediments were resampled at 2 cm resolutions for point sampling to locate the precise stratigraphic position of the cryptotephra horizon. Each extracted sample was mounted and examined for tephra shards using a polarizing microscope. Tephra concentrations were measured by counts normalized to shards per gram dry sediment (shard g^{-1}). Individual shards were hand-picked from the point-sample with the highest tephra counts and embedded in epoxy resin, which were then sectioned and polished for geochemical analysis.

Single-grain major and minor element concentrations were measured using wavelength-dispersive electron probe microanalysis (WDS-EPMA) at 1) the Research Laboratory for Archaeology and the History of Art, at the University of Oxford with a JEOL JXA-8600, and 2) the Grant Institute, School of Geosciences at the University of Edinburgh with a Cameca SX100. Spot sizes of 10 and 5 um were used depending on the size of the area available for analysis in different shards. Secondary glass standards were analysed in the same session in order to monitor instrumental accuracy and analytical precision (supplementary materials). Detailed machine set-up for the electron probe JEOL JXA-8600 at Oxford see Kuehn et al. (2011) (lab#25), and for the Cameca SX100 at Edinburgh see Hayward (2012). For comparative purposes, all data presented in text, table and plots were normalized to 100 wt% on a volatile-free basis.

4.4.2 Proximal volcano

Krakatau (or Krakatoa) was an island volcano situated in the Sunda Strait between the islands of Sumatra and Java along the Indonesian arc (Fig. 4.1a). After the 1883 CE eruption, a 300 m deep and 6 km wide submarine caldera remained (Sigurdsson et al., 1991; Fig. 4.1c). The eruption (VEI=6) on August 26-27, 1883, resulting in more than 36,000 fatalities, was ranked as one of the largest historic eruptions (Newhall and Self, 1982). An eruption column of about 40 km height and a bulk tephra volume of 18-21 km^3 were estimated (Self and Rampino, 1981; Rampino and self, 1982). The majority of the tephra was deposited at sea, generating some 30-40 m high tsunamis that inundated the coasts of west Java and Sumatra (Sigurdsson et al., 1991; Mandeville et al., 1996b). Average Northern Hemisphere temperatures fell by 0.25 °C for 2-3 years

following the eruption (Self et al., 1981), whereas the sea-level rise and ocean warming were slowed down for decades after the event (Gleckler et al., 2006).

4.5 Results and Discussion

4.5.1 Stratigraphy and Chronology

Investigation of RK12 core sediment between CD 750-930 cm reveals a prominent cryptotephra horizon in CD 818-820 cm (hereby named RK12-0819). In this layer, tephra concentration reaches a maximum of 168 shards/g, which is an order of magnitude higher than the adjacent point-samples (Fig. 4.2a). Tephra shards of the sample are dominantly bubble wall type and vesicular shards. The counting profile of the layer and a lack of evidence of mixing shard morphology clearly indicates that the RK12-0819 is a primary tephra deposit, which is consistent with the sheltered nature of the lake deposit (Chen et al., submitted). Radiocarbon based age model of the RK12 core provides an age estimate of 5279-4865 cal. yr BP (95.4%) for the tephra layer (Fig. 4.2b).

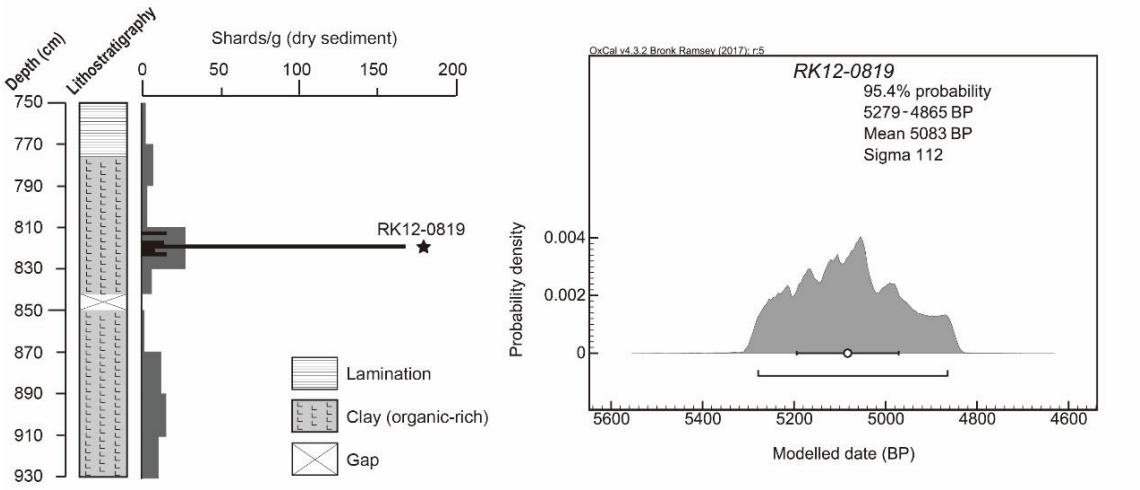

Fig. 4.2 (a) Lithostratigraphy and tephrostratigraphy for the segment of composite depth (CD) 750-930 cm of the RK12 composite core. The precise position of the RK12-0819 cryptotephra horizon is shown, indicating by the number of glass shards (shards/g dry sediment) counted in 20 cm range-finder samples (grey bars) then 2 cm point-samples (black bars). The cryptotephra horizon reaches a peak in glass shard concentration of 168 shards/g in CD 818-820 cm. (b) Posterior probability density function generated for the cryptotephra RK12-0819 using the RK12 Holocene age

model. The age model was constructed using AMS radiocarbon dates reported in Muller et al. (2016), with a high-resolution tephra age of the B-Tm tephra (Oppenheimer et al., 2017) inserted in the Late Holocene part of the RK12 sequence (Chen et al., 2016).

4.5.2 Glass chemistry and tephra correlation

Glasses of RK12-0819 (n=26, Table S4.3) are very heterogeneous with SiO_2 ranging from 65.8 to 74.4 wt%. They are dacitic to rhyolitic in composition (Fig. 4.3a) and mainly belong to the medium-K calc-alkaline series (Fig. 4.4a). Given that the Lake Kushu has recorded cryptotephra deposits from China/N Korea (Chen et al., 2016) and Kamchatka, Russia (Chen et al., submitted), the search of provenance for RK12-0819 tephra was first undertaken across the entire NE Asia, including Russia, Japan, China/N Korea, and S Korea (Fig. 4.1a). Table S4.1 lists sixty-two Holocene major marker tephras originating from NE Asia, whose compositions were well characterised by electron probe techniques, along with their VEI index, tephra volumes, ages as well as the source volcanoes or identification localities (see table for data sources). Detailed investigation of these glass chemistries reveals that only five of these sixty-two tephras exhibit dacitic to rhyolitic compositions with ca. 10 wt% variation in SiO_2 content (Table S4.1), whereas the others do not match (Fig. 4.3). The five comparable tephra layers are late Holocene Ra-1 and Ra-2 tephras erupted from Rausu volcano in eastern Hokkaido (Nakamura, 2016), early Holocene SG14-1185 tephra with unknown provenance identified in Lake Suigetsu, central Japan (McLean et al., 2018), late Holocene AV_1 tephra from Avachinsky volcano and mid-Holocene KS_2 tephra from Ksudach volcano in the Kamchatka peninsula (Kyle et al., 2011) (Table S4.1). Glass compositions of the Kamchatkan AV_1 and KS_2 tephras are mainly low-K series whereas those of the Suigetsu SG14-1185 are high-K series, thus they are different from the RK12-0819 compositions (Fig. 4.4a). Hokkaido Ra-1 and Ra-2 tephras match closely with the RK12-0819 on most of the major elements but can be easily distinguished from the latter on SiO_2-FeO_t bi-plot (Fig. 4.4a, b). Therefore, no match was found within the NE Asian Holocene tephra database (Table S4.1). Further comparison with available averaged compositions of sixty widespread late Quaternary tephras ranging from 15 ka to 1 Ma in age, erupted from over thirty major volcanic centres in Japan (Aoki and Machida, 2006; Appendix 1), again revealed no match for the RK12-0819 chemistry

(compositions of RK12-0819 see Table S4.3). Consequently, the geochemically distinctive RK12-0819 tephra is unlikely to originate from NE Asia.

Provenance studies were expanded to include the northern and western Pacific Ring of Fire, namely the Aleutians and Alaska, as well as the Philippines and Indonesia (Fig. 4.1a). Given the long distance between these regions and the Lake Kushu, we would expect an extremely large eruption to disperse tephra over this range, and thus for it to be well known. Table S4.2 lists tephras from eleven volcanoes with the largest known eruptions (e.g. Toba, Tambora, Samalas, Krakatau, Pinatubo etc) and eight geochemically well-characterised distal tephra deposits with unknown provenance within these regions. Only five tephras among them turned out to fit the criteria of a very heterogeneous (i.e. ca. 10 wt% variation in SiO_2 content) dacitic to rhyolitic composition (Table S4.2). These are tephras from the Philippine Pinatubo 1991 CE (VEI=6) and the Indonesian Krakatau 1883 CE (VEI=6) historic eruptions (Luhr and Melson, 1996; Pallister et al., 1996; Mandeville et al., 1996a), late Holocene V-4 tephra found in marine core 79PC near Sumatra (Salisbury et al., 2012), mid- to late Holocene 95-01/3 tephra found in Attu Island, Aleutians (Kyle et al., 2011), and LSP 4.7-ka tephra found in Lone Spruce Pond, SW Alaska (Kaufman et al., 2012) (Table S4.2). However, the compositions of Pinatubo 1991 tephra are more evolved than that of the RK12-0819 tephra, while the Alaskan LSP 4.7-ka and Aleutian Attu Island tephras have either higher or lower K_2O contents compared to the RK12-0819 (Fig. 4.4a), thus they are all ruled out as indicator of possible provenance for RK12-0819, leaving over only the V-4 and Krakatau 1883 tephra.

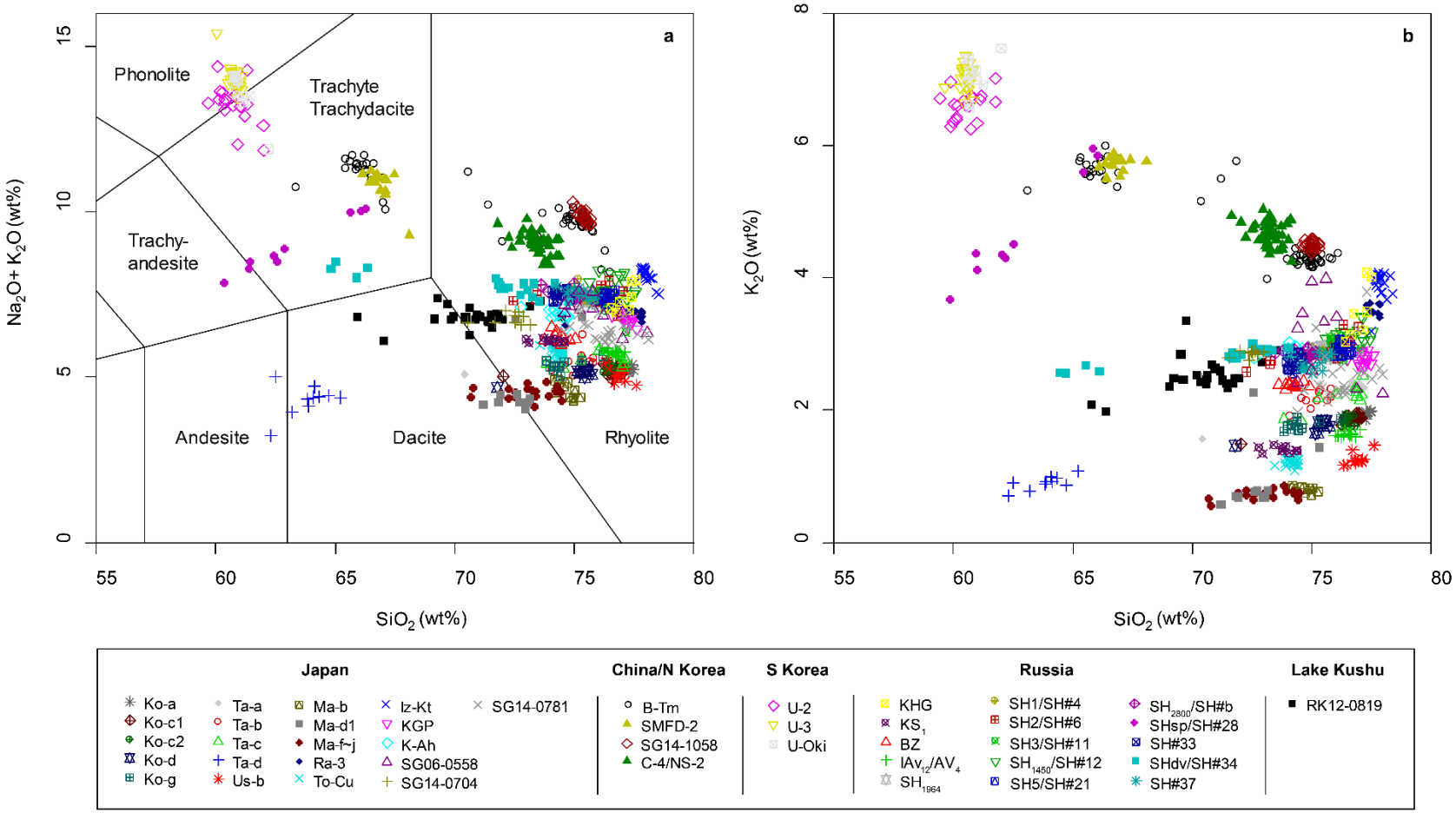

Fig. 4.3 (a) TAS diagram (classification scheme based on Le Bas et al. (1986)) and (b) SiO_2-K_2O bi-plot showing glass compositions of RK12-0819, along with other Holocene major marker tephras originating from NE Asia which do not match with the RK12-0819. Detailed information of the marker tephras and data sources see Table S4.1.

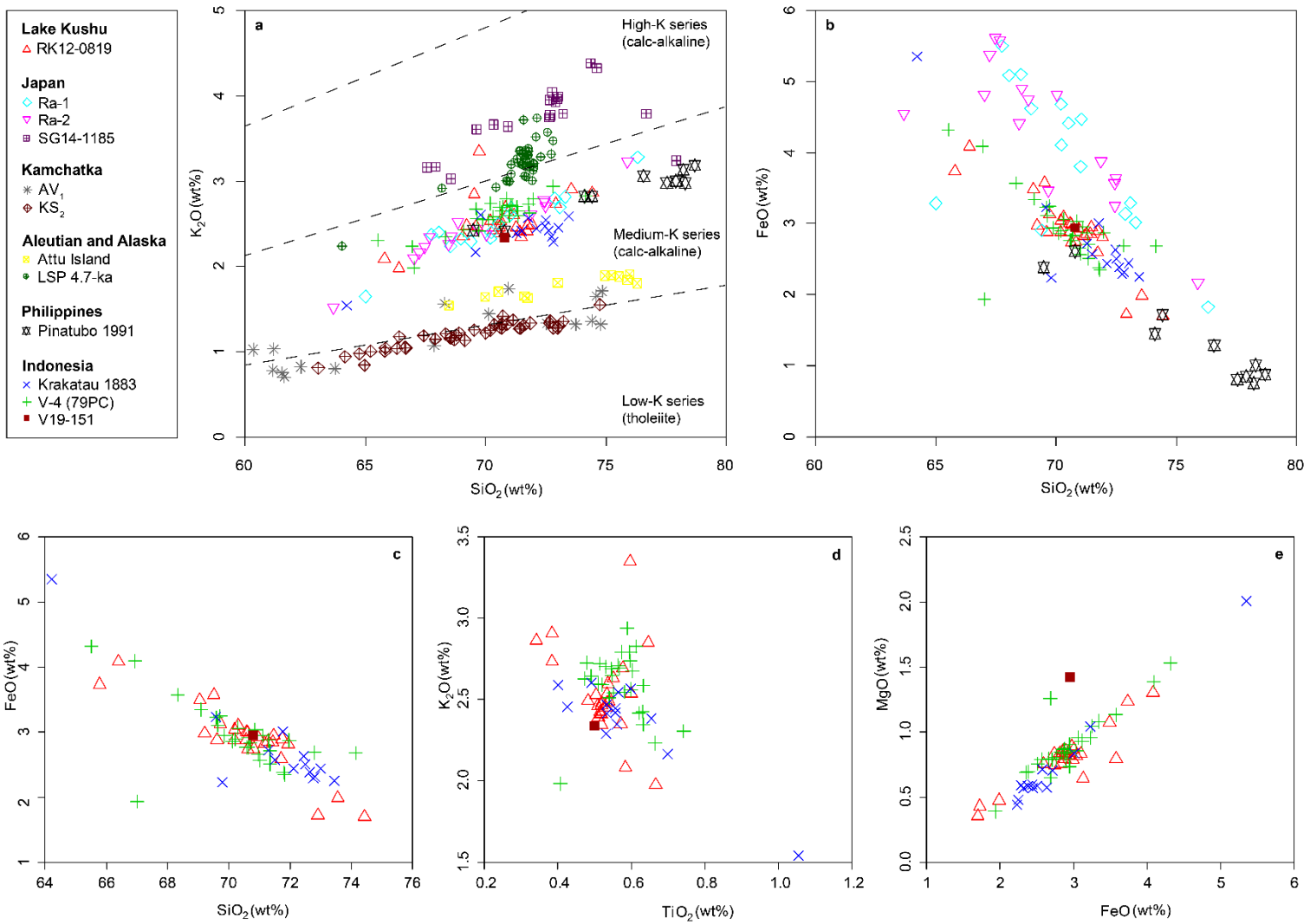
Lake Kushu
RK12-0819
Japan
Ra-1
Ra-2
SG14-1185
Kamchatka
AV1
KS2
Aleutian and Alaska
Attu Island
LSP 4.7-ka
Philippines
Pinatubo 1991
Indonesia
Krakatau 1883
V-4 (79PC)
V19-151
a
High-K series
(calc-alkaline)
Medium-K series
(calc-alkaline)
Low-K series
(tholeiite)
K2O(wt%)
SiO2(wt%)
b
FeO(wt%)
SiO2(wt%)
c
FeO(wt%)
SiO2(wt%)
d
K2O(wt%)
TiO2(wt%)
e
MgO(wt%)
FeO(wt%)

Fig. 4.4 Glass shard major element compositions of RK12-0819 along with tephras that have heterogeneous dacitic to rhyolitic glass chemistry, among major Holocene marker tephras occurred in the western Pacific Rim region (data sources see Table S4.1). (a) K-classification diagram (classification scheme based on Peccerillo and Taylor (1976)) showing glasses of RK12-0819 are classified into the medium-K calc-alkaline series thus are different from tephras with dacitic to rhyolitic compositions but are in high-K or low-K series. (b) SiO_2-FeO_t bi-plot showing that RK12-0819 can be distinguished from the Japanese Ra-1 and Ra-2 tephras originating from Rausu volcano, which also exhibit medium-K dacitic to rhyolitic glass compositions. (c-e) Bivariate plots showing the geochemical similarities between RK12-0819 and Indonesian V-4, Krakatau 1883 and V19-151 tephras.

The V-4 tephra, dacitic to rhyolitic in compositions and dated at ~1.9 cal ka BP, is a 3.5 cm thick distal layer found in marine core 79PC ca. 250 km off the central Sumatra Island (Salisbury et al., 2012; Fig. 4.1a). Owing to the scarcity of available microprobe data on Holocene Indonesian tephras, Salisbury et al. (2012) failed to establish a distal-proximal correlation, leaving the tephra distally-described only. The comparison of RK12-0819 with the V-4 tephra revealed identical compositions on major element level (Fig. 4.4, Table S4.3), suggesting that they were erupted from the same volcano and that the RK12-0819 tephra has an Indonesian origin. Mandeville et al. (1996a) characterized the glass chemistry of the proximal Krakatau 1883 tephra and reported heterogeneous dacitic to rhyolitic compositions with >9 wt% variation in SiO_2 content. These Krakatau compositions are remarkably similar to the geochemically identical V-4 and RK12-0819 tephras on the basis of major elements (Fig. 4.4, Table S4.3), strongly indicating a Krakatau origin for the two uncorrelated distal layers. More importantly, these distinctive Krakatau-type compositions are different from glass compositions of other Indonesian volcanoes with the largest known eruptions such as the Tambora, Samalas, Agung, Galunggung, Kelut, Merapi and the much older Toba caldera (Table S4.3). On these rigorous geochemical grounds, we thus propose that our ~5.1 ka RK12-0819 tephra and the ~1.9 ka V-4 tephra represent previously undocumented pre-historic eruptions of the Krakatau volcano.

4.5.3 Unravelling previously undocumented eruptions

In the equatorial islands region like Indonesia, proximal volcanic records are usually not very well preserved and studied. This is due to the extremely high erosion rates coupled with dense vegetation, and the inaccessibility of the islands (Salisbury et al., 2012). One of the examples is the Agung volcano in eastern Bali. The 1963 CE eruption (VEI=5) produced tephras with a bulk volume of ~1 km^3, but 15 years after the event, there was little or no trace of the tephra on the island (Rampino and Self, 1982). The case would have been even worse for Krakatau, as the 1883 eruption destroyed the pre-existent volcano/island (Fig. 4.1c), and the tephras generated from the volcano were mainly deposited in the submarine environment (Mandeville et al., 1996b). Apart from the ancient record from Javanese chronicles suggesting an eruption in 416 CE (Camus et al., 1987; and refs therein), very little is known about the pre-1883 eruptive history of the Krakatau volcano.

Ninkovich (1979) identified a Holocene tephra in a deep sea marine core (V19-151) near Sunda Strait. Without any precise age information Ninkovich (1979) described it as "recent tephra", and tentatively attributed the tephra to Krakatau eruption, on the basis of whole-rock chemistry and the geographic proximity between the marine core and the volcano. Geochemical comparison of the marine tephra with Krakatau 1883, V-4 and RK12-0819 tephras reveals comparable composition, except for elevated MgO content (Fig. 4.4, Table S4.3). As such the V19-151 tephra's presumed Krakatau origin and whether it can be attributed to the unconfirmed 416 CE event require further geochemical analysis and chronological constraints. Nevertheless, our proposed correlations of the ~5.1 ka RK12-0819 tephra and the ~1.9 ka V-4 tephra with the Krakatau volcano clearly for the first time, provide evidence on the volcano's pre-historic eruptions.

4.5.4 Implication for future study

This study suggests that the Lake Kushu preserves the most distal example of an transhemispheric tephra dispersal event. At present the only other example is the Toba ash in East Africa (Lane et al., 2013b), which was the largest known volcanic eruption in the late Quaternary. It is possible that correlation to Krakatau 1883, V-4 are the only other examples and that these events are extremely rare. If this is the case, then we have

presented an unusual but potentially very widespread and useful tephra isochron that may allow correlation of climate archives between the two hemispheres. Given the discussion above regarding the difficulty of reconstructing Indonesian volcanism, coupled with the lack of systematic application of cryptotephra studies in the region means, however, it is possible that we have just lifted the lid on a potential revolution in tephra studies and tephrochronology in the region. At present there are no long term cryptotephra studies published for East Asia, south of Lake Suigetsu. Even this important site has only one cryptotephra study published so far, and there are many unattributed geochemical analyses that have not been assigned to a known eruption or volcano (McLean et al., 2018). Large volume tropical eruptions are also known to have the greatest chance of influencing climate as the atmospheric dispersal pattern in the tropics is most likely to disperse globally (Robock, 2000). Therefore, we believe that there is considerable potential to develop an interhemispheric cryptotephra lattice in this region to facilitate the correlation of widespread palaeoclimatic archives. This would be important for a number of reasons not least testing proposed influences of past climate change on the Intertropical Convergence Zone and the Asian monsoon. However in order for this to be developed it is now essential that a more systematic approach to the application of cryptotephra method is applied to lacustrine and marine records from the region.

4.6 Supplementary materials

Table S4.1 Summary information of sixty-two Holocene major marker tephras originating from NE Asia which are used for compositional comparison. Tephra names in **Bold** indicate that the tephras exhibit dacitic to rhyolitic compositions similar to the RK12-0819 tephra and that their compositions were plotted for comparison in the main text.

Area	Volcano / Identification locality	Tephra	Volume (km3)	Age	Age ref	EPMA glass chemistry ref
Known regional marker tephras						
Northern Japan	Usu	Us-b (VEI=5)	2.78	1663 CE	Ōba et al 1983	Nakamura 2016
	Komagatake	Ko-a (VEI=4)	0.34	1929 CE	Katsui and Komuro 1984	Nakamura 2016
		Ko-c1 (VEI=4)	0.21	1856 CE	Katsui and Komuro 1984	Nakamura 2016
		Ko-c2 (VEI=4)	0.36	1694 CE	Katsui and Komuro 1984	Nakamura 2016
		Ko-d (VEI=5)	2.9	1640 CE	Katsui and Komuro 1984	Nakamura 2016
		Ko-g (VEI=5)	3.0	6.5-6.6 cal ka BP	Nakamura and Hirakawa 2004	Nakamura 2016
	Tarumai	Ta-a (VEI=5)	4.0	1739 CE	Nakamura 2016 and refs therein	Nakamura 2016
		Ta-b (VEI=5)	2.8	1667 CE	Nakamura 2016 and refs therein	Nakamura 2016
		Ta-c (VEI=5)	3.3	2.5-2.8 cal ka BP	Nakamura 2016 and refs therein	Nakamura 2016
		Ta-d (VEI=5)	1.9	9.0-9.7 cal ka BP	Nakamura 2016 and refs therein	Nakamura 2016
	Mashu	Ma-b (VEI=5)	4.6	1.0 cal ka BP	McLean et al 2018	Nakamura 2016
		Ma-d1 (VEI=4)	0.32	4.0 cal ka BP	Yamamoto et al 2010	Nakamura 2016
		Ma-f~j (VEI=6)	18.6	7.5-7.7 cal ka BP	Yamamoto et al 2010	Nakamura 2016
	Rausu	**Ra-1 (VEI=3)**	0.04	0.5-0.7 cal ka BP	Miyaji et al 2000	Nakamura 2016
		Ra-2 (VEI=4)	0.2	1.3-1.5 cal ka BP	Miyaji et al 2000	Nakamura 2016
		Ra-3		2.1-2.3 cal ka BP	Miyaji et al 2000	Nakamura 2016
Central Japan	Towada	To-a (VEI=5)	6.5	915 CE	Hayakawa and Koyama 1998	Aoki and Machida 2006
		To-Cu (VEI=5)	9.2	6.2-6.3 cal ka BP	Inoue et al 2011	McLean et al 2018
		To-Nb (VEI=5)	2.5	9.4 cal ka BP	Kudo and sasaki 2007	Aoki and Machida 2006
	Kozushima	Iz-Kt (VEI=4)	1	838 CE	Tsukui et al 2006	McLean et al 2018
	Kawagodaira	KGP (VEI=4)	1.04	3.1-3.2 cal ka BP	Tani et al 2013	McLean et al 2018
Southern Japan	Sakurajima	Sz-Ub/P12	<0.1	9.0 cal ka BP	Okuno et al 1997, Moriwaki et al 2016	Moriwaki et al 2017
		Sz-Tk3/P13	1.3	10.6 cal ka BP	Okuno et al 1997, Moriwaki et al 2016	Moriwaki et al 2017
		Sz-S/P14 (VEI=6)	14	*12.8 cal ka BP*	Okuno et al 1997, Moriwaki et al 2016	Moriwaki et al 2017
	Kikai	K-Ah (VEI=7)	170	7.2-7.3 cal ka BP	Smith et al 2013	Smith et al 2013
Kamchatka, Russia	Shiveluch	SH1964 (VEI=4)	0.6-0.8	1964 CE	Ponomareva et al 2017	Ponomareva et al 2015
		SH#4/SH1 (VEI=5)	≥2	0.3 cal ka BP	Ponomareva et al 2017	Ponomareva et al 2015
		SH#6/SH2 (VEI=5)	≥2	0.8 cal ka BP	Ponomareva et al 2017	Ponomareva et al 2015
		SH#11/SH3 (VEI=5)	≥2	1.3 cal ka BP	Ponomareva et al 2017	Ponomareva et al 2015
		SH#12/SH1450 (VEI=5)	≥2	1.3-1.4 cal ka BP	Ponomareva et al 2017	Ponomareva et al 2015
		SH#21/SH5 (VEI=4)	~1	1.9 cal ka BP	Ponomareva et al 2017	Ponomareva et al 2015
		SHb/SH2800 (VEI=5)	≥1	2.8-3.0 cal ka BP	Ponomareva et al 2017	Ponomareva et al 2015
		SH#28/SHsp (VEI=5)		3.9 cal ka BP	Ponomareva et al 2017	Ponomareva et al 2015
		SH#33		4.3-4.5 cal ka BP	Ponomareva et al 2017	Ponomareva et al 2015
		SH#34/SHdv (VEI=5)	≥2	4.6-4.8 cal ka BP	Ponomareva et al 2017	Ponomareva et al 2015
		SH#37		5.4-5.6 cal ka BP	Ponomareva et al 2017	Ponomareva et al 2015
	Kizimen	KZ (VEI=5)	4-5	7.5 14C ka BP	Kyle et al 2011 and refs therein	Kyle et al 2011
	Khangar	KHG6600		6.6 14C ka BP	Kyle et al 2011 and refs therein	Kyle et al 2011
		KHG6900 (VEI=6)	14-16	6.9 14C ka BP	Kyle et al 2011 and refs therein	Kyle et al 2011
	Karymsky	KRM (VEI=6)	13-16	7.9 14C ka BP	Kyle et al 2011 and refs therein	Kyle et al 2011
	Avachinsky	**AV1 (VEI=5)**	≥3.6	3.5 14C ka BP	Kyle et al 2011 and refs therein	Kyle et al 2011
		IAv12/AV4 (VEI=5)	≥4	6.3 cal ka BP	Ponomareva et al 2017	Ponomareva et al 2017
		IAv2 (VEI=5)	≥8	7.1 14C ka BP	Kyle et al 2011 and refs therein	Kyle et al 2011
	Opala	OP (VEI=5)	9-10	1.5 14C ka BP	Kyle et al 2011 and refs therein	Kyle et al 2011
	Khodutkinsky	KHD (VEI=5)	1-1.5	2.5 14C ka BP	Kyle et al 2011 and refs therein	Kyle et al 2011
	Ksudach	KSht3 (VEI=5)	1.5-2	1907 CE	Kyle et al 2011 and refs therein	Kyle et al 2011
		KS1 (VEI=6)	18-19	1.8 14C ka BP	Kyle et al 2011 and refs therein	Kyle et al 2011
		KS2 (VEI=5)	7-8	6.0 14C ka BP	Kyle et al 2011 and refs therein	Kyle et al 2011
		KS3 (VEI=5)	0.5-1	6.4 14C ka BP	Kyle et al 2011 and refs therein	Kyle et al 2011
	Kurile Lake	KO (VEI=7)	140-170	7.6 14C ka BP	Kyle et al 2011 and refs therein	Kyle et al 2011
	Bezymianny	BZ (VEI=4)		1.9 14C ka BP	Plunkett et al 2015	Ponomareva et al 2017
China/N Korea	Changbaishan	B-Tm (VEI=7)	77-115	946 CE	Oppenheimer et al 2017	Chen et al 2016
		C-4/NS-2		1.9-4.2 ka	Yang et al 2014, Sun et al 2017	Sun et al 2017
		SG14-1058		8.1 cal ka BP	McLean et al 2018	McLean et al 2018
		SMFD-2		1403 CE	Sun et al 2017	Sun et al 2017
S Korea	Ulleungdo	U-2		5.6 cal ka BP	Okuno et al 2010	McLean et al 2018
		U-3		8.4 cal ka BP	McLean et al 2018	McLean et al 2018
		U-Oki/U-4 (VEI=6)	>10	10.2 cal ka BP	Smith et al 2013	Smith et al 2011a
Distal tephras with unknown provenance						
Central Japan	Lake Suigetsu	SG06-0558		4.0 cal ka BP	Smith et al 2013	Smith et al 2013
		SG14-0704		4.8 cal ka BP	McLean et al 2018	McLean et al 2018
		SG14-0781		5.5 cal ka BP	McLean et al 2018	McLean et al 2018
		SG14-1185		8.4 cal ka BP	McLean et al 2018	McLean et al 2018

Note:

1. VEI data were compiled from: (1) Global Volcanism Program (Smithsonian Institution); (2) List of Quaternary volcanic eruptions (Wikipedia); (3) List of known large volcanic eruptions (Wikipedia); (4) Volcanoes of Japan (Geological Survey of Japan, AIST).

2. Tephra volume data were compiled from: Volcanoes of Japan (Geological Survey of Japan, AIST); List of Quaternary volcanic eruptions (Wikipedia); Kobayashi and Sasaki 2014; Braitseva et al., 1997; Kyle et al., 2011; Horn and Schmincke 2000.

Table S4.2 Summary information of nineteen major tephra layers originating from northern and western Pacific Ring of Fire which are used for compositional comparison. Tephra names in **Bold** indicate that the tephras exhibit dacitic to rhyolitic compositions similar to the RK12-0819 tephra and that their compositions were plotted for comparison in the main text.

Area	Volcano / Identification locality	Tephra	Volume (km3)	Age	Age ref	EPMA glass chemistry ref
Known regional marker tephras						
Philippines	Pinatubo	**1991 eruption (VEI=6)**	6-16	1991 CE	Westrich and Gerlach 1992	Westrich and Gerlach 1992, Rutherford and Devine 1996, Pallister et al 1996, Luhr and Melson 1996
Indonesia	Tambora	1815 eruption (VEI=7)	150	1815 CE	Self et al 1984	Self et al 2004
	Samalas/Rinjani	1257 eruption (VEI=7)	>40 (DRE)	1257 CE	Lavigne et al 2013	Alloway et al 2017
	Krakatau	**1883 eruption (VEI=6)**	18-21	1883 CE	Verbeek 1884	Mandeville et al 1996
	Agung	1963 eruption (VEI=5)	1	1963 CE	Self and King 1996	Self and King 1996
	Galunggung	1982 eruption (VEI=4)	>0.37	1982-1983 CE	Gerbe et al 1992	Gerbe et al 1992
	Merapi	1872 eruption (VEI=4)	0.33	1872 CE	Newhall et al 2000	*Gertisser and Keller 2003 (whole-rock composition)*
	Kelut	1990 eruption (VEI=4)	0.13	1990 CE	Bourdier et al 1997	Jeffery et al 2013
	Toba	YTT (VEI=8)	2500-3000	*~75 ka*	Ninkovich et al 1978	Smith et al 2011b
Alaska	Aniakchak	Aniakchak Tephra (VEI=6)	> 50	3.6 cal ka BP	Pearce et al 2004	Pearce et al 2004
	Churchill	White River Ash (VEI=6)	50	846-848 CE	Coulter et al 2012, Jensen et al 2014	Jensen et al 2014
Distal tephras with unknown provenance						
Indonesia	Marine core 79PC	**V-4 (VEI=5)**	>2	1.9 cal ka BP	Salisbury et al 2012	Salisbury et al 2012
		V-5 (VEI=5)	>4.7	4.8-4.9 cal ka BP	Salisbury et al 2012	Salisbury et al 2012
	Marine core V19-151	V19-151		ca. 2-3 ka BP	Age Inferred from Ninkovich 1979	*Ninkovich 1979 (Bulk analysis on pure glass)*
Aleutian Arc	Attu Island	**95-01/3**		3-5.1 14C ka BP	Kyle et al 2011 and refs therein	Kyle et al 2011
Alaska	Ahklun mountains	**LSP 4.7-ka tephra**		4.7 cal ka BP	Kaufman et al 2012	Kaufman et al 2012
		SP 5.3-ka tephra		5.3 cal ka BP	Kaufman et al 2012	Kaufman et al 2012
		Tephra B		6.1 cal ka BP	Kaufman et al 2012	Kaufman et al 2012
		8-ka tephra		8.0 cal ka BP	Kaufman et al 2012	Kaufman et al 2012

Note:

1. VEI data were compiled from: (1) Global Volcanism Program (Smithsonian Institution); (2) List of Quaternary volcanic eruptions (Wikipedia); (3) List of known large volcanic eruptions (Wikipedia); (4) List of volcanoes in Indonesia (Wikipedia).
2. Tephra volume data were compiled from: (1) List of Quaternary volcanic eruptions (Wikipedia); (2) List of volcanoes in Indonesia (Wikipedia)

Table S4.3 Average major element glass shard compositions of RK12-0819 and tephras of Indonesian origin. All data are normalised to 100% on a water-free basis. Data sources see Tables S4.2.

Tephra Layer	wt. (%)	SiO2	TiO2	Al2O3	FeOt	MnO	MgO	CaO	Na2O	K2O	P2O5	n
RK12-0819	Avg.	**70.61**	**0.53**	**14.81**	**2.90**	**0.11**	**0.81**	**3.16**	**4.27**	**2.54**	**0.15**	26
	±1σ	1.83	0.07	0.66	0.52	0.03	0.20	0.55	0.31	0.27	0.13	
V-4	Avg.	**70.33**	**0.57**	**15.63**	**2.93**	**0.09**	**0.89**	**3.15**	**3.57**	**2.59**	**N/A**	28
	±1σ	1.78	0.07	0.83	0.49	0.02	0.23	0.73	0.40	0.20	N/A	
Krakatau 1883	Avg.	**71.42**	**0.58**	**14.21**	**2.74**	**0.13**	**0.74**	**2.43**	**5.38**	**2.37**	**N/A**	14
	±1σ	2.36	0.16	0.53	0.80	0.04	0.40	0.91	0.15	0.27	N/A	
V19-151	whole-rock	**70.78**	**0.50**	**14.44**	**2.95**	**0.12**	**1.42**	**2.54**	**4.78**	**2.34**	**0.12**	1
Tambora 1815	Avg.	**58.59**	**0.53**	**19.42**	**4.56**	**0.18**	**1.38**	**3.26**	**5.46**	**6.28**	**0.35**	126
	±1σ	0.49	0.03	0.26	0.25	0.02	0.11	0.33	0.27	0.31	0.04	
Samalas 1257	Avg.	**68.86**	**0.48**	**16.49**	**2.47**	**0.11**	**0.53**	**2.22**	**4.43**	**4.21**	**N/A**	94
	±1σ	1.55	0.11	1.31	0.61	0.03	0.22	0.87	0.43	0.64	N/A	
Agung 1963	Avg.	**59.54**	**1.06**	**16.83**	**7.92**	**0.20**	**2.42**	**6.68**	**2.88**	**1.82**	**0.40**	20
	±1σ	1.25	0.19	1.37	0.93	0.04	0.53	0.70	0.99	0.33	0.075	
Galunggung 1982	Avg.	**66.02**	**0.90**	**15.01**	**5.72**	**0.13**	**1.69**	**4.90**	**3.79**	**1.58**	**0.00**	30
	±1σ	5.68	0.27	2.31	2.09	0.05	2.13	2.59	0.78	0.52	0.00	
Merapi 1872	whole-rock	**52.73**	**0.80**	**18.56**	**9.29**	**0.20**	**3.49**	**9.36**	**3.29**	**1.99**	**0.29**	1
Kelut 1990	Avg.	**54.89**	**0.65**	**18.63**	**8.75**	**0.21**	**3.85**	**9.17**	**3.05**	**0.72**	**0.09**	7
	±1σ	0.50	0.05	0.15	0.29	0.01	0.17	0.09	0.12	0.10	0.06	
Toba YTT	Avg.	**77.42**	**0.05**	**12.40**	**0.81**	**0.08**	**0.04**	**0.68**	**3.23**	**5.17**	**0.01**	22
	±1σ	0.23	0.02	0.15	0.10	0.06	0.01	0.05	0.15	0.09	0.01	
V-5	Avg.	**74.27**	**0.33**	**14.89**	**1.92**	**0.06**	**0.45**	**2.24**	**2.38**	**3.34**	**N/A**	28
	±1σ	0.97	0.05	0.61	0.20	0.01	0.08	0.34	0.39	0.17	N/A	

Chapter 5: An Integrated Holocene tephrostratigraphic framework for East Asia: implications for palaeoclimate research and future opportunities

5.1 Author List

Xuan-Yu Chen [a,b,c,d,*], Simon Blockley [b], Yi-Gang Xu [a], Martin Menzies [a,c]

[a] State Key Laboratory of Isotope Geochemistry, Guangzhou Institute of Geochemistry, Chinese Academy of Sciences, Guangzhou, 510640, China

[b] Department of Geography, Royal Holloway University of London, Egham, Surrey, TW20 0EX, UK

[c] Department of Earth Sciences, Royal Holloway University of London, Egham, Surrey, TW20 0EX, UK

[d] University of Chinese Academy of Sciences, Beijing, 100049, China

5.2 Abstract

Palaeoclimate records in East Asia are important for the understanding of monsoon dynamics and its links to the North Atlantic and the tropical climate systems. In Europe, a comprehensive regional tephrostratigraphic framework is proven to effectively facilitate the integration of proxy records from various sedimentary environments. East Asia is a volcanically active region that possesses the greatest potential for offering widespread volcanic ash layers that could aid precise comparison of palaeoclimate records. On the basis of previous extensive visible tephra studies and recent pioneering cryptotephra research in East Asia, we present in this study the first integrated Holocene tephrostratigraphic framework for the region. A total of twenty-two widespread tephras originating from Russia, China/N Korea, S Korea, Japan and Indonesia have been selected and incorporated in the framework, which is an essential first step towards a comprehensive master tephra framework. The current best age estimate, furthest known distribution, and precisely determined grain-specific glass chemistry for the tephra isochrons are reviewed and updated in this study, which are fundamental for future tephra correlation. The chronostratigraphic relationships between these tephras and climate change events were fully evaluated, in particular the extent to which these isochrons can be used to constrain regional variations of short-lived climate oscillations. A list of potential candidates are also discussed, with the suggestion of future work as the prerequisite for them to be included in the framework. Given the fruitful results derived from recent cryptotephra research in this region, we advocate a more systematic employment of the cryptotephra method in sedimentary sequences from the region, which may lead to a revolution in East Asian tephrochronology.

5.3 Introduction

Holocene climate variability has become increasingly important (e.g. Mayewski et al., 2004; Wanner et al., 2008) not only because it provides a detailed analogue for the study of interglacial climates, but also because it is essential for providing baseline for our understanding of future climate change. Palaeoclimate records in East Asia preserve valuable information on changes of the intertropical convergence zone and the Asian monsoon, as such are important for the understanding of monsoon dynamics and its links to the North Atlantic and the tropical climate systems (e.g. Dykoski et al., 2005; Wang et al., 2005). During the Holocene, numerous centennial- and multidecadal-scale oscillations are recorded in Chinese speleothems (Dykoski et al., 2005; Wang et al., 2005) and lacustrine records (Yancheva et al., 2007), however, these are not all reported from high northern latitudes (NGRIP members, 2004). Precise alignment of high resolution proxy records is essential for the investigation of global and regional variation of these short-lived climate oscillations. However, inherent dating uncertainties of various dating techniques that have been employed within different sedimentary archives make it extremely difficult to assess such variability (Lowe et al., 2015). Widely dispersed volcanic ash (i.e. tephra) layers preserved in sedimentary sequences provide ideal isochrons to facilitate synchronization of widespread palaeoclimate records (Lowe et al., 2008b; Davies et al., 2012; Blockley et al., 2012). Although tephra layers associated closely with climatic/cultural changes are particularly valuable (e.g. Lowe et al., 2012; Lane et al., 2013a), all widespread tephras are important for the development of a regional tephra framework (e.g. Blockley et al., 2014; Davies et al., 2014).

In Europe, the INTIMATE (INTegration of Ice core, Marine and Terrestrial records) project was initiated in 1995 to synchronise palaeoenvironmental records for the Last Termination (22-11.5 ka BP) around the North Atlantic region. The primary goal of the project being to test for leads and lags within the North Atlantic climate system by comparison of independently dated records, thus to understand the causal mechanisms driving the abrupt climate change events (Lowe et al., 2001, 2008b). Again, high-precision comparison is not easy to achieve, largely due to the inherent difficulties of integrating palaeoclimate records. Recently, however, the rapid developments in tephrochronology, particularly those derived from studies that focus on cryptotephra,

have demonstrated the growing potential to achieve the goals of the project (e.g. Davies et al., 2010; Lane et al., 2013a). To date, the protocol of integrating INTIMATE records using tephrochronology has been employed not only in the North Atlantic/Europe (Davies et al., 2012, 2014; Blockley et al., 2014) but also in Australasia (Alloway et al., 2007; Lowe et al., 2008a, 2013). Similarly, the RESET (RESponse of humans to abrupt Environmental Transitions) project was undertaken between 2008 and 2013 with the main focus on the causal links between abrupt environmental changes and human evolution/migration (Lowe et al., 2015). The project, through detailed analysis of tephra sequences at both proximal and distal sites, has partly refined the tephrostratigraphic framework for continental Europe and regions across the Mediterranean Sea, although the Eastern Mediterranean is still less well constrained. A RESET tephra lattice was established, with which key archaeological and palaeoenvironmental sites across the study area could be linked by tephra isochrons, and in particular cryptotephra horizons. This allows the disparate archives to be reliably integrated, providing an otherwise unattainable insight into the long-standing questions of the causative links between environmental changes and regional species extinctions (Lowe et al., 2012).

Volcanically active regions, for example East Asia, have great potential to offer a number of widely dispersed tephra isochrons (McLean et al., 2018). Combined with its important role in understanding the monsoon dynamics, East Asia is an ideal area for optimising the use of tephra layers to integrate palaeoclimate records. However, before records can be confidently correlated using these ash layers, a robust regional tephrostratigraphic framework needs be established to guide correlations and minimise miscorrelations. Tephra studies in and around Japan of the past few decades have provided a comprehensive picture for East Asian volcanism and allow detailed regional tephrostratigraphies to be established (e.g. Machida and Arai, 1983; Arai et al., 1986; Furuta et al., 1986; Machida, 1999; Aoki and Arai, 2000; Machida and Arai, 2003; Park et al., 2003; Nagahashi et al., 2004; Furukawa and Nanayama, 2006; Aoki et al., 2008; Takemura et al., 2010; Okuno et al., 2011; Smith et al., 2013; Moriwaki et al., 2016; Nakamura, 2016; Razzhigaeva et al., 2016; Tsuji et al., 2018). However, the reported tephrostratigraphies focus on different localities and timeframes, as such are either not regionally significant or do not fit with the goal to test Holocene climate variability. More importantly, the results of these studies are all based on identification of visible tephra layers, whereas employment of the cryptotephra method has been demonstrated

to effectively enlarge ash footprint of individual eruptions and to help identify previously unknown tephra isochrons (e.g. Sun et al., 2015; Chen et al., 2016; McLean et al., ,2018; Chen et al., submitted). McLean et al. (2018) provides an excellent example of the utility of cryptotephra method in East Asia. By applying the cryptotephra extraction techniques, the Holocene tephrostratigraphy in Lake Suigetsu has been extended from four to twenty ash layers (McLean et al., 2018). The study not only extended the ash dispersal of many key Holocene tephra markers but also identified a number of previously unreported distal tephra isochrons. As such, it provides currently the most comprehensive site-specific Holocene tephrostratigraphy in East Asia. Nevertheless, in order to develop the geographical range over which tephra isochrons can be applied, it is essential to integrate results from multiple sites within the region.

Following the tephrochronology protocols of the INTIMATE (Turney et al., 2004) and the RESET (Lowe et al., 2015) projects, and taking advantage of recent pioneering cryptotephra studies in East Asia (McLean et al., 2018; Chen et al., 2016; Chen et al., submitted; Chen et al., in preparation), it is attempted in this paper to establish a comprehensive and updated Holocene tephrostratigraphic framework for the region. A framework with twenty-two key tephra horizons is presented, which incorporates tephras originating from multiple regions in Russia, China/N Korea, S Korea, Japan and Indonesia. Their climatostratigraphic relationships with climate events are fully evaluated in this paper. The possibility of additional tephras being incorporated in this framework after further studies is also discussed. Finally, we highlight the opportunities for future tephrochronology studies in this region.

5.4 Holocene tephrostratigraphic framework for East Asia

For tephras layers to be of value in correlations they should (a) be regionally widespread, (b) have a unique geochemical fingerprint, (c) be precisely dated and (d) be closely associated in time with climatic/cultural transition (Davies et al., 2012). However, it is difficult to select tephras that perfectly fit all these criteria in a region such as the East Asia where the cryptotephra method has not yet been employed routinely. Consequently, we have slightly amended the criteria for this first attempt to bring together and summarise a Holocene tephra framework for East Asia. The tephras that are integrated in the framework have been 1) identified in at least one distal site, 2)

geochemically characterised using grain-specific techniques and attributed a provenance and 3) dated proximally or distally. The relationship of the timing between these tephras and climate changes are evaluated in this paper. Although the data quality could still be improved, these tephras represent the prime candidates for effecting precise correlation of East Asian palaeoclimate records that span the Holocene timeframe.

The East Asia Holocene tephra framework presented in this review contains twenty-two tephra layers with fifteen originating from Japan, three from South Korea, two from China/N Korea, one from Russia and one from Indonesia. Detailed information of tephra name, provenance, current best age, dispersal axis, furthest known distribution and data sources see Table 5.1. The related volcanic centres are shown in Fig. 5.1. The Japanese tephras mainly exhibit low-K to medium-K rhyolitic compositions with the exceptions of the Ma-f~j (low-K dacitic to rhyolitic) and Ta-d (low-K andesitic to dacitic) from Mashu and Tarumai volcanoes (Fig. 5.2). The Chinese/N Korean tephras (B-Tm, SG14-1058) from the Changbaishan volcano have very distinctive high-K trachytic to rhyolitic compositions (Fig. 5.2). South Korean tephras (U-2, U-3, U-Oki) from the Ulleungdo volcano compositionally straddle the phonolitic and trachytic boundary and are also very distinctive (Fig. 5.2). The Russian tephra from Shiveluch volcano (SH#12) has a medium-K rhyolitic composition but are different from other medium-K rhyolitic tephras from Japan (Fig. 5.2). And the far-travelled Indonesian tephra from Krakatau volcano (RK12-0819) has a unique medium-K dacitic to rhyolitic composition (Fig. 5.2). In summary, tephras in the framework from different volcanic settings possess unique glass compositions and can be effectively distinguished using the TAS (Le Bas et al., 1986) and K-classification (Peccerillo and Taylor, 1976) diagrams. However, separation of ash layers erupted from the same volcanic centres (e.g. Ta-a, Ta-b and Ta-c from Tarumai volcano) requires additional stratigraphic or chronological information.

Table 5.1 Summary information of twenty-two tephra isochrons within the proposed East Asian Holocene tephrostratigraphic framework.

Tephra	Source volcano (Country)	Current best age estimate (2σ)	Age ref	Dispersal axis	Furthest known distribution	Distribution ref	Glass Composition		EPMA data source ref
							K classification	TAS classification	
Ko-a	Komagatake (J)	1929 CE	Katsui et al 1984	ESE	V, >450 km	Razzhigaeva et al 2016	Medium-K	Rhyolitic	Nakamura 2016
Ko-c1	Komagatake (J)	1856 CE	Katsui et al 1984	ENE	V, >550 km	Razzhigaeva et al 2016	Medium-K	Rhyolitic	Nakamura 2016
Ta-a	Tarumai (J)	1739 CE	Nakamura 2016 and refs therein	ENE	V, >600 km	Razzhigaeva et al 2016	Medium-K	Rhyolitic	Nakamura 2016
Ko-c2	Komagatake (J)	1694 CE	Katsui et al 1984	ENE	V, >550 km	Razzhigaeva et al 2016	Medium-K	Rhyolitic	Nakamura 2016
Ta-b	Tarumai (J)	1667 CE	Nakamura 2016 and refs therein	E	V, >600 km	Razzhigaeva et al 2016	Medium-K	Rhyolitic	Nakamura 2016
Us-b	Usu (J)	1663 CE	Ōba et al 1983	E	V, >400 km	Furukawa and Nanayama 2006	Low-K	Rhyolitic	Nakamura 2016
Ko-d	Komagatake (J)	1640 CE	Katsui et al 1984	NW	V, >120 km	Machida and Arai 2003	Medium-K	Rhyolitic	Nakamura 2016
Ma-b	Mashu (J)	960-992 CE	McLean et al 2018	ENE	C, ~1150 km	McLean et al 2018	Low-K	Rhyolitic	Nakamura 2016
B-Tm	Changbaishan (C/N)	946 CE	Oppenheimer et al 2017	E	C, ~9000 km	Sun et al 2014	High-K	Trachytic-Rhyolitic	Chen et al 2016
SH#12	Shiveluch (R)	1408-1311 cal BP	Ponomareva et al 2017	SE	C, ~1900 km	Chen et al submittted	Medium-K	Rhyolitic	Ponomareva et al 2015/ Chen et al submitted
Ta-c	Tarumai (J)	2800-2500 cal BP/ 2500-2300 cal BP	Nakamura 2016/ Razzhigaeva et al 2016	E	V, >450 km	Razzhigaeva et al 2016	Medium-K	Rhyolitic	Nakamura 2016
KGP/Kg	Kawagodaira (J)	3160-3137 cal BP	Tani et al 2013	W	C, ~300 km	McLean et al 2018	Medium-K	Rhyolitic	McLean et al 2018
RK12-0819	Krakatau (I)	5287-4861 cal BP	Chen et al in preparation	N/A	C, ~6700 km	Chen et al in preparation	Medium-K	Dacitic-Rhyolitic	Chen et al in preparation
U-2	Ulleungdo (S)	5681-5619 cal BP	McLean et al 2018	SE	C, ~500 km	McLean et al 2018	High-K	Phonolitic-Trachytic	McLean et al 2018/ Shiihara et al 2011
To-Cu	Towada (J)	6313-6180 cal BP/ 5986-5899 cal BP	Inoue et al 2011/ McLean et al 2018	SE	C, ~700 km	McLean et al 2018	Low-K	Rhyolitic	McLean et al 2018
Ko-g	Komagatake (J)	6686-6520 cal BP	Chen et al submitted	ENE	V, >450 km	Razzhigaeva et al 2016	Medium-K	Rhyolitic	Nakamura 2016/Chen et al submitted
K-Ah	Kikai (J)	7303-7165 cal BP	Smith et al 2013	E	V, >1300 km	Machida and Arai 2003	Medium-K	Rhyolitic	Smith et al 2013
Ma-f~j	Mashu (J)	7581-7440 cal BP	Recal based on Yamamoto et al 2010	ESE	C, ~350 km	Chen et al submitted	Low-K	Dacitic-Rhyolitic	Razzhigaeva et al 2016 /Chen et al submitted
SG14-1058	Changbaishan (C/N)	8166-8099 cal BP	McLean et al 2018	N/A	C, ~1000 km	McLean et al 2018	High-K	Rhyolitic	McLean et al 2018
U-3	Ulleungdo (S)	8440-8360 cal BP	Im et al 2012	SE	V, >500 km	Nagahashi et al 2004, Shiihara et al 2011	High-K	Phonolitic	McLean et al 2018/ Shiihara et al 2011
Ta-d	Tarumai (J)	9700-9000 cal BP	Nakamura 2016 and refs therein	E	V, >200 km	Machida and Arai 2003	Low-K	Andesitic-Dacitic	Nakamura 2016
U-Oki/U-4	Ulleungdo (S)	10255-10177 cal BP	Smith et al 2011	ESE	V, >500 km	Machida et al 1984	High-K	Phonolitic-Trachytic	Smith et al 2011/ Shiihara et al 2011

Abbreviations: countries: J-Japan, C/N-China/N Korea, S-S Korea, R-Russia, I-Indonesia; distribution: V-visible layer, C-cryptotephra horizon.

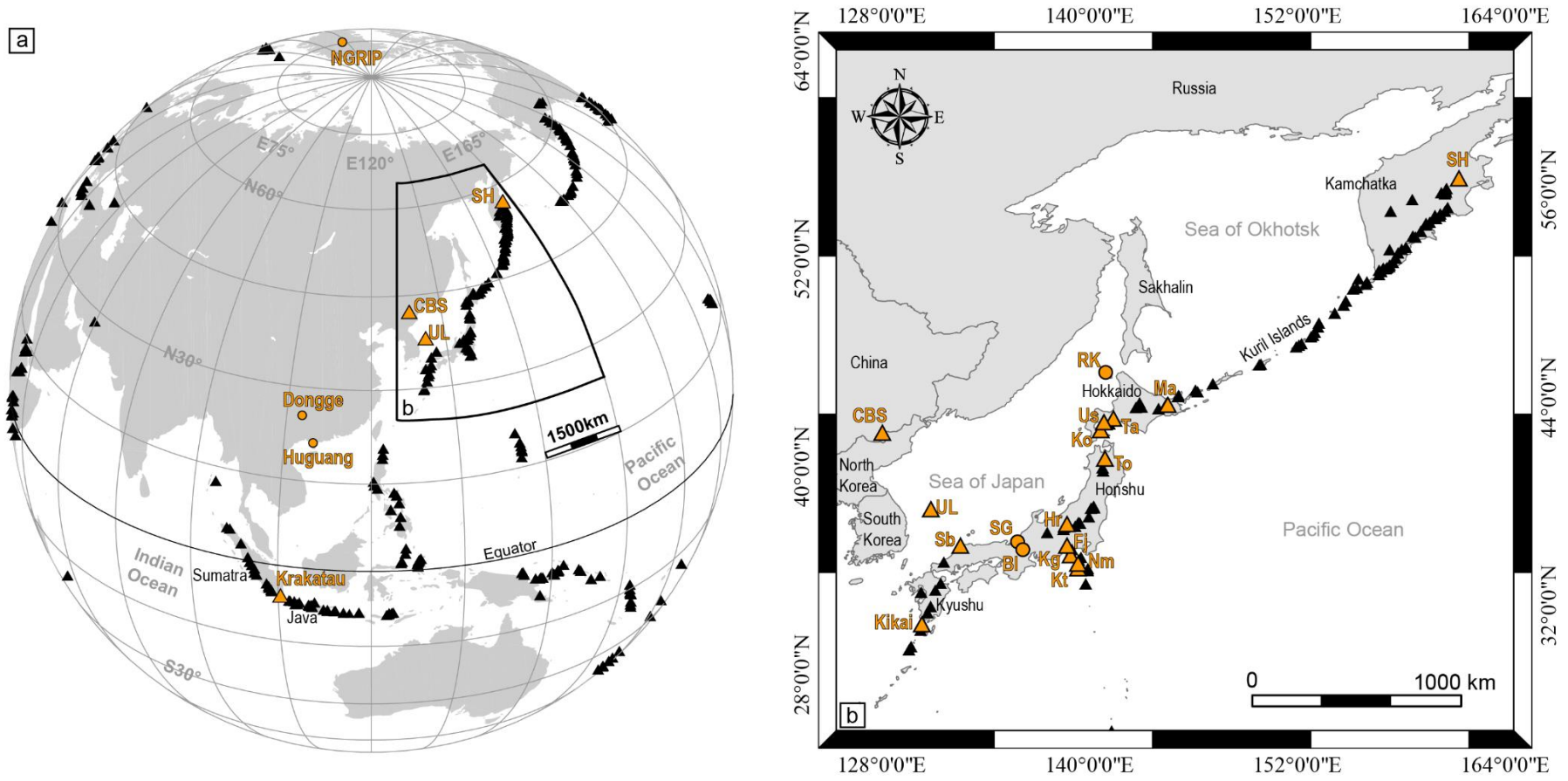

Fig. 5.1 (a) Map of the western Pacific rim and Greenland showing volcanoes (triangle) and palaeoclimatic archives (circle), with those related to the text highlighted using orange colour. The relevant Japanese volcanoes and lakes are not highlighted in this map given the limited space. (b)

Enlarged map of the NE Asia showing volcanoes (triangle) and distal archives for tephra studies (circle) in the region, with those mentioned in the text highlighted using orange colour. Abbreviations: Russia: SH-Shiveluch; China/N Korea: CBS-Changbaishan; S Korea: UL-Ulleungdo; Japan: Ma-Mashu, Ta-Tarumai, Us-Usu, Ko-Komagatake, To-Towada, Hr-Haruna, Fj-Fuji, Nm-Niijima, Kt-Kozushima, Kg-Kawagodaira, Sb-Sanbe, RK-Lake Kushu (Rebun Island), SG-Lake Suigetsu, BI-Lake Biwa. Kikai is a caldera in southern Kyushu, Krakatau is a submarine caldera in Indonesia. NGRIP, Dongge and Huguang are ice-core, cave and maar lake respectively.

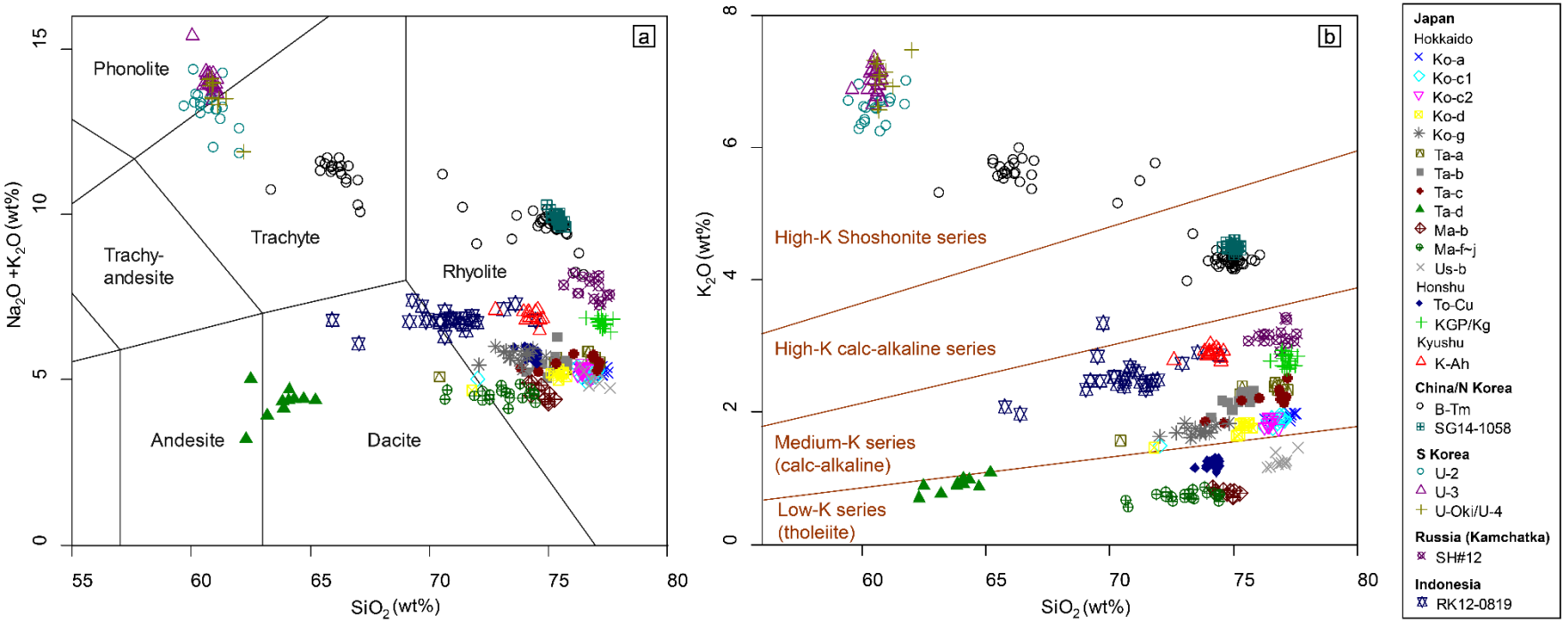

Fig. 5.2 Glass shard major element compositions of twenty-two tephra isochrons within the proposed East Asian Holocene tephrostratigraphic framework. (a) Total alkaline versus silica (TAS) diagram (classification scheme based on Le Bas et al. (1986)), (b) K-classification diagram (classification scheme based on Peccerillo and Taylor (1976)). The Ko-a, Ko-c1, Ko-c2, Ko-d, Ko-g are from Komagatake volcano. The Ta-a, Ta-b, Ta-c and Ta-d are from Tarumai volcano. The Ma-b and Ma-f~j are from Mashu volcano. The Us-b is from Usu volcano. The To-Cu is from Towada volcano. The KGP/Kg is from Kawagodaira volcano. The K-Ah is from Kikai caldera. The B-Tm and SG14-1058 are from Changbaishan volcano. The U-2, U-3, U-Oki/U-4 are from Ulleungdo. The SH#12 is from Shiveluch volcano. The RK12-0819 is from Krakatau volcano. Data sources see Table 5.1.

5.4.1 Tephra isochrons in Early Holocene (11.7-8.2 ka BP)

In this paper, subdivision of the Holocene Epoch follows the scheme proposed by Walker et al. (2012). Three tephras fall within the early Holocene period in the framework. They are the Ulleungdo U-Oki/U-4 and U-3 tephras, and Hokkaido Ta-d tephra (Table 5.1).

The U-Oki tephra represents the largest know Plinian eruption from the Ulleungdo volcano in the Sea of Japan (Fig. 5.1). It was dispersed towards the ESE and has been identified in a number of marine and terrestrial records (Machida and Arai, 1983; Machida et al., 1984). A detailed tephrostratigraphic study revealed that this tephra can be correlated to the proximal U-4 tephra (Shiihara et al., 2011). In both Lake Suigetsu and Lake Biwa in central Japan (Fig. 5.1), the tephra occurs as visible layers (Smith et al., 2011b, 2013; Takemura et al., 2010). It has been dated to 10255-10177 cal yr BP (2σ) in Lake Suigetsu by the SG06 chronology (Smith et al., 2011b). This distal age is slightly younger than the proximal ages derived from radiocarbon dating (OKuno et al., 2010) but supported by a high resolution proximal Ar-Ar age (Smith et al., 2011b). The known distribution of the tephra is based on visible tephra studies, which suggest a dispersal area covering the southwestern Sea of Japan and southwestern Honshu (Machida and Arai, 1983; Machida, 1999). A Holocene cryptotephra study in Lake Kushu, northern Japan (Fig. 5.1) failed to identify this marker tephra, which probably suggests that the northern limit of tephra dispersal did not reach northern Hokkaido (Chen et al., submitted). At the time of deposition of the U-Oki tephra, significant climate changes were not recorded in the Greenland ice core (NGRIP; NGRIP members, 2004) or the Chinese stalagmite (D4, Dongge Cave, location see Fig. 5.1; Dykoski et al., 2005) (Fig. 5.3). Interestingly, however, a high-resolution lacustrine record in SE China (Huguang Maar, location see Fig. 5.1) exhibits an apparent decrease of Ti content in the lake sediments (Fig. 5.3), which was interpreted as an indicator of a weakening East Asian winter monsoon (EAWM, Yancheva et al., 2007). The U-Oki tephra occurs at the end of this (around 300 yrs) low intensity winter monsoon period (Fig. 5.3). Sequences that contain this tephra, coupled with palaeoclimate proxy records allow verification of such a climate change event proposed by Yancheva et al. (2007).

The Ta-d tephra is one of the major tephra markers for northern Japan during the early Holocene (Nakamura, 2016). Erupted from Tarumai volcano in SW Hokkaido

(Fig. 5.1), the tephra was dispersed mainly toward the east and identified as visible tephra layers over 200 km away from the volcano (Machida and Arai, 2003). The age of this tephra, however, remains poorly constrained. Based on the calibration of radiocarbon dates, Nakamura (2016) calculated an age of 9700-9000 cal yr BP (2σ) for this tephra. The timing of this tephra, from a climatostratigraphic viewpoint, is very interesting. The proxy records from NGRIP, Dongge Cave and Huguang Maar all reveal significant climate oscillations during ca. 9.5-9.0 ka BP (Fig. 5.3). A rapid cooling event centred at ca. 9.3 ka BP was identified from multiple ice core records (Rasmussen et al., 2007), whereas the stalagmite record from Dongge Cave showed a dramatic decrease in the intensity of the East Asian summer monsoon (EASM) around 9165±75 yr BP (Dykoski et al., 2005). In contrast, the Huguang Maar record revealed a bimodal event around ca. 9.4 ka BP, indicating an intensified EAWM period (Yancheva et al., 2007). Based on these independently dated records, such events seem to differ from one other both in timing and duration (Fig. 5.3). At the moment, the age of the Ta-d tephra broadly overlaps with these climate events recorded in different regions. Once the tephra age is refined, combining with the future identification of the tephra in disparate archives, it is possible to precisely test the synchronicity of the climate events over a large geographic area and an inverse correlation between EASM and EAWM proposed by Yancheva et al. (2007).

The U-3 tephra from Ulleungdo volcano has a more limited known distribution compared to the U-Oki tephra, as the former has been identified in only a few sequences. In a Sea of Japan marine core KT96-17 P-2, the distal U-3 tephra exists as a cryptotephra (TRG1; Domitsu et al., 2002; Shiihara et al., 2011). In contrast, the tephra occurs as visible layers in both Lake Biwa (BT-4; Nagahashi et al., 2004; Shiihara et al., 2011) and Lake Suigetsu (SG14-1091; McLean et al., 2018) on Honshu Island. A proximal charcoal sample provides the current best age estimate for the tephra (8440-8360 cal BP (2σ); Im et al., 2012), which has been cross-validated by an independent distal age (8455-8367 cal BP (2σ); McLean et al., 2018). In terms of the climatostratigraphic positioning, the U-3 tephra is closely associated with a centennial scale climate oscillation recorded in the Huguang Maar (Fig. 5.3). Locating right at the beginning of a proposed weakened EAWM period (Yancheva et al., 2007), the U-3 tephra facilitates the verification of the reliability of the Ti content as an effective proxy for reconstructing the intensity of the winter monsoon, through comparison with other

palaeoclimate records that also bear this tephra. More importantly, if such climate events exist in other records, the tephra provides an opportunity for testing the synchronicity of the event between the marine and terrestrial realms.

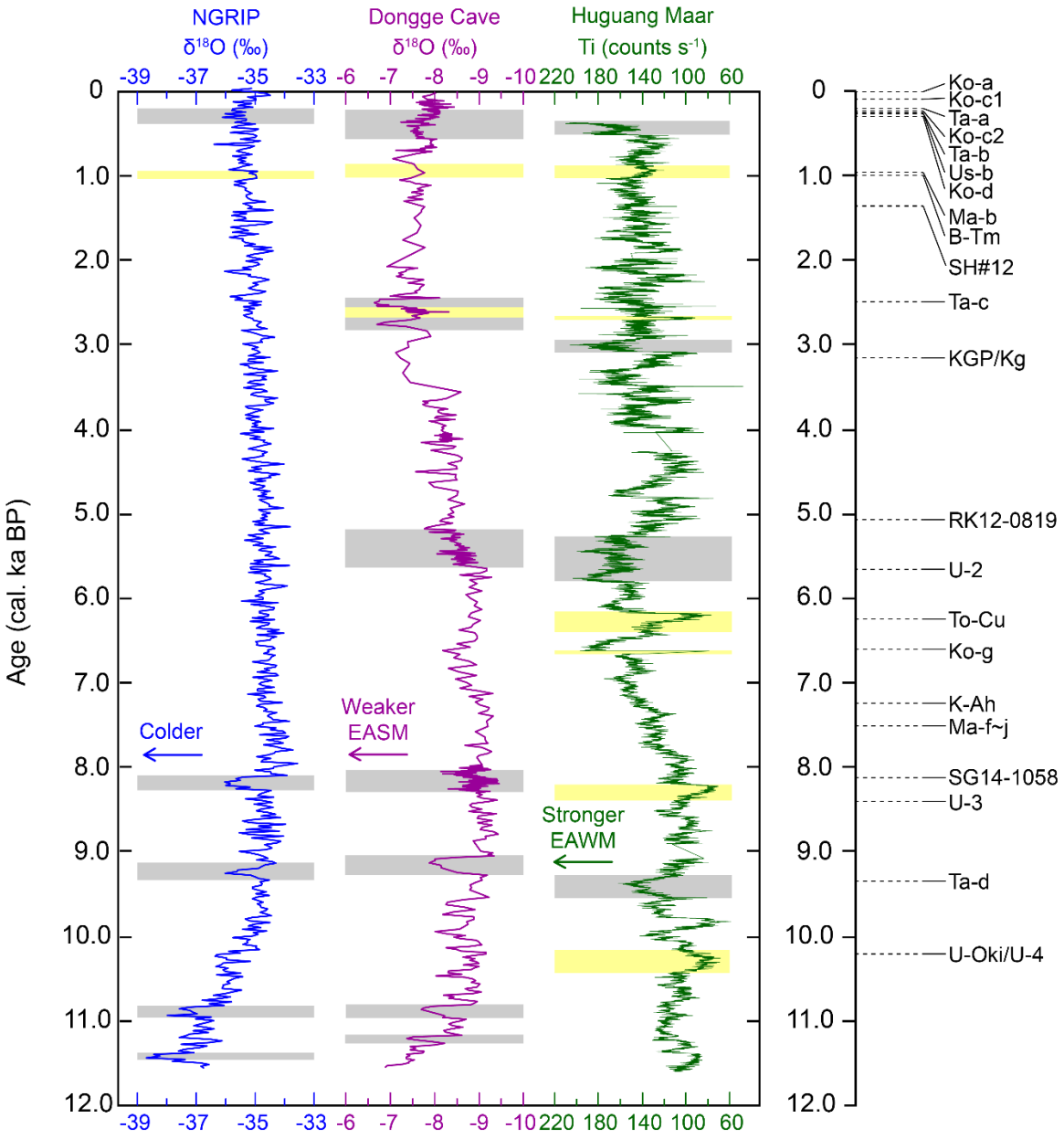

Fig. 5.3 The proposed East Asian Holocene tephrostratigraphic framework plotted against Greenland Ice-core (NGRIP) $\delta^{18}O$ record (NGRIP members, 2004), Chinese speleothem (D4, Dongge Cave) $\delta^{18}O$ record (Dykoski et al., 2005) and the Chinese lacustrine (Huguang Maar) Ti content record (Yancheva et al., 2007). The proxy records are plotted on their independent timescales (NGRIP converted from b2k to cal BP). The cooling events in Greenland, weakened East Asian summer monsoon (EASM) and intensified East Asian winter monsoon (EAWM) periods in East Asia are marked

with gray bars, whereas the warmer period in Greenland, intensified EASM and weakened EAWM periods in East Asia are marked with yellow bars. The chronostratigraphic positioning of the tephra layers is based on the median values of their age ranges (age ranges and data sources see Table 5.1).

5.4.2 Tephra isochrons in mid-Holocene (8.2-4.2 ka BP)

The mid-Holocene section of the tephra framework contains seven widespread tephra layers. They are the SG14-1058 tephra from China/N Korea, Ma-f~j, Ko-g and To-Cu tephras from northern Japan, K-Ah tephra from southern Japan, U-2 tephra from Ulleungdo and RK12-0819 tephra with a proposed Indonesian provenance (Table 5.1).

The SG14-1058 is a cryptotephra identified in Lake Suigetsu, which was correlated to the Changbaishan volcano (Fig. 5.1) (McLean et al., 2018) and specifically the Qixiangzhan eruption (Sun et al., 2018). Dated to 8166-8099 cal BP (2σ), the tephra presents an important isochron at the transition between the early and mid-Holocene, providing an opportunity to link palaeoclimate archives on both sides of the Sea of Japan. Climate in both the North Atlantic and East Asia have experienced centennial-scale oscillations at the time when the tephra was deposited, as shown in the NGRIP and Dongge Cave records (Fig. 5.3). At the moment correlations seem to exist between the cooling event in Greenland and a period of less intense EASM, though there could be different scenarios as the stalagmite recorded double events (Fig. 5.3). The high-resolution proxy records from Lake Suigetsu, would help test the correlation between the two climate systems. In addition, the identification of tephra in more palaeoclimate archives would facilitate the high-precision synchronisation of disparate records thus allowing us to test any regional variations in respond to the climate event. In spite of the palaeoclimate applications, the identification of the tephra has significant volcanological implications. For example the presence of a distal Changbaishan tephra at ~8.1 ka, contradicts known proximal ages (Wang et al., 2001; Yang et al., 2014), and reveals a previously undocumented period of explosive activity on the volcano (McLean et al., 2018). Another cryptotephra study in northern Japan, also identified several tephra layers from the volcano over the course of the Holocene period (Chen et al., submitted). These studies demonstrated the potential of distal archives to resolve the proximal explosive history of individual volcano. Although, at present, far more cryptotephra studies are required in the region to test this potential.

The Ma-f~j tephra represents the largest Holocene eruption of the Mashu volcano in eastern Hokkaido (Fig. 5.1). It was dispersed towards the ESE and had a bulk tephra volume of 18.6 km^3 (Kishimoto et al., 2009). Previous studies have revealed detailed proximal stratigraphy for this caldera-forming eruption (Katsui et al., 1975; Kishimoto et al., 2009), however, identification of the tephra has long remained in the proximal sites. The furthest known distribution of the visible layer was reported by Razzhigaeva et al. (2016), who traced the tephra following its main dispersal axis into the southern Kuril Islands, ~200 km away from the volcano. When the cryptotephra method was applied, the tephra footprint can be significantly enlarged. For example, Chen et al. (submitted) reported the presence of the Ma-f~j as a cryptotephra in Lake Kushu Rebun Island ~350 km NW of the Mashu volcano (Fig. 5.1), which is in the opposite direction to the primary plume dispersal axis. This indicates that the tephra has a much larger distribution area than defined from visible tephra studies, mantling most of the Hokkaido and the Kuril arc (Fig. 5.4). However, only the cryptotephra technique could help uncover its full potential in correlating disparate sequences. Radiocarbon dating of charcoal samples preserved within the tephra layer provides an age of 7581-7440 cal BP (2σ) for the tephra (calibrated based on two dates from Yamamoto et al. (2010)). Although there are some older dates derived from organic materials immediately below the tephra layers (c.f. Nakamura and Hirakawa, 2004; Razzhigaeva et al., 2016), Bayesian age modelling exercises (Chen et al., submitted) suggest that they might be too old. Palaeoclimate proxy records indicate that the deposition of the tephra occurred in a relatively stable period (Fig. 5.3). Nevertheless, identification of the tephra provides opportunity for precise dating and correlation of palaeoclimate records.

The K-Ah tephra from Kikai caldera in southern Kyushu (Fig. 5.1) is the most widespread Holocene tephra in East Asia (Machida and Arai, 1978; Machida and Arai, 1983; Machida, 1999). Discharging a bulk volume of ~170 km^3 tephra, the eruption dispersed the K-Ah ash over 1300 km mantling an area from southwest to central Japan, and the adjacent seas (Machida and Arai, 1983). Identified as a visible layer in Lake Suigetsu, central Japan, the K-Ah was precisely dated to 7303-7165 cal BP (2σ) (Smith et al., 2013). Despite its widespread (>1300 km) eastward distribution, the tephra did not reach Hokkaido, as a recent cryptotephra study failed to identify it in the Rebun Island (Chen et al., submitted). The extensive occurrences of the tephra on land and in the marine environments (e.g. Sea of Japan, Pacific Ocean and East China Sea) allow

precise dating of terrestrial and marine sequences, and the test of the correction factors for the marine reservoir effect. Moreover, the deposition of the tephra coincides with the timing of the maximum Holocene transgression reported in a locality near the South China Sea (Parham et al., 2014). As such the tephra is important for our understanding of palaeoenvironmental changes associated with postglacial sea level fluctuations and local tectonic movements (Machida, 1999).

The Ko-g tephra represents the largest Plinian eruption of the Komagatake volcano in SW Hokkaido (Fig. 5.1) during the Holocene (Yoshimoto et al., 2008). The tephra was dispersed towards the ENE, covering most of southern and eastern Hokkaido (Furukawa and Nanayama, 2006). The furthest identification of the visible Ko-g tephra was reported by Razzhigaeva et al. (2016), which extended its known limit from eastern Hokkaido (~350 km) to the southern Kuril Islands (~450 km). More importantly, a cryptotephra study revealed that the northern limit of the Ko-g is Lake Kushu Rebun Island (Chen et al., submitted), which confirmed that the tephra actually mantles Hokkaido rather than only its southern and eastern parts (Fig. 5.4). Several studies attempted to unravel the age of the tephra, and the results yield various but overlapping dates (e.g. 6661-6448 cal BP (2σ), Nakamura and Hirakawa, 2004; 7156-6551 cal BP (2σ), Yoshimoto et al., 2008; 6830-6640 cal BP (2σ), calibrated based on Razzhigaeva et al. (2016)). A recent Bayesian modelling study (Chen et al., submitted) taking into account all the available chronological, stratigraphic and depositional information of the Ko-g tephra, provides the current best age estimate for the tephra (6686-6520 cal BP (2σ)). The deposition of the tephra coincides with a decadal-scale oscillation revealed by a sudden decrease of Ti content in the Huguang Maar record (Fig. 5.3), which was interpreted as less intense EAWM (Yancheva et al., 2007). The identification of the tephra in other high resolution records would help verify the existence of such a rapid event.

The To-Cu tephra represents the largest-volume Plinian eruption of the Towada caldera in northern Honshu (Fig. 5.1) during the Holocene (Hayakawa, 1985). The eruption dispersed tephra over 200 km to the SE, covering parts of northern Honshu and coastal regions of the Pacific (Machida and Arai, 2003). A recent cryptotephra study has significantly increased its known distribution to ~700 km to the SW of the source in central Honshu (Fig. 5.4) (McLean et al., 2018). The age of the tephra varies from study to study. Proximally, Kudo et al. (2003) reported a date of 6282-5926 cal

BP (2σ) for soil below To-Cu, whereas Inoue et al. (2011) reported a slightly order age of 6313-6180 cal BP (2σ) for humin within soils below the tephra. Both the dates are in agreement within error with the age derived from charcoal preserved within the tephra (6480-5897 cal BP (2σ), calibrated based on Hayakawa (1983)). Distally, however, the tephra was dated to 5986-5899 cal BP (2σ) in lake Suigetsu (McLean et al., 2018), which is slightly younger than those proximal ages. The deposition of the To-Cu tephra occurred in a period where the Greenland ice core and the Chinese cave records show stabilized characteristics of regional climates whereas the lacustrine record in SE China displays remarkable multicentennial-scale climate oscillations (Fig. 5.3). The Lake Suigetsu proxy record might help understand these regional variations, and the To-Cu tephra would largely facilitate high precision proxy comparison.

The U-2 tephra from Ulleungdo volcano was thought to be generated by a smaller eruption compared to the U-Oki/U-4 and U-3, as the tephra has only been identified in the proximal sites for a long time (Machida et al., 1984; Shiihara et al., 2011; Kim et al., 2014). Recently it was identified as a distal cryptotephra in Lake Suigetsu (McLean et al., 2018). Identification of the tephra in central Japan indicates that it should cover an extensive area in the Sea of Japan, probably as a cryptotephra layer. The age of the tephra was dated to 5681-5619 cal BP (2σ) in Lake Suigetsu (McLean et al., 2018), which was supported by proximal ages derived from charcoal samples preserved within the tephra layer (OKuno et al., 2010). The deposition of the tephra coincides with climate change events recorded in both speleothem and lacustrine records in China. In the Dongge cave record, EASM intensity exhibited a gradual decline since ca. 5.6 ka BP (Dykoski et al., 2005). The intensity continuously decreased for ~400 years and did not rebound at the end of the event (Fig. 5.3). In contrast, the intensity of the EAWM recorded in Huguang Maar showed a multicentennial-scale intensified period at roughly the same time. The intensity of the winter monsoon experienced a dramatic decline at the end of the event (Fig. 5.3). An inverse correlation between the intensity of summer and winter monsoon proposed by Yancheva et al. (2007) seems to hold in this period, but the timing, duration and termination of the climate events vary in the two records. The Lake Suigetsu proxy record should shed light on these regional variations, and future identification of the U-2 tephra in other archives would facilitate high precision proxy comparison.

The RK12-0819 tephra, dated at 5287-4861 cal BP (2σ), is an exotic layer which was first identified as a cryptotephra in Lake Kushu northern Japan (Chen et al., in preparation). The tephra has a very heterogeneous medium-K dacitic to rhyolitic glass composition with ca. 10% variations in SiO_2 content (Fig. 5.2). These compositions are very distinctive compared to those of the tephras originating from East Asia. For example, the Japanese tephras have typically more evolved compositions (c.f. Aoki and Machida, 2006) whereas back-arc volcanism tends to produce tephra with high-K compositions (e.g. Changbaishan and Ulleungdo tephras; Fig. 5.2). There is no match with Holocene tephras from Kamchatka, but a full match of the major element glass chemistry with a visible marine tephra layer near Sumatra (Chen et al., in preparation). On this basis Chen et al. (in preparation) proposed an Indonesian provenance for the RK12-0819 tephra. Further investigations on large Holocene Indonesian eruptions suggested the Krakatau volcano (Fig. 5.1) as the most probable source (Chen et al., in preparation). If this is the case, then RK12-0819 represents the furthest known latitudinal tephra dispersal, which allows interhemispheric correlation of widespread palaeoclimate records, linking the low southern latitudes to mid-northern latitudes. We thus have included this tephra layer in our proposed tephra framework.

5.4.3 Tephra isochrons in Late Holocene (4.2-0 ka BP)

Twelve tephra isochrons are integrated within the tephra framework during the late Holocene. These include nine major markers from Hokkaido, one from Honshu, one from China/N Korea and one from Kamchatka (Table 5.1).

The oldest tephra within the late Holocene timeframe is the KGP/Kg tephra erupted from Kawagodaira volcano in SE Honshu (Fig. 5.1). With a bulk volume of 1.04 km^3, the tephra was mainly dispersed towards the west and covers some large areas of the central and western Honshu (Shimada, 2000; Tani et al., 2013). In Lake Biwa, the tephra was described as a dispersed ash horizon (Nagahashi et al., 2004; Takemura et al., 2010) whereas in a further west locality, Lake Suigetsu (~300 km from the source), the tephra occurred as a cryptotephra layer (McLean et al., 2018). The current best age estimate for the tephra was provided by radiocarbon wiggle-matching of a Japanese cedar timber found within the associated pyroclastic flow deposit, which dated the eruption to 3160-3137 cal BP (2σ) (Tani et al., 2013). Given its very precise age, the

tephra is important for the dating of archaeological sequences of the late and final Jōmon period in the Japanese prehistory.

Postdating the KGP tephra, the Ta-c tephra from Tarumai volcano is one of the major markers in Hokkaido during the late Holocene. Dispersed mainly towards the east, the tephra was found covering most of the southern and eastern Hokkaido (Furukawa and Nanayama, 2006; Nakamura, 2016) and has recently been traced into the southern Kuril Islands (Razzhigaeva et al., 2016). The age of the tephra is poorly constrained at the moment. Nakamura (2016) provided an age of 2800-2500 cal BP (2σ) based on calibration of previously reported dates. In contrast, Razzhigaeva et al. (2016) proposed a younger age of 2500-2300 cal BP (2σ) for the tephra. We are not able to determine which age is more reliable due to a lack of detailed information regarding the radiocarbon dates. This is unfortunate as the Ta-c tephra would serve as a useful isochron for dating and synchronising palaeoclimate records. It is worth noting that Mackay et al. (2016) proposed a possible correlation between a cryptotephra (FBB12-162) identified in east coast of North America and the Ta-c tephra. However, the correlation is not yet confirmed due to the limited amount of analyses on distal shards. Nevertheless, if this could be proven in the future, then the Ta-c tephra provides a valuable isochrons linking East Asia and North America across the Pacific Ocean.

The SH#12 (SH_{1450}) tephra is the other exotic layer that has been incorporated into the Holocene East Asian tephra framework. Erupted from the Shiveluch volcano in the Kamchatka Peninsula, Russia (Fig. 5.1), the tephra was dispersed towards the SE (Kyle et al., 2011; Ponomareva et al., 2015) and identified in a number of localities ~50-100 km to the east of the volcano (Ponomareva et al., 2017). Chen et al. (submitted) reported the occurrence of the tephra in Lake Kushu northern Japan (RK12-0225), which is the furthest known distribution of the tephra ~1900 km from the vent. More importantly, this is the first example of Russian tephra interlinked with Japanese eruptions, which allows connection between the East Asia and the further north Kamchatka region to be established (Fig. 5.4), significantly widening the geographical area over which precise correlations of palaeoclimate records can be achieved. In addition, it is reasonable to predict that the tephra can be traced following its main dispersal axis over 1900 km into the Aleutian Arc, the Bering Sea and probably the SW Alaska, which would serve as a potential correlation tool linking records in NE Asia and North America. The age of the tephra was dated proximally to 1408-1311 cal BP (2σ) (Ponomareva et al., 2017), which

is supported by and slightly more precise than the age determined distally (1389-1275 cal BP (2σ), Chen et al., submitted).

The B-Tm and the Ma-b tephras chronologically postdate the SH#12 tephra and are closely spaced in time (Table 5.1). The distal B-Tm tephra was first identified in a number of marine and terrestrial records in the Sea of Japan and northern Japan (Machida and Arai, 1983) and correlated to the Changbaishan volcano (Machida et al., 1990). Machida (1999) proposed the distribution for the B-Tm tephra based on tracing the visible tephra layer. Recently, the tephra was reported from a number of new localities including northeast China (Sun et al., 2015), the Russian Far East (Razjigaeva et al., 2017), northern Japan (Chen et al., 2016), central Japan (McLean et al., 2016), and as far as Greenland (Sun et al., 2014a). Moreover, the age of the tephra has been precisely dated to 946 CE, which is reliably cross-validated by ice-core chronology (Sigl et al., 2015) and ^{14}C spike-matching dendrochronology (Oppenheimer et al., 2017; Hakozaki et al., 2017). As such the tephra provides a valuable isochron for dating sequences and serves as a correlation tool directly linking records between East Asia and North Atlantic climate systems. Importantly, the B-Tm tephra was deposited right at the beginning of the Medieval Warm Period (ca. 950-1250 CE; Mann et al., 2009). It thus permits the investigation of the climate anomaly event in detail for its climatic forcing and environmental responses across a vast geographic area.

The Ma-b tephra represents the volumetrically second largest Holocene eruption of the Mashu volcano (Kishimoto et al., 2009). With a bulk volume of 4.6 km^3, the tephra was thought to be dispersed towards the north (Machida and Arai, 2003). Furukawa and Nanayama (2006), however, proposed that the tephra was dispersed easterly and this was supported by Razzhigaeva et al. (2016), who traced the tephra over 200 km towards the ENE into the southern Kuril Islands. All the above-mentioned studies were based on visible tephra layer, and recently, the Ma-b was identified as a cryptotephra layer in Lake Suigetsu (McLean et al., 2018). Lake Suigetsu is located over 1100 km SW of the Mashu volcano, in the opposite direction to the main dispersal axis. This indicates that the tephra has a much larger distribution area than is currently known (Fig. 5.4). The age of the tephra is best constrained in Lake Suigetsu, where it has been dated to 960-992 CE (2σ; McLean et al., 2018). Given its close chronostratigraphic relationship with the Medieval Warm Period (ca. 950-1250 CE), the widespread Ma-b tephra can be used to test the synchronicity of the climate event same as the B-Tm tephra.

In the uppermost section of the tephrostratigraphic framework, seven major marker tephras from Hokkaido volcanoes are integrated based on their ages and stratigraphic relationships observed at outcrops (Nakamura, 2016; Razzhigaeva et al., 2016). They are Ko-d, Us-b, Ta-b, Ko-c2, Ta-a, Ko-c1 and Ko-a dated by historic records to 1640 CE, 1663 CE, 1667 CE, 1694 CE, 1739 CE, 1856 CE and 1929 CE respectively (Ōba et al., 1983; Katsui and Komuro, 1984; Nakamura, 2016 and refs therein).

The Ko-d, Ko-c2, Ko-c1, and Ko-a tephras are from the Komagatake volcano in SW Hokkaido (Fig. 5.1) and have different dispersal directions (Machida and Arai, 2003; Furukawa and Nanayama, 2006; Nakamura, 2016). The Ko-d was known to disperse towards the NW and identified over 120 km away from the volcano as a visible layer (Machida and Arai, 2003). With a bulk volume of 2.9 km^3, it is therefore predictable that the tephra should mantle a large area of the northeastern Sea of Japan. The Ko-c2 and Ko-c1 tephras were both dispersed towards the ENE and covered most of the southern and eastern Hokkaido (Machida and Arai, 2003; Furukawa and Nanayama, 2006). Compared to the Ko-c1, the Ko-c2 tephra was identified in more outcrops and had a 3 cm thickness at a distance of 300 km away from the volcano whereas the Ko-c1 only had a 0.5 cm thickness at the same distance (Furukawa and Nanayama, 2006). A recent study has traced the visible Ko-c2 and Ko-c1 layers into the southern Kuril Islands over 550 km from the source volcano (Razzhigaeva et al., 2016). The Ko-a tephra was dispersed towards the ESE and identified on land in southern Hokkaido (Furukawa and Nanayama, 2006). Given its dispersal axis, the tephra was most probably deposited in the marine environment. Razzhigaeva et al. (2016) reported visible Ko-a in the southern Kuril Islands indicating dispersal of the tephra was more southern than previously thought.

The Us-b tephra is from the Usu volcano and Ta-b and Ta-a are from the Tarumai volcano. Both of the volcanoes are located in SW Hokkaido (Fig. 5.1). The Us-b and Ta-b were both dispersed towards the east and identified in much of southern Hokkaido (Machida and Arai, 2003). Both of the tephras were found over 350 km away from their source volcanoes but the difference is that the Ta-b was traced into eastern Hokkaido as a visible layer while the Us-b was not (Furukawa and Nanayama, 2006). As such the Ta-b seemed to have a wider distribution compared to the Us-b. A recent study confirmed this as the Ta-b has been reported from the southern Kuril Islands ca. 600 km away from the Tarumai volcano (Razzhigaeva et al., 2016). This has significantly

extended the known distribution of the visible Ta-b tephra and indicates a more southerly and easterly dispersal of the tephra. The Ta-a tephra was dispersed towards ENE and had the largest volume (4km^3) among the seven historic tephras (Machida and Arai, 2003). The tephra was known to cover most of the Hokkaido in a visible form (Furukawa and Nanayama, 2006). Its furthest known visible occurrence was reported from the southern Kuril Islands (ca. 600 km) same as the Ta-b, but it occurred in more outcrops in the study areas than the Ta-b layer (Razzhigaeva et al., 2016).

The tephras that were deposited in the historic time are chronologically associated with the Little Ice Age (ca. 1400-1700 CE; Mann et al., 2009). During the Little Ice Age, the Dongge cave recorded a declined EASM whereas the Huguang Maar record showed an intensified EAWM (Fig. 5.3). The NGRIP record, however, showed a less profound temperature decrease which occurred later than the events recorded in the East Asia region. The historic tephras can help precisely align different palaeoclimate records within East Asia thus facilitate the constraints of synchronicity of the climate event. More importantly, given that more and more Asian tephras were being reported from the Greenland ice core records (e.g. Sun et al., 2014a; Bourne et al., 2016; Cook et al., 2018b), it is possible to precisely test the leads and lags of the Little Ice Age between North Atlantic and East Asia systems once these tephras are identified in Greenland.

5.5 Potential improvement and future opportunities

5.5.1 Potential candidates

Most of the Japanese tephras within the framework are from northern Japan (i.e. Hokkaido), because these volcanoes (e.g. Komagatake, Usu, Tarumai, Mashu) produced large explosive eruptions during the Holocene, which dispersed tephra over long distances (Table 5.1). Volcanic centres in southern Japan (i.e. Kyushu) were very active during Holocene, but they mainly produced tephra layers with limited distribution in contrast to those large caldera-forming eruptions occurred in the Pleistocene (c.f. Moriwaki et al., 2016), except for the K-Ah tephra (Machida and Arai, 1978). Central Japan (i.e. Honshu) hosts a lot of active volcanoes with numerous Holocene eruptions, and there are widespread tephras with the potential to form regional marker horizons (Machida and Arai, 2003). However, tephras originating from

this region have not been widely researched. In this section, we describe several tephras from central Japan which we recommended as potential candidates to be incorporated in the framework in the future (Table 5.2), based on reviewing their known distribution. The reasons for them not being included at the moment were also highlighted.

The SG14-1185 is a cryptotephra layer which has been identified in Lake Suigetsu (McLean et al., 2018). It is precisely dated to 9372-9301 cal BP (2σ) by the SG14 chronology thus can serve as a tool for dating palaeoclimate records. However, its provenance is currently unknown and McLean et al. (2018) suggested that it could be a far-travelled tephra as its glass composition did not match sources in East Asia. We recommend that once the provenance of the tephra is unravelled, it should be included in the tephra framework and serves as a marker horizon in the early Holocene, given its well constrained age and glass composition (c.f. McLean et al., 2018).

The S-Oh tephra is from the Sanbe volcano in SW Honshu (Fig.1) (Miura and Hayashi, 1991; Fukuoka and Matsui, 2002). It was dispersed towards ENE and identified as a cryptotephra layer in Lake Biwa over 320 km from the source volcano (Takemura et al., 2010). The age of the tephra is poorly constrained (4143-3698 cal BP (2σ); Miura and Hayashi, 1991) and the grain-specific glass data are not available currently. Once the age and the glass chemistry are resolved, this tephra could be included in the tephra framework given its relatively wide distribution.

The Hr-FP tephra is from the Haruna volcano (named Hr-I in Soda 1989) in central Honshu (Fig. 5.1) and is one of the most widespread Holocene tephras originating from Honshu (Machida and Arai, 2003). Found in the archaeological sequences, the tephra was roughly dated to the mid- to late 6th century (Soda, 1989). The tephra was dispersed towards the NE and identified as a visible layer over 300 km from the source (Machida and Arai, 2003). Recently, Ikehara et al. (2017) reported the presence of the visible Hr-FP tephra in multiple marine cores off northeastern Honshu in the Pacific Ocean. This has extended the distribution of the tephra to ~600 km from the source. As such the Hr-FP is indeed a widespread layer that could be used to link terrestrial and marine sequences between central Japan and the Pacific Ocean. However, the current correlations are based on mineral assemblages and glass refractive index (Ikehara et al., 2017). Precisely determined glass chemistry and age estimate is needed before this widespread horizon can be included into the East Asian tephra framework.

The Iz-Kt tephra is from the Kozushima volcano in SE Honshu (Fig. 5.1) and dated precisely to 838 CE based on evidence from historical documents (Tsukui et al., 2006). It was dispersed towards the NNE and found as a visible layer over 100 km from the volcano (Machida and Arai, 2003). McLean et al. (2018) reported the Iz-Kt as a cryptotephra in Lake Suigetsu thus extending the tephra distribution to ~340 km. Unfortunately, there was another eruption from Niijima volcano (Fig. 5.1) that produced geochemically similar tephra in 886 CE (i.e. Iz-Nm tephra; Tsukui et al., 2006; McLean et al., 2018). This has created an issue for precise correlation in the distal site, as the two tephra are difficult to separate both geochemically and chronologically (McLean et al., 2018). Unless the two layers are both present in the same sequence (i.e. stratigraphic evidence), otherwise distal-proximal correlation based on glass geochemistry and geochronology can be tricky. Trace element glass chemistry might help resolve this problem, but until then, the tephra will not be included in the tephra framework.

The To-a tephra is from one of the two volumetrically largest Holocene eruptions of the Towada caldera (Hayakawa, 1985). The tephra was dispersed towards the south and found as a visible layer over 300 km from the volcano (Machida and Arai, 2003). Based on reviewing historical records, Hayakawa and Koyama (1998) confirmed that the eruption occurred in 915 CE. Therefore, the layer is closely associated with the Medieval Warm Period (ca. 950-1250 CE; Mann et al., 2009), as with the B-Tm and Ma-b, and may help constrain the precise starting time of the Medieval climate anomaly. However, full dataset of the grain-specific glass chemistry of the tephra is not reported from any literature at the moment. As such the tephra has not yet been included in the East Asian tephra framework.

The F-Ho tephra represents one of the largest Plinian eruptions of the Fuji volcano (Fig. 5.1) throughout its entire history (Miyaji et al., 2011). The tephra was dispersed towards the east and identified as a visible layer over 180 km from the volcano (Machida and Arai, 2003). Dated precisely to 1707 CE by historical records, the tephra provides an isochron right at the end of the Little Ice Age (ca. 1400-1700 CE; Mann et al., 2009). Given it close chronostratigraphic position with the Litter Ice Age, it is ideal for testing the synchronicity of the termination of the climate event across different regions. The issues for this tephra not being included in the tephra framework include

that on one hand, its known distribution is not wide enough currently, and on the other hand, grain-specific glass chemistry of the tephra is not yet available.

Table 5.2 Summary information of six additional tephra candidates which could be included in the East Asian Holocene tephrostratigraphic framework with further investigation.

Tephra	Source volcano	Age estimante (2σ)	Age Ref	Dispesal axis	Furthest known distribution	Distribution ref	Reason(s) for not being incorporated in the framework at the moment
F-Ho	Fuji	1707 CE	Miyaji et al 2011	E	V, >180 km	Miyaji et al 2011	Grain-specific glass data not available, whole-rock data only
To-a	Towada	915 CE	Hayakawa and Koyama 1998	S	V, >300 km	Machida and Arai 2003	Grain-specific glass data not available, average glass data only
Iz-Kt	Kozushima	838 CE	Tsukui et al 2006	NNE	C, ~340 km	McLean et al 2018	Stratigraphically and geochemically similar to the Iz-Nm tephra (886 CE)
Hr-FP	Haruna	Mid-sixth-century	Machida and Arai 2003	NE	V, >300 km	Machida and Arai 2003	Poorly constrained age, grain-specific glass data not available
S-Oh	Sanbe	4143-3698 cal BP	Miura and Hayashi 1991	ENE	C, ~320 km	Takemura et al 2010	Poorly constrained age, grain-specific glass data not available
SG14-1185	N/A	9372-9301 cal BP	McLean et al 2018	N/A	Lake Suigetsu	McLean et al 2018	Unknown provenance and unknown distribution

Note: V-visible layer, C-cryptotephra horizon.

5.5.2 Future opportunities for tephrochronology in East Asia

East Asian is a volcanically active region with great potential of offering numerous useful and widespread tephra isochrons (Machida, 1999; Machida and Arai, 2003). In light of recent identifications of Asian tephras in Greenland (Sun et al., 2014a; Bourne et al., 2016; Cook et al., 2018b), Artic circle (van der Bilt et al., 2017) and probably North America (Mackay et al., 2016), and the identification of Russian and Indonesian tephra in northern Japan (Chen et al., submitted; Chen et al., in preparation), East Asia is an ideal region for the search of widespread tephra isochrons. However, the cryptotephra method (e.g. Turney, 1998; Blockley et al., 2005) that is commonly employed in Europe and North Atlantic regions has very limited applications in East Asia. So far, probably only two studies have applied the method to systematically search for cryptotephra horizons in continuous sequences (Lake Suigetsu, McLean et al., 2018; Lake Kushu, Chen et al., submitted). Yet both studies have proven the method extremely useful, as on one hand, the known distributions of several key tephra markers have been significantly enlarged (Fig. 5.4), and on the other hand, a number of previously undocumented tephra horizons were reported from the studies (McLean et al., 2018; Chen et al., submitted). These findings have significantly augmented the effect of the related tephras as isochrons for synchronising widespread palaeoclimate records, and encouraged the search of more widespread tephra horizons occurred in or originating from the region. In terms of volcanological applications, these new findings derived from cryptotephra studies also allow a much clearer insight into the eruptive history of the volcanoes in the region (e.g. Changbaishan volcano; McLean et al., 2018; Chen et al., submitted), which in turn facilitate the volcanic hazard assessment and the prediction of future eruption. Given these fruitful results, we strongly advocate that the state-of-the-art cryptotephra method should be more systematically applied in this active volcanic region, preferably in distal archives, in order to fully unlock the potential of East Asian tephras as important dating and correlating tools with extensive applications in Quaternary researches.

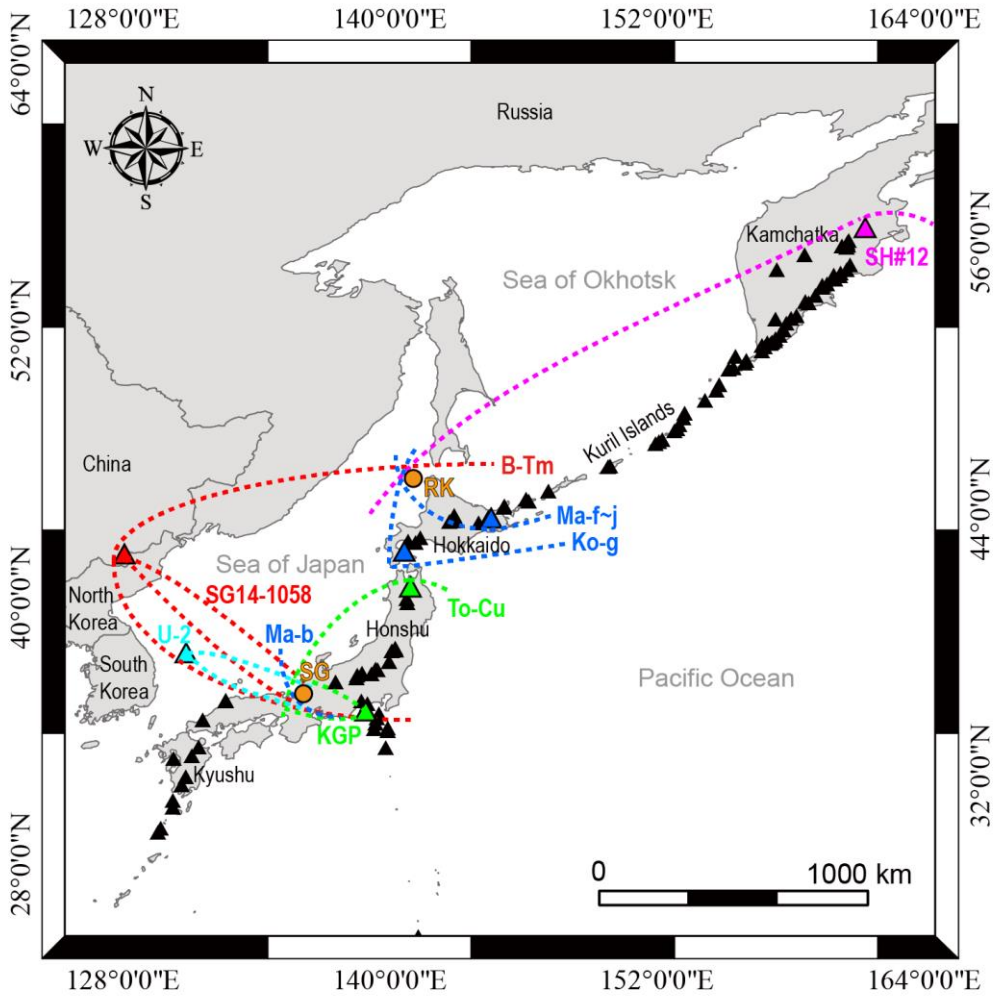

Fig. 5.4 Map of the NE Asia showing the up-to-date distribution of several key marker tephras based on recent pioneering cryptotephra studies in the region (McLean et al., 2018; Chen et al., 2016; Chen et al., submitted). In Lake Kushu (RK) northern Japan, Ko-g tephra from Komagatake volcano (SW Hokkaido), Ma-f~j tephra from Mashu volcano (E Hokkaido), B-Tm tephra from Changbaishan volcano (China/N Korea) and SH#12 tephra from Shiveluch volcano (Kamchatka Russia) are identified as cryptotephra horizons (Chen et al., 2016; Chen et al., submitted). In Lake Suigetsu (SG) central Japan, KGP tephra from Kawagodaira volcano (SE Honshu), To-Cu tephra from Towada volcano (N Honshu), Ma-b from Mashu volcano (E Hokkaido), U-2 tephra from Ulleungdo (S Korea), SG14-1058 tephra from Changbaishan volcano (China/N Korea) are recorded as cryptotephra horizons and B-Tm tephra from Changbaishan volcano (China/N Korea) is recorded as a visible layer (McLean et al., 2018). The identification of these tephra layers in the two studies is constraining the furthest edge of distribution of the correlative tephras thus provides the most important information on regional tephra dispersal.

5.6 Conclusions

The framework presented here is a basis for future cryptotephra studies and represents an essential first step towards a master Holocene tephrostratigraphy for East Asia. A total of twenty-two widespread tephras have been selected and incorporated in the framework, based on results from previous extensive visible tephra studies and recent pioneering cryptotephra research. All these tephra horizons are known to be widespread, reliably dated proximally or distally (Table 5.1), with grain-specific glass chemistry available which is fundamental for precise tephra correlation. We review and update the relevant information (e.g. age, distribution and chemistry) on these tephra layers and evaluate their chronostratigraphic relationships with abrupt climate oscillation events during the Holocene and discuss that how they can be used to facilitate high precision proxy comparison. A list of potential candidates, including six widespread tephras originating from Honshu, which have not yet been included in the framework are also discussed, with the suggestions of future work as the prerequisite for them to be eventually incorporated. The fruitful results derived from recent pioneering cryptotephra studies (McLean et al., 2018; Chen et al., 2016; Chen et al., submitted; Chen et al., in preparation), present significant encouragement for the continuous employment of the cryptotephra method in this region, which might eventually lead to a revolution in East Asian tephrochronology, as with the Europe and North Atlantic regions during the past few decades (Davies, 2015).

Chapter 6: Conclusions

The overall aim of this thesis is to develop an integrated Holocene tephrostratigraphy for East Asia and to explore its utility in palaeoclimate research. A summary of the main conclusions of each chapter is presented here, along with the suggestions for future work.

6.1 Tephrochronology of Changbaishan volcano (Chen et al., 2016)

In this study, tephra correlations between Changbaishan volcano NE China and Lake Kushu northern Japan are established, constrained by a full spectrum of glass chemistry (major, minor and trace element) and independent chronological data. This is then used to clarify the controversial proximal volcanic stratigraphy, which is largely due to the inherent difficulty in dating ultra-young (< 1ka) volcanic rocks. This study proposes that the three investigated proximal pyroclastic fall units are erupted as part of the Millennium eruption. In addition, the robust correlation of the analysed Kushu tephra with the Changbaishan Millennium eruption tephra allows the use of high-precision tephra ages to constrain the radiocarbon chronology in the related interval of the Lake Kushu sedimentary record.

This study reports the B-Tm tephra from Lake Kushu, which allows future palaeoclimate proxy records from the site to be synchronised with records in Greenland and central Japan (i.e., Lake Suigetsu). As such it directly addresses the aim of using tephra isochron to aid palaeoclimate research in the region.

6.2 Tephrostratigraphy in Lake Kushu northern Japan (Chen et al., submitted)

This study presents the first cryptotephra stratigraphy in northern Japan using the high resolution lacustrine archive from Lake Kushu, Rebun Island, which facilitates the construction of an integrated tephra framework for East Asia through providing an important northern element of a regional tephra lattice. The detailed RK12 Holocene tephrostratigraphy integrates local and far-travelled tephras originating from regions in Japan, China (Chen et al., 2016), Russia and as far south as Indonesia (Chen et al., in preparation). In this study, the distribution of several regional tephra markers is

significantly enlarged, and a number of previously undocumented tephra layers are identified. These results highlight the importance of cryptotephra studies in a volcanically active region. Given that there are extensive on-going high resolution proxy analyses from the sequence, and that the tephra isochrons recorded in the sequence have very wide distributions, connecting with the high northern latitudes (e.g. Greenland, Kamchatka) and the low southern latitudes (e.g. Indonesia), this tephra study makes the Kushu RK12 record a key archive for regional and global palaeoclimate research.

This study directly addresses the aim of constructing a Holocene tephrostratigraphy for northern Japan, which in turn aids the development of a regional tephra framework for East Asia. In addition, the study explores the possibility of combining tephra layer with proxy record to answer palaeoenvironmental questions.

6.3 Transhemispheric tephra dispersal (Chen et al., in preparation)

This study is based on the analyses of a mid-Holocene cryptotephra from Lake Kushu northern Japan. Cryptotephra layers from this site are predominantly correlated to volcanic eruptions in the northern Hemisphere, from Japan, China and Russia (Chen et al., 2016; Chen et al., submitted). However a remaining cryptotephra horizon exhibits chemical affinity that does not match with known Asian northern Hemisphere eruptions. With further investigation of southern Hemisphere tephra sources, this study proposes the identification of a cryptotephra from Krakatau volcano Indonesia, in northern Japan over 6700 km from the vent. This provides the first empirical evidence of transhemispheric latitudinal distribution of volcanic ash. The finding not only sheds light on a previously undocumented large eruption, but also opens up an opportunity for developing an interhemispheric cryptotephra lattice in the region.

This study finds new tephra isochron into the regional tephrostratigraphy thus addresses the aim of developing an integrated East Asian tephra framework.

6.4 An integrated Holocene tephrostratigraphic framework for East Asia (Chen et al., in preparation-b)

In this study, a thorough review of previous visible tephra studies and recent developments in cryptotephra research (McLean et al., 2018; Chen et al., 2016; Chen

et al., submitted; Chen et al., in preparation) is undertaken in order to establish criteria for selection of widely dispersed tephra horizons. An updated Holocene tephra framework for East Asia is proposed, which incorporates twenty-two widespread tephra isochrons originating from Russia, China/N Korea, S Korea, Japan and Indonesia (Fig. 6.1). In addition, the chronostratigraphic relationships between these tephras and climate change events are fully evaluated, in particular the extent to which these isochrons can be used to constrain regional variations of short-lived climate oscillations. A list of potential candidates are also discussed, with the suggestion of future work as the prerequisite for them to be included in the framework.

This study proposes a regional tephra framework for future tephrochronology studies and provides an evaluation of the utility of tephra isochrons in palaeoclimate research in East Asia. As such, it addresses the overall aim of this thesis.

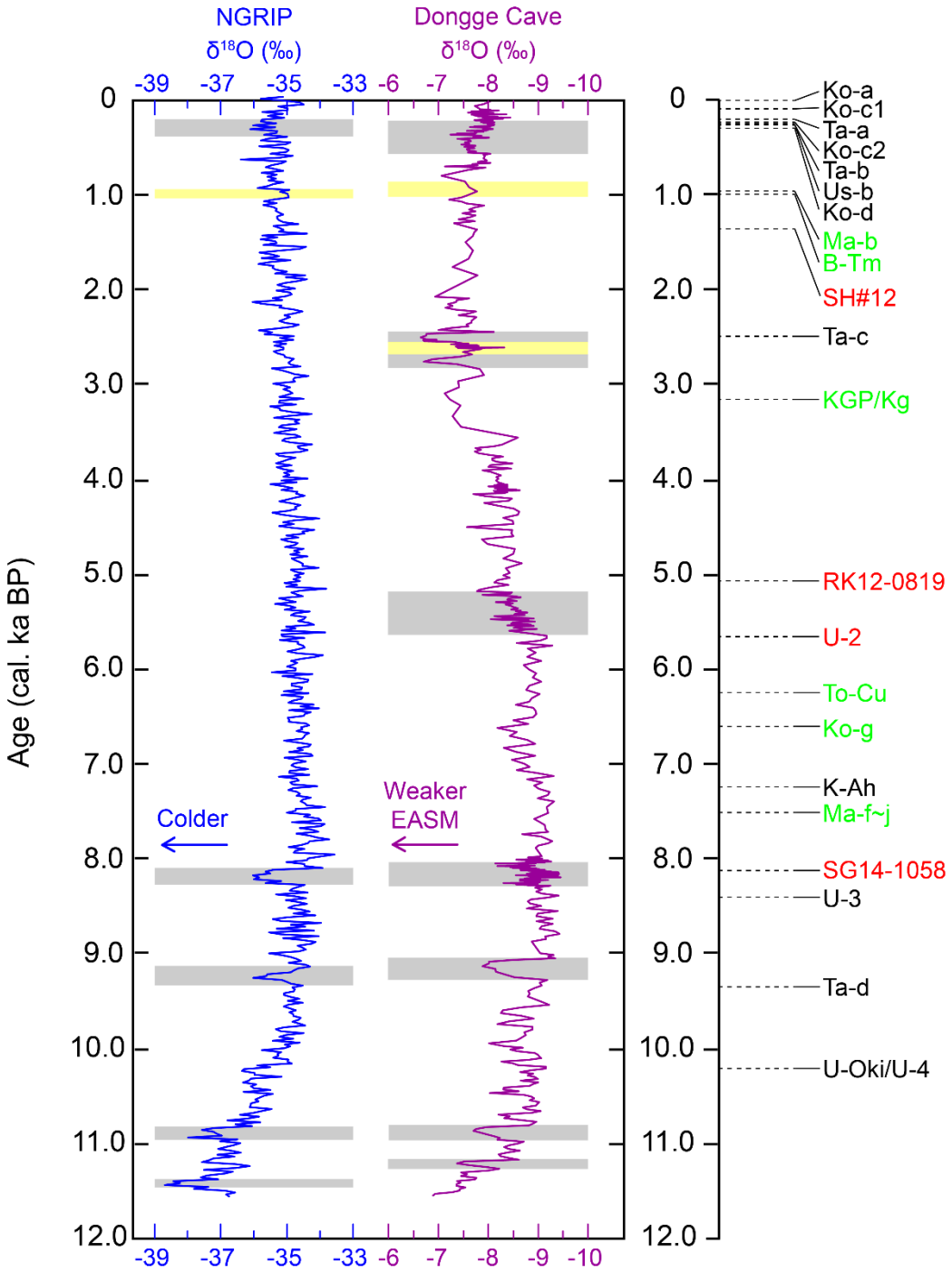

Fig. 6.1 An updated Holocene tephra framework for East Asia based on recent pioneering cryptotephra studies in the region (Chen et al., 2016; Chen et al., submitted; Chen et al., in preparation; McLean et al., 2018). The tephra layers were plotted based on their ages, against the proxy records from Greenland (NGRIP members, 2004) and Chinese speleothem (Dykoski et al., 2005). Tephra name in red indicates that the tephra isochron is newly identified using cryptotephra method, while tephra name in green

indicates that the dispersal to the tephra layer is significantly enlarged by cryptotephra technique (detailed information of the tephra layers see Table 5.1).

6.5 Future work

Through the process of this PhD project, it becomes increasingly apparent that sedimentary archives in East Asia possess great potential in the identification of widely dispersed tephra horizons and the development of important tephrostratigraphic framework. These would effectively facilitate the use of tephra isochrons for precise correlation of widespread palaeoclimate records. However, it is also apparent that the cryptotephra technique that are commonly employed in other parts of the world (e.g. Europe, North America) has very limited applications in this palaeoclimatologically significant region (i.e. monsoon climate system). As a consequence, in order for a more comprehensive regional tephra framework/lattice to be established, it is now essential that a more systematic approach to the application of cryptotephra studies is applied to terrestrial and marine records from the region.

Given that East Asia is an important region for our understanding of monsoon dynamics, one of the key applications of tephrochronological studies in this region is to utilise widespread tephra isochrons for testing leads and lags in climate archives. An example of exploring the use of tephra layer to constrain regional variations in response to climate changes has been discussed in section 3.9. With more and more proxy records from Lake Kushu being published, as well as the tephra layers reported from the lake being identified in other key palaeoclimate archives, there is significant potential for future studies, in terms of the use of tephra layer to synchronise disparate records thus to understand how climate changes propagate within the region.

In the study presented in Chapter 3, several previously unknown tephra horizons are revealed by subordinate population of analyses within individual geochemical samples. Based on a number of reasons (see section 3.6.2 and correlation sections related to each tephra), these tephra horizons are interpreted as primary deposits and thus represent previously undocumented eruptions (e.g. three of the early to mid-Holocene Changbaishan eruptions). In order to fully confirm that these newly identified geochemical signals are from primary tephra deposits, ideally it is essential to

systematically geochemically characterise the shards that surround the geochemical samples. If those signals were not presented in the stratigraphically adjacent samples, these subordinate populations could then be robustly defined as primary deposits. Nevertheless, given the limited analytical budgets and lake core sediments related to the project, these additional analyses are not undertaken in this study. As such these are now recommended as future work.

In the study presented in Chapter 4, a distal tephra identified in the Lake Kushu sequence is correlated to the Krakatau volcano based on cross-matching of major element glass chemistry. However, in order the nail the correlation down, it is necessary to carry out trace element analyses on both distal and proximal samples. As the proximal samples from Indonesia have been received shortly before the submission of this thesis, these further geochemical analyses are listed as future work and are planned to be undertaken soon.

Bibliography

Abbott, P.M., Bourne, A.J., Purcell, C.S., Davies, S.M., Scourse, J.D. and Pearce, N.J.G., 2016. Last glacial period cryptotephra deposits in an eastern North Atlantic marine sequence: Exploring linkages to the Greenland ice-cores. Quat Geochronol, 31: 62-76.

Albert, P.G., Hardiman, M., Keller, J., Tomlinson, E.L., Smith, V.C., Bourne, A.J., Wulf, S., Zanchetta, G., Sulpizio, R., Müller, U.C., Pross, J., Ottolini, L., Matthews, I.P., Blockley, S.P.E. and Menzies, M.A., 2015. Revisiting the Y-3 tephrostratigraphic marker: a new diagnostic glass geochemistry, age estimate, and details on its climatostratigraphical context. Quaternary Science Reviews, 118: 105-121.

Albert, P.G., Tomlinson, E.L., Lane, C.S., Wulf, S., Smith, V.C., Coltelli, M., Keller, J., Lo Castro, D., Manning, C.J., Müller, W. and Menzies, M.A., 2013. Late glacial explosive activity on Mount Etna: Implications for proximal–distal tephra correlations and the synchronisation of Mediterranean archives. Journal of Volcanology and Geothermal Research, 265(0): 9-26.

Albert, P.G., Tomlinson, E.L., Smith, V.C., Di Roberto, A., Todman, A., Rosi, M., Marani, M., Muller, W. and Menzies, M.A., 2012. Marine-continental tephra correlations: Volcanic glass geochemistry from the Marsili Basin and the Aeolian Islands, Southern Tyrrhenian Sea, Italy. Journal of Volcanology and Geothermal Research, 229–230: 74-94.

Allan, A.S.R., Baker, J.A., Carter, L. and Wysoczanksi, R.J., 2008. Reconstructing the Quaternary evolution of the world's most active silicic volcanic system: insights from an ~1.65 Ma deep ocean tephra record sourced from Taupo Volcanic Zone, New Zealand. Quaternary Science Reviews, 27(25–26): 2341-2360.

Alloway, B.V., Andreastuti, S., Setiawan, R., Miksic, J. and Hua, Q., 2017. Archaeological implications of a widespread 13th Century tephra marker across the central Indonesian Archipelago. Quaternary Science Reviews, 155: 86-99.

Alloway, B.V., Lowe, D.J., Barrell, D.J., Newnham, R.M., Almond, P.C., Augustinus, P.C., Bertler, N.A., Carter, L., Litchfield, N.J. and McGlone, M.S., 2007. Towards a climate event stratigraphy for New Zealand over the past 30 000 years (NZ-INTIMATE project). Journal of Quaternary Science, 22(1): 9-35.

An, Z., 2000. The history and variability of the East Asian paleomonsoon climate.

Quaternary Science Reviews, 19(1): 171-187.

An, Z., Kukla, G., Porter, S.C. and Xiao, J., 1991a. Late quaternary dust flow on the chinese Loess Plateau. CATENA, 18(2): 125-132.

An, Z., Kukla, G.J., Porter, S.C. and Xiao, J., 1991b. Magnetic susceptibility evidence of monsoon variation on the Loess Plateau of central China during the last 130,000 years. Quaternary Research, 36(1): 29-36.

Aoki, K., 2008. Revised age and distribution of ca. 87ka Aso-4 tephra based on new evidence from the northwest Pacific Ocean. Quaternary International, 178(1): 100-118.

Aoki, K. and Arai, F., 2000. Late Quaternary tephrostratigraphy of marine core KH94-3, LM-8 off Sanriku, Japan. The Quaternary Research (Daiyonki-kenkyu), 39(2): 107-120 (in Japanese with English abstract).

Aoki, K., Irino, T. and Oba, T., 2008. Late Pleistocene tephrostratigraphy of the sediment core MD01-2421 collected off the Kashima coast, Japan. The Quaternary Research (Daiyonki-kenkyu), 47: 391-407 (in Japanese with English abstract).

Aoki, K. and Machida, H., 2006. Major element composition of volcanic glass shards in the late Quaternary widespread tephras in Japan-Distinction of tephras using K2O-TiO2 diagrams. Bulletin of the Geological Survey of Japan, 57(7/8): 239-258 (in Japanese).

Arai, F., Machida, H., Okumura, K., Miyauchi, T., Soda, T. and Yamagata, K., 1986. Catalog for late quaternary marker-tephras in japan ii : tephras occurring in northeast honshu and hokkaido. Geographical reports of Tokyo Metropolitan University, 21: 223-250.

Barton, R., Lane, C.S., Albert, P., White, D., Collcutt, S., Bouzouggar, A., Ditchfield, P., Farr, L., Oh, A. and Ottolini, L., 2015. The role of cryptotephra in refining the chronology of Late Pleistocene human evolution and cultural change in North Africa. Quaternary Science Reviews, 118: 151-169.

Blockley, S.P.E., Bourne, A.J., Brauer, A., Davies, S.M., Hardiman, M., Harding, P.R., Lane, C.S., MacLeod, A., Matthews, I.P., Pyne-O'Donnell, S.D.F., Rasmussen, S.O., Wulf, S. and Zanchetta, G., 2014. Tephrochronology and the extended intimate (integration of ice-core, marine and terrestrial records) event stratigraphy 8–128 ka b2k. Quaternary Science Reviews, 106: 88-100.

Blockley, S.P.E., Bronk Ramsey, C. and Pyle, D.M., 2008. Improved age modelling and

high-precision age estimates of late Quaternary tephras, for accurate palaeoclimate reconstruction. Journal of Volcanology and Geothermal Research, 177(1): 251-262.

Blockley, S.P.E., Edwards, K.J., Schofield, J.E., Pyne-O'Donnell, S.D.F., Jensen, B.J.L., Matthews, I.P., Cook, G.T., Wallace, K.L. and Froese, D., 2015. First evidence of cryptotephra in palaeoenvironmental records associated with Norse occupation sites in Greenland. Quat Geochronol, 27: 145-157.

Blockley, S.P.E., Lane, C.S., Hardiman, M., Rasmussen, S.O., Seierstad, I.K., Steffensen, J.P., Svensson, A., Lotter, A.F., Turney, C.S.M. and Bronk Ramsey, C., 2012. Synchronisation of palaeoenvironmental records over the last 60,000 years, and an extended INTIMATE event stratigraphy to 48,000 b2k. Quaternary Science Reviews, 36: 2-10.

Blockley, S.P.E., Lane, C.S., Lotter, A.F. and Pollard, A.M., 2007. Evidence for the presence of the Vedde Ash in Central Europe. Quaternary Science Reviews, 26(25): 3030-3036.

Blockley, S.P.E., Pyne-O'Donnell, S.D.F., Lowe, J.J., Matthews, I.P., Stone, A., Pollard, A.M., Turney, C.S.M. and Molyneux, E.G., 2005. A new and less destructive laboratory procedure for the physical separation of distal glass tephra shards from sediments. Quaternary Science Reviews, 24(16–17): 1952-1960.

Bourdier, J.-L., Pratomo, I., Thouret, J.-C., Boudon, G. and Vincent, P.M., 1997. Observations, stratigraphy and eruptive processes of the 1990 eruption of Kelut volcano, Indonesia. Journal of volcanology and geothermal research, 79(3-4): 181-203.

Bourne, A.J., Abbott, P.M., Albert, P.G., Cook, E., Pearce, N.J.G., Ponomareva, V., Svensson, A. and Davies, S.M., 2016. Underestimated risks of recurrent long-range ash dispersal from northern Pacific Arc volcanoes. Scientific Reports, 6: 29837.

Bourne, A.J., Albert, P.G., Matthews, I.P., Trincardi, F., Wulf, S., Asioli, A., Blockley, S.P.E., Keller, J. and Lowe, J.J., 2015a. Tephrochronology of core PRAD 1-2 from the Adriatic Sea: insights into Italian explosive volcanism for the period 200–80 ka. Quaternary Science Reviews, 116: 28-43.

Bourne, A.J., Cook, E., Abbott, P.M., Seierstad, I.K., Steffensen, J.P., Svensson, A., Fischer, H., Schüpbach, S. and Davies, S.M., 2015b. A tephra lattice for Greenland and a reconstruction of volcanic events spanning 25–45 ka b2k.

Quaternary Science Reviews, 118: 122-141.

Bourne, A.J., Lowe, J.J., Trincardi, F., Asioli, A., Blockley, S.P.E., Wulf, S., Matthews, I.P., Piva, A. and Vigliotti, L., 2010. Distal tephra record for the last ca 105,000 years from core PRAD 1-2 in the central Adriatic Sea: implications for marine tephrostratigraphy. Quaternary Science Reviews, 29(23): 3079-3094.

Braitseva, O.A., Ponomareva, V.V., Sulerzhitsky, L.D., Melekestsev, I.V. and Bailey, J., 1997. Holocene key-marker tephra layers in Kamchatka, Russia. Quaternary research, 47(2): 125-139.

Bronk Ramsey, C., 2008. Deposition models for chronological records. Quaternary Science Reviews, 27(1–2): 42-60.

Bronk Ramsey, C., 2009a. Bayesian analysis of radiocarbon dates. Radiocarbon, 51(1): 337-360.

Bronk Ramsey, C., 2009b. Dealing with outliers and offsets in radiocarbon dating. Radiocarbon, 51(3): 1023-1045.

Bronk Ramsey, C., 2013. OxCal 4.2. Available from: http://c14.arch.ox.ac.uk/oxcal.

Bronk Ramsey, C. and Lee, S., 2013. Recent and planned developments of the program OxCal. Radiocarbon, 55(2): 720-730.

Bursik, M.I., Kobs, S.E., Burns, A., Braitseva, O.A., Bazanova, L.I., Melekestsev, I.V., Kurbatov, A. and Pieri, D.C., 2009. Volcanic plumes and wind: Jetstream interaction examples and implications for air traffic. Journal of Volcanology and Geothermal Research, 186(1): 60-67.

Camus, G., Gourgaud, A. and Vincent, P., 1987. Petrologic evolution of Krakatau (Indonesia): implications for a future activity. Journal of Volcanology and Geothermal Research, 33(4): 299-316.

Charlier, B., Namur, O., Toplis, M.J., Schiano, P., Cluzel, N., Higgins, M.D. and Auwera, J.V., 2011. Large-scale silicate liquid immiscibility during differentiation of tholeiitic basalt to granite and the origin of the Daly gap. Geology, 39(10): 907-910.

Chen, F., Xu, Q., Chen, J., Birks, H.J.B., Liu, J., Zhang, S., Jin, L., An, C., Telford, R.J. and Cao, X., 2015. East Asian summer monsoon precipitation variability since the last deglaciation. Scientific reports, 5: 11186.

Chen, X.-Y., Blockley, S.P.E., Tarasov, P.E., Xu, Y.-G., McLean, D., Tomlinson, E.L., Albert, P.G., Liu, J.-Q., Müller, S., Wagner, M. and Menzies, M.A., 2016. Clarifying the distal to proximal tephrochronology of the Millennium (B–Tm)

eruption, Changbaishan Volcano, northeast China. Quat Geochronol, 33: 61-75.

Chen, X.-Y., Blockley, S.P.E., Xu, Y.G. and Menzies, M., in preparation-b. An Integrated Holocene tephrostratigraphic framework for East Asia: implications for palaeoclimate research and future opportunities.

Chen, X.-Y., McLean, D., Blockley, S.P.E., Tarasov, P.E., Xu, Y.G. and Menzies, M., in preparation. Transhemispheric tephra dispersal: Krakatau tephra in northern Japan.

Chen, X.-Y., McLean, D., Blockley, S.P.E., Tarasov, P.E., Xu, Y.G. and Menzies, M., submitted for publication. Developing a Holocene tephrostratigraphy for northern Japan using the sedimentary record from Lake Kushu, Rebun Island.

Chen, X.Y., Xu, Y.G. and Menzies, M., 2014. Tephrochronology: Principles and applications. Acta Petrologica Sinica, 30(12): 3491-3500 (in Chinese with English abstract).

Chesner, C.A., Rose, W.I., Deino, A., Drake, R. and Westgate, J., 1991. Eruptive history of Earth's largest Quaternary caldera (Toba, Indonesia) clarified. Geology, 19(3): 200-203.

Clemens, S.C., Prell, W.L. and Sun, Y., 2010. Orbital-scale timing and mechanisms driving Late Pleistocene Indo-Asian summer monsoons: Reinterpreting cave speleothem δ18O. Paleoceanography, 25, PA4207, doi:10.1029/2010PA001926.

Cook, E., Davies, S.M., Guðmundsdóttir, E.R., Abbott, P.M. and Pearce, N.J.G., 2018a. First identification and characterization of Borrobol-type tephra in the Greenland ice cores: new deposits and improved age estimates. Journal of Quaternary Science, 33(2): 212-224.

Cook, E., Portnyagin, M., Ponomareva, V., Bazanova, L., Svensson, A. and Garbe-Schönberg, D., 2018b. First identification of cryptotephra from the Kamchatka Peninsula in a Greenland ice core: Implications of a widespread marker deposit that links Greenland to the Pacific northwest. Quaternary Science Reviews, 181: 200-206.

Coulter, S.E., Pilcher, J.R., Plunkett, G., Baillie, M., Hall, V.A., Steffensen, J.P., Vinther, B.M., Clausen, H.B. and Johnsen, S.J., 2012. Holocene tephras highlight complexity of volcanic signals in Greenland ice cores. Journal of Geophysical Research: Atmospheres, 117(D21303).

Crosweller, H.S., Arora, B., Brown, S.K., Cottrell, E., Deligne, N.I., Guerrero, N.O.,

Hobbs, L., Kiyosugi, K., Loughlin, S.C., Lowndes, J., Nayembil, M., Siebert, L., Sparks, R.S.J., Takarada, S. and Venzke, E., 2012. Global database on large magnitude explosive volcanic eruptions (LaMEVE). Journal of Applied Volcanology, 1(1): 4.

Cui, Z., Wei, H. and Liu, R., 1995. Historical documentation research of eruptions of the Tianchi Volcano, Changbaishan. In: Liu, R. (ed). Volcanism and Human Environment. Beijing: Seismology Press: 36-39 (in Chinese).

Davies, L.J., Appleby, P., Jensen, B.J.L., Magnan, G., Mullan-Boudreau, G., Noernberg, T., Shannon, B., Shotyk, W., van Bellen, S., Zaccone, C. and Froese, D.G., 2018. High-resolution age modelling of peat bogs from northern Alberta, Canada, using pre- and post-bomb 14C, 210Pb and historical cryptotephra. Quat Geochronol, 47: 138-162.

Davies, S.M., 2015. Cryptotephras: the revolution in correlation and precision dating. Journal of Quaternary Science, 30(2): 114-130.

Davies, S.M., Abbott, P.M., Meara, R.H., Pearce, N.J.G., Austin, W.E.N., Chapman, M.R., Svensson, A., Bigler, M., Rasmussen, T.L., Rasmussen, S.O. and Farmer, E.J., 2014. A North Atlantic tephrostratigraphical framework for 130–60 ka b2k: new tephra discoveries, marine-based correlations, and future challenges. Quaternary Science Reviews, 106: 101-121.

Davies, S.M., Abbott, P.M., Pearce, N.J.G., Wastegård, S. and Blockley, S.P.E., 2012. Integrating the INTIMATE records using tephrochronology: rising to the challenge. Quaternary Science Reviews, 36: 11-27.

Davies, S.M., Larsen, G., Wastegård, S., Turney, C.S., Hall, V.A., Coyle, L. and Thordarson, T., 2010a. Widespread dispersal of Icelandic tephra: how does the Eyjafjöll eruption of 2010 compare to past Icelandic events? Journal of Quaternary Science, 25(5): 605-611.

Davies, S.M., Wastegård, S., Abbott, P., Barbante, C., Bigler, M., Johnsen, S.J., Rasmussen, T.L., Steffensen, J.P. and Svensson, A., 2010b. Tracing volcanic events in the NGRIP ice-core and synchronising North Atlantic marine records during the last glacial period. Earth and Planetary Science Letters, 294(1-2): 69-79.

Ding, Z., Yu, Z., Rutter, N.W. and Liu, T., 1994. Towards an orbital time scale for chinese loess deposits. Quaternary Science Reviews, 13(1): 39-70.

Domitsu, H., Shiihara, M., Torii, M., Tsukawaki, S. and Oda, M., 2002.

Tephrostratigraphy of the piston cored sediment KT96-17 P-2 in the southern Japan Sea-the eruption age of Daisen-Kusadanihara Pumice (KsP). JOURNAL-GEOLOGICAL SOCIETY OF JAPAN, 108(9): 545-556.

Dufek, J. and Bachmann, O., 2010. Quantum magmatism: Magmatic compositional gaps generated by melt-crystal dynamics. Geology, 38(8): 687-690.

Dykoski, C.A., Edwards, R.L., Cheng, H., Yuan, D., Cai, Y., Zhang, M., Lin, Y., Qing, J., An, Z. and Revenaugh, J., 2005. A high-resolution, absolute-dated Holocene and deglacial Asian monsoon record from Dongge Cave, China. Earth and Planetary Science Letters, 233(1): 71-86.

Fan, Q., Liu, R., Wei, H., Sui, J. and Li, N., 1999. Petrogeochemical Characteristics of Holocene Eruption of the Tianchi Volcano, Changbai Mountains. Geological Review, 45(Sup.): 263-271 (in Chinese with English abstract).

Fukuoka, T. and Matsui, S., 2002. Stratigraphy of pyroclastic deposits post-dating the AT tephra, Sambe volcano. Earth Science (Chikyu kagaku), 56: 105-122 (in Japanese with English abstract).

Fukusawa, H., Tsukamoto, S., Tsukamoto, H., Ikeda, M., Okamura, M. and MAtsuoka, H., 1998. Falling age of Baegdusan-Tomakomai tephra (B-Tm) estimated by using non-glacial varves. Laguna, 5: 55-62 (in Japanese with English abstract).

Furukawa, R. and Nanayama, F., 2006. Holocene pyroclastic fall deposits along the Pacific coastal region of eastern Hokkaido. Bulletin of Volcanological Society of Japan, 51(6): 351-371 (in Japanese with English abstract).

Furuta, T., Fujioka, K. and Arai, F., 1986. Widespread submarine tephras around Japan — Petrographic and chemical properties. Marine Geology, 72(1): 125-142.

Ganzawa, Y., Kito, N., Yanai, S. and Sadakata, N., 2005. Discovery of primary tephra layers and research of the early stage of the volcanic history of Hokkaido-Komagatake volcano, Japan. Journal of the Geological Society of Japan, 111(10): 581-589 (in Japanese with English abstract).

Gerbe, M.-C., Gourgaud, A., Sigmarsson, O., Harmon, R.S., Joron, J.-L. and Provost, A., 1992. Mineralogical and geochemical evolution of the 1982–1983 Galunggung eruption (Indonesia). Bull Volcanol, 54(4): 284-298.

Gertisser, R. and Keller, J., 2003. Temporal variations in magma composition at Merapi Volcano (Central Java, Indonesia): magmatic cycles during the past 2000 years of explosive activity. Journal of Volcanology and Geothermal research, 123(1): 1-23.

Gleckler, P., Wigley, T., Santer, B., Gregory, J., AchutaRao, K. and Taylor, K., 2006. Volcanoes and climate: Krakatoa's signature persists in the ocean. Nature, 439(7077): 675.

Global Volcanism Program, 2018. Volcanoes of the World database. Smithsonian Institution Washington, DC.

Goto, Y., 2011. A Fallout Tephra from Tenchozan Volcano, Shiretoko Peninsula, Hokkaido, Japan. Bulletin of the Volcanological Society of Japan, 56(4-5): 137-145.

Grove, T.L. and Donnelly-Nolan, J.M., 1986. The evolution of young silicic lavas at Medicine Lake Volcano, California: Implications for the origin of compositional gaps in calc-alkaline series lavas. Contrib Mineral Petrol, 92(3): 281-302.

Guo, Z., Liu, J., Sui, S., Liu, Q., He, H. and Ni, Y., 2002. The mass estimation of volatile emission during 1199–1200 AD eruption of Baitoushan volcano and its significance. Science in China Series D: Earth Sciences, 45(6): 530-539.

Hakozaki, M., Miyake, F., Nakamura, T., Kimura, K., Masuda, K. and Okuno, M., 2018. Verification of the annual dating of the 10th century Baitoushan volcano eruption based on an ad 774–775 radiocarbon spike. Radiocarbon, 60(1): 261-268.

Hayakawa, Y., 1983. Chuseri tephra formation from Towada volcano, Japan. Bulletin of the Volcanological Society of Japan, 28: 263-273 (in Japanese with English abstract).

Hayakawa, Y., 1985. Pyroclastic geology of Towada volcano. Bull. Earthq. Res. Inst. Univ. Tokyo, 60: 507-592.

Hayakawa, Y. and Koyama, M., 1998. Dates of two major eruptions from Towada and Baitoushan in the 10th century. Bulletin of the Volcanological Society of Japan, 43(5): 403-407 (in Japanese).

Hayward, C., 2011. High spatial resolution electron probe microanalysis of tephras and melt inclusions without beam-induced chemical modification. The Holocene, 22(1): 119-125.

Horn, S. and Schmincke, H.-U., 2000. Volatile emission during the eruption of Baitoushan Volcano (China/North Korea) ca. 969 AD. Bull Volcanol, 61(8): 537-555.

Hughes, P.D.M., Mallon, G., Brown, A., Essex, H.J., Stanford, J.D. and Hotes, S., 2013. The impact of high tephra loading on late-Holocene carbon accumulation and

vegetation succession in peatland communities. Quaternary Science Reviews, 67(0): 160-175.

Ikehara, K., Usami, K., Kanamatsu, T., Danhara, T. and Yamashita, T., 2017. Three important Holocene tephras off the Pacific coast of the Tohoku region, Northeast Japan: implications for correlating onshore and offshore event deposits. Quaternary International, 456: 138-153.

Im, J.H., Shim, S.H., Choo, C.O., Jang, Y.D. and Lee, J.S., 2012. Volcanological and paleoenvironmental implications of charcoals of the Nari Formation in Nari Caldera, Ulleung Island, Korea. Geosciences Journal, 16(2): 105-114.

Inoue, Y., Hiradate, S., Sase, T., Hosono, M., Morita, S. and Matsuzaki, H., 2011. Using 14C dating of stable humin fractions to assess upbuilding pedogenesis of a buried Holocene humic soil horizon, Towada volcano, Japan. Geoderma, 167-168: 85-90.

Irvine, T.N. and Baragar, W.R.A., 1971. A Guide to the Chemical Classification of the Common Volcanic Rocks. Canadian Journal of Earth Sciences, 8(5): 523-548.

Ishizuka, K., 1999. Eruptive history of Rishiri volcano, northeastern Hokkaido, Japan. Bulletin of the Volcanological Society of Japan, 44: 23-40 (in Japanese with English abstract).

Jeffery, A.J., Gertisser, R., Troll, V.R., Jolis, E.M., Dahren, B., Harris, C., Tindle, A.G., Preece, K., O'Driscoll, B. and Humaida, H., 2013. The pre-eruptive magma plumbing system of the 2007–2008 dome-forming eruption of Kelut volcano, East Java, Indonesia. Contrib Mineral Petrol, 166(1): 275-308.

Jensen, B.J., Pyne-O'Donnell, S., Plunkett, G., Froese, D.G., Hughes, P.D., Sigl, M., McConnell, J.R., Amesbury, M.J., Blackwell, P.G., van den Bogaard, C., Buck, C.E., Charman, D.J., Clague, J.J., Hall, V., Koch, J., Mackay, H., Mallon, G., McColl, L. and Pilcher, J.R., 2014. Transatlantic distribution of the Alaskan white river ash. Geology, 42(10): 875-878.

Ji, F., Li, J. and Zheng, R., 1999. The preliminary study of TL chronology for recent eruptive materials in Changbaishan Tianchi Volcano. Geological Review, 45(Sup.): 282-286.

Jochum, K.P., Stoll, B., Herwig, K., Willbold, M., Hofmann, A.W., Amini, M., Aarburg, S., Abouchami, W., Hellebrand, E., Mocek, B., Raczek, I., Stracke, A., Alard, O., Bouman, C., Becker, S., Dücking, M., Brätz, H., Klemd, R., de Bruin, D., Canil, D., Cornell, D., de Hoog, C.-J., Dalpé, C., Danyushevsky, L., Eisenhauer,

A., Gao, Y., Snow, J.E., Groschopf, N., Günther, D., Latkoczy, C., Guillong, M., Hauri, E.H., Höfer, H.E., Lahaye, Y., Horz, K., Jacob, D.E., Kasemann, S.A., Kent, A.J.R., Ludwig, T., Zack, T., Mason, P.R.D., Meixner, A., Rosner, M., Misawa, K., Nash, B.P., Pfänder, J., Premo, W.R., Sun, W.D., Tiepolo, M., Vannucci, R., Vennemann, T., Wayne, D. and Woodhead, J.D., 2006. MPI-DING reference glasses for in situ microanalysis: New reference values for element concentrations and isotope ratios. Geochemistry, Geophysics, Geosystems, 7(2): Q02008.

Jones, G., Lane, C.S., Brauer, A., Davies, S.M., Bruijn, R., Engels, S., Haliuc, A., Hoek, W.Z., Merkt, J., Sachse, D., Turner, F. and Wagner-Cremer, F., 2017. The Lateglacial to early Holocene tephrochronological record from Lake Hämelsee, Germany: a key site within the European tephra framework. Boreas, 47(1): 28-40.

Kamite, M., Yamada, K., Saito-Kato, M., Okuno, M. and Yasuda, Y., 2010. Microscopic observations of varve sediments from Lake Ni-no-Megata and Lake San-no-Megata, Oga Peninsula, NE Japan, with reference to the fallout age of the B-Tm Tephra. Jour. Geol. Soc. Japan, 116(7): 349-359.

Katoh, S., Yamagata, K. and Okumura, K., 1995. AMS-14C dates of Late Quaternary tephra layers erupted from the Shikotsu and Kuttara volcanoes. The Quaternary Research (Daiyonki-Kenkyu), 34(4): 309-313 (in Japanese with English abstract).

Katsui, Y., 1963. Evolution and magmatic history of some Krakatoan calderas in Hokkaido, Japan. Journal of the Faculty of Science, Hokkaido University. Series 4, Geology and mineralogy, 11(4): 631-650.

Katsui, Y., Ando, S. and Inaba, K., 1975. Formation and magmatic evolution of Mashu volcano, east Hokkaido, Japan. Journal of the Faculty of Science, Hokkaido University. Series 4, Geology and mineralogy, 16(4): 533-552.

Katsui, Y. and Komuro, H., 1984. Formation of fractures in Komagatake volcano, Hokkaido. Journal of the Faculty of Science, Hokkaido University. Series 4, Geology and mineralogy, 21(2): 183-195.

Kaufman, D.S., Jensen, B.J., Reyes, A.V., Schiff, C.J., Froese, D.G. and Pearce, N.J., 2012. Late Quaternary tephrostratigraphy, Ahklun Mountains, SW Alaska. Journal of Quaternary Science, 27(4): 344-359.

Kearney, R., Albert, P.G., Staff, R.A., Pál, I., Veres, D., Magyari, E. and Bronk Ramsey,

C., 2018. Ultra-distal fine ash occurrences of the Icelandic Askja-S Plinian eruption deposits in Southern Carpathian lakes: New age constraints on a continental scale tephrostratigraphic marker. Quaternary Science Reviews, 188: 174-182.

Kim, G., Cronin, S., Yoon, W. and Sohn, Y., 2014. Post 19 ka BP eruptive history of Ulleung Island, Korea, inferred from an intra-caldera pyroclastic sequence. Bull Volcanol, 76(4): 802.

Kishimoto, H., Hasegawa, T., Nakagawa, M. and Wada, K., 2009. Tephrostratigraphy and eruption style of Mashu volcano, during the last 14,000 years, eastern Hokkaido, Japan. Bulletin of the Volcanological Society of Japan, 54: 15-36 (in Japanese with English abstract).

Kobayashi, T. and Sasaki, H., 2014. Sakurajima volcano. Journal of the Geological Society of Japan, 120(Supplement): 63-78 (in Japanese).

Kudo, T., Okuno, M. and Nakamura, T., 2003. Eruptive history of Kita-Hakkoda volcanic group during the last 6000 years, Northeast Japan. Journal of the Geological Society of Japan, 109(3): 151-165 (in Japanese with English abstract).

Kudo, T. and Sasaki, H., 2007. High-precision chronology of eruptive products during the post-caldera stage of Towada volcano, northeast Japan. Journal of Geography (Chigaku Zasshi), 116(5): 653-663 (in Japanese with English abstract).

Kuehn, S.C., Froese, D.G. and Shane, P.A.R., 2011. The INTAV intercomparison of electron-beam microanalysis of glass by tephrochronology laboratories: Results and recommendations. Quaternary International, 246(1): 19-47.

Kukla, G. and An, Z., 1989. Loess stratigraphy in Central China. Palaeogeography, Palaeoclimatology, Palaeoecology, 72: 203-225.

Kumano, S., Ihira, M., Kuromi, M., Maeda, Y., Matsumoto, E., Nakamura, T., Matsushima, Y., Sato, H. and Matsuda, I., 1990. Holocene sedimentary history of some coastal plains in Hokkaido, Japan V. Sedimentary history of Kushu Lake and Akkeshi. Ecol. Res., 5(3): 277-289.

Kyle, P.R., Ponomareva, V.V. and Rourke Schluep, R., 2011. Geochemical characterization of marker tephra layers from major Holocene eruptions, Kamchatka Peninsula, Russia. International Geology Review, 53(9): 1059-1097.

Lane, C.S., Andrič, M., Cullen, V.L. and Blockley, S.P.E., 2011. The occurrence of

distal Icelandic and Italian tephra in the Lateglacial of Lake Bled, Slovenia. Quaternary Science Reviews, 30(9): 1013-1018.

Lane, C.S., Blockley, S.P.E., Lotter, A.F., Finsinger, W., Filippi, M.L. and Matthews, I.P., 2012a. A regional tephrostratigraphic framework for central and southern European climate archives during the Last Glacial to Interglacial transition: comparisons north and south of the Alps. Quaternary Science Reviews, 36: 50-58.

Lane, C.S., Blockley, S.P.E., Mangerud, J., Smith, V.C., Lohne, Ø.S., Tomlinson, E.L., Matthews, I.P. and Lotter, A.F., 2012b. Was the 12.1 ka Icelandic Vedde Ash one of a kind? Quaternary Science Reviews, 33(0): 87-99.

Lane, C.S., Brauer, A., Blockley, S.P.E. and Dulski, P., 2013a. Volcanic ash reveals time-transgressive abrupt climate change during the Younger Dryas. Geology, 41(12): 1251-1254.

Lane, C.S., Brauer, A., Martín-Puertas, C., Blockley, S.P.E., Smith, V.C. and Tomlinson, E.L., 2015. The Late Quaternary tephrostratigraphy of annually laminated sediments from Meerfelder Maar, Germany. Quaternary Science Reviews, 122: 192-206.

Lane, C.S., Chorn, B.T. and Johnson, T.C., 2013b. Ash from the Toba supereruption in Lake Malawi shows no volcanic winter in East Africa at 75 ka. Proceedings of the National Academy of Sciences, 110(20): 8025.

Lane, C.S., Lowe, D.J., Blockley, S.P.E., Suzuki, T. and Smith, V.C., 2017. Advancing tephrochronology as a global dating tool: Applications in volcanology, archaeology, and palaeoclimatic research. Quat Geochronol, 40: 1-7.

Lavigne, F., Degeai, J.-P., Komorowski, J.-C., Guillet, S., Robert, V., Lahitte, P., Oppenheimer, C., Stoffel, M., Vidal, C.M. and Pratomo, I., 2013. Source of the great AD 1257 mystery eruption unveiled, Samalas volcano, Rinjani Volcanic Complex, Indonesia. Proceedings of the National Academy of Sciences: 201307520.

Le Bas, M.J., Le Maitre, R.W., Streckeisen, A. and Zanettin, B., 1986. A Chemical Classification of Volcanic Rocks Based on the Total Alkali-Silica Diagram. Journal of Petrology, 27(3): 745-750.

Lee, M.-Y., Chen, C.-H., Wei, K.-Y., Iizuka, Y. and Carey, S., 2004. First Toba supereruption revival. Geology, 32(1): 61-64.

Leipe, C., Müller, S., Hille, K., Kato, H., Kobe, F., Schmidt, M., Seyffert, K., Spengler,

R., Wagner, M., Weber, A.W. and Tarasov, P.E., 2018. Vegetation change and human impacts on Rebun Island (Northwest Pacific) over the last 6000 years. Quaternary Science Reviews, 193: 129-144.

Leipe, C., Sergusheva, E.A., Müller, S., Spengler III, R.N., Goslar, T., Kato, H., Wagner, M., Weber, A.W. and Tarasov, P.E., 2017. Barley (Hordeum vulgare) in the Okhotsk culture (5th–10th century AD) of northern Japan and the role of cultivated plants in hunter–gatherer economies. PloS one, 12(3): e0174397.

Liu, R., Fan, Q., Wei, H. and Li, N., 1999. Study on Active Volcanoes of China. Geological Review, 45(Sup.): 3-15 (in Chinese with English abstract).

Liu, R., Wei, H. and Li, J., 1998. The latest eruptions from Tianchi volcano, Changbaishan. SciencePress, Beijing (in Chinese).

Lowe, D.J., 2011. Tephrochronology and its application: A review. Quat Geochronol, 6(2): 107-153.

Lowe, D.J., Blaauw, M., Hogg, A.G. and Newnham, R.M., 2013. Ages of 24 widespread tephras erupted since 30,000 years ago in New Zealand, with re-evaluation of the timing and palaeoclimatic implications of the Lateglacial cool episode recorded at Kaipo bog. Quaternary Science Reviews, 74: 170-194.

Lowe, D.J., Shane, P.A.R., Alloway, B.V. and Newnham, R.M., 2008a. Fingerprints and age models for widespread New Zealand tephra marker beds erupted since 30,000 years ago: a framework for NZ-INTIMATE. Quaternary Science Reviews, 27(1): 95-126.

Lowe, J.J., Barton, N., Blockley, S., Ramsey, C.B., Cullen, V.L., Davies, W., Gamble, C., Grant, K., Hardiman, M., Housley, R., Lane, C.S., Lee, S., Lewis, M., MacLeod, A., Menzies, M., Mueller, W., Pollard, M., Price, C., Roberts, A.P., Rohling, E.J., Satow, C., Smith, V.C., Stringer, C.B., Tomlinson, E.L., White, D., Albert, P., Arienzo, I., Barker, G., Boric, S., Carandente, A., Civetta, L., Ferrier, C., Guadelli, J.-L., Karkanas, P., Koumouzelis, M., Mueller, U.C., Orsi, G., Pross, J., Rosi, M., Shalamanov-Korobar, L., Sirakov, N. and Tzedakis, P.C., 2012. Volcanic ash layers illuminate the resilience of Neanderthals and early modern humans to natural hazards. Proceedings of the National Academy of Sciences of the United States of America, 109(34): 13532-13537.

Lowe, J.J., Hoek, W.Z. and INTIMATE group, 2001. Inter-regional correlation of palaeoclimatic records for the Last Glacial–Interglacial Transition: a protocol for improved precision recommended by the INTIMATE project group.

Quaternary Science Reviews, 20(11): 1175-1187.

Lowe, J.J., Ramsey, C.B., Housley, R.A., Lane, C.S. and Tomlinson, E.L., 2015. The RESET project: constructing a European tephra lattice for refined synchronisation of environmental and archaeological events during the last c. 100 ka. Quaternary Science Reviews, 118: 1-17.

Lowe, J.J., Rasmussen, S.O., Björck, S., Hoek, W.Z., Steffensen, J.P., Walker, M.J.C. and Yu, Z.C., 2008b. Synchronisation of palaeoenvironmental events in the North Atlantic region during the Last Termination: a revised protocol recommended by the INTIMATE group. Quaternary Science Reviews, 27(1): 6-17.

Luhr, J.F. and Melson, W.G., 1996. Mineral and glass compositions in June 15, 1991, pumices: Evidence for dynamic disequilibrium in the dacite of Mount Pinatubo. Fire and Mud: Eruptions and Lahars of Mount Pinatubo, Philippines: 733-750.

MacDonald, R., 1974. Nomenclature and petrochemistry of the peralkaline oversaturated extrusive rocks. Bulletin Volcanologique, 38(2): 498-516.

Machida, H., 1999. The stratigraphy, chronology and distribution of distal marker-tephras in and around Japan. Global and Planetary Change, 21(1): 71-94.

Machida, H. and Arai, F., 1978. Akahoya ash-a Holocene widespread tephra erupted from the Kikai caldera, south Kyushu, Japan. The Quaternary Research (Daiyonki-Kenkyu), 17(3): 143-163 (in Japanese with English abstract).

Machida, H. and Arai, F., 1983. Extensive ash falls in and around the sea of Japan from large late quaternary eruptions. Journal of Volcanology and Geothermal Research, 18(1–4): 151-164.

Machida, H. and Arai, F., 2003. Atlas of Tephra in and around Japan, Revised ed. University of Tokyo press, Tokyo, Japan (In Japanese).

Machida, H., Arai, F., Lee, B.-S., Moriwaki, H. and Furuta, T., 1984. Late Quaternary tephras in Ulreung-do island, Korea. Journal of Geography (Chigaku Zasshi), 93(1): 1-14 (in Japanese with English abstract).

Machida, H., Moriwaki, H. and Zhao, D.-C., 1990. The recent major eruption of Changbai Volcano and its environmental effects. Geographical Reports of Tokyo Metropolitan University(25): 1-20.

Mackay, H., Hughes, P.D.M., Jensen, B.J.L., Langdon, P.G., Pyne-O'Donnell, S.D.F., Plunkett, G., Froese, D.G., Coulter, S. and Gardner, J.E., 2016. A mid to late Holocene cryptotephra framework from eastern North America. Quaternary

Science Reviews, 132: 101-113.

MacLeod, A., Matthews, I.P., Lowe, J.J., Palmer, A.P. and Albert, P.G., 2015. A second tephra isochron for the Younger Dryas period in northern Europe: The Abernethy Tephra. Quat Geochronol, 28: 1-11.

Maher, B.A. and Thompson, R., 2012. Oxygen isotopes from Chinese caves: records not of monsoon rainfall but of circulation regime. Journal of Quaternary Science, 27(6): 615-624.

Mandeville, C.W., Carey, S. and Sigurdsson, H., 1996a. Magma mixing, fractional crystallization and volatile degassing during the 1883 eruption of Krakatau volcano, Indonesia. Journal of Volcanology and Geothermal Research, 74(3): 243-274.

Mandeville, C.W., Carey, S. and Sigurdsson, H., 1996b. Sedimentology of the Krakatau 1883 submarine pyroclastic deposits. Bull Volcanol, 57(7): 512-529.

Mann, M.E., Zhang, Z., Rutherford, S., Bradley, R.S., Hughes, M.K., Shindell, D., Ammann, C., Faluvegi, G. and Ni, F., 2009. Global signatures and dynamical origins of the Little Ice Age and Medieval Climate Anomaly. Science, 326(5957): 1256-1260.

Mark, D.F., Petraglia, M., Smith, V.C., Morgan, L.E., Barfod, D.N., Ellis, B.S., Pearce, N.J., Pal, J.N. and Korisettar, R., 2014. A high-precision 40Ar/39Ar age for the Young Toba Tuff and dating of ultra-distal tephra: Forcing of Quaternary climate and implications for hominin occupation of India. Quat Geochronol, 21: 90-103.

Matsu'ura, T., Kimura, J.-I., Chang, Q. and Komatsubara, J., 2017. Using tephrostratigraphy and cryptotephrostratigraphy to re-evaluate and improve the Middle Pleistocene age model for marine sequences in northeast Japan (Chikyu C9001C). Quat Geochronol, 40: 129-145.

Matthews, I.P., Trincardi, F., Lowe, J.J., Bourne, A.J., MacLeod, A., Abbott, P.M., Andersen, N., Asioli, A., Blockley, S.P.E., Lane, C.S., Oh, Y.A., Satow, C.S., Staff, R.A. and Wulf, S., 2015. Developing a robust tephrochronological framework for Late Quaternary marine records in the Southern Adriatic Sea: new data from core station SA03-11. Quaternary Science Reviews, 118: 84-104.

Mayewski, P.A., Rohling, E.E., Curt Stager, J., Karlén, W., Maasch, K.A., Meeker, L.D., Meyerson, E.A., Gasse, F., van Kreveld, S., Holmgren, K., Lee-Thorp, J., Rosqvist, G., Rack, F., Staubwasser, M., Schneider, R.R. and Steig, E.J., 2017.

Holocene climate variability. Quaternary Research, 62(3): 243-255.

McLean, D., 2013. Identification and correlation of cryptotephra from Lake Kushu, Rebun Island, Japan (MSc thesis). University of London, p. 101.

McLean, D., Albert, P.G., Nakagawa, T., Staff, R.A., Suzuki, T. and Smith, V.C., 2016. Identification of the Changbaishan 'Millennium'(B-Tm) eruption deposit in the Lake Suigetsu (SG06) sedimentary archive, Japan: synchronisation of hemispheric-wide palaeoclimate archives. Quaternary Science Reviews, 150: 301-307.

McLean, D., Albert, P.G., Nakagawa, T., Suzuki, T., Staff, R.A., Yamada, K., Kitaba, I., Haraguchi, T., Kitagawa, J. and Smith, V.C., 2018. Integrating the Holocene tephrostratigraphy for East Asia using a high-resolution cryptotephra study from Lake Suigetsu (SG14 core), central Japan. Quaternary Science Reviews, 183: 36-58.

Miura, K. and Hayashi, M., 1991. Quarternary Tephra Studies in the Chugoku and Shikoku Districts. The Quaternary Research (Daiyonki-Kenkyu), 30(5): 339-351 (in Japanese with English abstract).

Miyaji, N., Kan'no, A., Kanamaru, T. and Mannen, K., 2011. High-resolution reconstruction of the Hoei eruption (AD 1707) of Fuji volcano, Japan. Journal of Volcanology and Geothermal Research, 207(3-4): 113-129.

Miyaji, N., Nakagawa, M. and Yoshida, M., 2000. Eruptive history of Rausudake volcano during the last 2200 years. Bulletin of the Volcanological Society of Japan, 45: 75-85 (in Japanese with English abstract).

Moriwaki, H., Nagasako, T., Nishizawa, F., Matsushima, Y., Suzuki, T. and Tanaka, G., 2017. Chronology and Significance of Marine Deposits on Shinjima (Moeshima) Island, Kagoshima Bay, Based on Tephrochronology and C-14 Ages. JOURNAL OF GEOGRAPHY-CHIGAKU ZASSHI, 126(5): 557-579 (in Japanese with English abstract).

Moriwaki, H., Nakamura, N., Nagasako, T., Lowe, D.J. and Sangawa, T., 2016. The role of tephras in developing a high-precision chronostratigraphy for palaeoenvironmental reconstruction and archaeology in southern Kyushu, Japan, since 30,000 cal. BP: An integration. Quaternary International, 397: 79-92.

Moriwaki, H., Suzuki, T., Murata, M., Ikehara, M., Machida, H. and Lowe, D.J., 2011. Sakurajima-Satsuma (Sz-S) and Noike-Yumugi (N-Ym) tephras: New tephrochronological marker beds for the last deglaciation, southern Kyushu,

Japan. Quaternary International, 246(1): 203-212.

Müller, S., Schmidt, M., Kossler, A., Leipe, C., Irino, T., Yamamoto, M., Yonenobu, H., Goslar, T., Kato, H., Wagner, M., Weber, A.W. and Tarasov, P.E., 2016. Palaeobotanical records from Rebun Island and their potential for improving the chronological control and understanding human–environment interactions in the Hokkaido Region, Japan. The Holocene, 26(10): 1646-1660.

Nagahashi, Y., Yoshikawa, S., Miyakawa, C., Uchiyama, T. and Inouchi, Y., 2004. Stratigraphy and Chronology of Widespread Tephra Layers during the Past 430ky in the Kinki District and the Yatsugatake Mountains. The Quaternary Research (Daiyonki-Kenkyu), 43(1): 15-35 (in Japanese with English abstract).

NAKAGAWA, M., NOGAMI, K., ISHIZUKA, Y., YOSHIMOTO, M., TAKAHASHI, R., ISHII, E., EGUSA, M., MIYAMURA, J.-i., SHIGA, T. and OKAZAKI, N., 2002. The 2000 eruption of Hokkaido-Komagatake volcano and its significance: evidence for increasing effect of magma deduced from temporal variations of eruptive materials and adhered gas component on ash. Bulletin of the Volcanological Society of Japan, 46(6): 295-304 (in Japanese with English abstract).

Nakagawa, T., Gotanda, K., Haraguchi, T., Danhara, T., Yonenobu, H., Brauer, A., Yokoyama, Y., Tada, R., Takemura, K., Staff, R.A., Payne, R., Bronk Ramsey, C., Bryant, C., Brock, F., Schlolaut, G., Marshall, M., Tarasov, P. and Lamb, H., 2012. SG06, a fully continuous and varved sediment core from Lake Suigetsu, Japan: stratigraphy and potential for improving the radiocarbon calibration model and understanding of late Quaternary climate changes. Quaternary Science Reviews, 36: 164-176.

Nakamura, T., Okuno, M., Kimura, K., Mitsutani, T., Moriwaki, H., Ishizuka, Y., Kim, K.H., Jing, B.L., Oda, H., Minami, M. and Takada, H., 2007. Application of 14C Wiggle-Matching to Support Dendrochronological Analysis in Japan. Tree-Ring Research, 63(1): 37-46.

Nakamura, Y., 2016. Stratigraphy, distribution, and petrographic properties of Holocene tephras in Hokkaido, northern Japan. Quaternary International, 397: 52-62.

Nakamura, Y. and Hirakawa, K., 2004. Mid-Holocene widespread tephra, Komagatake-g (Ko-g) in Hokkaido, northern Japan. The Quaternary Research (Daiyonki-Kenkyu), 43(3): 189-200 (in Japanese with English abstract).

Nanayama, F., Satake, K., Furukawa, R., Shimokawa, K., Atwater, B.F., Shigeno, K.

and Yamaki, S., 2003. Unusually large earthquakes inferred from tsunami deposits along the Kuril trench. Nature, 424(6949): 660-663.

Newhall, C., Bronto, S., Alloway, B., Banks, N., Bahar, I., Del Marmol, M., Hadisantono, R., Holcomb, R., McGeehin, J. and Miksic, J., 2000. 10,000 Years of explosive eruptions of Merapi Volcano, Central Java: archaeological and modern implications. Journal of Volcanology and Geothermal Research, 100(1-4): 9-50.

Newhall, C.G. and Self, S., 1982. The volcanic explosivity index (VEI) an estimate of explosive magnitude for historical volcanism. Journal of Geophysical Research: Oceans, 87(C2): 1231-1238.

Ninkovich, D., 1979. Distribution, age and chemical composition of tephra layers in deep-sea sediments off western Indonesia. Journal of Volcanology and Geothermal Research, 5(1-2): 67-86.

Ninkovich, D., Shackleton, N.J., Abdel-Monem, A.A., Obradovich, J.D. and Izett, G., 1978. K–Ar age of the late Pleistocene eruption of Toba, north Sumatra. Nature, 276(5688): 574.

North Greenland Ice Core Project, m., Andersen, K.K., Azuma, N., Barnola, J.M., Bigler, M., Biscaye, P., Caillon, N., Chappellaz, J., Clausen, H.B., Dahl-Jensen, D., Fischer, H., Flückiger, J., Fritzsche, D., Fujii, Y., Goto-Azuma, K., Grønvold, K., Gundestrup, N.S., Hansson, M., Huber, C., Hvidberg, C.S., Johnsen, S.J., Jonsell, U., Jouzel, J., Kipfstuhl, S., Landais, A., Leuenberger, M., Lorrain, R., Masson-Delmotte, V., Miller, H., Motoyama, H., Narita, H., Popp, T., Rasmussen, S.O., Raynaud, D., Rothlisberger, R., Ruth, U., Samyn, D., Schwander, J., Shoji, H., Siggard-Andersen, M.L., Steffensen, J.P., Stocker, T., Sveinbjörnsdóttir, A.E., Svensson, A., Takata, M., Tison, J.L., Thorsteinsson, T., Watanabe, O., Wilhelms, F. and White, J.W.C., 2004. High-resolution record of Northern Hemisphere climate extending into the last interglacial period. Nature, 431: 147-151.

Ōba, Y., Katsui, Y., Kurasawa, H., Ikeda, Y. and Uda, T., 1983. Petrology of historic rhyolite and dacite from Usu volcano, North Japan. Journal of the Faculty of Science, Hokkaido University. Series 4, Geology and mineralogy, 20(4): 275-290.

Okuno, M., Nakamura, T., Moriwaki, H. and Kobayashi, T., 1997. AMS radiocarbon dating of the Sakurajima tephra group, southern Kyushu, Japan. Nuclear

Instruments and Methods in Physics Research Section B: Beam Interactions with Materials and Atoms, 123(1-4): 470-474.

Okuno, M., Shiihara, M., Torii, M., Nakamura, T., Kim, K.H., Domitsu, H., Moriwaki, H. and Oda, M., 2010. AMS radiocarbon dating of Holocene tephra layers on Ulleung Island, South Korea. Radiocarbon, 52(3): 1465-1470.

Okuno, M., Torii, M., Yamada, K., Shinozuka, Y., Danhara, T., Gotanda, K., Yonenobu, H. and Yasuda, Y., 2011. Widespread tephras in sediments from lake Ichi-no-Megata in northern Japan: Their description, correlation and significance. Quaternary International, 246(1–2): 270-277.

Okuno, M., Yoshimoto, M., Arai, K.-i., Nakamura, T., Ui, T. and Wada, K., 1999. AMS radiocarbon age of the Ko-f tephra from Hokkaido-Komagatake volcano, southwestern Hokkaido, Japan. Journal of the Geological Society of Japan, 105(5): 364-369 (in Japanese with English abstract).

Oppenheimer, C., Wacker, L., Xu, J., Galván, J.D., Stoffel, M., Guillet, S., Corona, C., Sigl, M., Di Cosmo, N., Hajdas, I., Pan, B., Breuker, R., Schneider, L., Esper, J., Fei, J., Hammond, J.O.S. and Büntgen, U., 2017. Multi-proxy dating the 'Millennium Eruption' of Changbaishan to late 946 CE. Quaternary Science Reviews, 158: 164-171.

Pallister, J.S., Hoblitt, R.P., Meeker, G.P., Knight, R.J. and Siems, D.F., 1996. Magma mixing at Mount Pinatubo: petrographic and chemical evidence from the 1991 deposits. Fire and mud: eruptions and lahars of Mount Pinatubo, Philippines: 687-731.

Pan, B., de Silva, S.L., Xu, J., Chen, Z., Miggins, D.P. and Wei, H., 2017. The VEI-7 Millennium eruption, Changbaishan-Tianchi volcano, China/DPRK: New field, petrological, and chemical constraints on stratigraphy, volcanology, and magma dynamics. Journal of Volcanology and Geothermal Research, 343: 45-59.

Parham, P.R., Saito, Y., Sapon, N., Suriadi, R. and Mohtar, N.A., 2014. Evidence for ca. 7-ka maximum Holocene transgression on the Peninsular Malaysia east coast. Journal of Quaternary Science, 29(5): 414-422.

Park, M.-H., Kim, I.-S. and Shin, J.-B., 2003. Characteristics of the late Quaternary tephra layers in the East/Japan Sea and their new occurrences in western Ulleung Basin sediments. Marine Geology, 202(3-4): 135-142.

Pearce, N.J., Westgate, J.A., Preece, S.J., Eastwood, W.J. and Perkins, W.T., 2004. Identification of Aniakchak (Alaska) tephra in Greenland ice core challenges

the 1645 BC date for Minoan eruption of Santorini. Geochemistry, Geophysics, Geosystems, 5(3).

Peccerillo, A. and Taylor, S., 1976. Geochemistry of Eocene calc-alkaline volcanic rocks from the Kastamonu area, northern Turkey. Contrib Mineral Petrol, 58(1): 63-81.

Plunkett, G., Coulter, S.E., Ponomareva, V.V., Blaauw, M., Klimaschewski, A. and Hammarlund, D., 2015. Distal tephrochronology in volcanic regions: challenges and insights from Kamchatkan lake sediments. Global and Planetary Change, 134: 26-40.

Ponomareva, V., Portnyagin, M., Pendea, I.F., Zelenin, E., Bourgeois, J., Pinegina, T. and Kozhurin, A., 2017. A full holocene tephrochronology for the Kamchatsky Peninsula region: Applications from Kamchatka to North America. Quaternary Science Reviews, 168: 101-122.

Ponomareva, V., Portnyagin, M., Pevzner, M., Blaauw, M., Kyle, P. and Derkachev, A., 2015. Tephra from andesitic Shiveluch volcano, Kamchatka, NW Pacific: chronology of explosive eruptions and geochemical fingerprinting of volcanic glass. International Journal of Earth Sciences, 104(5): 1459-1482.

Pyne-O'Donnell, S.D.F., Cwynar, L.C., Jensen, B.J.L., Vincent, J.H., Kuehn, S.C., Spear, R. and Froese, D.G., 2016. West Coast volcanic ashes provide a new continental-scale Lateglacial isochron. Quaternary Science Reviews, 142: 16-25.

Pyne-O'Donnell, S.D.F., Hughes, P.D.M., Froese, D.G., Jensen, B.J.L., Kuehn, S.C., Mallon, G., Amesbury, M.J., Charman, D.J., Daley, T.J., Loader, N.J., Mauquoy, D., Street-Perrott, F.A. and Woodman-Ralph, J., 2012. High-precision ultra-distal Holocene tephrochronology in North America. Quaternary Science Reviews, 52: 6-11.

Ramos, F.C., Heizler, M., Buettner, J., Gill, J., Wei, H., Dimond, C. and Scott, S., 2016. U-series and 40Ar/39Ar ages of Holocene volcanic rocks at Changbaishan volcano, China. Geology, 44(7): 511-514.

Rampino, M.R. and Self, S., 1982. Historic eruptions of Tambora (1815), Krakatau (1883), and Agung (1963), their stratospheric aerosols, and climatic impact. Quaternary Research, 18(2): 127-143.

Ramsey, C.B., Albert, P.G., Blockley, S.P., Hardiman, M., Housley, R.A., Lane, C.S., Lee, S., Matthews, I.P., Smith, V.C. and Lowe, J.J., 2015. Improved age

estimates for key Late Quaternary European tephra horizons in the RESET lattice. Quaternary Science Reviews, 118: 18-32.

Rasmussen, S.O., Vinther, B.M., Clausen, H.B. and Andersen, K.K., 2007. Early Holocene climate oscillations recorded in three Greenland ice cores. Quaternary Science Reviews, 26(15-16): 1907-1914.

Razjigaeva, N., Ganzey, L., Lyaschevskaya, M., Makarova, T., Kudryavtseva, E., Grebennikova, T., Panichev, A., Arslanov, K., Maksimov, F. and Petrov, A.Y., 2017. Climatic and human impacts on landscape development of the Murav'ev Amursky Peninsula (Russian South Far East) in the Middle/Late Holocene and historical time. Quaternary International: In press.

Razzhigaeva, N.G., Matsumoto, A. and Nakagawa, M., 2016. Age, source, and distribution of Holocene tephra in the southern Kurile Islands: Evaluation of Holocene eruptive activities in the southern Kurile arc. Quaternary International, 397: 63-78.

Reimer, P.J., Bard, E., Bayliss, A., Beck, J.W., Blackwell, P.G., Bronk Ramsey, C., Buck, C.E., Cheng, H., Edwards, R.L., Friedrich, M., Grootes, P.M., Guilderson, T.P., Haflidason, H., Hajdas, I., Hatté, C., Heaton, T.J., Hoffmann, D.L., Hogg, A.G., Hughen, K.A., Kaiser, K.F., Kromer, B., Manning, S.W., Niu, M., Reimer, R.W., Richards, D.A., Scott, E.M., Southon, J.R., Staff, R.A., Turney, C.S.M. and van der Plicht, J., 2013. IntCal13 and Marine13 Radiocarbon Age Calibration Curves 0–50,000 Years cal BP. Radiocarbon, 55(4): 1869-1887.

Robock, A., 2000. Volcanic eruptions and climate. Reviews of Geophysics, 38(2): 191-219.

Rutherford, M.J. and Devine, J.D., 1996. Preeruption pressure-temperature conditions and volatiles in the 1991 dacitic magma of Mount Pinatubo. Fire and mud: eruptions and lahars of Mount Pinatubo, Philippines: 751-766.

Salisbury, M.J., Patton, J.R., Kent, A.J.R., Goldfinger, C., Djadjadihardja, Y. and Hanifa, U., 2012. Deep-sea ash layers reveal evidence for large, late Pleistocene and Holocene explosive activity from Sumatra, Indonesia. Journal of Volcanology and Geothermal Research, 231-232: 61-71.

Sato, H., Kumano, S., Maeda, Y., Nakamura, T. and Matsuda, I., 1998. The Holocene development of Kushu Lake on Rebun Island in Hokkaido, Japan. Journal of Paleolimnology, 20(1): 57-69.

Schmidt, M., Leipe, C., Becker, F., Goslar, T., Hoelzmann, P., Mingram, J., Müller, S.,

Tjallingii, R., Wagner, M. and Tarasov, P.E., 2019. A multi-proxy palaeolimnological record of the last 16,600 years from coastal Lake Kushu in northern Japan. Palaeogeography, Palaeoclimatology, Palaeoecology, 514: 613-626.

Schmidt, M., Tarasov, P.E., Hoelzmann, P., Meyer, H. and Leipe, C., 2016. Diatoms from Lake Kushu: A pilot study to test the potential of a Late Quaternary palaeoenvironmental archive from Rebun Island (Hokkaido Region, Japan). Journal of Asian Earth Sciences, 122: 106-122.

Self, S., Gertisser, R., Thordarson, T., Rampino, M. and Wolff, J., 2004. Magma volume, volatile emissions, and stratospheric aerosols from the 1815 eruption of Tambora. Geophysical Research Letters, 31(20).

Self, S. and King, A.J., 1996. Petrology and sulfur and chlorine emissions of the 1963 eruption of Gunung Agung, Bali, Indonesia. Bull Volcanol, 58(4): 263-285.

Self, S., Rampino, M., Newton, M. and Wolff, J., 1984. Volcanological study of the great Tambora eruption of 1815. Geology, 12(11): 659-663.

Self, S. and Rampino, M.R., 1981. The 1883 eruption of Krakatau. Nature, 294: 699-704.

Self, S., Rampino, M.R. and Barbera, J.J., 1981. The possible effects of large 19th and 20th century volcanic eruptions on zonal and hemispheric surface temperatures. Journal of Volcanology and Geothermal Research, 11(1): 41-60.

Shen, C., Beer, J., Liu, T., Oeschger, H., Bonani, G., Suter, M. and Wölfli, W., 1992. ^{10}Be in Chinese loess. Earth and Planetary Science Letters, 109(1): 169-177.

Shiihara, M., Torii, M., Okuno, M., Domitsu, H., Nakamura, T., Kim, K.-H., Moriwaki, H. and Oda, M., 2011. Revised stratigraphy of Holocene tephras on Ulleung Island, South Korea, and possible correlatives for the U-Oki tephra. Quaternary International, 246(1): 222-232.

Shimada, S., 2000. Eruption of the Amagi-Kawagodaira volcano and paleo-environments in the Late and Latest Jomon Periods around the Izu Peninsula. The Quaternary Research (Daiyonki-kenkyu), 39(2): 151-164 (in Japanese with English abstract).

Sigl, M., Winstrup, M., McConnell, J.R., Welten, K.C., Plunkett, G., Ludlow, F., Buntgen, U., Caffee, M., Chellman, N., Dahl-Jensen, D., Fischer, H., Kipfstuhl, S., Kostick, C., Maselli, O.J., Mekhaldi, F., Mulvaney, R., Muscheler, R., Pasteris, D.R., Pilcher, J.R., Salzer, M., Schupbach, S., Steffensen, J.P., Vinther,

B.M. and Woodruff, T.E., 2015. Timing and climate forcing of volcanic eruptions for the past 2,500 years. Nature, 523(7562): 543-549.

Sigurdsson, H., Carey, S., Mandeville, C. and Bronto, S., 1991. Pyroclastic flows of the 1883 Krakatau eruption. Eos, Transactions American Geophysical Union, 72(36): 377-381.

Smith, V.C., Isaia, R. and Pearce, N.J.G., 2011a. Tephrostratigraphy and glass compositions of post-15 kyr Campi Flegrei eruptions: implications for eruption history and chronostratigraphic markers. Quaternary Science Reviews, 30(25–26): 3638-3660.

Smith, V.C., Mark, D.F., Staff, R.A., Blockley, S.P.E., Ramsey, C.B., Bryant, C.L., Nakagawa, T., Han, K.K., Weh, A., Takemura, K. and Danhara, T., 2011b. Toward establishing precise 40Ar/39Ar chronologies for Late Pleistocene palaeoclimate archives: an example from the Lake Suigetsu (Japan) sedimentary record. Quaternary Science Reviews, 30(21–22): 2845-2850.

Smith, V.C., Pearce, N.J.G., Matthews, N.E., Westgate, J.A., Petraglia, M.D., Haslam, M., Lane, C.S., Korisettar, R. and Pal, J.N., 2011c. Geochemical fingerprinting of the widespread Toba tephra using biotite compositions. Quaternary International, 246(1–2): 97-104.

Smith, V.C., Staff, R.A., Blockley, S.P.E., Bronk Ramsey, C., Nakagawa, T., Mark, D.F., Takemura, K. and Danhara, T., 2013. Identification and correlation of visible tephras in the Lake Suigetsu SG06 sedimentary archive, Japan: chronostratigraphic markers for synchronising of east Asian/west Pacific palaeoclimatic records across the last 150 ka. Quaternary Science Reviews, 67(0): 121-137.

Soda, T., 1989. Two 6th century eruptions of Haruna volcano, central Japan. The Quaternary Research (Daiyonki-Kenkyu), 27(4): 297-312 (in Japanese with English abstract).

Spano, N.G., Lane, C.S., Francis, S.W. and Johnson, T.C., 2017. Discovery of Mount Mazama cryptotephra in Lake Superior (North America): Implications and potential applications. Geology, 45(12): 1071-1074.

Stebich, M., Mingram, J., Han, J. and Liu, J., 2009. Late Pleistocene spread of (cool-)temperate forests in Northeast China and climate changes synchronous with the North Atlantic region. Global and Planetary Change, 65(1–2): 56-70.

Stebich, M., Rehfeld, K., Schlütz, F., Tarasov, P.E., Liu, J. and Mingram, J., 2015.

Holocene vegetation and climate dynamics of NE China based on the pollen record from Sihailongwan Maar Lake. Quaternary Science Reviews, 124: 275-289.

Sun, C., Liu, J., You, H. and Nemeth, K., 2017. Tephrostratigraphy of Changbaishan volcano, northeast China, since the mid-Holocene. Quaternary Science Reviews, 177: 104-119.

Sun, C., Plunkett, G., Liu, J., Zhao, H., Sigl, M., McConnell, J.R., Pilcher, J.R., Vinther, B., Steffensen, J.P. and Hall, V., 2014a. Ash from Changbaishan Millennium eruption recorded in Greenland ice: Implications for determining the eruption's timing and impact. Geophysical Research Letters: 2013GL058642.

Sun, C., Wang, L., Plunkett, G., You, H., Zhu, Z., Zhang, L., Zhang, B., Chu, G. and Liu, J., 2018. Ash from the Changbaishan Qixiangzhan eruption: A new early Holocene marker horizon across East Asia. Journal of Geophysical Research: Solid Earth, 123. https://doi.org/10.1029/2018JB015983.

Sun, C., You, H., He, H., Zhang, L., Gao, J., Guo, W., Chen, S., Mao, Q., Liu, Q., Chu, G. and Liu, J., 2015. New evidence for the presence of Changbaishan Millennium eruption ash in the Longgang volcanic field, Northeast China. Gondwana Research, 28(1): 52-60.

Sun, C.Q., You, H.T., Liu, J.Q., Li, X., Gao, J.L. and Chen, S.S., 2014b. Distribution, geochemistry and age of the Millennium eruptives of Changbaishan volcano, Northeast China - A review. Front. Earth Sci., 8(2): 216-230.

Sun, S.-s. and McDonough, W.F., 1989. Chemical and isotopic systematics of oceanic basalts: implications for mantle composition and processes. Geological Society, London, Special Publications, 42(1): 313-345.

TAKAHASHI, M., OTSUKA, T., SAKO, H., KAWAMATA, H., YASUI, M., KANAMARU, T., OTSUKI, M., KOBAYASHI, T., ISHIHARA, K. and MIKI, D., 2013. Temporal Variation for Magmatic Chemistry of the Sakurajima Volcano and Aira Caldera Region, Southern Kyushu, Southwest Japan since 61 ka and Its Implications for the Evolution of Magma Chamber System. Bulletin of the Volcanological Society of Japan, 58(1): 19-42.

Takemura, K., Iwabe, C., Hayashida, A., Danhara, T., Kitagawa, H., Haraguchi, T., Sato, T. and Ishikawa, N., 2010. Stratigraphy of marker tephras and sediments during the past 50,000 years from multiple sites in Lake Biwa, Japan. Quaternary Research, 49(3): 147-160 (in Japanese with English abstract).

Tani, S., Kitagawa, H., Hong, W., Park, J.H., Sung, K.S. and Park, G., 2013. Age determination of the Kawagodaira volcanic eruption in Japan by 14 C wiggle-matching. Radiocarbon, 55(2): 748-752.

Timms, R.G.O., Matthews, I.P., Palmer, A.P. and Candy, I., 2018. Toward a tephrostratigraphic framework for the British Isles: A Last Glacial to Interglacial Transition (LGIT c. 16-8 ka) case study from Crudale Meadow, Orkney. Quat Geochronol, 46: 28-44.

Timms, R.G.O., Matthews, I.P., Palmer, A.P., Candy, I. and Abel, L., 2017. A high-resolution tephrostratigraphy from Quoyloo Meadow, Orkney, Scotland: Implications for the tephrostratigraphy of NW Europe during the Last Glacial-Interglacial Transition. Quat Geochronol, 40: 67-81.

Tomlinson, E.L., Albert, P.G., Wulf, S., Brown, R.J., Smith, V.C., Keller, J., Orsi, G., Bourne, A.J. and Menzies, M.A., 2014. Age and geochemistry of tephra layers from Ischia, Italy: constraints from proximal-distal correlations with Lago Grande di Monticchio. Journal of Volcanology and Geothermal Research, 287: 22-39.

Tomlinson, E.L., Arienzo, I., Civetta, L., Wulf, S., Smith, V.C., Hardiman, M., Lane, C.S., Carandente, A., Orsi, G., Rosi, M., Müller, W. and Menzies, M.A., 2012. Geochemistry of the Phlegraean Fields (Italy) proximal sources for major Mediterranean tephras: Implications for the dispersal of Plinian and co-ignimbritic components of explosive eruptions. Geochimica et Cosmochimica Acta, 93(0): 102-128.

Tomlinson, E.L., Smith, V.C., Albert, P.G., Aydar, E., Civetta, L., Cioni, R., Cubukcu, E., Gertisser, R., Isaia, R., Menzies, M.A., Orsi, G., Rosi, M. and Zanchetta, G., 2015. The major and trace element glass compositions of the productive Mediterranean volcanic sources: tools for correlating distal tephra layers in and around Europe. Quaternary Science Reviews, 118: 48-66.

Tomlinson, E.L., Thordarson, T., Müller, W., Thirlwall, M. and Menzies, M.A., 2010. Microanalysis of tephra by LA-ICP-MS — Strategies, advantages and limitations assessed using the Thorsmörk ignimbrite (Southern Iceland). Chemical Geology, 279(3–4): 73-89.

Tsuji, T., Ikeda, M., Furusawa, A., Nakamura, C., Ichikawa, K., Yanagida, M., Nishizaka, N., Ohnishi, K. and Ohno, Y., 2018. High resolution record of Quaternary explosive volcanism recorded in fluvio-lacustrine sediments of the

Uwa basin, southwest Japan. Quaternary International, 471: 278-297.

Tsukui, M., Saito, K. and Hayashi, K., 2006. Frequent and intensive eruptions in the 9th century, Izu Islands, Japan: Revision of volcanostratigraphy based on tephras and historical document. Bulletin of Volcanological Society of Japan, 1: 327-338 (in Japanese with English abstract).

Turney, C.S., Lowe, J.J., Davies, S.M., Hall, V., Lowe, D.J., Wastegård, S., Hoek, W.Z. and Alloway, B., 2004. Tephrochronology of Last Termination sequences in Europe: a protocol for improved analytical precision and robust correlation procedures (a joint SCOTAV–INTIMATE proposal). Journal of Quaternary Science, 19(2): 111-120.

Turney, C.S.M., 1998. Extraction of rhyolitic component of Vedde microtephra from minerogenic lake sediments. Journal of Paleolimnology, 19(2): 199-206.

Ukstins Peate, I., Baker, J.A., Kent, A.J.R., Al-Kadasi, M., Al-Subbary, A., Ayalew, D. and Menzies, M., 2003. Correlation of Indian Ocean tephra to individual Oligocene silicic eruptions from Afro-Arabian flood volcanism. Earth and Planetary Science Letters, 211(3–4): 311-327.

Ukstins Peate, I., Kent, A.J.R., Baker, J.A. and Menzies, M.A., 2008. Extreme geochemical heterogeneity in Afro-Arabian Oligocene tephras: Preserving fractional crystallization and mafic recharge processes in silicic magma chambers. Lithos, 102(1–2): 260-278.

van der Bilt, W.G.M., Lane, C.S. and Bakke, J., 2017. Ultra-distal Kamchatkan ash on Arctic Svalbard: Towards hemispheric cryptotephra correlation. Quaternary Science Reviews, 164: 230-235.

Verbeek, R.D.M., 1884. The Krakatoa Eruption. Nature, 30: 10.

Walker, M.J., Berkelhammer, M., Björck, S., Cwynar, L.C., Fisher, D.A., Long, A.J., Lowe, J.J., Newnham, R.M., Rasmussen, S.O. and Weiss, H., 2012. Formal subdivision of the Holocene Series/Epoch: a Discussion Paper by a Working Group of INTIMATE (Integration of ice‐core, marine and terrestrial records) and the Subcommission on Quaternary Stratigraphy (International Commission on Stratigraphy). Journal of Quaternary Science, 27(7): 649-659.

Wang, F., Chen, W.-j., Peng, Z.-c. and Li, Q., 2001. Activity of Cangbaishan Tianchi Volcano since Late Pleistocene: The constrain from geochronology of high precision U-series TIMS method. Geochimica, 30(1): 88-94 (in Chinese with

English abstract).

Wang, L., Li, J., Lu, H., Gu, Z., Rioual, P., Hao, Q., Mackay, A.W., Jiang, W., Cai, B., Xu, B., Han, J. and Chu, G., 2012. The East Asian winter monsoon over the last 15,000 years: its links to high-latitudes and tropical climate systems and complex correlation to the summer monsoon. Quaternary Science Reviews, 32: 131-142.

Wang, X., Chu, G., Sheng, M., Zhang, S., Li, J., Chen, Y., Tang, L., Su, Y., Pei, J. and Yang, Z., 2016. Millennial-scale Asian summer monsoon variations in South China since the last deglaciation. Earth and Planetary Science Letters, 451: 22-30.

Wang, Y.J., Cheng, H., Edwards, R.L., An, Z.S., Wu, J.Y., Shen, C.-C. and Dorale, J.A., 2001. A High-Resolution Absolute-Dated Late Pleistocene Monsoon Record from Hulu Cave, China. Science, 294(5550): 2345-2348.

Wang, Y., Cheng, H., Edwards, R.L., He, Y., Kong, X., An, Z., Wu, J., Kelly, M.J., Dykoski, C.A. and Li, X., 2005. The Holocene Asian Monsoon: Links to Solar Changes and North Atlantic Climate. Science, 308(5723): 854-857.

Wang, Y., Cheng, H., Edwards, R.L., Kong, X., Shao, X., Chen, S., Wu, J., Jiang, X., Wang, X. and An, Z., 2008. Millennial- and orbital-scale changes in the East Asian monsoon over the past 224,000 years. Nature, 451: 1090.

Wanner, H., Beer, J., Bütikofer, J., Crowley, T.J., Cubasch, U., Flückiger, J., Goosse, H., Grosjean, M., Joos, F., Kaplan, J.O., Küttel, M., Müller, S.A., Prentice, I.C., Solomina, O., Stocker, T.F., Tarasov, P., Wagner, M. and Widmann, M., 2008. Mid- to Late Holocene climate change: an overview. Quaternary Science Reviews, 27(19): 1791-1828.

Watson, E.J., Swindles, G.T., Lawson, I.T. and Savov, I.P., 2016. Do peatlands or lakes provide the most comprehensive distal tephra records? Quaternary Science Reviews, 139: 110-128.

Watson, E.J., Swindles, G.T., Lawson, I.T., Savov, I.P. and Wastegård, S., 2017. The presence of Holocene cryptotephra in Wales and southern England. Journal of Quaternary Science, 32(4): 493-500.

Weber, A.W., Jordan, P. and Kato, H., 2013. Environmental change and cultural dynamics of Holocene hunter–gatherers in Northeast Asia: Comparative analyses and research potentials in Cis-Baikal (Siberia, Russia) and Hokkaido (Japan). Quaternary International, 290–291: 3-20.

Wei, H., Liu, G. and Gill, J., 2013. Review of eruptive activity at Tianchi volcano, Changbaishan, northeast China: implications for possible future eruptions. Bull Volcanol, 75(4): 1-14.

Wei, H., Wang, Y., Jin, J., Gao, L., Yun, S.-H. and Jin, B., 2007. Timescale and evolution of the intracontinental Tianchi volcanic shield and ignimbrite-forming eruption, Changbaishan, Northeast China. Lithos, 96(1–2): 315-324.

Westrich, H. and Gerlach, T., 1992. Magmatic gas source for the stratospheric SO2 cloud from the June 15, 1991, eruption of Mount Pinatubo. Geology, 20(10): 867-870.

Wulf, S., Dräger, N., Ott, F., Serb, J., Appelt, O., Guðmundsdóttir, E., van den Bogaard, C., Słowiński, M., Błaszkiewicz, M. and Brauer, A., 2016. Holocene tephrostratigraphy of varved sediment records from Lakes Tiefer See (NE Germany) and Czechowskie (N Poland). Quaternary Science Reviews, 132: 1-14.

Wulf, S., Hardiman, M.J., Staff, R.A., Koutsodendris, A., Appelt, O., Blockley, S.P.E., Lowe, J.J., Manning, C.J., Ottolini, L., Schmitt, A.K., Smith, V.C., Tomlinson, E.L., Vakhrameeva, P., Knipping, M., Kotthoff, U., Milner, A.M., Müller, U.C., Christanis, K., Kalaitzidis, S., Tzedakis, P.C., Schmiedl, G. and Pross, J., 2018. The marine isotope stage 1–5 cryptotephra record of Tenaghi Philippon, Greece: Towards a detailed tephrostratigraphic framework for the Eastern Mediterranean region. Quaternary Science Reviews, 186: 236-262.

Xiao, J., Porter, S.C., An, Z., Kumai, H. and Yoshikawa, S., 1995. Grain Size of Quartz as an Indicator of Winter Monsoon Strength on the Loess Plateau of Central China during the Last 130,000 Yr. Quaternary Research, 43(1): 22-29.

Xu, J., Pan, B., Liu, T., Hajdas, I., Zhao, B., Yu, H., Liu, R. and Zhao, P., 2013. Climatic impact of the Millennium eruption of Changbaishan volcano in China: New insights from high-precision radiocarbon wiggle-match dating. Geophysical Research Letters, 40(1): 54-59.

Yamamoto, T., Ito, J.-i., Nakagawa, M., Hasegawa, T. and Kishimoto, H., 2010. 14 C ages for the ejecta from Kutcharo and Mashu calderas, eastern Hokkaido, Japan. Bulletin of the Geological Survey of Japan, 61(5-6): 161-170 (in Japanese with English abstract).

Yancheva, G., Nowaczyk, N.R., Mingram, J., Dulski, P., Schettler, G., Negendank, J.F.W., Liu, J., Sigman, D.M., Peterson, L.C. and Haug, G.H., 2007. Influence

of the intertropical convergence zone on the East Asian monsoon. Nature, 445: 74-77.

Yang, L., Wang, F., Feng, H., Wu, L. and Shi, W., 2014. 40Ar/39Ar geochronology of Holocene volcanic activity at Changbaishan Tianchi volcano, Northeast China. Quat Geochronol, 21: 106-114.

Yatsuzuka, S., Okuno, M., Nakamura, T., Kimura, K., Setoma, Y., Miyamoto, T., Kim, K.H., Moriwaki, H., Nagase, T. and Jin, X., 2010. 14C wiggle-matching of the B-Tm tephra, Baitoushan volcano, China/North Korea. Radiocarbon, 52(3): 933-940.

Yin, J., Jull, A.J.T., Burr, G.S. and Zheng, Y., 2012. A wiggle-match age for the Millennium eruption of Tianchi Volcano at Changbaishan, Northeastern China. Quaternary Science Reviews, 47(0): 150-159.

Yoshimoto, M., Amma-Miyasaka, M., Takahashi, R., Nakagawa, M. and Yoshida, K., 2008. Reevaluation of the pre–1640 AD eruptive history of Hokkaido-Komagatake volcano, northern Japan. Journal of the Geological Society of Japan, 114: 336-347 (in Japanese with English abstract).

Yu, H., Wu, J., Xu, J., Lin, C., Shi, L. and Chen, X., 2012. Microstructural Characteristics of the Holocene Pumice Erupted from Changbaishan Tianchi Volcano and Their Volcanological Implications. Journal of Jilin University (Earth Science Edition), 42(Sup. 3): 132-144 (in Chinese with English abstract).

Zdanowicz, C.M., Zielinski, G.A. and Germani, M.S., 1999. Mount Mazama eruption: Calendrical age verified and atmospheric impact assessed. Geology, 27(7): 621-624.

Appendix

Averaged compositions of sixty late Quaternary marker tephras ranging from 15 ka to 1 Ma in age, erupted from over thirty major volcanic centres in Japan (detailed information of source volcanoes see Aoki and Machida (2006)). These compositions were used to compare with the averaged composition of RK12-0819 (see Table S4.3). The results revealed no match.

Tephra	SiO2	TiO2	Al2O3	FeO*	MnO	MgO	CaO	Na2O	K2O	n	Total
Ng (pfl)	**78.47**	**0.17**	**12.19**	**1.17**	**0.08**	**0.23**	**1.55**	**3.33**	**2.82**	**23**	**95.05**
	0.2	0	0.1	0.1	0	0	0.1	0.1	0.1		0.9
WT (u)	**76.36**	**0.35**	**13.55**	**1.45**	**0.1**	**0.31**	**1.71**	**4.04**	**2.14**	**22**	**96.28**
	2.1	0.1	1.6	0.4	0	0.1	0.6	0.3	0.3		1.6
WT (m)	**76.39**	**0.37**	**13.38**	**1.63**	**0.08**	**0.35**	**1.68**	**4.06**	**2.06**	**28**	**97.07**
	0.7	0.1	0.3	0.2	0	0.1	0.1	0.2	0.1		1.8
WT (l)	**76.81**	**0.36**	**13.28**	**1.53**	**0.09**	**0.32**	**1.59**	**3.89**	**2.12**	**27**	**95.38**
	0.5	0	0.2	0.1	0	0	0.1	0.2	0.1		1.6
A (pfl)	**75.19**	**0.51**	**13.63**	**2.01**	**0.1**	**0.46**	**2.04**	**3.98**	**2.06**	**30**	**97.75**
	0.4	0	0.2	0.1	0	0	0.1	0.1	0		1.4
En-a	**76.22**	**0.31**	**13.1**	**1.83**	**0.06**	**0.34**	**2.05**	**3.58**	**2.51**	**12**	**97.01**
	0.6	0.1	0.4	0.1	0.1	0	0.3	0.1	0.1		1.2
YmP	**72.07**	**0.63**	**14.87**	**3.15**	**0.16**	**0.9**	**3.6**	**4.03**	**0.59**	**11**	**97.28**
	1.1	0.1	0.4	0.4	0	0.1	0.3	0.1	0		2.1
D-Oh (pfa)	**78.45**	**0.21**	**11.94**	**0.88**	**0.04**	**0.15**	**0.93**	**2.59**	**4.82**	**20**	**97.4**
	0.4	0	0.2	0.3	0	0	0.1	0.1	0.1		1.3
D-Oh (pfa)	**78.63**	**0.18**	**11.78**	**1.05**	**0.04**	**0.13**	**0.82**	**2.75**	**4.61**	**15**	**95.5**
	0.3	0	0.2	0.1	0	0	0	0.1	0.1		2.1
Kc-Sr	**78.52**	**0.26**	**12.14**	**1.33**	**0.07**	**0.25**	**1.34**	**3.69**	**2.4**	**21**	**97.85**

	0.4	0	0.2	0.1	0	0	0.1	0.1	0.1		1.2
Spfl	**78.56**	**0.15**	**12.45**	**1.37**	**0.05**	**0.13**	**1.23**	**3.41**	**2.64**	**21**	**98.1**
	0.5	0	0.3	0.1	0	0	0.1	0.1	0.1		2
Spfa-1	**77.99**	**0.15**	**12.53**	**1.47**	**0.08**	**0.13**	**1.3**	**3.78**	**2.58**	**23**	**93.03**
	0.5	0	0.2	0.1	0	0	0	0.2	0.1		1.4
Spfa-1	**78.55**	**0.14**	**12.16**	**1.69**	**0.04**	**0.13**	**1.18**	**3.69**	**2.42**	**16**	**97.63**
	0.3	0	0.1	0.1	0	0	0	0.2	0.1		1.4
Kt-1	**78.57**	**0.17**	**12.1**	**1.5**	**0.06**	**0.17**	**1.36**	**3.47**	**2.59**	**16**	**98.38**
	0.4	0	0.3	0.1	0.1	0	0	0.2	0.1		1.5
Kt-2	**76.8**	**0.3**	**12.75**	**2.31**	**0.07**	**0.33**	**2.2**	**3.62**	**1.62**	**14**	**97.19**
	1.3	0.1	0.5	0.4	0	0.1	0.4	0.1	0.1		1.7
Kt-3	**76.32**	**0.37**	**12.6**	**3.27**	**0.1**	**0.43**	**2.77**	**2.69**	**1.46**	**13**	**95.71**
	0.7	0.1	0.2	0.1	0	0	0.1	0.5	0.1		1.8
Kt-4	**76.5**	**0.34**	**12.76**	**2.39**	**0.06**	**0.37**	**2.34**	**3.56**	**1.68**	**14**	**96.16**
	0.2	0.1	0.1	0.1	0.1	0	0.1	0.1	0.1		2.1
Kt-5	**76.54**	**0.29**	**12.29**	**2.73**	**0.07**	**0.36**	**2.43**	**3.82**	**1.46**	**12**	**96.71**
	0.3	0	0.2	0.1	0	0	0.1	0.1	0.1		1.3
Kt-6	**76.41**	**0.28**	**13.07**	**2.33**	**0.08**	**0.33**	**2.36**	**3.62**	**1.52**	**26**	**97.2**
	0.8	0.1	0.3	0.4	0.1	0.1	0.3	0.2	0.2		1.8
Kt-7	**76.63**	**0.31**	**13.01**	**2.19**	**0.1**	**0.39**	**2.4**	**3.6**	**1.36**	**23**	**95.55**
	1.1	0.1	0.4	0.5	0.1	0.1	0.6	0.2	0.4		0.9
Kt-8	**77.56**	**0.25**	**12.84**	**2.21**	**0.07**	**0.38**	**2.38**	**3.14**	**1.17**	**12**	**93.73**
	0.6	0.1	0.2	0.2	0.1	0.1	0.2	0.3	0.2		1.7
Kc-2/3 (pfl)	**77.54**	**0.35**	**12.67**	**1.81**	**0.08**	**0.32**	**1.63**	**3.77**	**1.83**	**18**	**96.56**
	1.9	0.2	0.5	0.7	0	0.2	0.5	0.2	0.1		1.1
Toya	**79.06**	**0.05**	**12.44**	**0.88**	**0.1**	**0.03**	**0.33**	**4.3**	**2.8**	**14**	**94.22**
	0.2	0	0.2	0.1	0	0	0	0.1	0.1		1.4

Toya	**78.52**	**0.04**	**12.67**	**0.9**	**0.1**	**0.03**	**0.33**	**4.49**	**2.92**	**11**	**93.35**
	0.3	0	0.2	0.1	0.1	0	0	0.1	0.1		1
Kc-Hb (pfl)	**78.32**	**0.33**	**12.07**	**1.49**	**0.11**	**0.23**	**1.29**	**4.14**	**2.02**	**17**	**97.95**
	0.5	0	0.3	0.1	0	0	0.1	0.1	0.1		1.6
Kc-5 (pfl)	**76.06**	**0.28**	**13.25**	**2.18**	**0.04**	**0.37**	**1.66**	**4.23**	**1.92**	**12**	**94.32**
	0.3	0.1	0.2	0.2	0	0	0.1	0.1	0.1		1.3
Kc-6 (pfl)	**77.18**	**0.21**	**12.88**	**1.71**	**0.05**	**0.29**	**1.44**	**4.04**	**2.19**	**19**	**94.36**
	0.5	0	0.2	0.2	0	0	0.1	0.1	0.1		0.9
Kc-7 (pfl)	**73.66**	**0.42**	**14.01**	**2.87**	**0.1**	**0.62**	**2.16**	**4.27**	**1.9**	**20**	**94.11**
	1.1	0.1	0.3	0.5	0	0.2	0.3	0.1	0.1		1.5
Kc-8 (pfl)	**77.89**	**0.19**	**12.34**	**1.57**	**0.06**	**0.24**	**1.27**	**3.82**	**2.62**	**20**	**93.95**
	0.4	0	0.2	0.1	0	0	0	0.1	0.1		1.1
AUP (pfl)	**77.05**	**0.25**	**12.55**	**2.02**	**0.03**	**0.25**	**1.42**	**3.7**	**2.73**	**19**	**95.11**
	0.4	0	0.2	0.1	0	0	0	0.1	0.1		1.4
AWT (pfl)	**74.3**	**0.31**	**13.14**	**3.75**	**0.07**	**0.28**	**1.77**	**3.58**	**2.8**	**17**	**93.98**
	1.1	0	0.4	0.6	0	0	0.2	0.6	0.1		1.7
ALP (pfl)	**73.45**	**0.42**	**13.81**	**3.43**	**0.09**	**0.57**	**2.23**	**4.35**	**1.66**	**17**	**94.57**
	0.5	0	0.3	0.1	0	0	0.1	0.2	0.1		1.2
To-H (pfa, m)	**76.61**	**0.44**	**12.83**	**1.86**	**0.1**	**0.66**	**2.44**	**4.02**	**1.05**	**15**	**98.23**
	0.5	0.1	0.3	0.2	0.1	0	0.1	0.1	0		1.5
To-H (pfa, l)	**77.68**	**0.4**	**12.24**	**1.61**	**0.11**	**0.54**	**2.22**	**4.08**	**1.12**	**16**	**97.26**
	0.8	0.1	0.2	0.3	0.1	0.1	0.2	0.1	0.1		2.2
	78.09	**0.38**	**12.17**	**1.48**	**0.09**	**0.49**	**2.11**	**4.05**	**1.13**	**12**	**97.2**
	0.3	0.1	0.2	0.1	0	0.1	0.1	0.1	0.1		2.3
	76.45	**0.46**	**12.45**	**1.99**	**0.15**	**0.69**	**2.55**	**4.17**	**1.09**	**4**	**97.46**
	0.6	0	0.1	0.1	0.1	0.1	0.2	0.2	0.1		2.3
To-H (pfl, u)	**77.8**	**0.32**	**12.89**	**1.62**	**0.08**	**0.36**	**1.98**	**3.72**	**1.23**	**22**	**97.94**

	1.6	0.1	0.7	0.4	0.1	0.1	0.5	0.4	0.1		1.2
To-H (pfl, u)	**77.75**	**0.33**	**12.89**	**1.63**	**0.08**	**0.33**	**1.87**	**3.85**	**1.28**	**21**	**95.93**
	1	0.1	0.5	0.2	0.1	0.1	0.3	0.1	0.1		2
	78.3	**0.29**	**12.67**	**1.52**	**0.06**	**0.29**	**1.73**	**3.84**	**1.3**	**15**	**95.68**
	0.5	0	0.4	0.1	0	0	0.1	0.1	0.1		1.9
	76.38	**0.4**	**13.43**	**1.9**	**0.11**	**0.44**	**2.22**	**3.88**	**1.24**	**6**	**96.56**
	0.2	0.1	0.1	0.1	0	0.1	0.1	0.1	0.1		2.3
To-H (pfl, u)	**77.61**	**0.33**	**12.89**	**1.56**	**0.09**	**0.33**	**1.84**	**3.96**	**1.38**	**34**	**97.39**
	0.7	0.1	0.3	0.2	0	0.1	0.2	0.1	0.1		1.4
To-H (pfl, l)	**77.32**	**0.34**	**12.96**	**1.67**	**0.09**	**0.36**	**1.89**	**4**	**1.37**	**30**	**97.5**
	1.2	0.1	0.5	0.3	0	0.1	0.3	0.1	0.1		1.6
To-Of (pfa)	**77.6**	**0.35**	**12.58**	**1.96**	**0.08**	**0.37**	**2.03**	**3.86**	**1.16**	**13**	**97.31**
	1.1	0	0.5	0.2	0.1	0.1	0.3	0.1	0.1		1.6
To-Of (pfl)	**77.82**	**0.36**	**12.45**	**1.88**	**0.08**	**0.33**	**1.87**	**3.97**	**1.25**	**21**	**98.25**
	1.3	0.1	0.4	0.5	0	0.1	0.3	0.1	0.1		1.2
To-GP	**75.62**	**0.48**	**13.39**	**2.07**	**0.1**	**0.65**	**2.53**	**4.12**	**1.04**	**15**	**97.52**
	1.1	0.1	0.7	0.3	0	0.1	0.2	0.1	0		1.8
Iw-Y	**77**	**0.28**	**12.46**	**2.04**	**0.04**	**0.29**	**1.59**	**3.5**	**2.8**	**15**	**92.55**
	0.9	0	0.4	0.3	0	0.1	0.2	0.2	0.2		1.4
Nr-Y (afa)	**79.67**	**0.16**	**11.94**	**1.3**	**0.06**	**0.17**	**1.31**	**3.62**	**1.78**	**40**	**96.64**
	0.3	0	0.2	0.1	0	0	0.1	0.1	0.1		1.4
Nr-Y (pfl)	**79.35**	**0.19**	**12.06**	**1.24**	**0.05**	**0.18**	**1.32**	**3.7**	**1.89**	**11**	**98.89**
	0.2	0	0.2	0.1	0	0	0.1	0.1	0.1		0.9
Yk-Y	**79.49**	**0.19**	**11.65**	**1.38**	**0.05**	**0.17**	**1.43**	**3.18**	**2.46**	**16**	**97.86**
	0.4	0	**0.3**	0.1	0	0	0.1	0.1	0.1		1.5
Yk-Y (u)	**78.81**	**0.2**	**11.94**	**1.54**	**0.05**	**0.2**	**1.47**	**3.17**	**2.63**	**5**	**96.7**
	0.2	0.1	0.1	0.1	0	0	0	0.1	0		1.6

Yk-Y (m)	**78.74**	**0.21**	**12.15**	**0.9**	**0.03**	**0.19**	**1.53**	**3.5**	**2.75**	**3**	**93.17**
	0.1	0.1	0.2	0.1	0	0	0	0	0.1		1.1
Yk-Y (l)	**78.59**	**0.2**	**12.08**	**1.43**	**0.04**	**0.17**	**1.49**	**3.26**	**2.75**	**12**	**95.06**
	0.8	0.1	0.5	0.4	0	0.1	0.2	0.2	0.3		2.2
Yk-MP	**78.71**	**0.2**	**11.73**	**1.52**	**0.04**	**0.19**	**1.67**	**3.38**	**2.56**	**25**	**95.04**
	0.3	0	0.2	0.1	0	0	0.1	0.1	0.1		1.8
Nr-N (afa)	**78.09**	**0.17**	**12.55**	**1.9**	**0.04**	**0.17**	**1.32**	**4.08**	**1.68**	**24**	**94.75**
	0.9	0	0.4	0.3	0	0.1	0.3	0.2	0.2		1.6
Nr-N (pfl)	**78.08**	**0.14**	**12.38**	**1.79**	**0.06**	**0.15**	**1.18**	**4.33**	**1.9**	**19**	**97.08**
	0.5	0	0.3	0.1	0	0	0.1	0.2	0.1		1.5
Smy (pfl)	**78.59**	**0.11**	**12.42**	**1.39**	**0.05**	**0.14**	**1.12**	**4.08**	**2.11**	**20**	**94.8**
	0.5	0	0.3	0.1	0	0	0.1	0.2	0.1		1.1
O-Ik (pfl)	**79.01**	**0.21**	**12.25**	**1**	**0.04**	**0.16**	**1.13**	**3.9**	**2.3**	**24**	**97.5**
	0.5	0	0.3	0.1	0	0	0.1	0.2	0.1		1.3
Tn-A (pfl)	**78.7**	**0.12**	**12.47**	**1.56**	**0.05**	**0.22**	**1.53**	**3.85**	**1.5**	**5**	**98.55**
	0.3	0	0.2	0.1	0	0	0	0	0.1		0.5
Tn-C (pfl)	**78.74**	**0.23**	**12.36**	**1.88**	**0.05**	**0.28**	**1.71**	**3.23**	**1.52**	**9**	**94.94**
	0.9	0.1	0.3	0.4	0	0.1	0.4	0.7	0.6		2.3
Tn-C (pfa)	**78.92**	**0.18**	**11.92**	**1.82**	**0.05**	**0.22**	**1.64**	**3.66**	**1.58**	**13**	**96.52**
	0.6	0.1	0.3	0.3	0	0	0.1	0.1	0.2		1.4
Oga pmt	**77.65**	**0.07**	**12.65**	**0.4**	**0.08**	**0.04**	**0.6**	**3.23**	**5.28**	**20**	**95.31**
	0.3	0	0.2	0.1	0	0	0	0.2	0.2		1.5
Ag-KP	**77.03**	**0.18**	**13.34**	**1.41**	**0.05**	**0.39**	**2**	**3.19**	**2.42**	**24**	**92.99**
	0.3	0.1	0.1	0.1	0	0	0.1	0.1	0.1		0.6
Hk-TP (pfa)	**75.67**	**0.47**	**12.89**	**2.49**	**0.11**	**0.53**	**2.46**	**4.17**	**1.2**	**15**	**94.7**
	0.6	0.1	0.5	0.2	0	0.1	0.1	0.2	0.1		1.2
Hk-TP (pfl)	**73.69**	**0.54**	**13.58**	**3.01**	**0.09**	**0.76**	**2.99**	**4.25**	**1.07**	**13**	**93.05**

	1.5	0.1	0.6	0.5	0	0.2	0.5	0.2	0.1		1.2
Tt-E (pfa)	**76.81**	**0.19**	**12.69**	**1.13**	**0.03**	**0.15**	**1.07**	**2.67**	**5.25**	**9**	**99.72**
	0.4	0	0.3	0.1	0	0	0.1	0.1	0.1		1.2
On-Pm1	**75.53**	**0.09**	**14.24**	**1.01**	**0.09**	**0.23**	**1.56**	**3.44**	**3.8**	**14**	**94.29**
	0.2	0.1	0.1	0.1	0.1	0	0.1	0.1	0.1		1
Nm-Tg (pfl)	**78.26**	**0.06**	**12.79**	**0.54**	**0.13**	**0.13**	**0.45**	**4.22**	**3.42**	**23**	**95.65**
	0.8	0	0.7	0.1	0	0	0	0.3	0.1		2.4
AT	**78.23**	**0.13**	**12.43**	**1.22**	**0.03**	**0.12**	**1**	**3.3**	**3.54**	**47**	**95.66**
	0.5	0	0.3	0.1	0	0	0	0.1	0.1		2
Aso-4	**73.23**	**0.4**	**14.57**	**1.56**	**0.09**	**0.3**	**1.03**	**4.23**	**4.58**	**26**	**96.91**
	0.9	0.1	0.5	0.2	0	0.1	0.2	0.2	0.3		1.9
Aso-4	**72.3**	**0.41**	**14.74**	**1.74**	**0.1**	**0.38**	**1.15**	**4.14**	**5.04**	**33**	**95.8**
	0.5	0.1	0.3	0.2	0	0.1	0.2	0.1	0.2		1.2
K-Tz	**76.8**	**0.21**	**13.17**	**1.07**	**0.04**	**0.25**	**1.14**	**3.2**	**4.11**	**19**	**96.92**
	0.3	0	0.2	0.1	0	0	0.1	0.1	0.1		0.9
Ata (pfl)	**75.72**	**0.45**	**13.15**	**1.8**	**0.08**	**0.39**	**1.64**	**3.52**	**3.25**	**15**	**98.44**
	0.2	0	0.1	0.1	0	0	0	0.1	0.1		0.7
Ata (pfl)	**75.74**	**0.46**	**13.05**	**1.83**	**0.07**	**0.4**	**1.62**	**3.61**	**3.22**	**35**	**98.28**
	0.3	0	0.2	0.1	0	0	0.1	0.1	0.1		1.1
SK	**76.37**	**0.11**	**13.98**	**0.81**	**0.11**	**0.2**	**0.8**	**3.64**	**3.99**	**3**	**94.74**
	1.5	0	0.5	0.4	0	0.1	0.2	0.3	0.1		0.8
SK	**77.2**	**0.05**	**13.5**	**0.6**	**0.09**	**0.12**	**0.66**	**3.63**	**4.15**	**25**	**94.16**
	0.3	0	0.2	0	0	0	0.1	0.1	0.1		0.9
SK	**77.34**	**0.05**	**13.59**	**0.52**	**0.1**	**0.1**	**0.65**	**3.73**	**3.91**	**21**	**94.3**
	0.5	0	0.4	0	0	0	0	0.3	0.1		1.1
Aso-3	**70.18**	**0.64**	**15.56**	**2.14**	**0.09**	**0.54**	**1.63**	**4.17**	**5.06**	**29**	**94.35**
	0.4	0	0.2	0.1	0	0	0.1	0.1	0.1		1.4

Ata-Th (pfl)	**78.19**	**0.15**	**12.78**	**0.91**	**0.06**	**0.15**	**1.03**	**3.39**	**3.34**	**29**	**95.04**
	0.6	0.1	0.3	0.2	0	0.1	0.1	0.2	0.3		1
Aso-1	**68.55**	**0.64**	**15.72**	**3.17**	**0.08**	**0.55**	**1.92**	**3.69**	**5.67**	**38**	**93.47**
	0.4	0.1	0.2	0.2	0	0	0.1	0.1	0.1		1.1
Kkt	**77.19**	**0.17**	**12.56**	**1.13**	**0.03**	**0.11**	**0.8**	**3.4**	**4.61**	**19**	**96.16**
	0.3	0	0.1	0.1	0	0	0	0.1	0.1		1
Yb-1	**78.38**	**0.11**	**11.91**	**0.84**	**0.04**	**0.06**	**0.7**	**2.71**	**5.25**	**15**	**95.88**
	0.3	0	0.2	0.1	0	0	0.1	0.2	0.3		2
Tky-Ng1	**78.1**	**0.13**	**12.22**	**0.69**	**0.03**	**0.09**	**0.72**	**2.65**	**5.38**	**18**	**96.31**
	0.4	0	0.3	0.1	0	0	0	0.1	0.2		1.9
TE-5	**78.38**	**0.07**	**12.16**	**0.88**	**0.05**	**0.06**	**0.72**	**2.7**	**4.98**	**18**	**94.56**
	0.3	0	0.2	0.1	0	0	0.1	0.1	0.3		1.2
TE-5	**78.12**	**0.08**	**12.39**	**0.69**	**0.03**	**0.05**	**0.68**	**2.91**	**5.05**	**20**	**96.36**
	0.5	0	0.3	0.1	0	0	0	0.1	0.2		1.5
Ks-5	**77.02**	**0.3**	**12.98**	**1.24**	**0.05**	**0.24**	**1.21**	**3.74**	**3.21**	**39**	**96.05**
	0.3	0	0.2	0.1	0	0	0.1	0.1	0.1		0.9
Kb-Ks	**74.77**	**0.27**	**14.22**	**1.12**	**0.06**	**0.22**	**0.99**	**3.89**	**4.46**	**44**	**96.22**
	0.8	0.1	0.4	0.1	0	0	0.1	0.1	0.2		1.3
Ss-Pk	**78.39**	**0.21**	**12.16**	**0.97**	**0.05**	**0.16**	**0.91**	**2.76**	**4.4**	**17**	**94.23**
	0.3	0	0.2	0.1	0	0	0	0.1	0.2		1